

https://dspace.org/

Multi-objective optimization of thermo-mechanical modelling of friction stir welding

Topper, Candice Catherine

2015-05-07
http://hdl.handle.net/10539/17664

Downloaded from a DSpace repository. https://dspace.org/

University of the Witwatersrand

Multi-Objective Optimization of Thermo-Mechanical Modelling Of Friction Stir Welding

Candice Catherine Topper

5/28/2014

0701434Y

Supervisor: Prof. C Polese (University of the Witwatersrand)

Co-Supervisor: Mr F Pietra (University of Pretoria)

A dissertation submitted to the Faculty of Engineering and the Built Environment, University of the Witwatersrand, Johannesburg, in fulfilment of the requirements for the degree of Master of Science in Engineering.

Declaration

I, Candice Catherine Topper (Student number 0701434Y), a student registered for the degree of Master of Science in Engineering in the academic year(s) 2012-2013.

I hereby declare the following:

- I am aware that plagiarism (the use of someone else's work without their permission and/or without acknowledging the original source) is wrong.
- I confirm that the work submitted for assessment for the above degree is my own unaided work except where I have explicitly indicated otherwise.
- I have followed the required convections in referencing the thoughts and ideas of others.
- I understand that the University of the Witwatersrand may take disciplinary action against me if there is a belief that this is not my own unaided work or that I have failed to acknowledge the source of the ideas or words in my writing.

Signature: _____ Date: _____

Abstract

This research work is primarily focused on the simulation of the thermal effects on the Friction Stir Welding (FSW) process on aluminium alloys for aerospace applications. The main objective is to be able to realistically characterise the thermal input of a FSW process by means of an accurate parametric Finite Element thermal model, verified using thermal imaging camera data as a benchmark.

FSW is a solid state joining process. A rotating tool is plunged into the joint line between two clamped plates. The heat transfer input mechanism in the FSW process is due to the frictional contact between the tool and the work-piece plates. Since the FSW process occurs at solid state, no melting occurs and hence the yield strength of the material is temperature dependent.

Obtaining accurate measurements of temperature for the FSW process has proven to be challenging. Preliminary experimental observations in obtaining temperature variations in the material was performed using thermocouples but issues arose, one being the inability to obtain a complete thermal representation of the tool and the work-piece as thermocouples were placed along the FS weld only as control points. Research was undertaken using a thermal imaging camera. The type of camera used has a sensitivity that is able to detect temperature differences as small as 0.04°C. This experimental approach gives direct information of the temperature at all points of the work-piece, obtaining a complete external thermal assessment of the process. This is also beneficial in obtaining images of the temperature distribution in the tool itself also if it is rotating and partly submerged into the work-piece.

Since the temperature field directly affects the final residual stress distribution in the joint, an accurate thermal model of the FSW process is required to assimilate the numerical simulation with the process that actually occurs in reality. The new release of the Finite Element (FE) software ANSYS Release 14 was used. This novel version is capable of modelling the specific features required to assimilate the FSW process by using the ANSYS Parametric Design Language (APDL). The APDL language has new specific features designed for frictional heat generation, plastic heat generation and temperature controlled bonding contacts. The formulation of the model is based upon the thermal-mechanical model specifically developed by Zhu and Chao [20]. ANSYS APDL language is parametric by nature as such, it is well suited to be efficiently implemented into a multi-objective optimization platform, such as the modeFRONTIER software, in order to further improve the FSW simulation.

The quantitative experimental data obtained from the thermal imaging camera was used to match and verify the numerical results of the FSW FE model. An accurate FSW thermal model

will help to achieve a deeper understanding of the different phases of the process and an enhanced control of the key parameters of this technology, significantly reducing the required testing phase. It has many benefits over previous models including;

- The model is a fully developed thermal-structural model whereby the thermal and structural effects of each other are modelled together
- The model does not incorporate symmetry to account for the advance and retreating side of the weld as this has an effect on the temperature distribution and can be seen in the frictional stress developed where the one side clearly depicts a higher stress than the other
- It incorporates material properties changing with temperature

Results obtained prove to be of some comparison with not only the literature but experimentally as well. Although there is some comparison, further investigation needs to be conducted on the convection coefficients as well as the friction coefficient and recommendations have been suggested for these parameters. However, a fully parametric thermo-mechanical model has been developed and it is able to be implemented into an optimisation tool such as modeFRONTIER.

Acknowledgements

I would like to thank the following people for all their support and guidance during the completion of my Masters study.

Prof C. Polese. For her guidance and inspiration to always achieve for further goals other than the ones laid out before one. I would also like to thank her for support through any challenge that I was faced with and in believing in my capabilities from the very beginning.

Mr F. Pietra. For all his help and knowledge with ANSYS as well as his support through all the conferences that I presented.

National Research Foundation (NRF). For their financial contributions towards the research of FSW, who without their contributions this work would have been difficult to achieve.

University of the Witwatersrand. For generously giving me a travel grant in order to present my work in the USA. The experience and opportunity is one that will forever be cherished and for that I am greatly honoured.

My parents. Thank you for all your support throughout the years, it is because of you as to where I am now and I will always be grateful for that extra nudge to sometimes keep me going just a little further. Your loving care and guidance has not gone un-noticed and that I am very proud to be your daughter.

Loved ones. A special thank you to the specially loved people in my life. You have played an important role in your support with the completion of this challenge in my life. Thank you for always being there.

Table of Contents

Declaration i

Abstract ii

Acknowledgements iv

List of Tables viii

List of Figures xi

Nomenclature xiv

1. Introduction 1

1.1 Background of Friction Stir Welding 1

1.2 Purpose of study 3

1.3 Problem Statement 4

2. Literature Survey 6

2.1 Friction Stir Welding 6

2.2 Phases of the FSW process 6

2.3 FSW models 8

2.3.1 Numerical models 14

2.3.2 Analytical models 30

2.3.3 Experimental findings 40

2.3.4 Current model features versus previous models developed 44

2.3.5 Parameters of interest based on prior models 45

2.4 Material properties 50

2.4.1 Aluminium Alloys 50

2.4.2 H13 Tool steel 50

2.4.3 Material properties affected by temperature 51

2.5 Objectives 54

2.6 Summary 54

3. Finite Element Modelling 56

3.1 Introduction 56

3.2 Apparatus 56
3.3 Methodology 57
3.3.1 Material property inputs 58
3.3.2 Geometry 60
3.3.3 Boundary conditions and contacts 61
3.3.4 Analysis 68
3.3.5 Parametric model features 70
3.4 Summary 71
4. Experimental Weld Trials 72
4.1 Introduction 72
4.2 Apparatus 72
4.2.1 CNC machine 72
4.2.2 FLIR Systems 73
4.2.3 Tool and work piece properties 75
4.3 Methodology 77
4.3.1 CNC Setup 77
4.3.2 Thermal camera setup 77
4.4 Summary 78
5. Data Processing 79
5.1 Introduction 79
5.2 Finite Element Modelling 79
5.2.1 Sample calculation for heat flux for FEA model 83
5.2.2 Heat transfer values for FEA model 84
5.3 Weld Trials 85
5.3.1 Sample calculation for heat transfer values 87
5.3.2 Convection coefficients and heat transfer values of weld trials 91
5.4 Summary 97
6. Results 99
6.1 Introduction 99

6.2 Finite Element Modelling 99
6.3 Weld Trials 100
6.4 Comparison of FEA and weld trial results 104
6.5 Processing data based on result findings 108
6.6 Summary 109
7. Discussion 110
7.1 Introduction 110
7.2 Model development 110
7.3 FEA model processed data 112
7.4 Weld trial processed data 113
7.5 Results comparison 115
7.6 Optimisation of parametric model 117
7.7 Summary 118
8. Conclusions and recommendations 119
8.1 Introduction 119
8.2 Conclusions 119
8.3 Recommendations 120
9. References 122
10. APPENDIX 128
10.1 Appendix 1: Further information on literature models 128
10.2 Appendix 2: Material properties 140
10.3 Appendix 3: ANSYS APDL commands 161
10.4 Appendix 4: CNC information 173
10.5 Appendix 5: Tool and Pin Geometry 175
10.6 Appendix 6: FEA model processed data 176
10.7 Appendix 7: Average temperature plots 183
10.8 Appendix 8: Conferences and workshops 192
Workshop HPC 194
Conference IASSA 197

Conference AeroMat 202

List of Tables

Table 2.1: Effects of each parameter and influence on temperature development in FSW process 7
Table 2.2: Material properties changing with temperature ASTM 36 steel 15
Table 2.3: Temperature dependent properties for aluminium alloy 6061-T6 18
Table 2.4: Weld parameters and heat generated from the tool 28
Table 2.5: Convection coefficients for the work piece surface 29
Table 2.6 Table for material properties under consideration for the energy model 32
Table 2.7: Axial force with varying process parameters 33
Table 2.8: Optimised values for parameters affecting heat generation 36
Table 2.9: Temperatures for various parameters and materials 36
Table 2.10: Temperature result for various rpm 36
Table 2.11: Maximum temperatures for different rpm input 37
Table 2.12: Axial force and resulting temperatures for various models 39
Table 2.13: Contact condition 48
Table 2.14: Emissivity value dependant on view 53
Table 3.1: properties of materials as given in Engineering Data 58
Table 3.2: Material properties inserted into engineering data in ANSYS 58
Table 3.3: Depiction of pilot node setting in ANSYS workbench 70
Table 4.1: Thermal camera specification 74
Table 4.2: Material properties of tool and work piece 75
Table 4.3: Tool and work piece geometry 76
Table 5.1: Model log book for different inputs 80
Table 5.2: Heat flux transfer (kW/m^2) for various FEA models 84
Table 5.3: Weld trial parameters with images 85
Table 5.4: Tool parameters values 87
Table 5.5: Convection coefficients estimation for each contributing surface 90
Table 5.6: Average convection coefficients for the tool during dwell time 91
Table 5.7: Average convection coefficients on work piece surfaces during the dwell period 93
Table 5.8: Heat transfer for sliding and sticking for dwell period 93
Table 5.9: Spot locations for temperature graphs 94
Table 6.1: Heat flux transfer values for certain FEA models specified 99
Table 6.2: Total heat flux transfer for FEA models 100

Table 6.3: Average increase in temperature for FEA models 100
Table 6.4: Total heat flux along radius for both contact conditions 100
Table 6.5: Average for work piece of weld trials 101
Table 6.6: Average heat convection coefficients before the first 2 seconds of the weld trial 101
Table 6.7: Convection coefficients for the tool for first 2 seconds of dwell time..... 102
Table 6.8: Average change in temperature for the first 2 seconds of work piece and tool . 102
Table 6.9: Average increase in temperature for work piece and tool for the entire dwell duration as well for the first 2 seconds of the dwell period are recorded. 103
Table 6.10: Heat flux for work piece and tool during first 2 seconds of dwell time 103
Table 6.11: Error for total heat flux values on surfaces for weld trials of the same parameters 104
Table 6.12: Revision of heat flux values for weld trials 108
Table 7.1: Percentage contributions for each part of the tool..... 111
Table 10.1: Numerical models investigated..... 128
Table 10.2: Results and issues discussed for numerical models..... 132
Table 10.3: Analytical models investigated..... 135
Table 10.4: Results for analytical models..... 137
Table 10.5: Experimental studies investigated 138
Table 10.6: Aluminium alloy 2024 properties changing with temperature 140
Table 10.7: Aluminium Alloy 2024 T3..... 140
Table 10.8: Aluminium Alloy 2024 T6..... 146
Table 10.9: Overview of hot-work tool steel..... 150
Table 10.10: H13 Hot work tool steel 152
Table 10.11: Conversion of U.S units to standard Unit's 154
Table 10.12: Emissivity of material with different finishes..... 156
Table 10.13: Thermal expansion coefficient increasing with temperature for H13 tool steel 157
Table 10.14: Emissivity for Aluminium alloy of various surface specifications 158
Table 10.15: Theoretical emissivity values for various materials 159
Table 10.16: Values of thermal properties of some materials..... 159
Table 10.17: Yield stress at various conditions..... 160
Table 10.18: Average heat flux for FEA models 176
Table 10.19: Average heat flux for FEA models 177
Table 10.20: Heat flux transfer for FEA model..... 179
Table 10.21: Heat flux transfer for FEA model..... 180
Table 10.22: Temperature plots for average temperatures on work piece..... 183

Table 10.23: Calculated values used for processed data 184
Table 10.24: 1250 RPM and 500mm/min processes data 185
Table 10.25: 1600 RPM and 400mm/min processes data 187
Table 10.26: 1250 RPM and 400mm/min processes data 188
Table 10.27: 1600 RPM and 400mm/min processes data 190

List of Figures

Figure 1.1: Depiction of FSW process 1
Figure 1.2: Eclipse aircraft which uses FSW on primary parts of their aircraft 2
Figure 1.3: Depiction of the external tank on the Space Shuttle that uses FSW 3
Figure 1.4: Marine application where FSW is used on naval materials 3
Figure 2.1: FSW phases in FSW in general 7
Figure 2.2: FSW depicting the sides of the weld and an in depth view of the pin in the work piece 8
Figure 2.3: COMSOL Multiphysics model depicting the 3-D model coupled with the 2-D model 9
Figure 2.4: Depiction of STIR 3D model described as "3D particle dynamics at the tool leading edge" 10
Figure 2.5: Boundary condition set for model 15
Figure 2.6: Boundary conditions set for FEA model 16
Figure 2.7: Full depiction of boundary conditions set 19
Figure 2.8: Material properties changing with temperature AA2195 20
Figure 2.9: Mesh of model developed by Keiereddine 21
Figure 2.10: Pathways for the heat (thermal boundary conditions) described by Colgrove 23
Figure 2.11: Material properties changing with temperature for aluminium alloy 5000 series 24
Figure 2.12: Temperature profile over weld for advance and retreating side 27
Figure 2.13: Temperature dependent properties 34
Figure 2.14: Coefficient of friction versus temperature 34
Figure 2.15: Heat generation for various conditions 35
Figure 2.16: Percentage contributions form welding paramerts 38
Figure 2.17: Influence of parameters on heat generation (Variables have the same description as outlined in the Nomenclature 41
Figure 2.18: Results for various feed rates and rotation speeds for experimental findings 42
Figure 2.19: Friction coefficient versus time for experimental findings 43
Figure 2.20: Heat generation contributions from each part of the model 46
Figure 2.21: Increase in heat capacity with increasing temperature at constant volume 52
Figure 3.1: ANSYS mechanical logo 56
Figure 3.2: SOLID226 element geometry 57
Figure 3.3: Geometry of model built in ANSYS version 14.5 60
Figure 3.4: Element type command 61
Figure 3.5: ANSYS Workbench model tree 62

Figure 3.6: Thermal boundary command 63
Figure 3.7: Contact condition command for the tool surface and work piece surface contacts 65
Figure 3.8: Thermal boundary conditions between tool shoulder surface and work piece surface 67
Figure 3.9: Thermal boundary condition command between work piece surfaces 67
Figure 3.10: Frictionless contact between two plates 68
Figure 3.11: Remote point located for the two time steps for plunge and rotation 69
Figure 4.1: CNC Machine 72
Figure 4.2: T640 thermal camera 74
Figure 4.3: Tool geometry 76
Figure 5.1: Temperature comparisons with various models 83
Figure 5.2: Heat distribution and frictional stress from tool to work piece 84
Figure 5.3: Frictional stress region between tool surface and work piece surface 85
Figure 5.4: Temperature plot versus weld time for 1250 RPM and 500 mm/min feed rate weld trial 95
Figure 5.5: Temperature plot versus weld time for 1600 RPM and 400 mm/min feed rate weld trial 4 96
Figure 5.6: Temperature plot versus weld time for 1250 RPM and 400 mm/min feed rate weld 1a 96
Figure 5.7: Temperature plot versus weld time for 1600 RPM and 400 mm/min feed rate weld 1b 97
Figure 6.1: Heat flux comparison for each contributing surface for the FEA and weld trials 105
Figure 6.2: Convection contributions for each surface for the FEA and weld trials 106
Figure 6.3: Temperature increase over time for the FEA and weld trials to compare 106
Figure 6.4: Weld trial temperature trend data 107
Figure 6.5: FEA temperature trend data 108
Figure 6.6: Work piece convection coefficients for FEA and weld trials after adjusted data contributions 109
Figure 7.1: Extract from the contact command in FEA methodology 111
Figure 10.1: Flow model depicting coupling for thermal model 131
Figure 10.2: Rotational speed versus temperature result for numerical model 1 132
Figure 10.3: Efficiency of weld over time for numerical model 2 133
Figure 10.4: Numerical model 6 modelling result 133
Figure 10.5: Stress along weld line result for numerical model 8 133
Figure 10.6: Temperature results for numerical model 15 134
Figure 10.7: Table of welding parameters for experimental work 2 139

Figure 10.8: Tool dimensions for experimental work 139
Figure 10.9: Table of tool parameters for experimental work 5 139
Figure 10.10: Ultimate tensile strength of AL2024 changing with 154
Figure 10.11: Young's modulus of Al2024 changing with temperature 155
Figure 10.12: Modulus of Elasticity changing with temperature for Aluminium 2024..... 155
Figure 10.13: Variation with temperature for aluminium material properties relative to their value of 300K 156
Figure 10.14: Table representation of typical values for material properties 156
Figure 10.15: CNC specification 173
Figure 10.16: CNC technical data specification 174
Figure 10.17: Pin geometry 175
Figure 10.18: Tool geometry 175
Figure 10.19: Extract for prize winners from AeSSA newsletter of October 2012 194
Figure 10.20: Application to attend HPC workshop, part 1 194
Figure 10.21: Application to attend HPC workshop, part 2 195
Figure 10.22: Acceptance letter from HPC 196
Figure 10.23: Organising committee and acknowledgements as found in IASSSA book of abstracts 197
Figure 10.24: Featured title in IASSA book of abstracts 199
Figure 10.25: Abstract as found in IASSA book of Abstracts 200
Figure 10.26: Prize awarded for presentation at IASSA 2012 201
Figure 10.27: Extract of Abstract submitted from AeroMat website 202
Figure 10.28: Travel grant in Student account 203
Figure 10.29: Acceptance letter for travel grant 203
Figure 10.30: Acceptance letter to attend AeroMat conference 205
Figure 10.31: Overview of presentation 209

Nomenclature

Symbol	Definition	Units
Q	Total heat transfer	W
Q_1	Heat generated from shoulder	W
Q_2	Heat generated from probe	W
Q_3	Heat generated from probe tip surface	W
Q_{Total}	Total heat generation	W or W/m^2
$\tau_{contact}$	Shear stress contact	MPa
ω	Tool rotation	rad/s
$R_{Shoulder}$	Shoulder radius	m
R_{Probe}	Probe radius	m
H_{Probe}	Probe height	m
Q_1	Heat flux into the model due to the friction between tool and work piece surface	W/m^2
Q_3	Heat flux from the friction between tool and work piece surface	W/m^2
Q_2	Heat conducted from the bottom of the work piece to the backing plate	W/m^2
q_2	Convection due to heat lost from work piece surface to the air	W/m^2
Q	Increase of heat content in the work piece	W/m^2
Q_4	Heat flux transferred from the clamped tool to the machine bushing	W/m^2
q_1	Convection due to heat lost from the tool surface to the air	W/m^2
h_{q2}	Convection coefficient for top surface of work piece	W/m^2K
h_{Q2}	Convection coefficient for bottom surface of work piece	W/m^2K
h_4	Convection coefficient for clamped tool	W/m^2K
A_C	Area of clamped tool section	m^4
A_S	Area of shoulder tool section	m^4
T	Temperature	°C
T_O	Ambient temperature = 25°C	°C
F_1	Force	N
ε	Emissivity	
σ_{SB}	Stephan Boltzman constant = 5.	

F	Force acting due to plunge of tool	N
q(r)	Total heat flux for the tool	W/m^2K
r	Radial output until tool shoulder radius	m
δ	Contact condition	
γ	Slip condition	
v_{tool}	Velocity of tool	m/s
v_{matrix}	Matrix velocity	m/s

Chapter 1

1. Introduction

1.1 Background of Friction Stir Welding

Friction Stir Welding (FSW) is a solid state joining process as depicted in Figure 1.1 [1]. A rotating tool is plunged into the join line between two clamped plates. The heat transfer input mechanism in the FSW process is due to the frictional contact between the tool and the work piece plates. Since the FSW process occurs at solid state, no melting occurs and hence the yield strength of the material is temperature dependent as are a few other properties of the material.



Figure 1.1: Depiction of FSW process

Due to its finer grain recrystallization, the following material advantages of the FSW technique include:

- Reduces residual stresses
- Lower distortion, shrinkage and porosity
- Strong ductile joints

Other advantages for the FSW process are as follows;

- Wider range of materials can be welded
    - Some of the materials include, magnesium, titanium, zinc, mild steel, selected stainless steels, nickel alloys and aluminium alloys [1]
    - It is a great benefit for aluminium and its alloys since in the past it has always been difficult to weld aluminium alloys due to its high thermal conductivity and

rapid formation of an oxide film over liquid weld puddles causing weaknesses in the weld properties [1]
    - Investigation into welding dissimilar materials has also been investigated
- Consumes less energy
    - One tool can be used to weld 1000 metres of a joint length [2]
    - No extra processes in between is required for the weld such as, grinding, brushing or pickling [2] especially when it comes to mass production, this improves production time, which in turn helps with cost
- Environmentally friendly
    - The use of filler wire are eliminated, hence no harmful gases are emitted during the process [1]

FSW is being used in a variety of applications for various industries due to the advantages listed above. Some of the areas where FSW is being implemented are in the aircraft and aerospace industry. One aircraft company already using this process for production on their primary parts of their aircraft is Eclipse Aviation, where an example of one of their aircraft is shown in Figure 1.2 [3] below.



Figure 1.2: Eclipse aircraft which uses FSW on primary parts of their aircraft

The aerospace industry has used FSW process on the external tanks on the Space Shuttle [4]. The Shuttle's External Tank project (The external tank can be seen in Figure 1.3 [4]) developed a tool pin that is described as a through-spindle and is retractable, this was designed as such so that the pin tip could be retracted or expanded within the material depending on the material thickness [4]. Reason for this is because it was found that a fixed pin is limited to a constant material thickness.



Figure 1.3: Depiction of the external tank on the Space Shuttle that uses FSW

The last two industries where this process is applicable are in the automotive and marine industries, where the marine industry is particularly interested in the naval ships as depicted in Figure 1.4 [5]. The Navy is interested in joining naval materials and with the improved property-to-weight ratio for high strength low alloy steels and also aluminium alloys; thinner gauge sections can be used which results in lighter weight designs [5].



Figure 1.4: Marine application where FSW is used on naval materials

Since the FSW process has many applications in the industry, it is important for the FSW process to be proven a reliable and improved manufacturing process as compared to previous welding and joining techniques. In order to introduce this process into industry, experimental findings of the process need to be conducted.

1.2 Purpose of study

Moving away from the physical approach of the FSW process and towards the computational approach, it is found that there is a desirable need for it. There are multiple advantages in using a computational approach, which are;

- It eliminates the need to do actual weld tests which has benefits in that being
    - Saving material cost

    - Saving time spent in doing the actual welds
- Can input various different parameters and run them parallel to each other and find the effects of the different parameters
- Can optimise the model which again eliminates the need for actual weld tests

The next step in improving the computational finite element model would be to optimise it using a multi-objective optimisation tool. The optimisation tool predicts the best quality weld parameters that should be used in the process. Some of the parameters to be considered that would be an advantage in finding the best quality weld include;

- Tools rotational speed
- Feed rate
- Dwell time

These parameters are important attributes when considering the phases of the FSW process and will be discussed further for each phase and its influences.

Some limitations attributing to the model and have an effect on the quality of the weld from an examined perspective are the following;

- Some thermal parameters that are not found in the literature such as the thermal convection coefficient for a specific material while temperature changes
- Friction coefficient of a specific material while temperature changes

To better understand what the problem involves when modelling the FSW process, previous work were reviewed to see what method of computation they used, with respect if it was a user interface or a numerical coding computation. Other aspects noted include whether a 2-D or 3-D model was used, what the outcomes were and what features they were looking at of the FSW process.

1.3 Problem Statement

Much research has been investigated with respect to the FSW process whereby actual weld tests have been done. Some of the research includes looking at the microstructure of the weld and for any defects it might contain as well as the material flow and different regions that exist within the welded region. This is important when investigating the reliability of the weld and hence to prove it as a reliable process. Other areas include investigating the temperature distribution around the weld. Certain methods have been used in the past where thermocouples have been placed along certain points and measurements have been taken,

but a lot of care needs to be done when doing this. Another approach to represent the temperature variation is to use a thermal imaging camera.

In the current study, this method was used experimentally using the FLIR thermal T640 camera together with the FLIR tools + software.

Based on the previous models discussed in the literature, main conclusions drawn were the parameters that influenced the welding process. Other points of interest are the developments of the model used and assumptions made with respect to how the heat is generated. This information is useful when developing the model and what assumptions can be made and what could be neglected.

The model was investigated for the heat generated within the tool to the work piece and using relevant boundary conditions one was able to relate the process in a realistic way in terms of heat generation. The modelling software used is the ANSYS version 14 which has new command features that enable a contact point to generate heat within the work piece from the tool. This frictional contact is what assimilates the heat generation within the model and is able to depict the heat flow from the tool into the work piece. This new model is a structural-thermal analysis. The model created is a mechanical structure with thermal input commands. This improved model consists of structural and thermal degrees of freedom, since the temperature and mechanical properties are both coupled to each other for the FSW process. In the new ANSYS version 14, the new features allow one to model the process more realistically using a rotating and moving tool piece.

Chapter 2

2. Literature Survey

2.1 Friction Stir Welding

In 1991 [7], TWI (The Welding Institute) developed an innovative welding technique that used the heat created by friction between materials to be welded together. Since then, many other research institutions and companies have delved into the finer details of the process, asking questions as to what makes the process work well for welds that are acceptable for use in aeronautical applications and what is occurring in the microstructure of the materials that allows for this to be chosen as a viable option.

Friction Stir Welding encompasses many advantages, such as having finer recrystallisation within the grain structure and a more environmentally and economic option when compared to other welding techniques currently being used. With these advantages, many industries are taking advantage of using this technique in the manufacturing of their products. While industry is using this technique various institutions including industry themselves are researching into the process under a microscope. One area of particular interest has been the computational modelling of the process. This has included looking at the stirring motion of the material around the tool to the heat developed in the material caused by the rotating tool creating heat due to friction between the two surfaces.

Developing a computational model involves researching what has been accomplished so far, as well as understanding the short comings that previous researchers came up with as well as what important considerations were considered in their models and what is important for the current model. To understand, one needs to ask questions and to answer these questions, one needs to discover and delve into the knowledge that is available.

2.2 Phases of the FSW process

The process for the FSW can be separated into theoretically three or four phases. The fourth phase which is sometimes considered is the retraction of the tool from the work piece [6] for the purpose of this study in terms of heat generation and effects thereof, only the first three phases are deemed important and consist of the following;

- Plunge
- Dwell
- Feed rate

Shown in Figure 2.1 [8] is a simple schematic for the various 3 phases of the FSW weld, where the first picture is merely the initial tool rotation before it plunges into the work piece followed by the three main phases of the FSW process.

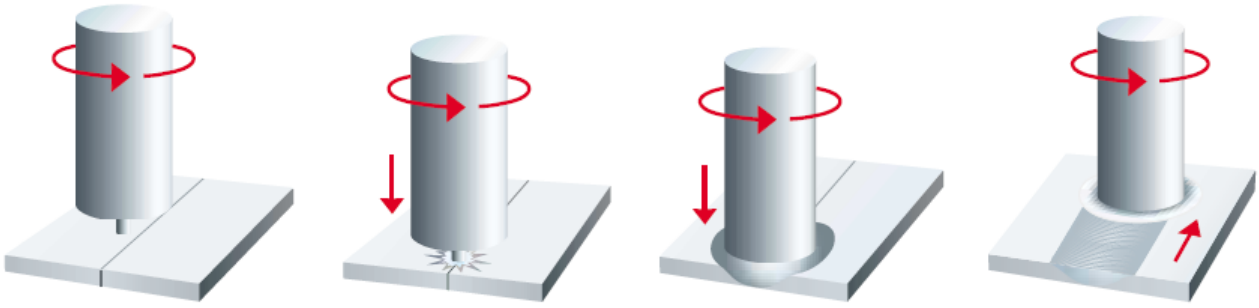


Figure 2.1: FSW phases in FSW in general

- Plunge
    - This consists of the tool penetrating into the work piece by a downward force whilst rotating at a particular speed. This is the initial phase of heat generation created.
- Dwell
    - This consists of the tool rotating for a period of time creating friction between the two surfaces and thereby generating heat between the two surfaces until the material plasticises to a particular temperature.
- Feed rate
    - Feed rate is when the tool begins to move in a lateral direction along the weld line, creating the weld. This phase consists of not only the tool rotating generating heat between the surfaces but also a weld speed in m/s. This feed rate has a significant effect on the quality of the weld.

Each parameter has an effect on the temperature condition of the FSW process and is described in Table 2.1 [9].

Table 2.1: Effects of each parameter and influence on temperature development in FSW process

Parameter	Effects
Rotation speed	Frictional heat, "stirring", oxide layer breaking and mixing of material.
Tilting angle	The appearance of the weld, thinning.
Welding speed	Appearance, heat control.
Down force	Frictional heat, maintaining contact conditions.

Rotation of the tool has a profound effect on the work piece material being stirred. This results in the weld having an advance and retreating side of the weld. This is depicted in Figure 2.2 [10], where the advancing side is where the rotation of the tool stirs the material away in the direction of the rotation and the retreating side is where that point of rotation has left behind. It is assumed that the temperatures on each side of the weld should also depict a difference since one side is stirring the heated material to the side while the other collects it. As to which side has the higher temperature is little is known, but according to Arbegast and Hartley [10] the advance side depicted has a slightly higher temperature.

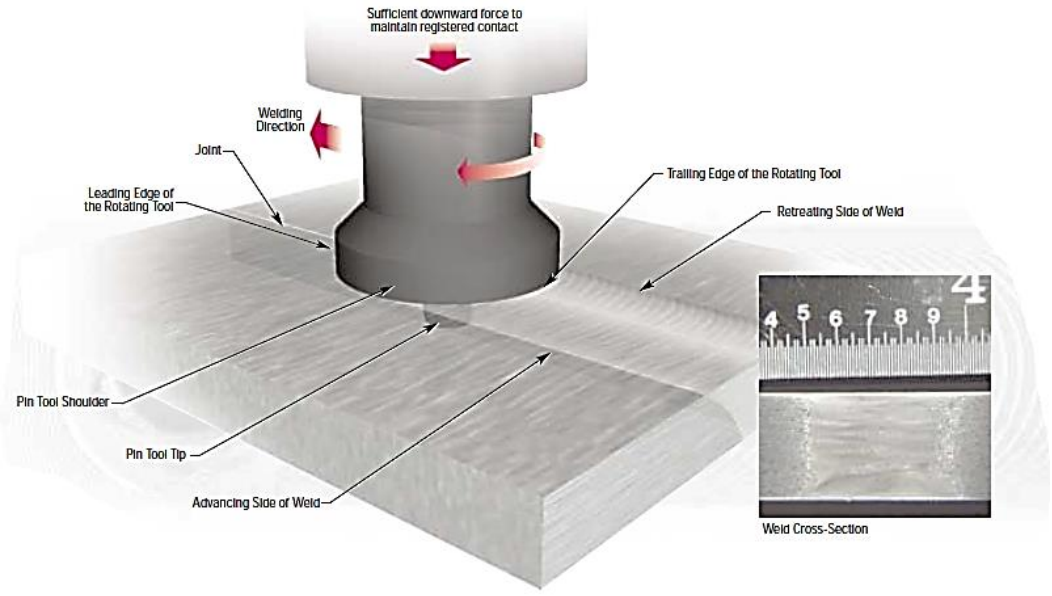


Figure 2.2: FSW depicting the sides of the weld and an in depth view of the pin in the work piece

2.3 FSW models

Previous work has been performed by developing models of the FSW process with many different objectives in mind. Models involve the material flow simulation, the effect of process parameters on the residual stresses produced, a thermal model predicting temperatures in the heat affected zone. Various assumptions have been made for each of the models and various considerations have been included in relation to the output of the model.

Previous works done for the modelling of the FSW process via computational means are described under each relevant researcher who was involved with the respective modelling;

- Xu, *et al* [10]
    - Developed two finite element models
        - Slipping interface model
        - Frictional contact model

- Finite element models compared qualitatively well with experimental measured patterns by means of marker insert technique

- Colegrove and Shercliff [10]
  - Used CFD code (FLUENT ‘slip’ model developed)
    - Interface conditions governed by local shear stresses
  - Findings with slip model;
    - Slip model revealed differences in flow with different tool shapes
    - Slip model showed different flow behaviour by common assumption of material stick
    - Deformation region is smaller on advancing side than retreating side
    - Material in path of pin is swept round the retreating side of tool- Corresponds to studies done by London and Guerra
    - Streamlines show bulge behind tool
    - Dragging material behind the advancing side – corresponds to studies with previous embedded marker experiments done by Reynolds et al [10]
- Colegrove [2]
  - Together with Airbus investigated to develop a mathematical model to enable one to look “inside” the weld to examine the temperature changes and distributions within the microstructure [2].
  - Uses a COMSOL Multiphysics model as depicted in Figure 2.3 [2]
    - Couples a 3-D thermal analysis to a 2-D axisymmetric swirl flow simulation [2] which can be seen in Figure 2.3 [2]

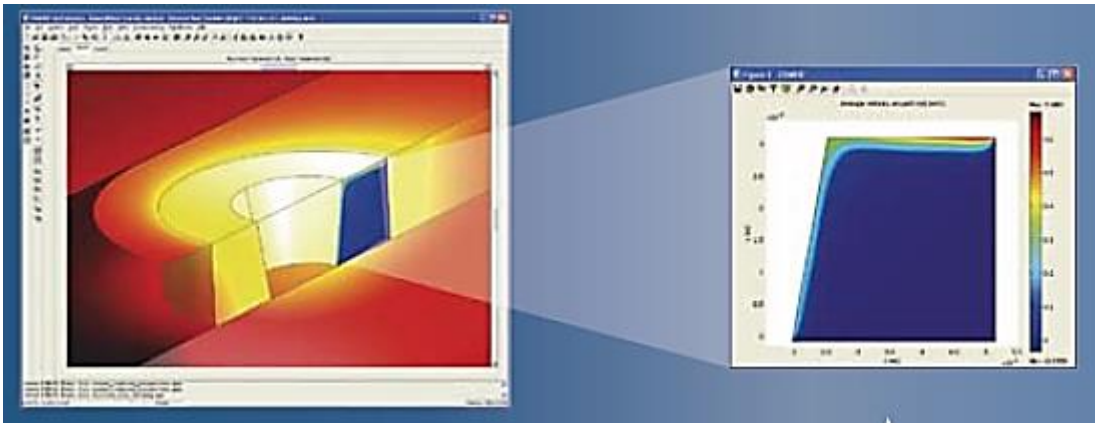


Figure 2.3: COMSOL Multiphysics model depicting the 3-D model coupled with the 2-D model

  - A follow on project is being funded to refine the model in terms of thermal and microstructural analysis
- Smith and Bendzsak [12]

- Developed thermo-mechanical flow model (STIR-3D) as depicted in Figure 2.4 [11]
    - Fluid mechanics applied in model for flow patterns [12]
    - Assumes viscous heat dissipation (opposed to frictional heating)
    - Inputs into model [12];
        - Tool geometry
        - Material properties
        - Operational conditions
    - Outputs for analysis and design [12];
        - Material flow profile
        - Shear and stress maps
        - Force distributions on all tool surfaces and tool forces and torques
        - Thermal profiles which are the temperature and heat generation fields
    - Assumptions made for the model [12]
        - Variations of the thermal profiles around the tool and within the weld of the nugget are assumed to only have secondary effects on the flow dynamics
    - Three distinct flow regimes are formed below tool shoulder and the following conclusions are made [12]
        - Region of rotation immediately below shoulder – flow occurred in direction of tool rotation
        - Region where material extruded past rotating tool- this occurred towards base of pin
        - Region of transition in between first two points – Flow had chaotic behaviour

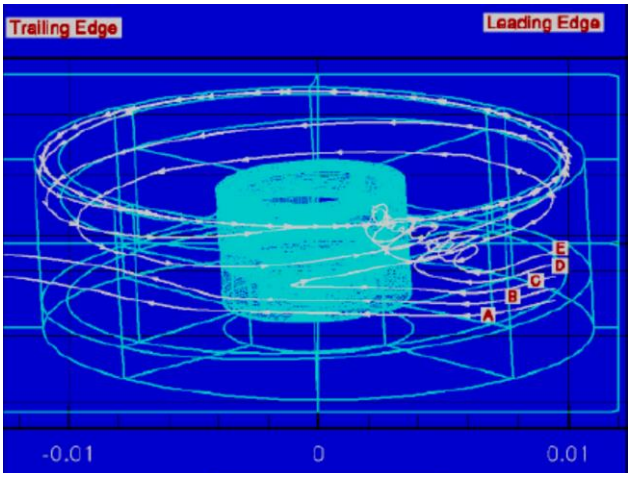


Figure 2.4: Depiction of STIR 3D model described as "3D particle dynamics at the tool leading edge"

- Askari, *et al* (CTH code) [10]
  - 3-D code- able to solve time dependent equations of continuum mechanics and thermodynamics
  - Predicts
    - Strain
    - Strain rate
    - Temperature distribution
  - Validity of model verified by marker insert technique
- Goetz and Jata [10]
  - 2-D FEM code – DEFORM
  - Simulated material flow in FSW of 1100Al and Ti-6Al-4V alloys
  - Non-isothermal simulation – depicted highly localised metal flow likely to occur
  - Simulation predicts strain rates of 2-12s^{-1} and strains of 2-5 in localised flow zone
- Stewart *et al* [10]
  - Mixed zone model
    - Assumes metal in plastic zone flows in a vortex system at an angular velocity of the tool
    - Metal interface and angular velocity drops to zero at edge of plastic zone
  - Single slip surface model
    - Principal rotational slip takes place at contracted slip surface outside tool (work-piece interface)
    - Using limited region of slip, thermal field, force and weld region corresponded well to experimental measurements
- Song and Kovecevic [13]
  - Model using a moving co-ordinate system
    - A non-uniform mesh is generated in order to solve the model
    - Includes tool pin in the model
    - Divided into three stages
      - Penetration
      - Weld period
      - Tool pulling out
    - Assumptions for model
      - Heat generated at interface is frictional heat
      - Thread of pin is neglected
      - No heat flows into the work-piece if the material melting temperature is reached via the local temperature

    - Model results and conclusions
        - Detailed information can be provided by model results which is sometimes difficult to see experimentally
        - Difficulty in depicting the temperature distribution has been reduced
        - No moving heat source needs to be modelled
- Arbegast [10]
    - Resultant microstructure and metal flow features of FSW resemble hot worked microstructure of typical Aluminium extrusion and forging – FSW modelled as a metal working process
    - Models the equivalent stage of the extrusion zone
        - Uses mass balance considerations and reveals;
        - Relationship between;
            - Tool geometry
            - Operating parameters
            - Flow stress of material being joined
    - Indicated that calculated temperature, width of extrusion zone, strain rate and extrusion pressure – consistent with experimental observations

From the above models, the following points need to be noted when modelling the FSW process.

- Many factors influence material flow during FSW
    - Tool geometry
        - Pin and shoulder design
        - Relative dimensions of pin and shoulder
    - Welding parameters
        - Tool rotation rate
        - Tool direction (Clock wise/Counter clock wise)
        - Traverse speed
        - Plunge depth
        - Spindle angle
    - Material type
    - Work piece temperature
- Likely material flow within nugget consists of several independent deformation processes

The models described above are brief explanations of what has been done, to follow, is a more concise account of various types of models and what each has to offer. However, based on the above information, the following is concluded as to what the above models can offer.

- The slip condition of the model is mentioned more than once and this is important regarding the tool geometry being used but the tool geometry has an effect on the heat generated, so the slip contact condition is important for the current study as well.
- Many of the papers described above concentrate on the material flow describing at times full detail as to what occurs at the pin which has been included in their model. Also mentioned is the deformation that occurs from this material flow. This is not seen as an important matter for the current study, but what is important to consider is that one should expect a heat distribution almost depicting material flow and the heat although is distributed outwards, one can also expect one side to have a higher temperature than on the other.
- Phases of the FSW process has been included with welding parameters mentioned according to what being tested.
- Thermal models had many various assumptions made. The ones mentioned are those that are to be considered for the current model.
    - One assumes a viscous heat dissipation as opposed to another that assumes frictional heat generates the heat at the interface of the two surfaces.
    - Physicality of the tool is modelled differently, some include the pin and other ignore it.

Based on the above findings, more is to be found in order to gain valuable information regards to parameters which should be included in the model and what these important parameters are. There are a lot of various ways in analysing a situation, so each will be divided into the relevant sections as outlined below.

The development of various depiction categories for the FSW can be summarised in each of the following sections;

- Analytical model- uses a mathematical approach, whereby it describes relationships between variables that might or are inter-dependent on one another using mathematical concepts. Also described as a “closed form” solution [10]
- Numerical models- Determining the state of the model by using incremental time steps with different input conditions for each time step procedure [10]

Based on the above definitions, the following models are categorised into the two different sections, also only the important information relating to any temperature information given in their models is looked at and discussed.

2.3.1 Numerical models

The following numerical models relate to thermal and thermal mechanical models that have been developed. The first part discusses the models and their assumptions made were the second part discusses their results obtained. These models are an important part in discovering what has been achieved and where discrepancies lie. As the models are discussed, mentions as to which properties are important and why will be revealed as well as in the results what lastly issues might arrive and where the current study can improve.

2.3.1.1 Model properties for papers discussed

Due to the vast amount of literature available on the thermal and thermal mechanical models, certain attributes of the models will be discussed and more detail can be found in in Appendix 1. Each of the papers discussed will be categorised according to software where various considerations have been considered.

ANSYS software

The following papers utilise the ANSYS software in order to develop their FSW process model.

Kural *et al* [15]

A thermal model is developed with the following model characteristics

- A moving heat source is used to simulate the heat distribution from the friction between the tool and work piece surface
- 3D models are developed using the ANSYS APDL to develop the moving heat source and HyperXtrude
- The pin is considered in the model
- Material properties changing with temperature are used
    - Thermal conductivity
    - Heat capacity
- Convection coefficients are applied to top and bottom surface of the work piece as shown in Figure 2.5 [15]
- Heat flux is applied at the surfaces between the tool shoulder and pin on the work piece as shown in Figure 2.5 [15]

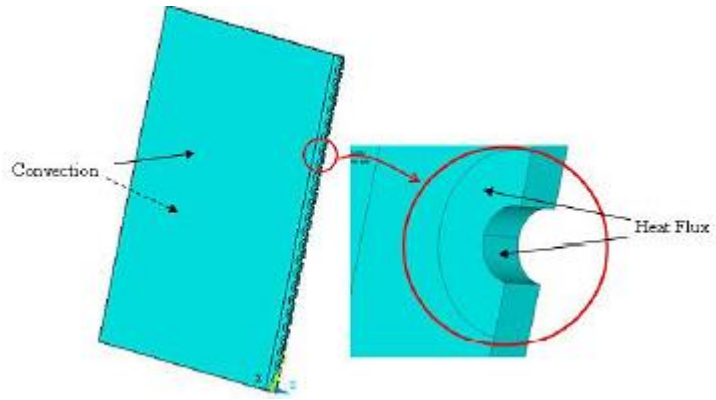


Figure 2.5: Boundary condition set for model

Stamenkovic [16]

A thermo mechanical model is developed with the following characteristics

- A moving heat source is used
- Assumptions for the thermal model
    - Displacement of the work pieces during the weld does not affect the thermal distribution
    - All material properties are defined until the liquid phase of the material is reached
    - Convection and radiation are considered
    - Element birth and death technique is employed
- SOLID 70 was used for the thermal analysis and SOLID45 was used for the structural analysis
- Material properties changing with temperature are given below in Table 2.2 [16]

Table 2.2: Material properties changing with temperature ASTM 36 steel

Temperature (°C)	Specific heat (J/kg°C)	Conductivity (W/m°C)	Density (kgm-3)	Yield stress (MPa)	Thermal expansion coefficient (10-5/°C)	Young´s modulus (GPa)	Poisson´s ratio
0	480	60	7880	380	1.15	210	0.3
100	500	50	7880	340	1.2	200	0.3
200	520	45	7800	315	1.3	200	0.3
400	650	38	7760	230	1.42	170	0.3
600	750	30	7600	110	1.45	80	0.3
800	1000	25	7520	30	1.45	35	0.3
1000	1200	26	7390	25	1.45	20	0.3
1200	1400	28	7300	20	1.45	15	0.3
1400	1600	37	7250	18	1.45	10	0.3
1550	1700	37	7180	15	1.45	10	0.3

Muhsin *et al* [17]

Thermal model is developed using the APDL of ANSYS with the following characteristics

- Element SOLID70 is used
- Following assumption are made
    - The work piece material is considered to be isotropic and homogenous
    - Density, specific heat and thermal conductivity change with temperature
    - During the process of the FSW, no melting occurs
    - Thermal boundary conditions are symmetrical over the weld line
        - This is not a good assumption, since it is known that the retreating side and advance side do depict variation in temperature and there cannot be considered symmetrical over the weld line.
    - Between the clamp and work piece, heat transfer is negligible
- Convection coefficient and heat flux is used for the boundary conditions and can be seen in Figure 2.6 [17]

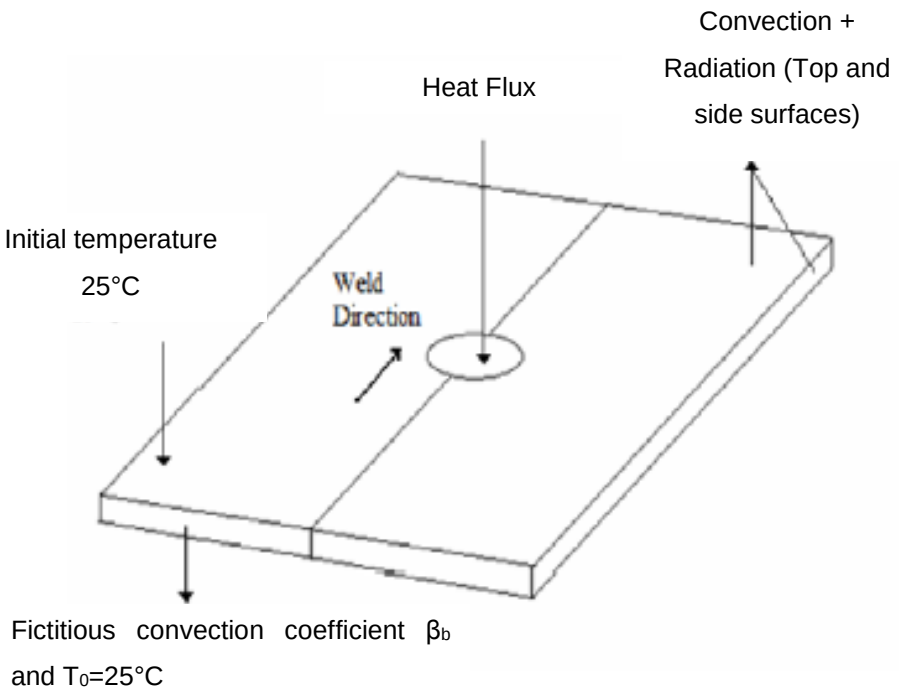


Figure 2.6: Boundary conditions set for FEA model

Chen *et al* [18]

A 3D model to study the thermal history and thermo-mechanical process in butt welds is developed.

- A thermal model is set up and then a mechanical model which are then coupled after the thermal temperature data is used to evaluate those mechanical properties with thermal parameters
- Only half of the model is considered due to symmetry
    - This is again, not a valid assumption due to the retreating and advancing sides differing in temperature as mentioned before

Malde [19]

A thermo mechanical model is replicated using ANSYS based on a model developed by Zhu and Chao [20].

- A non-linear transient 3D heat transfer model is developed which is then coupled to a 3D non-linear transient structural model
- The same assumptions as used in Muhsin [17] are applied
- SOLID70 is used for the thermal model and SOLID185 is used for the structural model
- Boundary conditions are as described in Muhsin [17]
- Yield stress, Youngs modulus and thermal expansion are changing with temperature
- Assumptions for the structural model
    - Deformation occurs symmetrically and only one half of the work piece is considered
        - This is not a valid assumption based on the knowledge that each side depending on retreating and advance side does depict variations in properties
    - Work piece material is homogenous
- Command ETCHG is used to switch between the elements
- Simulation was performed over two stages
    - First the transient thermal model was solved

- Non-linear structural model was solved after the previous point
    - Since each model is solved separately but the second is coupled, and that only half the model is considered, this allows for processing time to be reduced. This is based on the assumptions given, as one will realise at the end of the current study, is that the processing time points toward an imperative role for the model to process results accordingly. And if a full model is developed and is used this time is considerably extensive to those performed above.

ABAQUS/EXPLICIT software

Awang *et al* [21]

Finite Element modelling for friction stir spot welding is developed. A 3D coupled thermal-stress model is analysed

- Adaptive mesh scheme is used when elements are highly distorted and the mesh is regenerated
- Assumptions
    - Only the work piece is able to deform
    - Pin tool and backing anvil are considered to be rigid
    - Elastic-plastic behaviour of the work piece is assumed
    - Friction coefficient is dependent on temperature and is described by Coulombs law. This coefficient is zero at melting point of the work piece. Other temperature dependent properties are found in Table 2.3 [21]

Table 2.3: Temperature dependent properties for aluminium alloy 6061-T6

Temperature	^{0}C	37.8	93.3	148.9	204.4	260	315.6	371.1	426.7
Thermal Cond.	W/m^{0}C	0.0162	0.0177	0.0184	0.0192	0.0201	0.0207	0.0217	0.0223
Heat Capacity	J/Kg^{0}C	945	978	1004	1028	1052	1078	1104	1133
Density	Kg/m^3	2685	2685	2667	2657	2657	2630	2630	2602
Young's Modulus	GPa	68.54	66.19	63.09	59.16	53.99	47.48	40.34	31.72
Yield Strength	MPa	274.4	264.6	248.2	218.6	159.7	66.2	34.5	17.9
Thermal Exp.	μ/^{0}C	23.45	24.61	25.67	26.60	27.56	28.53	29.57	30.71

Temperature (^{0}C)	22.0	34.7	93.3	147.5	210.6	260.0	315.6	371.1	426.7	582.0*
Friction Coefficient, μ	0.610	0.545	0.259	0.115	0.064	0.047	0.035	0.020	0.007	0

- Boundary conditions
    - Edges of the work piece do not transfer any heat
    - Convection coefficient is applied to top and bottom surface and assumed to be the same value. A full depiction of the boundary conditions is seen below in Figure 2.7 [21]

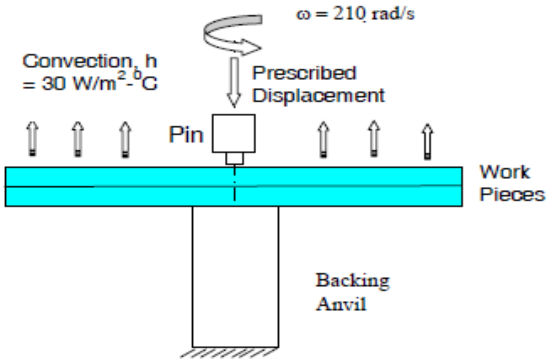


Figure 5 Boundary conditions

Figure 2.7: Full depiction of boundary conditions set

Grujicic *et al* [22] fully coupled thermo-mechanical finite element analysis of material evolution during friction stir welding of AA6063 model

- Nodal degrees of freedom include nodal velocity and nodal temperature
- Arbitrary Langrangian-Eulerian formulation is used, where adaptive re-meshing is performed

Chao *et al* [23]

A thermal model is developed to determine heat flux based on the temperature fields obtained by measurement.

- Thermal boundary conditions are described extensively for each surface of the work piece and tool
- Element type DCAX4 is used
- Material properties affected by temperature are considered and a relationship for specific heat and thermal conductivity changing with temperature is given below in Figure 2.8 [23].

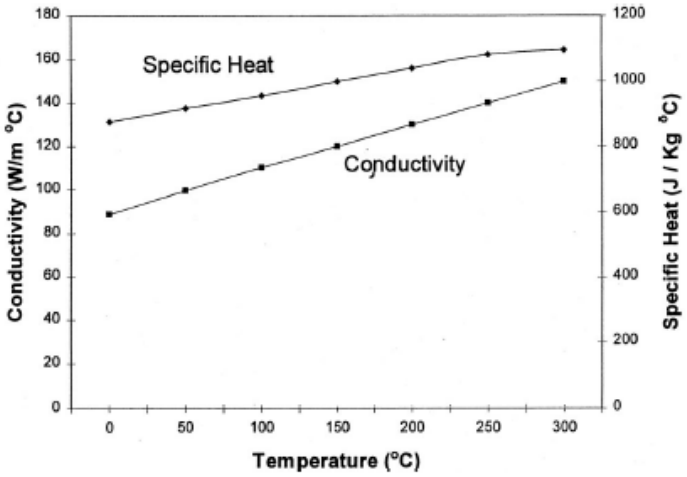


Figure 2.8: Material properties changing with temperature AA2195

- The work piece was modelled using WELDSIM
    - 3D transient non-linear finite element code for heat transfer and solid mechanical analysis
    - Half of the work piece is modelled due to symmetry
    - A larger heat conduction coefficient is applied to the surface area where tool shoulder is located

Grujicic *et al* [24] Modelling of AA5083 material-microstructure evolution during butt friction stir welding

Fully coupled thermo-mechanical model is employed;

- It uses first-order, 8 node reduced integration hexahedral thermo-mechanically coupled solid elements
- Interactions between surfaces are given specific algorithms applicable to contact pressure and shear stresses developed between tool and work piece surface
- Tool is modelled as a rigid material and the work piece material is isotropic and linear-elastic

Li *et al* [25]

Fully coupled thermo-mechanical model is created;

- Temperature displacement coupled element C3D8RT is used

- Convection coefficients are applied to all surfaces of the work piece, where the bottom surface has a higher convection to the rest of the surfaces
- Constant friction coefficient is used
- Contact conditions were simulated using a contact pair algorithm
- Tool pin is considered in the model

DEFORM 3D software

Kheireddine *et al* [26]

Thermo-mechanical model is developed using the DEFORM 3D software. The model is shown in Figure 2.9 [26]

- Tool and backing plate of the work piece are modelled as rigid undeformable bodies and only heat transfer is accounted for
- Two work pieces are modelled as one block and as a plastic body which is able to deform and has the effect of heat in it

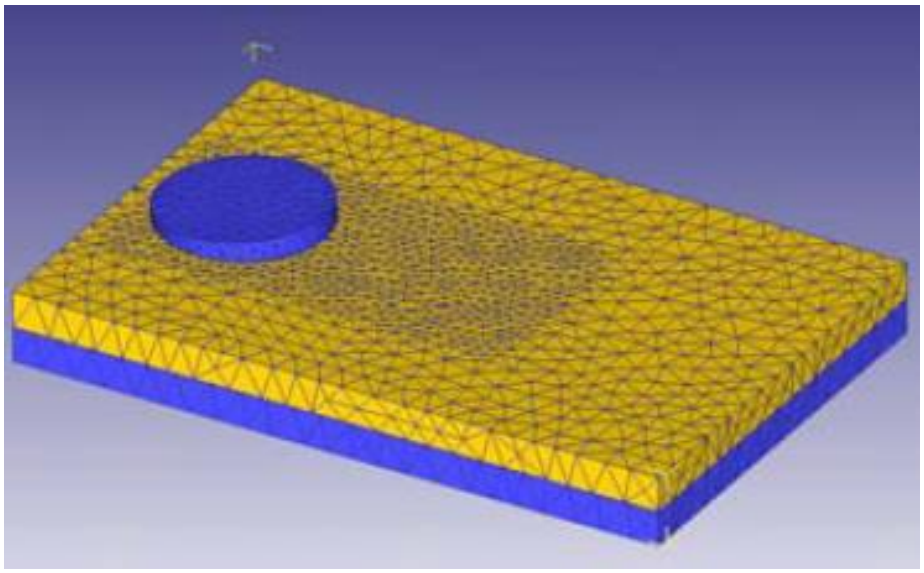


Figure 2.9: Mesh of model developed by Keiereddine

- Tetrahedral elements were used for the thermal analysis
- At the tool and work piece surface interaction rectangular mesh control was used for finer mesh elements

- Constant mechanical material properties were employed
- A thermo-visco-plastic formula was used to describe the stress of the material
- Friction coefficient was calculated based on the percentage of sticking
- Local remeshing was incorporated to allow for the deformation effects occurring on the work piece

STIR3D software

Bendzak *et a*l [27]

3D heat and material flow simulation using the STIR3D software

- Each sub-divided region is further divided into a set of non-orthogonal control volumes
- Meshes in each region have varied densities allowing for a finer structure for the flow near the tool to be shown
- Meshing does not require matching between each of the regions interfaces
- Assumptions
    - Viscosity is assumed constant and temperature conditions in each region are constant

FLUENT software

Colegrove *et al* [28]

Model involves a 2D axisymmetric flow model for calculating heat generation, coupled with a 3D thermal model to calculate the heat flow to be input into the 2D model.

- The 3D thermal model was modelled using the FLUENT software and calculates the heat flow
    - Four pathways for the heat transfer are described in Figure 2.10 [28] and constant thermal conductivity is applied to the model
    - Values for h_b and h_v are 1000 W/m^{2}K and 10 W/m^{2}K respectively

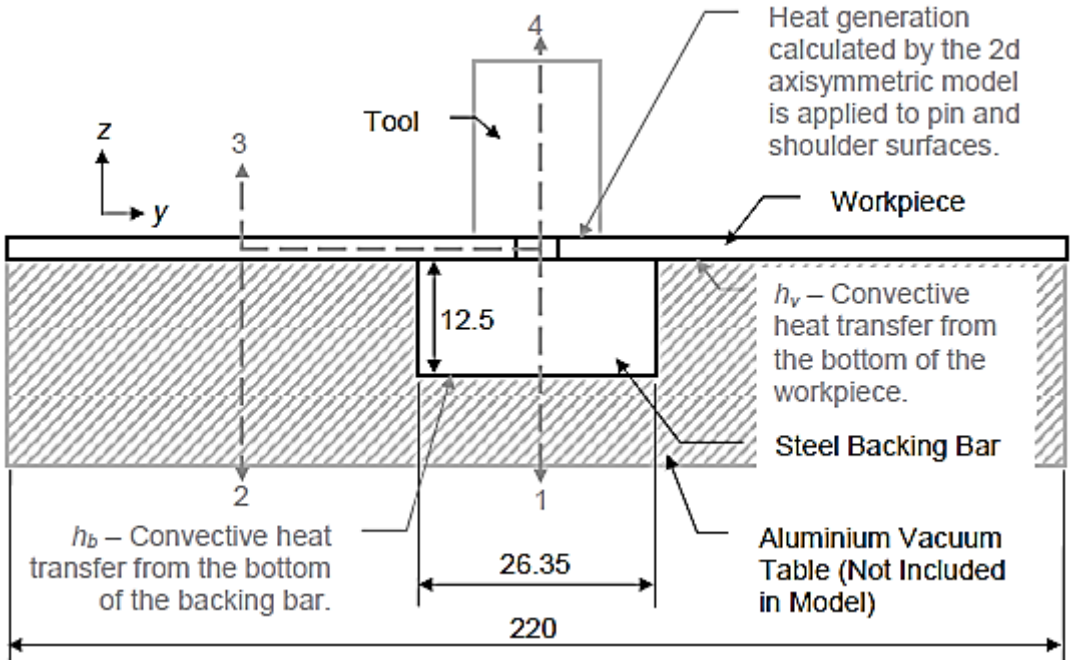


Figure 2.10: Pathways for the heat (thermal boundary conditions) described by Colgrove

- 2D axisymmetric flow model predicts the rotational flow around the tool

Colegrove [29]

A thermal model was developed with flow characterisation of the FSW process

- A coupled thermal and flow analysis was performed
    - Thermal model was considered as well as an isothermal model
- Viscous dissipation was used to describe the heat generation
- Material softening (to assimilate the effect of the material heating) could not be fully defines with the FLUENT software as it caused unstable solutions
- Specific heat and thermal conductivity is changing with temperature

WELDSIM code

Zhu *et al* [20]

3D thermal and thermo-mechanical model was carried out using WELDSIM code

- Material properties changing with temperature as can be seen in Figure 2.11 [20] for various material properties

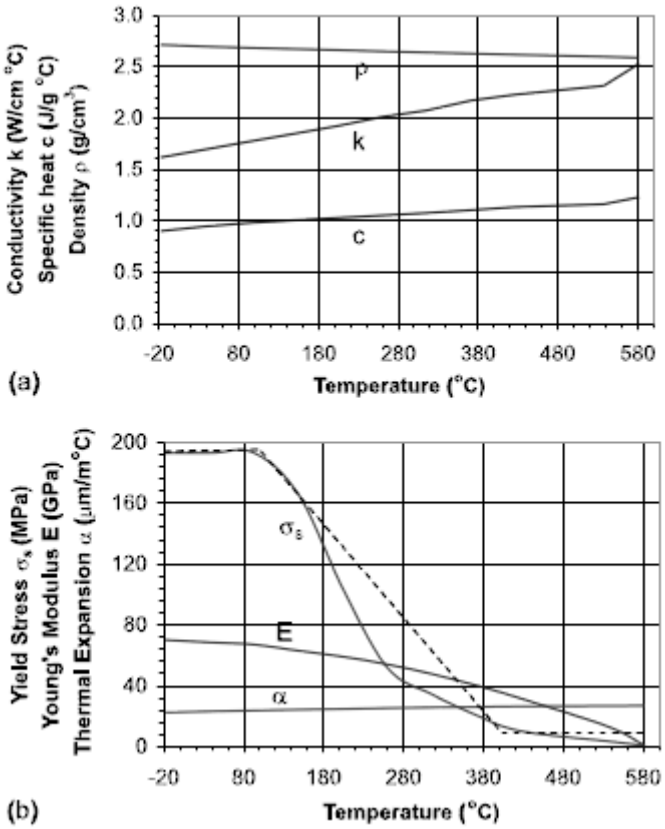


Figure 2.11: Material properties changing with temperature for aluminium alloy 5000 series

- Due to symmetry only half the model is used for analysis
    - As previously mentioned, this assumption does not account for the retreating and advance side of the weld that is present and the effects thereof
- A thermal analysis was performed first whereby the temperature output was used for the thermo-mechanical model
- Heat flux is modelled as a moving source on the boundary

Other numerical models are discussed, where the software being utilised is not at times fully explained but other times is a discussion of the various software packages available.

Tasic *et al* [30]

FEM simulation possibilities regarding the heat transfer are proposed

- Two different descriptions for heat generation are given:

    - Direct way, explicit expressions describe the amount of heat generated by the physical parameters of the FSW process and material properties
    - Temperatures are measured and a relationship between heat generation, friction coefficient , rotational speed etc. are found and reached temperatures are calculated
- Boundary conditions are important parameters to be considered and need to be described fully

Nandan *et al* [31]

3D visco-plastic and temperature field was mathematically modelled

- Heat is generated at a constant rate
- Mass flow is treated as a Non-Newtonian, incompressible visco-plastic material
- Assumes constant material properties such as friction coefficient
- Assumes a contact condition where percentage of sticking is given at 0.7

Song *et al* [13]

3D heat transfer model is developed

- A moving co-ordinate is used to represent the movement of the tool
- Only one plate is modelled

Sharma *et al* [32]

Discusses various FEA models and the various software available to model the FSW process.

Vilaca *et al* [33]

- Experiments of the FSW welding process are presented with results
- Difficulty in computational modelling is discussed
- Analytical modelling is discussed with special reference to iSTIR code
- Numerical modelling approach is also discussed

The last few papers discussing various attributes of the FSW and the modelling considerations are probably one of the most important to consider when beginning to understand the work involved in modelling the FSW process. It offers valid input into what has been developed and what various inputs and conditions have been used as well as where some of the heat generated properties are coming from and how it is developed in the numerical models.

The numerical models use various software packages available and consider many different objectives. The various considerations for these models are:

- Moving heat source or moving co-ordinate system is created and this simulates the heat generation
    - Current model will use a frictional contact that generates heat. This is more realistic than previous studies as it is known that it is this friction between surfaces that generates the heat.
- Various elements are used that are able to describe various degrees of freedom i.e. thermal, structural or certain nodal qualities are present such as velocity
    - The current model will use an element type that is able to describe both structural and thermal degrees of freedom
- Some models only use half the geometry since they consider symmetry, but for heat generation this is not the case since the advance side and retreat side do have a different heat profile that needs to be considered.

Assumptions made for the various models are mentioned below, where these assumptions are to be considered especially for the input of particular parameters that affect the heat generated

- Certain material properties are affected by temperature. Some models do not consider this but since a true reflection of the heat generated is required, it is imperative to consider these properties
    - Thermal conductivity
    - Specific heat
    - Density
    - Heat transfer coefficient
- Convection coefficients are mentioned for various surfaces and these values range for the top plate and backing plate respectively as follows:
    - 10 $W/m^2.K$-30 $W/m^2.K$
    - 300 $W/m^2.K$ -1000 $W/m^2.K$
    - It has also been mentioned with reference to a specific paper [23] that the heat transfer from the tool to the work piece is 11kW/ $m^2.K$. This value is very higher, but will be kept into consideration when analysing the comparison of experimental and FEA models performed in the current study
- Friction coefficient
    - This is at times considered changing with temperature and at others a constant value. The current study will consider a friction coefficient changing with

temperature and more data will be researched on this and of which is also recorded in the numerical and experimental sections that follow this.

The points mentioned above retrieve that information which is most important and deemed viable considerations for the current study. However, the more information that is known, the better assumptions that can be made when developing the model.

2.3.1.2 Results for numerical models

A general observation of results are discovered, where more detail for each specific model can be found in Appendix 1. These common similarities include:

- Temperatures on advance side are higher than on the retreating side of the weld. This is useful when comparing and relating models and ensuring it is according to literature.
    - Temperature profiles across the weld for Awang *et al* [21] depict that from the centre of the tool to the outer radial distance, the temperature is within a fairly close region. However, the stress increases further from the centre of the tool. Other temperature profiles across the weld depict a bell shape curve for the temperature across the weld as can be seen in results for Chen *et al* [18] and Malde [19].
    - Temperature profiles across the weld over time can be seen in Kheireddine *et al* [23] and Muhsin *et al* [17] temperature results. It also indicates in Muhsin *et al* [17] that the advance side has a slightly higher temperature than on the retreating side. This result profile is shown in Figure 2.12 [17]

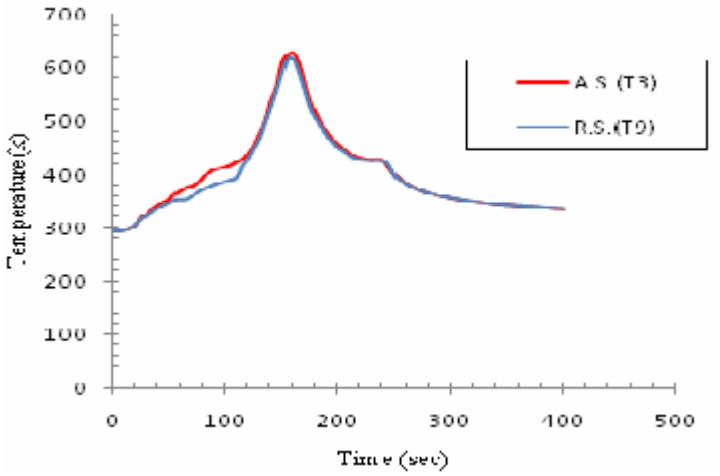


Figure 2.12: Temperature profile over weld for advance and retreating

- Higher rotational speeds increase the heat generated and hence temperature. The following Table 2.4 [31] from Nandan *et al* [31] depicts the heat input from various aspects of the tool together with the maximum temperatures. This result shows an

increase of heat generated by the shoulder and tool as the weld speed increases and these values further increase with increase in rotation speed. However, the maximum temperatures recorded drop with these increasing weld parameters.

Table 2.4: Weld parameters and heat generated from the tool

Weld speed, mm s^{-1}	Rotational speed, rev min^{-1}	Heat input from shoulder, W	Heat input from tool pin, W	Maximum temperature, K
0·85	300	496	63	1316
1·70	300	602	91	1241
2·55	300	705	113	1200
0·85	400	558	54	1412
1·70	400	668	88	1313
2·55	400	771	117	1256
0·85	500	617	42	1518
1·70	500	729	80	1385
2·55	500	835	114	1314

- Yield stress changing with temperature needs to be considered as it is a function of temperature. This must be considered when entering material properties into the FEA model under consideration for this study.
- Slip condition for a smaller contact radius can assume a pure sticking condition which is used to predict heat generation. This contact condition although won't be physically modelled, but will appear in the distortion of the model, when analysing this will help to determine the condition based on the experimental results and conclusions drawn.

2.3.1.3 Contributions from numerical findings to be considered

A list of the following factors are derived from those discussed for the numerical models:

- Material properties changing with temperature
  - Density
  - Specific heat
  - Thermal conductivity
  - Yield strength
  - Friction coefficient
- Convection coefficients are given in Table 2.5 and are along the assumptions that the backing plate has a higher value than that of the top surface of the plate. This assumption, as the values depict is an unknown value since this is a simplification factor of the model since this surface is not under convection exactly since the bottom surface is in contact with a backing plate and not air.

Table 2.5: Convection coefficients for the work piece surface

	Convection coefficient for top of work piece ($W/m^2.K$)	Convection coefficient for bottom of work piece ($W/m^2.K$)
Kural *et al* [15]	30	300
Chao *et al* [20]	30	Is dependent on the measured temperature
Kheireddine *et al* [26]	20	11000
Li *et al* [25]	10	1000
Colegrove [29]	10	1000

- Temperature profiles across the weld need to conform to a bell shape curve and the advance side should have a higher temperature than that found on the retreating side.
- Weld parameters have an effect on the temperature results

Some issues raised with various models mentioned and where the current study will improve.

- Some are only pure thermal models which is not a true reflection of the FSW process since the thermal and structural effects of the process are interlinked together. This is where the current model will improve as it is a structural-thermal model
- Some variables which should be changing with temperature are considered constant, although mentioned previously this is another improvement set out for the current study as this will consider these properties changing with temperature.

2.3.2 Analytical models

The analytical models described below are important when understanding the effects of process parameters on the heat generation for a particular material. Parameters and assumptions made for each model will be useful when deducing which will be important considerations based on what is required to be investigated and what the goals for the final study consist of. These models will give a brief explanation into understanding these decisions.

2.3.2.1 Model properties for papers discussed

Each model will be discussed, outlining certain properties that are considered important to the current study at hand.

Schmidt *et al* [34]

- Mentioned in the introduction according to other models the following is said;
    - The analytical has a certain flexibility with respect to the contact condition and tool design
    - With comparison to experimental results the contact condition will be present at the interface of the tool/matrix
- The contact condition is affected by the friction coefficient value as well as the tool geometry
- A ratio for the each of the tools contribution to heat is also concluded based on the equations allocated for slipping, sticking and combination contact conditions.

Nandan *et al* [35]

- Friction and slip between the surfaces as well as heat transfer was investigated for effects on model reliability
    - Its mathematical model created and relationships determined for the following parameters;
        - Friction coefficient
        - Extent of sticking
        - Heat transfer coefficient for the bottom surface of the work piece
        - Extent of viscous dissipation converted to heat
    - Bottom surface heat transfer is obtained by optimisation and given by the following equation [35]

$$k\left.\frac{\partial T}{\partial z}\right|_{bottom} = h_b\left(T-T_a\right) \tag{2.1}$$

- The top surface has both radiation and convection and is expressed in the following equation [35]

$$k\left.\frac{\partial T}{\partial z}\right|_{top} = h_b\left(T - T_a\right) + \sigma\left(T^4 - T_a^4\right) \quad (2.2)$$

These equations will be important when considering one's own model for the surface conditions and the values obtained for comparison.

- Understanding more of the parameters and the influences that affect them is very useful when considering what needs to be incorporated and what should be considered as an important input. This mathematical model presented with equations is therefore a useful tool to use.

Hamilton *et al* [36]

- Empirical relationship is derived amongst the temperature and weld energy
  - Relationship obtained could be valid based on the results obtained to compare with current study parameters and temperatures obtained.
  - Tool rotation, weld velocity and applied force contribute to the energy imparted to the work piece.
    - These process parameters can relate to each phase of the FSW process and will be considered when developing current model.
  - Friction coefficient is set at different values for various contact conditions for aluminium alloy and mild steel material;
    - Sticking-0.5
    - Sliding-0.25
  - Increasing solidus temperature will increase the maximum temperature for a given energy level.

Emam *et al* [37]

- Energy based thermal model is used and investigates the heat generated due to plastic deformation and the friction between the surfaces of the tool and work piece
  - Various material properties are given for the materials under scrutiny and these values for each property are given in Table 2.6 [37]

Table 2.6 Table for material properties under consideration for the energy model

Aluminum Alloy	6061-T6	6061-T651	6082-T6	7050-T7451	7050-T7451
t(mm)	6.4	8.13	6.0	6.4	19.1
$\rho(\mathrm{kg/m^3})$	2700	2700	2700	2830	2830
$c_p(\mathrm{J/kg\,K})$	896	896	889	860	860
k(W/m K)	167	167	170	157	157
α $(\times 10^{-5}\mathrm{m^2/s})$	6.9	6.9	7.1	6.5	6.5
$T_s(\mathrm{K})$	855	855	879	761	761

- Energy per mm were found similar to those outlined in Hamilton [34]

Song *et al* [13]

- Uses a moving coordinate system to model the moving tool
  - Mathematical model is created whereby heat generation from the tool shoulder and pin is included
  - Friction coefficient is known to vary and therefore an effective coefficient is assumed and 0.4 is used
  - Yield stress changes with temperature
  - Heat conductivity is set to 167 W/mK
- The above parameters are important and it should be noted that these parameters are for the material of the 6000 series of Aluminium alloy

Durdanovic *et al* [38]

- Mathematical which describes the stages of the FSW process for heat generation of the model
  - Considers 5 phases for the FSW process
    - Plunging
    - Dwelling
    - Welding
    - Final dwell time
    - Extraction of the tool from the work piece
  - Heat treatment of the weld is described in 4 phases

        - Dwell, the rotating tool achieves an acceptable temperature ahead of the tool that will allow for ease of forward motion
        - Transient heating, this occurs when the tool is moving along the weld line
        - Pseudo steady-state, thermal field around the tool that remains fairly constant
        - Post steady-state, additional heating around the tool occurs at the end of the weld due to the backing plate and end of weld pieces
    - Heat is generated during two tribological processes
        - Pure sliding or pure sticking
        - Contact interface is described as a Coulomb friction condition
    - Uncertainties
        - Some parameters involved in the mathematical model lead to uncertain results as the model has mainly geometrical inputs. If these are excluded together with the welding conditions, the main influences then include:
            - Contact state variable
            - Friction coefficient between surfaces
            - Contact pressure
            - Shear stress of the weld

Lakshminarayanan *et al* [39]

- Using a Taguchi parametric design approach, properties of the FSW process are optimised to improve tensile strength in weld joints
    - Process parameters are chosen and an orthogonal array is selected
    - Optimised parameters contribute to the understanding of the effects it has on the weld and one can also make conclusions based on heat generation for the parameters that have the most influence
- Process parameters are given and the range for axial force is shown in Table 2.7 [39]

Table 2.7: Axial force with varying process parameters

Rotational speed, R/(r·min^{-1})	Traverse speed, T/(mm·min^{-1})	Axial force, F/kN
1 200−1 600	22−75	4−8
1 200	22	4
1 400	45	6
1 600	75	8

Khairuddin *et al* [40]

- Various cases are considered for predicting transient temperature profiles
    - Full sliding contact condition where the theoretical plunge force is based on temperature dependent tensile strength
    - Full sliding contact condition where the theoretical plunge force is based on temperature dependent yield strength
    - Sticking contact condition where the theoretical plunge force is based on temperature dependent shear strength
    - Experimental plunge force and plunge depth control
- Some material temperature dependent properties are shown below in Figure 2.13 [40]

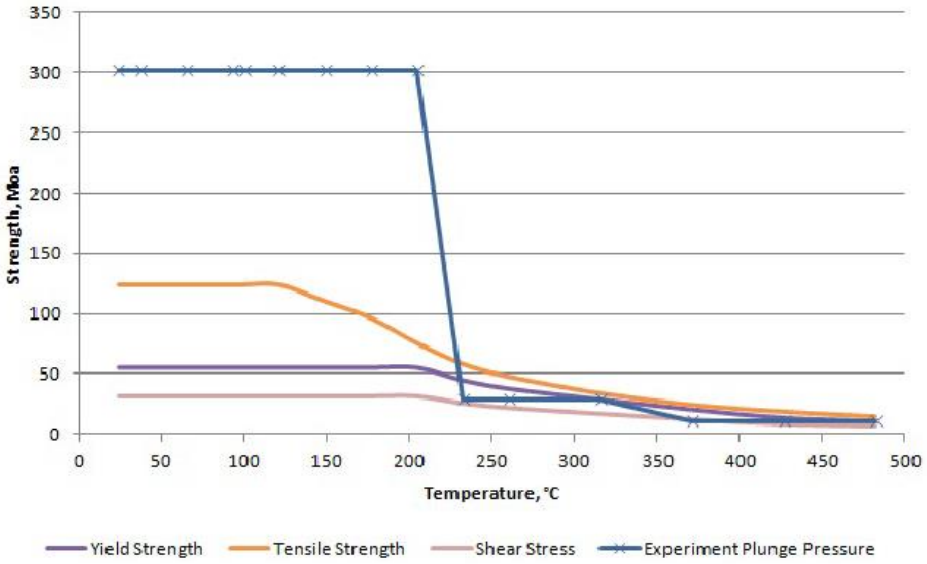


Figure 2.13: Temperature dependent properties

- Friction coefficient changing with temperature is considered, this is for the kinetic friction taken into account. This is shown below in Figure 2.14 [40]

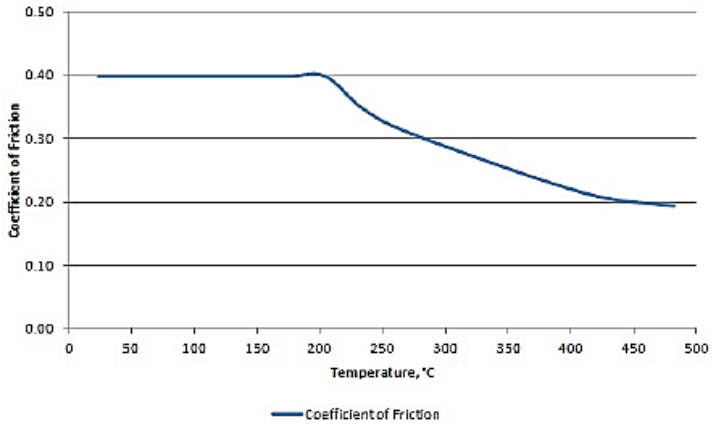


Figure 2.14: Coefficient of friction versus temperature

2.3.2.2 Results for analytical models discussed

Results for the analytical models are outlined below

Schmidt *et al* [34]

- Heat generation is shown in Figure 2.15 [34] , where a constant sticking condition is deduced

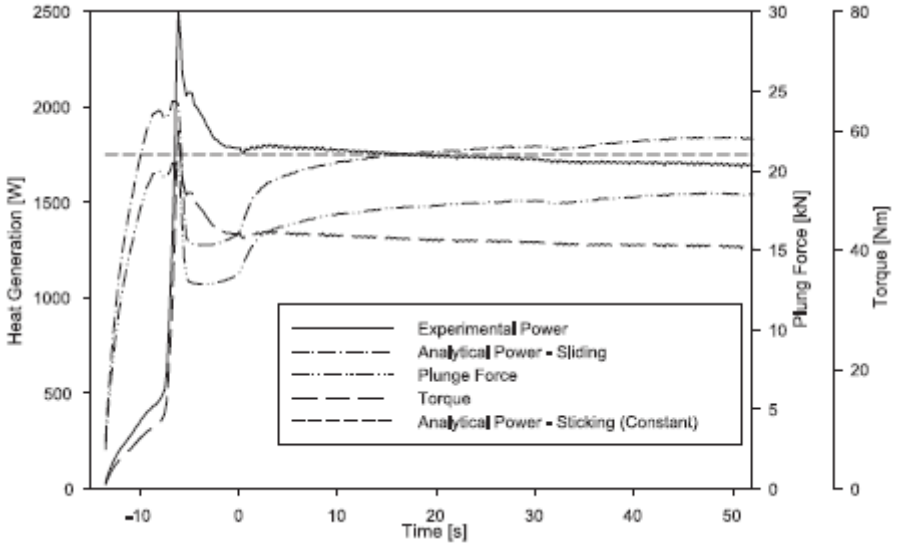


Figure 2.15: Heat generation for various conditions

- Torque does not change indicates a steady state welding condition
- Contact state variable is defined and each contact condition is related to a specific variable range for this state variable
- Sliding conditions give a fairly known range of friction coefficient for material surfaces interacting
- For the sticking condition, yield shear stress at elevated temperatures is used to obtain these frictional coefficients

Nandan *et al* [33]

- Conclusions were drawn that the parameters observed and investigated affected the temperature fields
- Optimised values of three of the important parameters are shown in Table 2.8 [35], where it can be observed for the chosen material the parameters fall in the following ranges;
    - Friction coefficient 0.488-0.499
    - Frictional slip 0.01-0.022
    - Heat transfer coefficient (cal/cm^2.s) 0.01-0.012

Table 2.8: Optimised values for parameters affecting heat generation

Friction Coefficient μ_0	Fractional Slip δ_0	Heat Transfer Coefficient h (cal/cm^2-s)
0.488	0.022	0.010
0.487	0.014	0.010
0.484	0.014	0.010
0.482	0.017	0.011
0.479	0.016	0.011
0.489	0.012	0.010
0.49	0.015	0.010
0.492	0.012	0.012
0.499	0.010	0.012
0.499	0.017	0.010

Hamilton *et al* [36]

- Resulting temperatures for different materials, welding parameters and tool geometry are outlined in the Table 2.9 [36] below.

Table 2.9: Temperatures for various parameters and materials

Alloy	Tool Geometry r_o (mm)	r_i (mm)	h (mm)	Rev/Min	Welding Parameters v_w (mm/s)	F (kN)	E (J/mm)	Measured Max. T (K)
AA7108-T79	7.5	2.5	6.0	1500	5.0	7	696	648
				1500	8.0	7	435	563
				1500	12.0	7	290	523
AA6061-T6	12.0	9.5	6.0	344	2.2	13	1639	698
AA6061-T651	12.7	5.0	8.0	390	2.4	22	1896	739
AA6082-T6	7.5	2.5	6.0	1500	5.0	7	696	594
				1500	8.0	7	435	548
				1500	12.0	7	290	523
				180	0.85	20	1845	628
				180	1.3	25	1513	623
				180	1.7	28	1273	593
AA7050-T7451	10.2	3.6	6.1	360	1.7	24	1978	673
				540	2.5	34	2464	663
				810	3.8	39	2868	703
AA7050-T7451	9.5	3.2	6.4	490	1.4	20	2916	493
				700	1.0	13	3710	533
				700	1.9	16	2403	493
				700	2.6	18	2229	483

- An empirical formula is proposed to estimate the maximum temperature from the tool geometry. The following Table 2.10 [36] outlines the maximum temperatures reached for various welding rotational speeds

Table 2.10: Temperature result for various rpm

Rev/Min	$(E_l)_{eff}$ (J/mm)	Maximum Welding Temperature (°C) Experimental	Predicted
225	938	346	363
250	977	350	371
300	1331	372	442
400	1567	390	490

- Equation 2.3 [36] used to calculate the maximum temperature (based on the welding energy) does not account for plastic deformation affecting heat generation

$$\frac{T_{max}}{T_s} = (0.0013 - 16.5\alpha)(E_l)_{eff} + 0.56 \tag{2.3}$$

Emam *et al* [37]

- Heat generated is due to friction and plastic deformation
- Plastic deformation has a profound effect on the temperature results. Temperatures for various revolution speeds are given in Figure 2.11 [37]

Table 2.11: Maximum temperatures for different rpm input

rpm	Welding properties for AA6061-T6 $r_o = 12.7$ mm, $r_i = 5.0$ mm, $h = 8.0$ mm, $v_o = 2.4$ mm/s, $F = 22$ kN			
	E(J/mm) Ref[12]	E(J/mm) Ours	T_{max} Ref[12]	T_{max} Ours
50	333	643	398	547
100	664	971	479	591
175	1163	1432	570	653
200	1329	1562	594	670
225	1495	1692	615	687
250	1661	1822	635	705
300	1993	2081	667	739
350	2325	2341	691	774
450	2691	2660	758	816
550	3289	3251	776	895

Song *et al* [13]

- Model accurately depicts the FSW process where the temperature distribution near the tool pin has been reduced
- A preheat of the temperature of the work piece in front of the tool piece will aid the weld in helping the material flow easily around

Durdanovic *et al* [38]

- Ambiguity lies in the value of the friction coefficient

- Contact conditions are described and friction values assumed for each are determined

Lakshminarayanan *et al* [39]

- Optimum values for the FSW parameters were found for the particular material investigated
- Percentage contribution for each parameter was found, these percentages can be seen in the pie chart in Figure 2.16 [39]. This is useful when developing the model under the current study, as to what parameters one can change in order to see various temperature effects

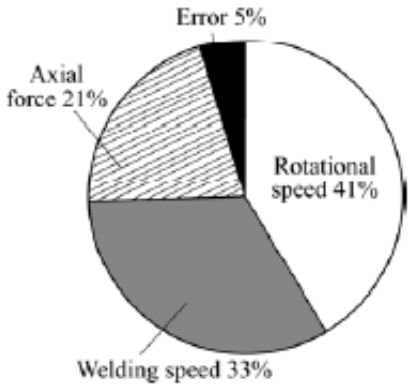


Figure 2.16: Percentage contributions form welding paramerts

Khairuddin *et al* [40]

- Heat generation and heat transfer are important parameters in determining the success of the joining process
- Issues from this model is that it only assumes either a slip condition or a sticking condition, which is not always the case for the FSW process

2.3.2.3 Contributions from analytical findings to be considered

The main contributions taken from these models are the following:

- Material properties influenced by temperature
- Equations relating specific welding properties to heat generation
- Certain values outlined for contact conditions, friction coefficient and convection coefficients.

Each of the material properties given in the papers, offer some consideration that is required to be accounted for when inputting values into the model. In both Schmidt *et al* [34] and Song *et al* [13], yield stress is dependent on temperature. However, in Nandan *et al* [35], it gives

equations for specific heat and thermal conductivity which are temperature dependant and these are again, other material properties which need to be accounted for in temperature variance.

One particular welding property which is given is the axial force exerted and is a property that is dependent on the machines parameters but an overview of this is given below in Table 2.12. It can be noted that at higher rotation speeds, the axial force is smaller and resulting temperatures are not only affected by the property but by material and other welding conditions.

Table 2.12: Axial force and resulting temperatures for various models

	Rotational speed (rpm)	Feed rate (mm/s)	Axial force (kN)
Hamilton *et al* [34]	1500	5	7
	180	1.7	28
	360	1.7	24
Emam *et al* [35]	1500	5	7
	520	1.9	24
	700	1.9	16
Lakshminarayanan *et al* [37]	1200	0.37	4
	1400	0.75	6
	1600	1.25	8

The last important parameters mentioned is the friction coefficient and contact surface condition, being either sticking, sliding or combination of the two. Schmidt *et al* [34] outlines the equations that are required to calculate the heat flux based on the friction coefficient, although it uses various contact conditions to estimate the heat generated, which in the end it is concluded that a sticking condition occurs. Hamilton *et al* [36] gives an equation for torque which has friction coefficient present and indicates that friction coefficient is dependent on temperature. Although, it is kept constant at 0.5 for energy levels smaller than 2000J/min and decreases to 0.45 at higher energy levels. This indicates that the friction coefficient decreases with increasing temperature as it is assumed that the contact condition between the surfaces is between a combination of sticking and sliding and more towards the sliding condition. Emam *et al* [37] uses the same notion as Hamilton *et al* [36] for the friction coefficient and ranges the friction coefficient between 0.5-0.25 for sticking and slip conditions respectively.

However, Durdanovic *et al* [38] assumes a constant friction coefficient throughout the mathematical model. This we know is for simplification purposes as there is definitely a change in this value as temperature changes. Khairuddin *et al* [40] on the hand, similar to Emam *et al* [37] and Hamilton *et al* [36], considers constant and changing friction coefficient based on the static and dynamic phases of the FSW process.

These are key parameters which affect the result of the FSW process and therefore care and attention is required to make the best assumptions for the model inputs and analysis of experimental data.

2.3.3 Experimental findings

Experimental work is briefly looked at to find any physical qualities that have been found that one may include as an initial estimation for any unknown values that are to be used in the current model investigation.

2.3.3.1 Model properties for papers discussed

Each experimental approach will be discussed, outlining properties that were considered important and if any result or information that has been included in the studies that is relevant to the current study, will therefore be commented on.

Khodir *et al* [41]

- Investigates the effects of the rotational speed in joining dissimilar material
    - Investigates dissimilar materials located at the advancing side and then retreating side
    - Observes the macrostructure and microstructure of the joints
    - Results obtained discuss the various effects of the material properties at various rotation speeds

This information was important since it listed the material properties of the Aluminium alloy 2024 T3 at room temperature (Which is the material we are interested in for the current study) and it is interesting to note the effects these material properties have at various welding parameter conditions.

Cederqvist and Reynolds [42]

- Investigate the lap joints of FSW

An interesting conclusion is the mention of the lower rotational speeds causing less vertical mixing on the retreating side of the weld. When looking at results of one's own developed

model, it is then expected that for lower rotational inputs, one can expect lower temperatures on this side, since there is less frictional stress and therefore heat generation occurring.

Hussain *et al* [43]

- Investigates the strength and hardness under various process parameters

It was interesting to note the effect of process parameters on the weld material property of tensile strength. Since this is a parameter to input into the model, understanding its behaviour helps to observe these issues experimentally since one of the conclusions is that misalignment will produce weaker strength in the material and this is a care that needs to be considered when performing the weld trials since the model will be analysed assuming perfect alignment of the work pieces.

Mijajlovi *et al* [44]

- Parameters affecting heat generation are investigated
    - Discusses the influence of the parameters on the heat generation which include
        - Tool geometry
        - Loads
        - Tribological parameters which include friction coefficient, contact pressure and shear stress
    - Experimental study was performed,
        - Estimated torque and axial force was recorded
        - Estimation of the friction was also performed
    - The interlinking between these parameters is shown in Figure 2.17 [44]

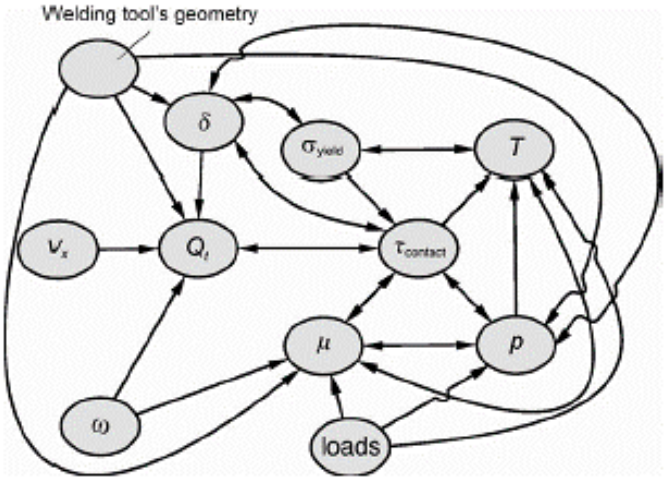


Figure 2.17: Influence of parameters on heat generation (Variables have the same description as outlined in the Nomenclature

2.3.3.2 Results for experimental finding as discussed

Experimental results based on the investigations above yield the following;

Khodir *et al* [41]

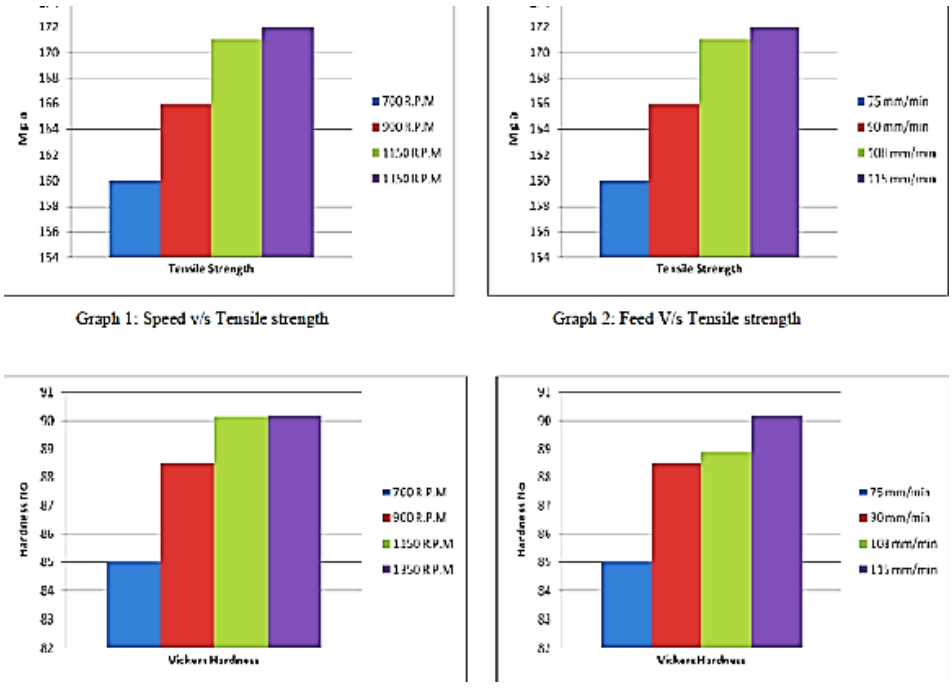
- Rotation speeds influence the following
    - Grain sizes increase with higher rotation speeds
    - Tensile properties for the 7000 series were higher when located on advancing side of the weld

Cederqvist and Reynolds [42]

- “Cold” welds cause less mixing on the retreating side, which this is assumed to have an effect on the frictional stress it is produced on that side which has an effect on the heat generated on that area.

Hussain *et al* [43]

- Increase in rotational speed increases tensile strength due finer grain structure developing in weld. Tensile strength is higher at a lower weld speed.
- Results for various rotation speeds and feed rate versus the tensile strength and hardness are shown in Figure 2.18 [43]



Graph 1: Speed v/s Tensile strength

Graph 2: Feed V/s Tensile strength

Figure 2.18: Results for various feed rates and rotation speeds for experimental findings

Mijajlovi *et al* [44]

- For experimental findings, the following aspects of the friction coefficient are found over time and this is shown in Figure 2.19 [44]

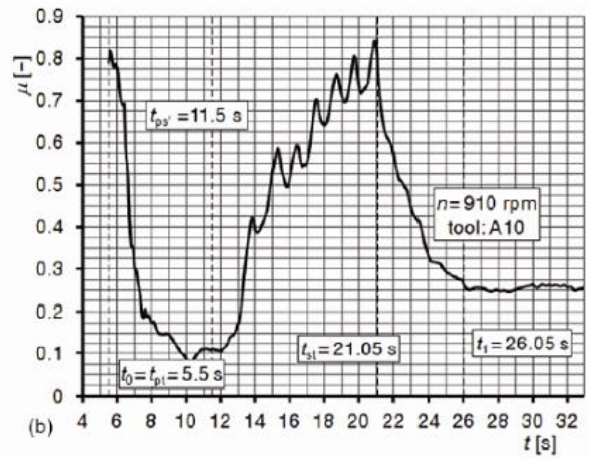


Figure 2.19: Friction coefficient versus time for experimental findings

2.3.3.3 Contributions from experimental findings to be considered

Based on the above discussion of experimental work and results, the following contributions from the study are considered and which will be used going forward.

Three most important findings are taken forward when conducting own experimental work and development of model. This is the experimental set up with regards to precautions of misalignment which needs to be considered, especially in comparison of FEA model and experimental findings of temperature, which leads to the consideration to ensure that the advance side depicts a higher temperature in the model and experimental weld trials.

The next important finding is that of the contributing factors influencing the heat generation. This is predominantly important when setting up both experimental and FE model work as to what considerations need to be made in order to depict a comparison or the reasoning behind differences of the processed data for results.

The third finding is that of the friction coefficient over the FSW process time. Further conclusions are drawn from the experimental findings based on Mijajlovi *et al* [44]. Coefficient of friction is dependent on tangential force, length of force pole, diameter of weld tool probe. And it shows that the friction coefficient changes between 0.1 and 1 depending on the phase of FSW process.

2.3.4 Current model features versus previous models developed

Based on the models discussed in each section with their contributing parameters of importance, the following is related to the development of the current model and what sets it apart from all the rest.

Many of the models described are either thermal models only or are specified as thermo mechanical models, relating either two variations of models that first utilises the one property of either thermal or structural and inserts it into another model for the counter part for it to be considered a thermo mechanical model. The current model utilises both thermal and structural in one model. With the new command feature in ANSYS 14.5, heat is generated by friction within the model and this command feature sets it apart from the rest. Other models have implemented moving heat sources and moving co-ordinate systems. This command feature allows the model to be analysed in a more realistic way by implementing the mechanical features of the process and therefore resulting in a thermal output which is especially relevant not only to the FSW process but towards other approaches such as simulation of brake discs whereby heat is also generated by friction.

Although there are those models which have used the software ANSYS, and have compared well to their literary experimental findings, the approaches used for each are different.

- Moving heat source [16]
- Thermal model only is considered [17] The element SOLID70 is used which has only a single degree of freedom for the temperature at each node defined
- Heat transfer model and mechanical model are coupled [18] half of the welded plate is considered but this limits the effects of temperature on the advance and retreating sides of the weld.
- Model is based on that developed by Zhu and Chao [20]. A moving heat flux is used to assimilate the heat generation by friction [22]

The current model being developed enhances and embraces those new features in a more recent ANSYS version whereby, a different element (SOLID226) is specified whereby an alternative command feature that generates heat within the work piece by friction is used as it allows for a structural-thermal model to be developed instead of a coupled models of thermal and mechanical. Also to note that the current model is also that based on the model by Zhu and Chao [20], it is modelled with the workbench interface and not that of the APDL.

The current model will invest in the notion of as many material properties changing with temperature are included and where these properties may be inserted as parameters resulting in a parametric model being developed for further implementation for optimisation. This too

sets it apart from the previously developed models as previously these properties are either assumed constant for simpler analysis or it's a combination of properties changing with temperature and others remaining constant. This approach, though it may be valid for their particular study, in order to have a true representation of the process, it is imperative to take these properties under consideration.

In terms of the actual model geometry, each model is specific to the tool geometry and work piece used. With this being said, it is difficult to compare any temperature results obtained for their models as various other studies have also shown the effect the geometry of the tool and the parameters inserted into the model have an effect of the weld and hence the temperature result of the FSW process. This is where the experimental weld trials for our study needs to be done, and based on the experimental studies, we are able to at least ensure that our study is representative of the parameter findings in literature. Also based on their approaches and being aware of the trouble with thermo couples being used, it is also decided to improve on this method of approach by utilising a thermal camera.

2.3.5 Parameters of interest based on prior models

The following parameters are important when considering those which are relevant to the model to be developed. Based on the previous models, the heat generated on each surface is looked at in more detail as well as what previous models have used and assumed on the convection and friction coefficients. The contact condition is also discussed further since it has been found that this incorporates not only if the weld is of a good quality but the friction coefficient as well as tool geometry. Since friction is created by the two surfaces interacting with one another and this generates heat, the slip condition is then an important parameter to investigate since it can also be related to the temperature the weld produces.

2.3.5.1 Heat generation

The amount of heat generated in the model is predominantly caused by the tools properties and the friction between the tool and work piece surfaces. The total amount of energy is the sum of the heat generated from the tools probe and shoulder surface.

$$Q = Q_1 + Q_2 + Q_3 \tag{2.4}$$

Q_1= Heat generated from shoulder [34]

Q_2= Heat generated from probe [34]

Q_3= Heat generated from probe tip surface [34]

The final result after integration of above with respect to the radii of each, the following total heat generation can be calculated as follows according to [34]

$$Q_{Total} = \frac{2}{3}\pi\tau_{contact}\omega\left(R^3_{shoulder} + 3R^2_{probe}H_{probe}\right) \quad (2.5)$$

Based on Chao-Qi-Tang, [23] concludes that 5% of the heat generated by friction flows to the tool and the remaining 95% flows through the work piece

The following heat generation continues from the above and describes the surfaces of interest that need to be accounted for during the FSW process. These heat contributions on the surfaces are shown in Figure 2.20.

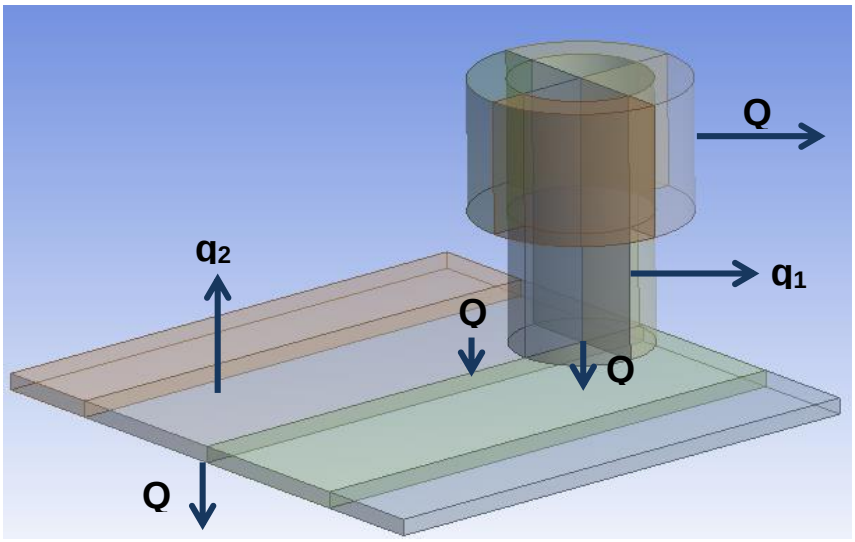


Figure 2.20: Heat generation contributions from each part of the model

From Figure 2.20, the following heat generation contribution is as follows and is according to Chao-Qi-Tang [23]

$$Q_3 = Q_4 + q_1 \quad (2.6)$$

$$Q_1 = Q_2 + q_2 + Q \quad (2.7)$$

Q_1 = Heat flux into the model due to the friction between tool and work piece surface

Q_2 = Heat conducted from the bottom of the work piece to the backing plate

Q_3 = Heat flux from the friction between tool and work piece surface

Q_4 = Heat transferred from the clamped tool to the machine bushing

q_1 = Convection due to heat lost from the tool surface to the air

q_2 = Convection due to heat lost from work piece surface to the air

Q = Increase of heat content in the work piece

Since Q_3 is the heat generation coming from the tool and Q_1 is the heat generation into the work piece from the tool, the assumption is;

$$Q_3 = Q_1 = Q_{total} \tag{2.8}$$

We can describe these two as the total heat generated by each of the contributing factors as described in the above equations.

Each of the definitions above can be represented in their own form. For the work piece Q_2 and q_2 are described in terms of heat flux loss, according to Muhsin *et al* [17]

$$q_2 = h_{q2}(T - T_0) + \varepsilon F_1 \sigma_{SB}(T^4 - T_0^4) \tag{2.9}$$

$$Q_2 = h_{Q2}(T - T_0) \tag{2.10}$$

Then, based on convection, the heat transfer and heat flux [13] for the tool pieces can be defined as;

$$Q_4 = h_4 A_c (T - T_0) \tag{2.11}$$

$$q_1 = \mu F \omega R_{shoulder} 2\pi \tag{2.12}$$

Where A_c and A_s are the surface areas for the clamped tool surface and shoulder surface respectively.

Additional heat transfer into the work piece is described as

$$Q = h_Q (T - T_0) \tag{2.13}$$

Heat flux along the tool into the work piece is expressed as follows with reference to Chao-Qi-Tang [20]

$$q(r) = \frac{3Q_3 r}{2\pi r_0^3} \quad \text{for } r \leqslant r_0 \tag{2.14}$$

2.3.5.2 Contact states for slip condition

The contact condition between surfaces is important as it affects the friction coefficient variable. Three contact conditions exist;

- Sticking
- Sticking and sliding combination
- Sliding

Contact condition variable is expressed as δ and the slip condition as γ [34].

$$\delta = \frac{v_{matrix}}{v_{tool}} = 1 - \frac{\dot{\gamma}}{v_{tool}} \tag{2.15}$$

Where;

$$v_{tool} = \omega r \; and \; \dot{\gamma} = v_{tool} - v_{matrix} \tag{2.16}$$

The following Table 2.13 [34] outlines the contact conditions and the results of each for the state variable value and the shear stress and matrix velocity conditions.

Table 2.13: Contact condition

Condition	Matrix velocity	Tool velocity	Shear stress	State variable
Sticking	$v_{\text{matrix}} = v_{\text{tool}}$	$v_{\text{tool}} = \omega r$	$\tau_{\text{friction}} > \tau_{\text{yield}}$	$\delta = 1$
Sticking/sliding	$v_{\text{matrix}} < v_{\text{tool}}$	$v_{\text{tool}} = \omega r$	$\tau_{\text{friction}} \geqslant \tau_{\text{yield}}$	$0 < \delta < 1$
Sliding	$v_{\text{matrix}} = 0$	$v_{\text{tool}} = \omega r$	$\tau_{\text{friction}} < \tau_{\text{yield}}$	$\delta = 0$

Based on the heat generated in equation 2.3, each of the above conditions change with contact shear conditions [34]

For sticking conditions, the contact shear is equal to the yield stress divided by the root of three. Yield stress is temperature dependent and the heat generated for pure sticking conditions is as follows;

$$Q_{\text{total, sticking}} = \frac{2}{3}\pi \frac{\sigma_{\text{yield}}}{\sqrt{3}} \omega((R^3_{\text{shoulder}} - R^3_{\text{probe}})(1 + \tan\alpha) + R^3_{\text{probe}} + 3R^2_{\text{probe}} H_{\text{probe}}) \tag{2.17}$$

For pure sliding, the contact shear stress is the friction coefficient multiplied by the contact pressures [34] and the heat generated is expressed as

$$Q_{\text{total, sliding}} = \tfrac{2}{3}\pi \mu p \omega((R^3_{\text{shoulder}} - R^3_{\text{probe}})(1 + \tan\alpha) + R^3_{\text{probe}} + 3R^2_{\text{probe}} H_{\text{probe}}) \tag{2.18}$$

Combination of sliding and sticking condition takes into account the contact condition variable (δ)

$$Q_{total} = \delta Q_{total,sticking} + (1-\delta) Q_{total,sliding} \quad (2.19)$$

2.3.5.3 Friction coefficient

Friction coefficient is affected by the changes in temperature. An example appears on waxed-wood skis, where the friction coefficient differs at 0.02 for temperatures above -10°C but 0.4 for temperatures below this amount [45].

Based on [28] it is concluded that for sliding conditions, friction coefficient lies within known values between surface conditions and for sticking conditions, yield shear stress relating to work piece material for varying temperatures is used.

M. Mijajlovic *et al* [44] predicts the friction coefficient in terms of the momentum of friction and axial force which is dominantly expressed for the plunge phase

$$\mu = \frac{3F_t L}{F_z d} \quad (2.20)$$

Where;

- d is the diameter of the tool probe
- F_t is the tangential force
- L is the length of the force/friction pole
- F_z is the axial force

For the slip condition to be taken into account which is affected by the temperature and strain rate conditions, the friction coefficient is expressed as follows with reference to A.H Kheireddine [26]

$$\mu_f = \mu_0 \exp(-\lambda \delta \omega r) \quad (2.21)$$

2.3.5.4 Convection coefficient

The convection coefficient is expressed as follows;

$$h = \frac{Q}{A\Delta T} \quad (2.22)$$

Where;

A=Surface area

ΔT = Difference in temperature between surface temperature and fluid temperature (In our case is air)

Q=Heat transfer

2.4 Material properties

The following materials describe those used for the work piece and tool piece respectively, describing as to why the selected material was chosen and more details relating to each of the material properties can be found in the Appendix 2.

2.4.1 Aluminium Alloys

Aluminium is a light weight, white metal. It has a melting temperature of 650 degrees Celsius [46]. Aluminium alloys improve mechanical properties and strength [46]. The two aluminium alloys of interest are the 2xxx and 6xxx series. Copper for the 2xxx series is the main alloying element and are commonly used in aircraft applications and for the 6xxx series, magnesium and silicone are the alloying elements [47]. The 6xxx class of aluminium alloy has intermediate strength capabilities as to the 2xxx aluminium class [46]. Apart from its advantage in being light weight, it also has exceptional resistance to atomic oxygen erosion [64] as well as its advantage in machinability and weld ability.

Forging temperature for Aluminium alloys in the range of 315 to 550 Degrees Celsius [47], this temperature is important to note since the FSW process requires the material to plasticize and not melt.

Applications of aluminium alloys;

- Skin panels for aircraft or anywhere in the aircraft where fatigue performance and good strength properties are required [48]
- Blades and pistons for aircraft engines
- Fuel tanks for rockets

2.4.2 H13 Tool steel

Tool steel is used for the shaping, cutting or forming a material into a component or part that is according to application [49]. Some other applications where tool steel is used include, pressure casting tools, hot shear knives as well as tools for the plastic industry [50]. It is especially suited for die casting of aluminium and copper [51]

Particular interest will be noted for the tool steel used experimentally, as well as material properties of it included for the finite element model analysis, which is commonly known as H13 Tool steel (USA) (4659 BH13 4659 H13 according to B.S.) [49]

H13 Tool steel falls under the category of Chromium hot work steels. [49] This is suitable for the application of use since there is a considerable amount of heat produced within the

process it is being used in. The melting temperature range for this particular tool steel is between 1200-1500 Degrees Celsius [46]. This particular material is able to withstand combinations of heat and pressure which is also applicable to current application use.

Advantages for H13 Tool steel (Chromium hot-work steel)

- Good resistance to softening due to chromium content, and therefore includes ease of forming and working [49]
- Resistance to erosive wear on material at high temperatures (due to Vanadium content [46, 49]

Relatively low thermal expansion coefficient

2.4.3 Material properties affected by temperature

The following properties [45] relate to properties of a material that are influenced by temperature and affect the values thereof. Results of increasing temperature of the above material properties include grain recrystallization which is an important result in the FSW process. This is due to the heat input which causes the dislocations in the material structure to decrease which increases its ductility and reduces its resistance [45]. Typical recrystallization temperatures are approximately 0.4 at melting temperature. Specifically for aluminium the recrystallization temperature is 150°C taking the melting temperature at 660°C [45]

An increase in temperature usually has a decrease in mechanical properties [45]. Typical values of material properties at room temperature can be found in the Appendix: Material properties and include typical values of those mentioned properties below;

- Density
- Elastic Modulus

A list of material properties changing with temperature is specified below. These material properties increase in value when the temperature increases. These thermal material properties are important for the FSW process since heat generation due to friction is the main cause and the components associated with a materials thermal properties need to be understood clearly in order for a fully defined model that consists of all important parameters to be described.

- Friction coefficient
    - Has common assumptions that it is independent of area contact and velocity of motion between surfaces [52]

- The friction independent of velocity is not true for the case of FSW. It has been noted that with a high increase in speed and air friction is come upon as part of this, the friction is dependent on the speed and also might be affected as much as the square or even higher powers of the speed has an influence. [53]
- An increase in friction occurs near the melting point of a material and decreases after the melting point temperature of that specific material [51]. This increase in friction is due to an increase in shear area as the adhesive effects become more pronounced between the surfaces [53]
- Applicable to FSW process is that at high velocities, frictional sliding may exceed the rate of heat conduction and hence the temperature changes may be quite significant [54] and hence this results in frictional heating being a primary factor.

- Specific heat capacity
  - This is the amount of energy per unit mass the material requires to produce a temperature rise by one degree [55]
  - Relationship of specific heat capacity with temperature is shown in Figure 2.21 [55]. Specific heat capacity increases when temperature increases.

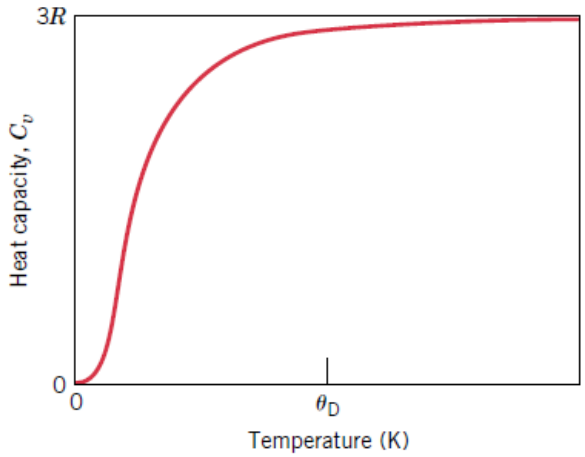


Figure 2.21: Increase in heat capacity with increasing temperature at constant volume

- Thermal expansion coefficient
  - It's the materials capability of expanding with temperature and its units are the inverse of temperature.
- Thermal conductivity
  - Refers to the materials ability to transfer heat
  - Heat flows from higher temperatures to low temperatures [56]

- Heat transfer coefficient
    - As the fluids velocity increases, the heat transfer coefficient increases [56]
- Emissivity
    - Influencing factors [57]
        - Surface condition
        - Opacity
        - Reflectivity
    - It is defined as the ratio of the actual amount of infrared energy emitted compared to the theoretical amount of energy that could be emitted [57]
    - The values range between 0.000 and 1. [57]
    - It is best to measure the emissivity of a material within the cone of maximum emissivity. Viewing angles influence the emissivity value and for molten metals this emissivity value is the highest within a 45° cone [57]
    - The emissivity value varying with the angle can be shown in Table 2.14 [58], where the angle after 45° (from the vertical point, where 90° is the parallel angle measurement) shows some discrepancy with published values. [58]
    - Effects of visible light on the area in question being evaluated also affects the emissivity value [58]

Table 2.14: Emissivity value dependant on view

	Angle (Degrees from perpendicular)				
Material	**0**	**45**	**60**	**75**	**Published Value**
Super 88 Tape- Calibration	*0.95*	*0.90*	*0.87*	*0.78*	*0.95*
Painted Aluminum Window Frame	0.91	0.85	0.82	0.73	
EIFS Top Coat	0.96	0.97	0.97	0.97	0.912
Vinyl Window Frame	0.93	0.86	0.87	0.87	0.91 to 0.93[2]
Cementitious Base (EIFS)	0.91	0.89	0.90	0.90	
Wood Stud	0.85	0.81	0.81	0.77	0.862
Oriented Strand Board (OSB)	0.93	0.94	0.92	0.90	0.912
Building Paper	0.95	0.91	0.89	0.82	0.86 to 0.88 [1]
Artificial Stone	0.93	0.92	0.92	0.91	0.92 [1]
Stucco Top Coat	0.87	0.86	0.82	0.83	0.89 [1]
Plaster (Stucco Scratch/Brown Coat)	0.88	0.87	0.84	0.83	0.86 to 0.89 [2]
Flexible Flashing Membrane	0.95	0.95	0.95	0.92	
Hardboard Siding (Painted)	0.93	0.92	0.91	0.86	0.77 to 0.94[2]
Hardboard Trim (Painted)	0.95	0.93	0.91	0.89	0.77 to 0.94[2]
Concrete	0.93	0.92	0.91	0.87	0.91 [1] 0.92[2]
Real Stone	0.94	0.92	0.92	0.90	0.932
Thermo Ply	N/A	0.03	0.04	0.07	
Galvanized Flashing	N/A	0.43	0.46	0.52	0.462
Densglass Exterior Sheathing	0.86	0.85	0.84	0.80	0.852
EPDM Roofing	0.95	0.93	0.91	0.85	

2.5 Objectives

From the literature, it is evident that a thermal mechanical model is needed, which is capable of implementing temperature dependent material properties as well. Various models which have been developed make various assumptions on these temperature dependant properties in order to simplify the model, but there is concern with this as it does not truly represent the actual FSW process. Therefore, it is imperative to consider these properties and investigate the effects further as well by a comparison of experimental and FEA model.

- Use the new command features in ANSYS version 14 to develop a thermo-mechanical model of the Friction Stir Welding Process depicting relevant phases of the process in one model
- To asses weld trials of various tool parameters that are to be considered best quality welds. These welds will be captured using a thermal imaging camera whereby the temperature can be obtained at specific points along the weld
- Compare the temperature results obtained from the experimental weld trials to that of the Finite Element model created in ANSYS for the same parameter settings and therefore validate the numerical model

2.6 Summary

The objectives outline the work that is required to be conducted in order to achieve the set goals. Based on the knowledge gathered for the various models, the initial step is to setup a FEA model which is capable of having thermal and mechanical properties input into it and the effects of each other with another needs to be implemented as well. This is outlined in the next section, after which the experimental weld simulation are performed where the temperatures are recorded on the surface of the plates and tool.

The material properties that are required and which are temperature dependant are as follows;

- Density
- Elastic Young’s modulus
- Coefficient of thermal expansion
- Specific heat
- Thermal conductivity

These properties are important when inserting information in to the model, as previous models have outlined. For the experimental weld trials, the emissivity value set on the camera needs to be calibrated and checked.

Those parameters for friction coefficient, convection coefficients for the surfaces of the work piece and tool are given estimations in the model based on theory suggestions and then will be compared to those calculated from the experimental data obtained from the weld trials performed.

Chapter 3

3. Finite Element Modelling

3.1 Introduction

The software used to develop the model is ANSYS version 14.5 and the methodology is set out describing the development of the model in full detail. The geometry of the model is described as well as the boundary conditions are set on the model as to describe the physical behaviour of the system in engineering terms by constraining areas in various directions to represent clamped or rigid surfaces. The contact conditions used are explained together with the input commands used to represent the thermal inputs of the mechanical model.

3.2 Apparatus

ANSYS version 14.5 (The start-up logo is shown in Figure 3.1 [59] was used to carry out the analysis for the FSW process. ANSYS mechanical is used to develop the model and it allows one to create the model using the Design Modeller interface. With a user-friendly workbench navigation window, one is able to insert conditions under the Mechanical model interface, once the analysis type has been chosen. With its advanced numerical methods for solving problems it is a useful tool to analyse non-linear problems. The software provides an advanced post-processing capabilities that allows the user to obtain not only visual details of the model but colour contour planes but has results which can be exported to spread sheets for further analysis. Also capable of slicing through models, it can reveal more details within the model.

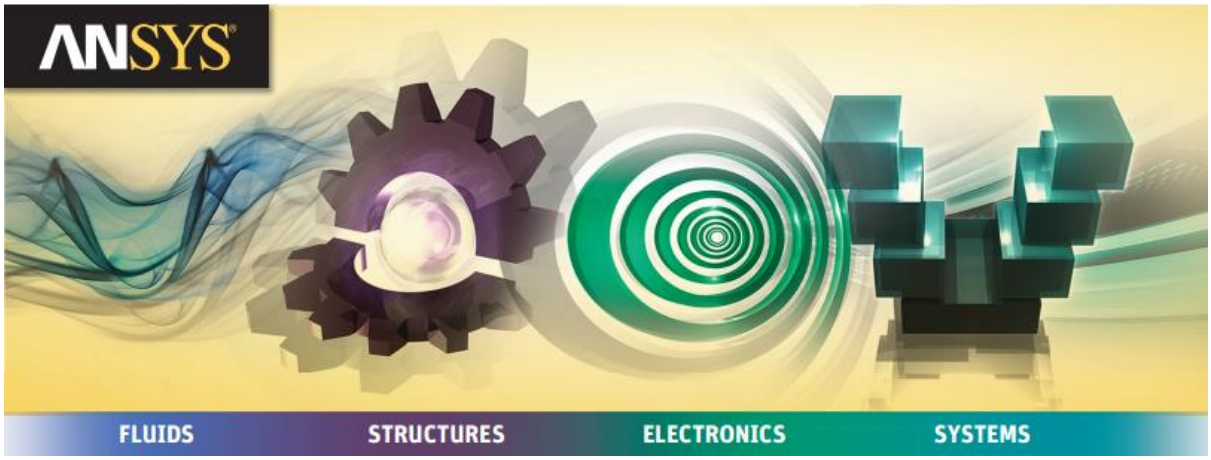


Figure 3.1: ANSYS mechanical logo

The computer used was a DELL Optiplex 790, with a core i7.

3.3 Methodology

The following steps are the guidelines that were taken into developing the model in the FEA software ANSYS version 14.5. This version incorporates new elements, such as the SOLID226, which allows for thermal commands to be implemented within the mechanical interface are capable of a thermal structural analysis and has new features enabling one to define contact points which simulate heat being generated.

SOLID226 has various capabilities, predominantly incorporating thermal effects to structural nodal points. The KEYOPT number indicates the degrees of freedom set for the element as well as determines the corresponding force and reaction solution. For the current study the field key for the structural field is set it to one and the field key for the thermal is set to 10, therefore the 11 is used to define the structural-thermal element.

It has up to 4 degrees of freedom (DOF) [59] and is a 3-D element consisting of 20 nodes. The DOF include for the x,y,z axis as well as a thermal DOF. The 3-D element with each node is shown below in Figure 3.2 [59]

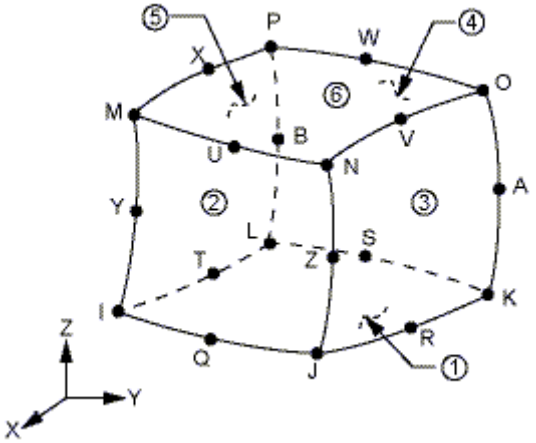


Figure 3.2: SOLID226 element geometry

The structural-thermal analysis can be used for full transient type of analysis and with its degrees of freedom in the x,y,z and temperature planes, one is also able to insert additional material properties relating to a materials thermal properties as well as its mechanical properties. Convection, heat flux and radiation can be applied to the surface of the model and the heat generation is applied to the body of the model when using this element type. This last point is the most important as it is the heat generation within the work piece one is trying to visualise.

A transient structural analysis tree is created, whereby all the information required is input into the work bench and all thermal aspects of the model are inserted as commands within the structural analysis, this is because the SOLID226 is being used.

The following procedure outlined for the modelling in ANSYS workbench is guided by the model created by Zhu and Chao [20], which uses a moving heat and modelled in the APDL of ANSYS with is new features in version 14.

3.3.1 Material property inputs

In the engineering data of the ANSYS work interface, this is where the following properties for the tool and work piece will be defined. For the current study, the following material properties are as follows (Table 3.1) and for those material properties changing with temperature are clearly indicated.

Table 3.1: properties of materials as given in Engineering Data

Property	Value
⊞ Density	Tabular
⊞ Isotropic Secant Coefficient of Thermal Expansion	
⊞ Isotropic Elasticity	Tabular
⊞ Alternating Stress R-Ratio	Tabular
Tensile Yield Strength	2.9E+08
Compressive Yield Strength	2.8E+08
Tensile Ultimate Strength	4.35E+08
Compressive Ultimate Strength	0
⊞ Isotropic Thermal Conductivity	Tabular
⊞ Specific Heat	Tabular
Isotropic Relative Permeability	1
⊞ Isotropic Resistivity	Tabular

The above table does not depict the values, but indicates those properties which have “Tabular” alongside as those properties which are changing with temperature. The following table (Table 3.2) outlines those properties changing with temperature with the corresponding values clearly indicated as well.

Table 3.2: Material properties inserted into engineering data in ANSYS

Aluminium Alloy 2024		H13 Tool Steel	
Material Property and Temperature (°C)		Material Property and Temperature (°C)	
Temperature (°C)	Density (kg/m^3)	Temperature (°C)	Density (kg/m^3)
0	2780	0	7750

200	2700	25	7740
400	2650	200	7740
600	2600	400	7700
800	2550	600	7650
Temperature (°C)	Coefficient of thermal expansion /°C	Temperature (°C)	Coefficient of thermal expansion /°C
0	1.40E-05	0	1.02E-05
20	2.11E-05	20	1.02E-05
100	2.29E-05	100	1.04E-05
200	2.38E-05	200	1.12E-05
300	2.47E-05	425	1.22E-05
400	2.56E-05	650	1.31E-05
500	2.66E-05	816	1.35E-05
Temperature (°C)	Young's Modulus (Pa)	Temperature (°C)	Young's Modulus (Pa)
0	7.31E+10	0	2.07E+11
20	7.24E+10	200	1.84E+11
100	6.89E+10	400	1.75E+11
200	6.35E+10	600	1.54E+11
260	5.75E+10		
300	5.00E+10		
371	3.44E+10		
Temperature (°C)	Thermal Conductivity (W/mK)	Temperature (°C)	Thermal Conductivity (W/mK)
0	144	0	30
20	164	215	28.6
100	182	350	28.4
200	194	475	28.4
300	202	605	28.7
400	210		
500	220		
Temperature (°C)	Specific Heat (J/kg°C)	Temperature (°C)	Specific Heat (J/kg°C)
0	875	25	434

20	881		
100	927		
200	1047		
300	1130		
400	1210		
500	1300		

3.3.2 Geometry

The geometry of the aluminium work piece and tool are modelled as shown. The tool geometry is that based in Appendix 5, Figure 10.18 [60] and the work piece thickness was kept consistent to that used in the experimental weld trials. Previous models created in ANSYS depicted the whole length and breadth of the work piece under consideration, but due to number of elements and processing time, the work piece was reduced as close to the tool area as this area of contact was the point of interest. Processing time was an immense property affecting the solution of the work and was therefore deemed an appropriate option in order for the running time to decrease, the number of elements could be reduced by shortening the plate dimension in terms of length and width, but the tool geometry and thickness of the plate is to be kept the same. The geometry created in the ANSYS geometry is seen below in Figure 3.3.

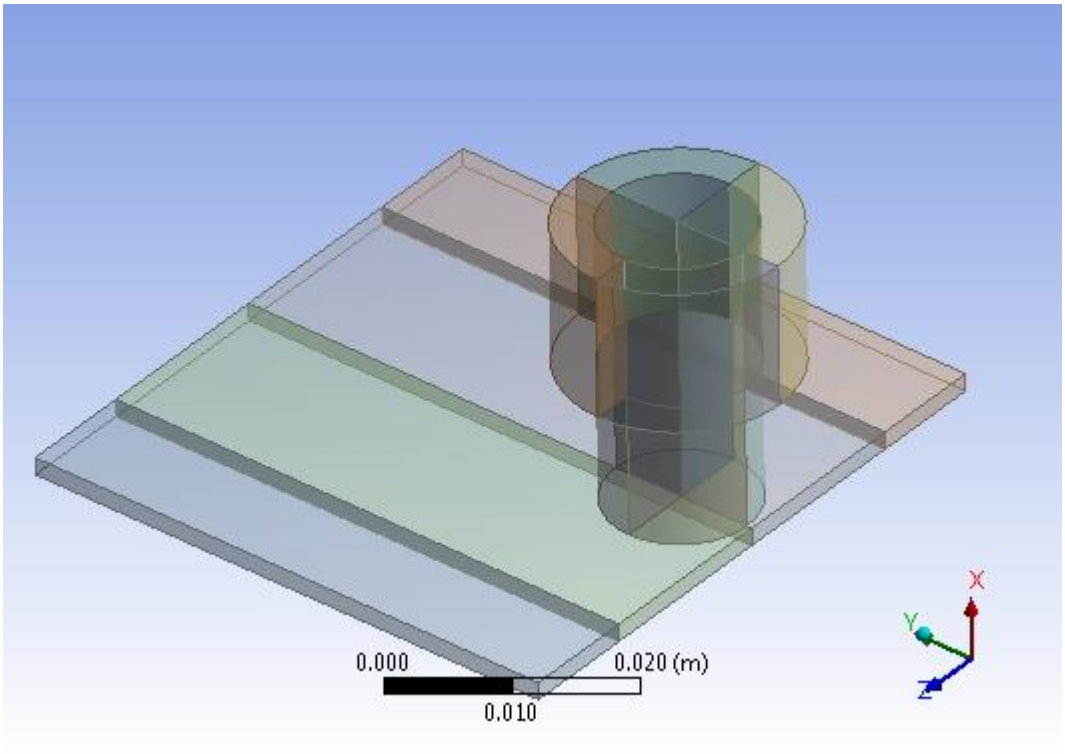


Figure 3.3: Geometry of model built in ANSYS version 14.5

Sliced planes are used as to divide certain areas for particular boundary conditions and contact points. These sliced areas can be clearly seen in Figure 3.3.

3.3.3 Boundary conditions and contacts

The contacts between the surfaces (Two work piece edges and the surfaces between the tool and work piece) are described as frictionless. Due to the new feature in ANSYS version 14.5, commands are inserted within the model tree as shown in Figure 3.5 and under each relevant contact, the commands relate to the thermal conditions for that particular contact point. The commands are expanded upon and it can be seen that the APDL is used to set these thermal commands within the structural analysis. This is only possible to due to the command labelled *Element Type*. This *Element Type* command is explained in detail in Figure 3.4.

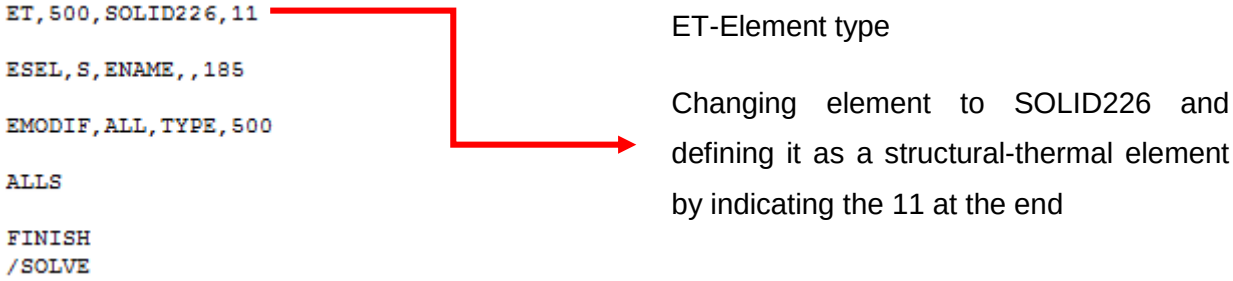


Figure 3.4: Element type command

ET

ET, *ITYPE, Ename, KOP1, KOP2, KOP3, KOP4, KOP5, KOP6, INOPR*
Defines a local element type from the element library.

First line indicates the element type (ET) the current elements need to be changed to ITYPE is 500 and later this is set to CID to correspond to the contact type parameter, which will be able to insert these thermal commands for the element type described as SOLID226. Solid226 is the desired element type and it is defined as structural-thermal by the number 11 as explained for the SOLID226 elements.

The element select command (ESEL) is explained below and taken from the ANSYS help file. It explains each part of the command in detail.

ESEL

ESEL, *Type, Item, Comp, VMIN, VMAX, VINC, KABS*
Selects a subset of elements.

The type S represents a new set of elements is selected.

The item is defined by the ENAME, which uses the element name to identify the elements to redefine to a different element name (EMODIF).

EMODIF

EMODIF, *IEL, STLOC, I1, I2, I3, I4, I5, I6, I7, I8*
Modifies a previously defined element.

The IEL is specified as ALL so that it modifies all the elements which is linked with the ESEL command.

STLOC-Startling location for the first node to be modified, where TYPE is used to modify only those elements as indicated by the I1 value which is 500, and this corresponds to the elements changed to the element type of SOLID226.

The model tree is depicted below, Figure 3.5, indicating the commands inserted under each section required to have a thermal input.

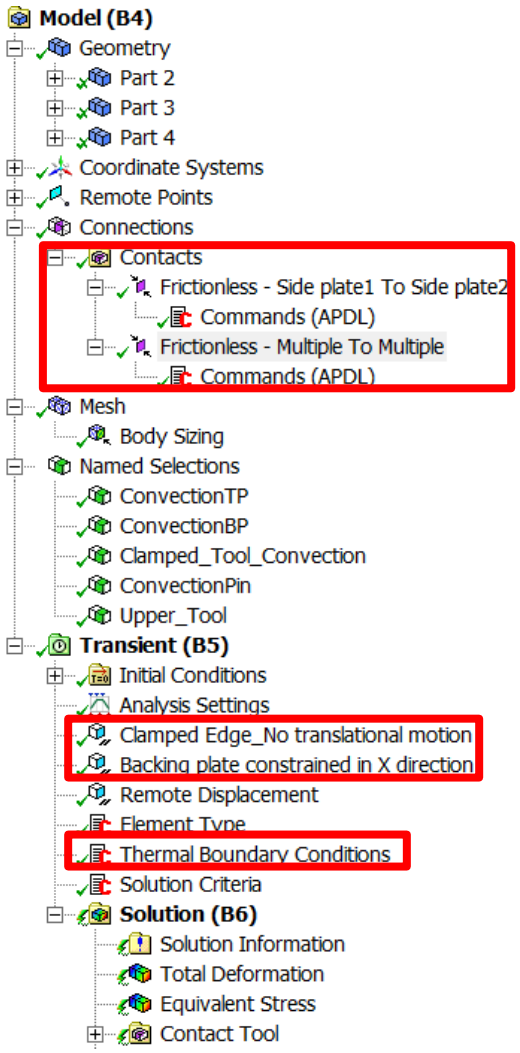


Figure 3.5: ANSYS Workbench model tree

Two types of boundary conditions are considered, mechanical and thermal. The following mechanical boundary conditions are;

- Since the plate is clamped on the edges, these outside edges are constrained in all directions
- The bottom of the work piece is constrained in the vertical direction

The thermal boundary conditions are inserted as commands within the “Transient” branch. It is the convection coefficients given to each relative surface. From previous studies, this figure is kept fairly similar, so for initial simulations these values were considered as first approximations. The convection coefficients were applied to the following surfaces;

- Top of the work piece
- Tool shoulder
- Tool part considered clamped in its bushing
- Bottom surface of the work piece which lies on a backing plate

This command is detailed below in Figure 3.6, where each of the ARG values are specified to each convection coefficient.

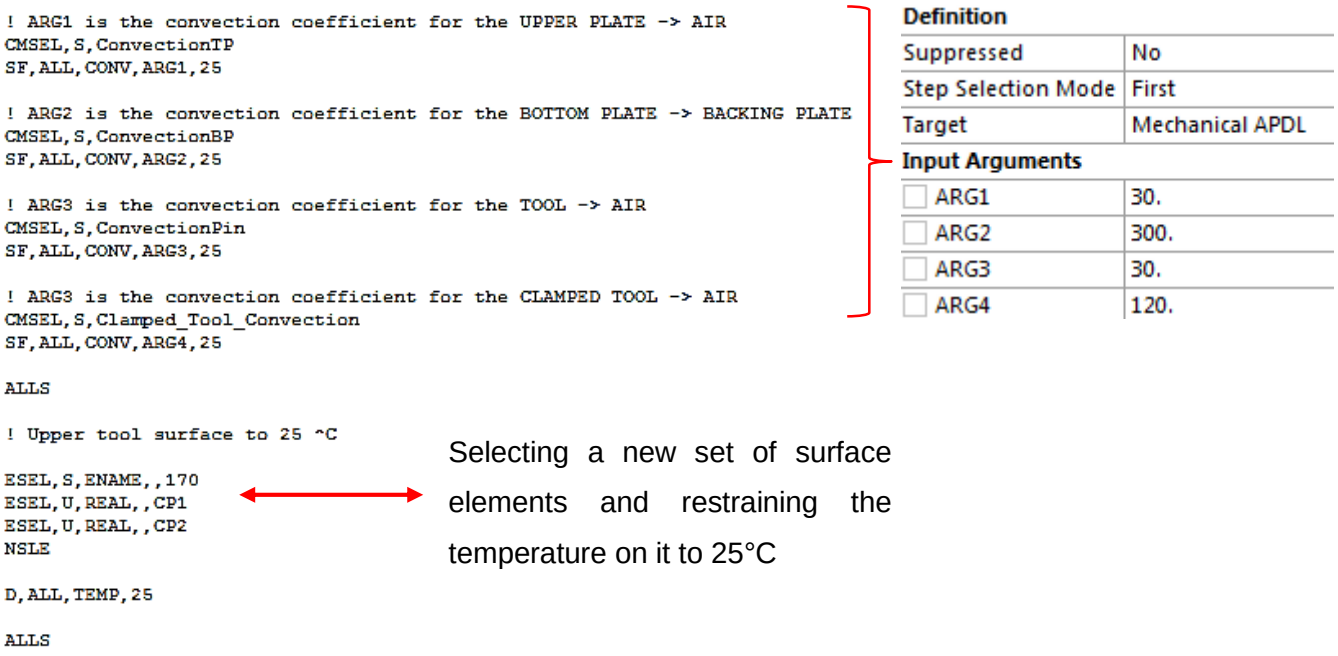


Figure 3.6: Thermal boundary command

CMSEL

CMSEL, *Type, Name, Entity*
Selects a subset of components and assemblies.

The Type is set to S- Selects the new set which in this situation the surfaces where given named selections and correspond to each surface according to its name.

SF

SF, *Nlist, Lab, VALUE, VALUE2*
Specifies surface loads on nodes.

Nlist is specified to ALL, so all nodes that are selected are to be used with which the surface load to be applied is set.

Lab is the surface load label and this is defined, for the thermal input, which CONV is used which indicates the convection on the surface.

VALUE is the surface load value that one sets and this is set to the ARG whereby an input value can be inserted easily instead of inserting it here on the command. Instead it reads the ARG value set under the workbench tree.

VALUE2 is the second load value if applicable. It is set to 25 to and this is the bulk temperature for the thermal analysis when the CONV command is used.

These above thermal boundary conditions assume the following;

- The clamped tool piece and backing plate is assumed to be exposed to air and given convection coefficients instead of conduction (since it is between material to material and not material to air) Their values are therefore an estimate and although is not a true representation it is a good estimation for the model in order to process the heat generated from the tool to work piece.

The commands inserted for the contact conditions are as follows for each contact surface beginning with the multiple contact and then the contact between the two work pieces which come together;

- Friction coefficient changing with temperature is defined for the contact between the tool shoulder surface and top work piece surface
- Thermal contact conductance is specified between the tool and work piece surface
- The amount of frictional energy converted to heat is specified

- Heat distribution from tool surface to work piece is specified. This number is that corresponding to the amount of heat generated by the shoulder to the work piece and is related to the tool geometry.

The KEYOPT command selects the relevant elements for the command to apply.

KEYOPT

KEYOPT, *ITYPE, KNUM, VALUE*
Sets element key options.

ITYPE is the element type number which corresponds to various options set out in the ET command. This is the contact type which is equal to the parameter and is defined as the CID. Two CID variations exist, where one indicates “The type number for the contact type is equal to the parameter CID”, the other refers to the following, “The real and mat number for asymmetric contact pair is equal to the parameter CID”. Depending on each command, each is applicable.

The command for the friction coefficient changing with temperature, frictional heat dissipated which is converted to heat and the heat distribution is depicted below in Figure 3.7 for the command between tool surface and work piece contact.

```
KEYOPT,CID,1,1

tb,fric,CID,6          !Definition of friction coefficient at
                       !different temp
tbtemp,25
tbdata,1,0.4           !friction co-efficiet at temp 25
tbtemp,200
tbdata,1,0.4           !friction co-efficiet at temp 200
tbtemp,400
tbdata,1,0.4           !friction co-efficiet at temp 400
tbtemp,600
tbdata,1,0.3           !friction co-efficiet at temp 600
tbtemp,800
tbdata,1,0.3           !friction co-efficiet at temp 800
tbtemp,1000
tbdata,1,0.2           !friction co-efficiet at temp 1000

rmodif,CID,9,500e6     !Max.friction stress
rmodif,CID,14,ARG1     !Thermal contact conductance b/w tool and
                       !workpiece, 10 W/m^2'C
rmodif,CID,15,1         !A real constant FHTG,the fraction of
                       !frictional dissipated energy converted
                       !into heat
rmodif,CID,18,ARG2     !A real constant  FWGT, weight factor for
                       !the distribution of heat between the
                       !contact and target surfaces, 0.95

CP2=CID
```

Definition	
Suppressed	No
Target	Mechanical APDL
Input Arguments	
ARG1	10.
ARG2	0.95

Figure 3.7: Contact condition command for the tool surface and work piece surface contacts

TB

TB, *Lab, MAT, NTEMP, NPTS, TBOPT, EOSOPT, FuncName*
Activates a data table for material properties or special element input.

This command activates the table for material properties to be set. For the current study since friction is changing with temperature, a table for the friction coefficients changing with temperature are set.

Lab is set to *fric* and this is the material model data type that is being specified to be the friction coefficient

TBTEMP

TBTEMP, *TEMP, KMOD*
Defines a temperature for a material data table.

The TEMP is set to a value corresponding to that value as outlined in C1 in TBDATA.

KMOD is left for blank for a new temperature to be redefined and reactivated

TBDATA

TBDATA, *STLOC, C1, C2, C3, C4, C5, C6*
Defines data for the material data table.

STLOC is set to 1 in order for this value to correspond to the first value set for the table constant.

C1 is the value defined for the chosen property, for this command in particular is the friction coefficient value set for a particular temperature.

RMODIF

RMODIF, *NSET, STLOC, V1, V2, V3, V4, V5, V6*
Modifies real constant sets.

NSET is the existing set to be modified which is defined as the CID.

STLOC is the starting location for the modified data and is required to be greater than 1. This data input corresponds to the number defined for that constant set. For each various input, a different number is defined for this.

V1 is the value set for each property indicated with the comments alongside.

The thermal boundary conditions as explained, are shown visually in Figure 3.8.

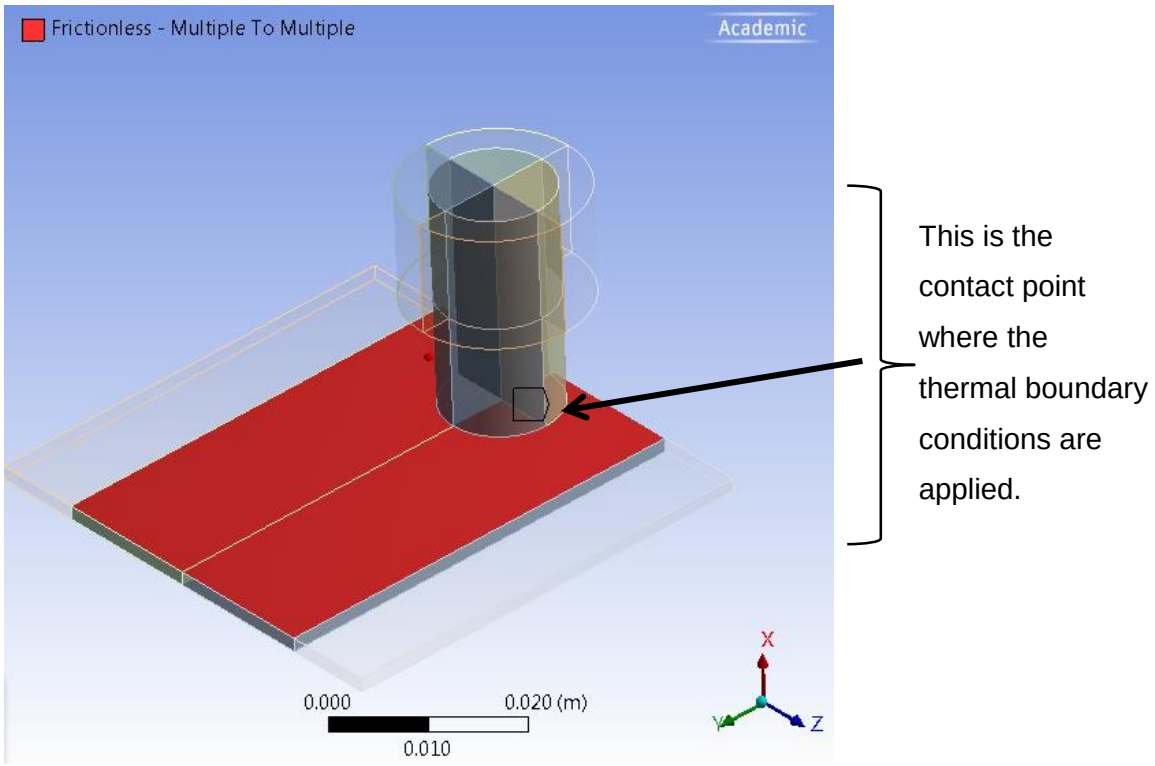


Figure 3.8: Thermal boundary conditions between tool shoulder surface and work piece surface

The command set for the contact surfaces between the two plates are as follows and shown in Figure 3.9 in detail relating to each argument set.

- Thermal contact conductance coefficient is given between the two work piece contacts
- A bonding temperature is given between the two work piece contacts. This command changes the frictionless contact to a bonded contact once the specific temperature is exceeded. (This temperature is set to approximately 80% the melting temperature for work piece material since the material under consideration is to only plasticize and not melt.

```
KEYOPT,CID,1,1
KEYOPT,CID,4,3

RMODIF,CID,14,ARG1   !A real constant TCC,Thermal contact
                     !conductance coeffi. b/w the plates, W/m^2'C
RMODIF,CID,35,ARG2   !A real constant TBND,Bonding temperature
                     !for welding, 'C

CP1=CID
```

Definition	
Suppressed	No
Target	Mechanical APDL
Input Arguments	
ARG1	2.e+006
ARG2	451.8

Figure 3.9: Thermal boundary condition command between work piece surfaces

The above command set out for RMODIF is outlined previously but as indicated, the various ARG values correspond to different aspects of the model. Again, with the set up as above with the ARG values as inputs, it is easy for these parameters to be inserted into an optimisation

tool since the model is parametric and these values can be easily called into the optimisation tool.

The frictionless contact is shown within the ANSYS model in Figure 3.10, where the thermal boundary conditions as explained above are inserted.

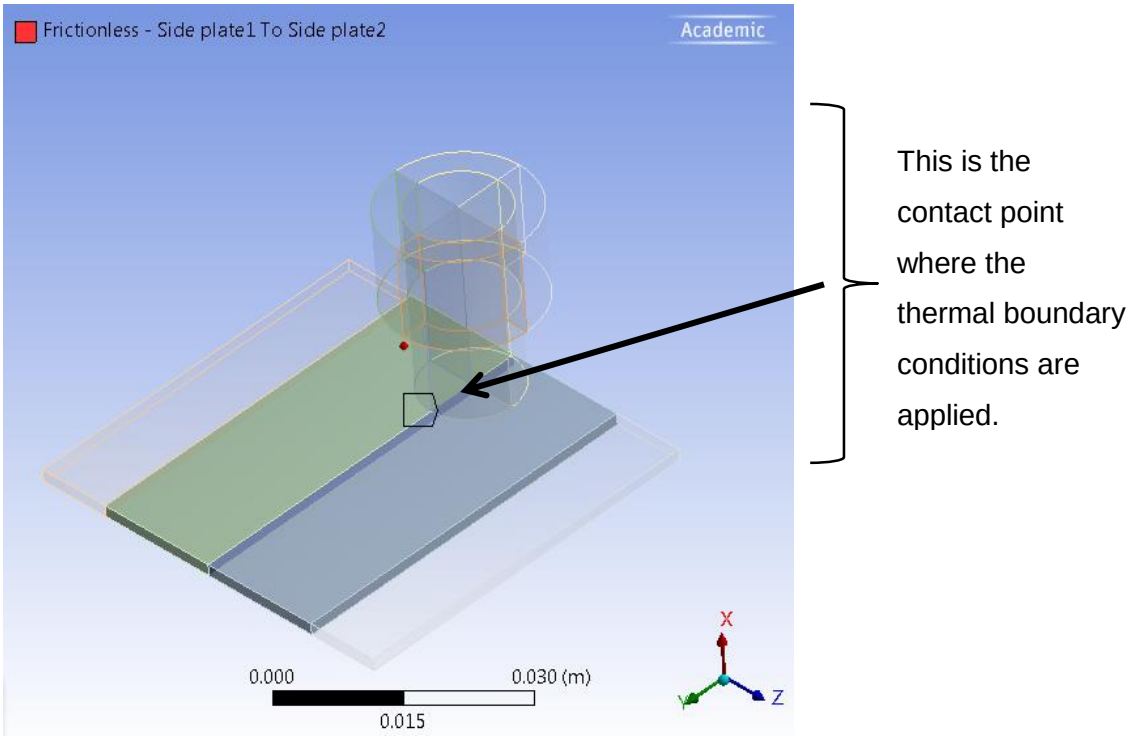


Figure 3.10: Frictionless contact between two plates

3.3.4 Analysis

From previous models, all three steps of the FSW process are considered (Plunge, dwell and transverse speed). For simplification purposes and time constraint, the model was reduced to the first two steps of the FSW process. A pilot node was created (Figure 3.11) on the top of the tool, to allow for plunging force and rotation conditions to be applied. This based on the different phases for the model as described in Figure 2.1. We assume three phases, plunge, dwell and transverse speed or feed rate. Since each phase has a condition set to it, this pilot node allows an easy way of inserting these parameters for each phase.

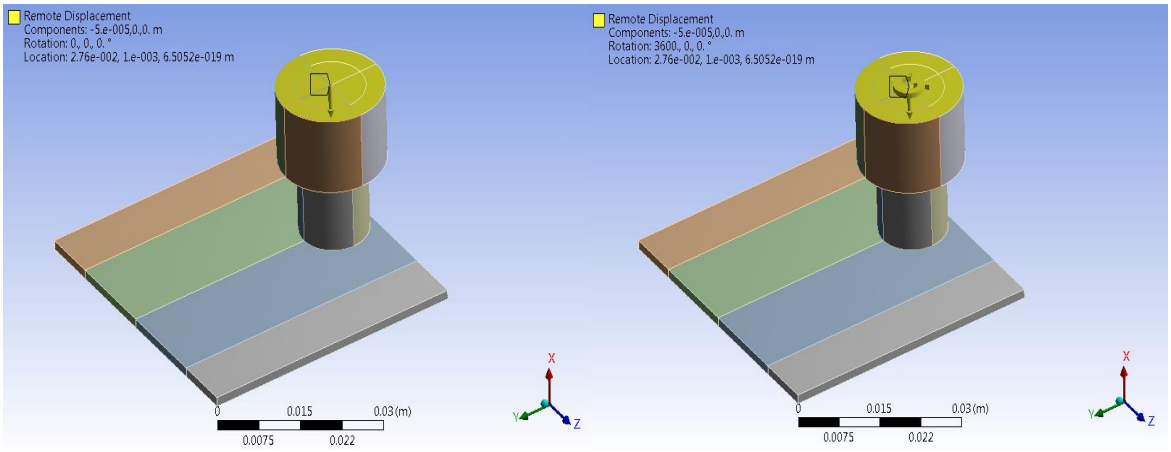


Figure 3.11: Remote point located for the two time steps for plunge and rotation

Initial models had all three phases represented in the model and the dwell time set to 10 seconds since this was the time allocated for the weld trials of the dwell time. The third phase had a time set to the same time corresponding to that of the weld trial time taken to complete a weld.

The initial time step is fairly quick, having 5 iteration steps most of the time since the 1 second is analysed after every 0.2 seconds. This is the initial plunge into the work piece.

The second time step is more involved. Initially it was solving for every time increment of 0.001 seconds and converging for the force, heat flux and moment conditions. This proved to take a lot of processing time, since convergence sometimes only happened after 10-20 iterations for that time step of increment 0.001 seconds and sometimes only increasing by the minimum set number of 0.0001 seconds. The time for the dwell time was then decreased to a lower number. This still proved to take a lot of processing time and so sub-steps was chosen that it analyses every few degrees until a certain degree and this takes the time allocated and distributes it accordingly. This proved to be better than before but still a lot of processing time took place, except convergence took less iterations, but time increment was smaller than before. It was then decided since this second phase took a long time, the third part of the model was to be taken out and until the second phase of the modelled solved sufficiently and had produced results of an acceptable standard, this could then be used to be inserted in the final phase of a model, whereby this model would only consist of the third phase. The third model is essentially set up based on the model already created except without the first two time steps. However, this final model was never run since the current model with two time steps still continued to solve without exact completion, due to at times large deformation effects or allocated memory to be exceeded.

Time steps are put into place for each part with the corresponding plunge depth and rotation value. These inputs for the plunge depth and rotation example can be seen in Table 3.3.

Table 3.3: Depiction of pilot node setting in ANSYS workbench

	Steps	Time [s]	X [m]	Y [m]	Z [m]	RX [°]	RY [°]	RZ [°]
1	1	0.	0.	0.	0.	0.	0.	0.
2	1	1.	-5.e-005	0.	0.	0.	0.	0.
3	2	3.	= -5.e-005	0.	0.	3600.	0.	0.

A command is inserted whereby the elements are changed to a SOLID226, this enables the elements to be analysed in a structural setting with thermal inputs, since this model is a thermo-mechanical one.

Various rotational calculations were done in order to insert the correct value in the Rx column in the table above.

Method 1

1. RPM x 2π/60=rad/sec X time (indicated in table) = radians
2. Convert to degrees

Method 2

Indicate 3600°

In the side property sheet number of sub steps in stage two indicate the degrees the tool turns in that space of time. E.g. for the tool to move 5°, the sub step is made 720 (For a set number of 3600°)

3.3.5 Parametric model features

It is important to note the following features of the developed model as described above. Based on the APDL commands set in section 3.3.3 Boundary conditions and contacts, it allows these parameters that have been inserted as physical values, to be integrated into an optimisation platform such as modeFRONTIER. These parameters include;

- Convection coefficients set for the various surfaces
- Friction coefficient changing with temperature
- Heat dissipation factor for the contact surfaces between the tool and work piece
- Fraction of the heat dissipated by means of frictional energy which is converted to heat
- Contact conductance coefficient set between the two work piece surfaces on the join line.

It is imperative for the following considerations to be mentioned with the above as this limits the results obtained and hence the optimisation of the model itself. This model has been developed as a parametric model which allows it to be easily integrated with an optimisation platform but the limit of the whole model comes in terms of the computational capability of the computer itself. As mentioned briefly in the analysis with regards to the time allocated for each step and the actual computational processing time.

In order for computational capability to be at its best it is, it is suggested that a cluster to be used in order to process the data faster and hence more results for comparison can be obtained. But due to limited resources available and the real time taken to process a set of results, the final results obtained are extremely valuable for the current study not only for result comparison with experimental data but for the implementation of it into an optimisation tool.

3.4 Summary

A FE model has been created using ANSYS version 14.5 software. Whereby it makes use of the SOLID226 elements. This element allows for a thermal mechanical model to be created as thermal inputs can be inserted within the mechanical interface of workbench.

With set geometry specified according to the same geometric properties of the tool which is to be used in the weld trials, these same geometric dimensions are used to create the geometry of the model. The boundary conditions are explained where certain thermal input commands have been inserted to account for material properties changing with temperature. One particular command is of essential use to the simulation of FSW process as it generates heat within the model by changing the frictionless contact to a bonded contact.

Analysis of the model includes the phases of the FSW process, and explains the individual steps used via a pilot node which was created on the top surface of the tool. The phases included in the model is for the plunge and dwell. The transverse phases has been eliminated for the moment for the time period of the study.

Important parameters of the model, have been outlined and are important when optimising the model in an optimisation tool such as modeFRONTIER.

Chapter 4

4. Experimental Weld Trials

4.1 Introduction

Weld trials were performed whereby certain parameters such as the rotational speed and the feed rate were specified and programmed into the CNC machine. The material for the work piece and tool piece is described briefly and needs to be known since different material properties relate to various values affected by temperature and in order to make a fair comparison with the FEA model, these properties need to be specified accordingly. The whole FSW process was recorded using the thermal imaging camera T640. Using the FLIR Tools + software one is able to process the temperature field of the FSW process.

4.2 Apparatus

The apparatus used for the experimental weld trials include the programmable CNC machine and FLIR thermal imaging camera T640.

4.2.1 CNC machine

Depicted below in Figure 4.1 is a representation of the experimental setup of the tool within the CNC machine together with the two plates clamped on either side.

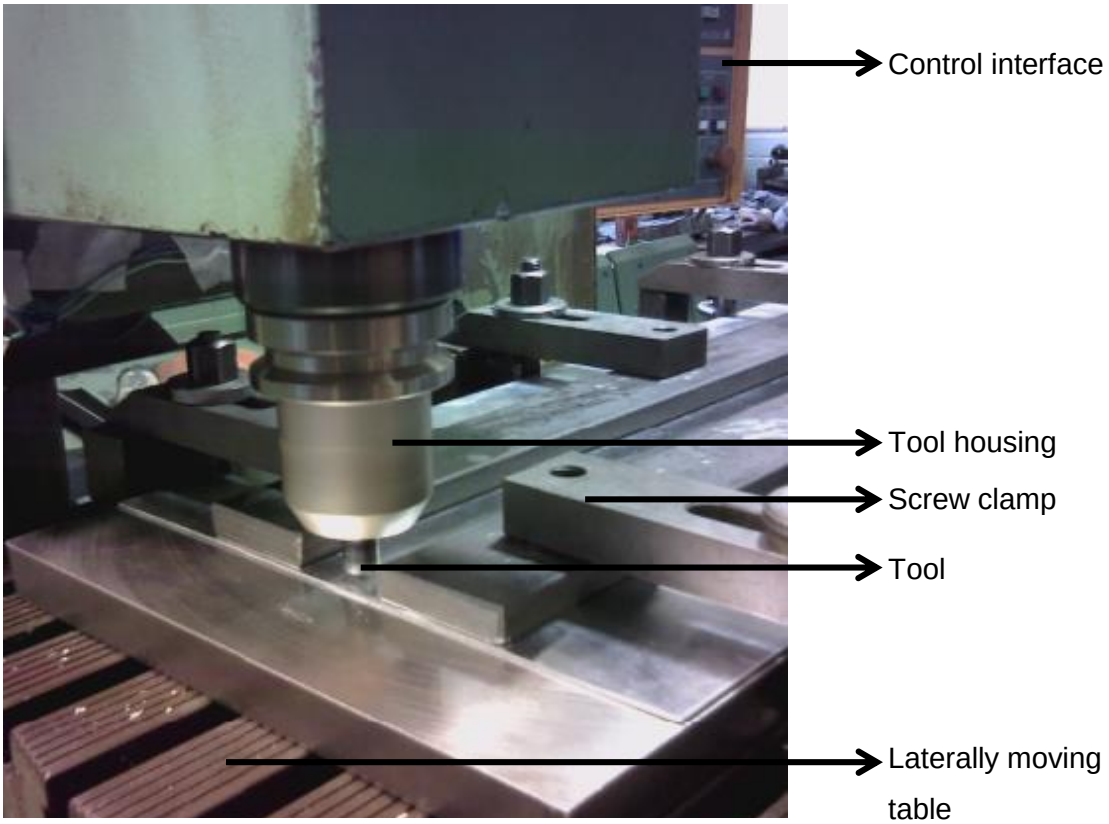


Figure 4.1: CNC Machine

Technical specifications for the CNC machine area are outlined in Appendix 4: CNC information.

4.2.2 FLIR Systems

The company was started in 1978 [61] and is a world leader in the design, manufacture and marketing of thermal imaging infrared cameras. They cater for various industries which are categorised as follows;

- Commercial
- Industrial
- Government

The above categories rely on different uses and developments within the infrared thermal imaging camera. It measures the emitted infrared from an object and dependent on the emissivity of the object as well as radiation [62]. The emissivity of various aluminium specifications can be found in the

The current use is associated with the research and development of the infrared thermal camera. Some advantages of using this method for capturing and recording thermal distribution [63]

- Real time recording allows for an accurate measurement of heat patterns across surfaces during processes
- Particularly to manufacturing it enables an improvement in adjusting process parameters by detecting defects on the material in a non-destructive way

Together with the thermal imaging camera the FLIR tools + is used to process the temperature information, whereby inspection reports can be created.

4.2.2.1 Thermal camera T640

For visual purposes and with new technology reaching into the photography industry, one is able to examine surfaces and see the varying temperature of the surface through the lens of a camera. For the purpose of the study being undertaken, the T640 thermal camera is to be used to help capture the varying temperature of the tool on the work piece.

The T640 thermal camera has many qualities contributing to its use. It has a 640 x 480 pixel resolution [64]. This high definition will enable a more accurate inspection of the image. Other attributes include a high sensitivity to temperature variations as small as 0.04°C as well as a “radiometric IR video streaming” which can be connected to a PC and using the FLIR tools

software can record live video streams which can be analysed at a later stage using the FLIR tools + software. [64]

The T640 thermal camera has three standard temperature ranges that are required to be set when operating the camera. The accuracy of these temperatures is within a ±2°C or ±2% of the reading [63]. The standard temperature ranges are listed as follows;

- -40°C – 150°C
- 100°C – 650°C
- 300°C – 2000°C

With these temperature ranges set and used with the specified software a profile measurement analysis can be done which depicts a live graph of temperature across a specified line on the image [65]. This is an important feature when one is required to process the information once the stream of video has taken place. The camera used is represented in Figure 4.2 [66]



Figure 4.2: T640 thermal camera

4.2.2.2 Specifications

The following specifications [67] relate to the FLIR T640 thermal camera

Table 4.1: Thermal camera specification

Specification detail	**Value**
Infrared resolution	640 x 480 pixels
Thermal sensitivity	40mk
Accuracy	±2°C
Temperature range	-40°C to 2000°C
Focal length	25mm
Emissivity correction	0.01-1

4.2.2.3 Calibration

In order to read the correct temperature of the reflected surface, the emissivity value needs to be determined. Based on a simple test, using a thermocouple and thermal camera the following calibration procedure was performed.

1. Heat the aluminium sheets and tool in an oven to temperature of about 200.
2. Remove the test piece carefully and place on a surface that will not absorb the heat quicker than one will be able to record the temperature.
3. Place the thermal couple on a position of the test piece.
4. At the same time, using the thermal camera, locate the same area in which the thermocouple is placed.
5. Reading the thermal couple temperature value, match the temperature on the thermal camera by changing the emissivity value.
6. When the temperature value on the thermal camera is matching the thermo couple temperature, use the emissivity used as the calibrated emissivity of that particular surface.

4.2.2.4 Precautions

1. Ensure the angle which the temperature is being read on thermal camera is less than 45° to the test piece surface as this will affect the emissivity value.

4.2.3 Tool and work piece properties

The information used in the FEA model was taken from Figure 4.3 [60]. This is also the tool that was used to perform the weld trials. It depicts a more detailed dimension of the tool and one is able to see clearly the shoulder geometry as well as where the pin is inserted into the tool. These dimensions are important when developing the model as well as analysing the heat generation since the surface of the tool is which dominantly creates this.

Material of the work piece and tool are Aluminium alloy 6056 (Although the properties of this material are very similar to AA2024, hence these properties will be used) and H13 tool steel respectively. Each of the properties for each are briefly described in Table 4.2

Table 4.2: Material properties of tool and work piece

Material property	Aluminium alloy 2024	H13 Tool steel
Density (kg/m^3)	2780	7760
Young's Modulus (GPa)	73.1	210

Ultimate tensile strength (Mpa)	475	1400
Coefficient of thermal expansion (/°C)	22.9	12.3
Specific heat (J/g-°C)	0.875	0.457
Thermal conductivity (W/m-K)	121	27.7
Melting temperature (°C)	502°C -638°C	817

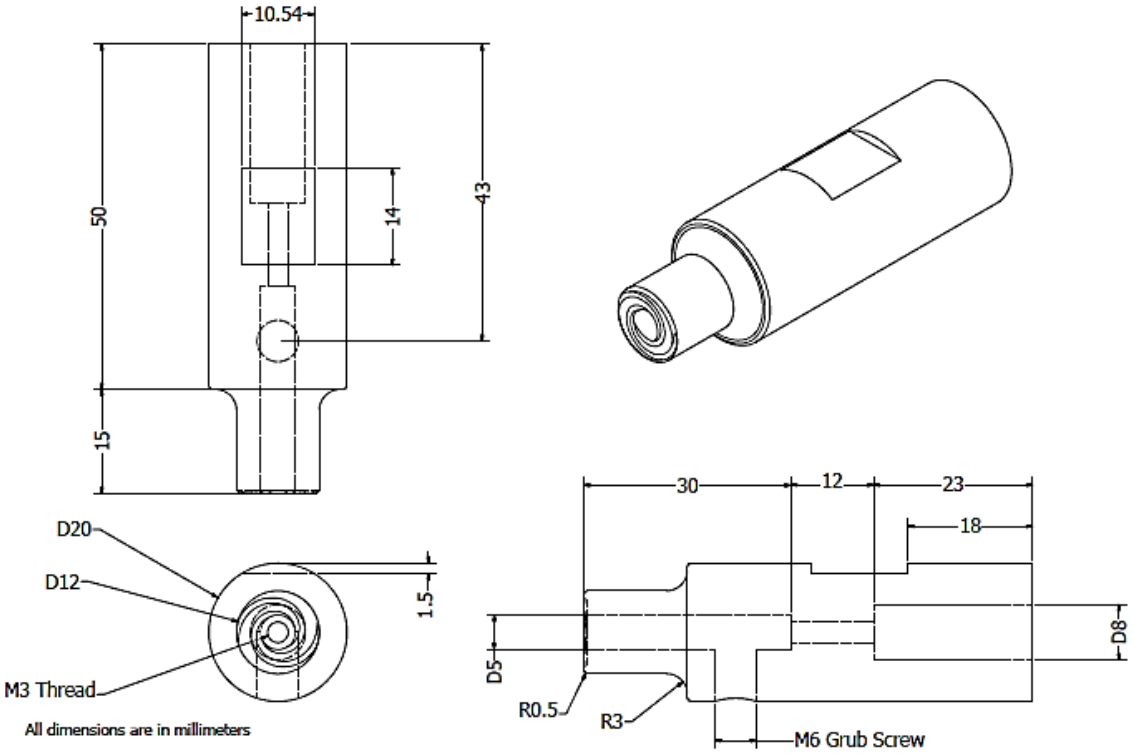
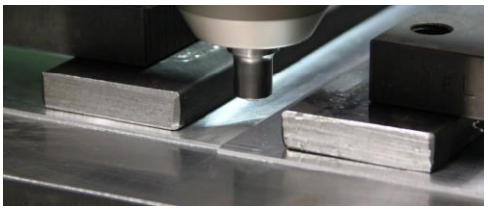


Figure 4.3: Tool geometry

The material and geometry of the tool and the work pieces is given in the Table 4.3. This information is especially important when the FEA model is developed.

Table 4.3: Tool and work piece geometry

Properties	Work piece	
Material	AA 6056 (Similar to AA2024)	
Length	400 mm	
Breadth	250 mm	
Thickness	1.6 mm	Clamped work piece

	Tool	
Material	H13 Tool steel	
Shoulder radius	12 mm	
Pin radius	5 mm	
Outer tool radius	20 mm	
Shoulder height	15 mm	
Pin height	1.4 mm	
Overall tool height	50 mm	

4.3 Methodology

The setup of the CNC machine and of the thermal camera are given in the following sections. Precautions are given as a guidance for those wanting to repeat the experiment and have results which are able to be repeated for the same inputs and dynamics of the machine and materials used.

4.3.1 CNC Setup

1. The two plates are cleaned with alcohol/acetone and placed onto the CNC table where it is clamped down.
2. The tool is inserted into the bushing and into the CNC machine spindle.
3. Position the tool so it touches the line of the plates to be welded.
4. The parameters for the tool are inserted into the machines settings.
    a. Rotation
    b. Plunge
    c. Dwell time
    d. Feed rate

4.3.1.1 Precautions

- Ensure the alignment of the tool is in position of the line of the two plates to be joined. This is achieved by running a needle along the one plate line and ensuring its running along the same line, then the other plate is aligned to it.

4.3.2 Thermal camera setup

1. Connect the camera to the computer.
2. Open the FLIR Tool + software
3. The camera settings are programmed for the respective temperature ranges and the emissivity value is adjusted according to the calibration.

4. The camera is placed on a tripod, above the work piece, with a clear view of the weldment that is to take place.
5. The angle of the camera is positioned so that it is not greater than 45° to the vertical. (this is based on the information described in the emissivity literature)

4.3.2.1 Precautions

- Ensure the correct temperature range is set for the respective weld trial
- Confirm the angle is not greater than 45° to the vertical

4.4 Summary

The setup of the apparatus for the experimental FSW process has been described. The CNC machine has been clearly defined together with the tool and work piece geometry and ambient material properties have been given.

The thermal camera functions and precautions have been detailed where the emissivity value defined when recording the temperature of the surface needs to be calibrated. Essential precautions for the setup of the thermal camera have been highlighted especially the angle at which the camera is positioned is also very important as this affects the emissivity value defined.

Chapter 5

5. Data Processing

5.1 Introduction

The data obtained from the FEA modelling is analysed and based on section 2.3.5 Parameters of interest based on prior models, these variables are calculated and compared to information captured experimentally with the thermal imaging camera. Temperature and heat variables are concentrated on since this will be used for the comparison of data and since experimentally, we have temperature data readily available it reasons to use this for comparison.

The FEA model parameters are initially discussed to obtain the variables for various thermal outputs obtained as is the experimental data also done in this way. Since the FEA model has defined inputs for these thermal properties, and is therefore available for comparison once these thermal properties have been calculated for the experimental weld trials. For both the FEA and weld trials however, heat flux can be calculated and compared as well.

5.2 Finite Element Modelling

The following outlines the various models developed with different inputs.

- The number of load steps with the time for each step indicated in seconds
    - First time step always 1 second and represent the plunging force.
        - Plunge depth of 0.1mm for model number 1-2 and 4-5.
        - Model number 3 has a smaller depth of 0.0008mm.
        - Model number 6 plunge depth is 0.01mm
        - Thereafter, model 7-16 plunge depth is set to 0.05mm
    - Second time step
        - Initial models time allocated was according to weld trial times set of 10 seconds for dwell time. This is later changed to a lower number for processing purposes.
        - Rotational speed is allocated at this step
    - Third time step
        - Model 1- 6 have a distance along the y-axis allocated to the length of the plate in the model, 230mm
        - Remaining models do not have the last time step (allocated to the feed rate along the weld line) due to excessive running time

        - The time set initially for this step is 46 seconds as this is the time worked out for the particular feed rate
        - $Feed\ rate = \frac{Distance}{time}$ therefore, $time = \frac{Distance}{Feed\ rate} = \frac{230\ mm}{300 mm/min} \times 60 = 46\ sec$
- Tool rotation- as seen in ANSYS model tabular data for rotation in x(RX (°))
- Convection coefficients
    - ARG1-Convection coefficient between top plate surface and air
    - ARG2- Convection coefficient between bottom plate surface and backing plate
    - ARG3- Convection coefficient between tool shoulder surface and air
    - ARG4- Convection coefficient between clamped tool surface and air
- Further comments are given on any parameters on interest, especially when changes are made to following models.

The following Table 5.1 represents the models that gave relevant results to be used for analysis. Although, more models were processed, it is important to extrapolate that data which is most useful for the current study.

Table 5.1: Model log book for different inputs

Model number	Tool rotation RPM (°)	Convection coefficient (W/mK)	Comments
1	1250 (130.83°)	• ARG1- 15 • ARG2- 300 • ARG3- 150 • ARG4- 360	Material properties for the aluminium alloy and H13 tool steel do not account for change in temperature for thermal conductivity and specific heat. 3 load steps are considered, for the plunge, dwell and feed rate respectively
2	1250 (130.83°)	• ARG1- 15 • ARG2- 3000 • ARG3- 150 • ARG4- 3600	
3	(209.44°)	• ARG1- 15 • ARG2- 300 • ARG3- 150 • ARG4- 360	

4	2 –(75000°) 3 – (345000°)	• ARG1- 15 • ARG2- 300 • ARG3- 150 • ARG4- 360	
5	2 –(7500°) 3 – (34500°)	• ARG1- 30 • ARG2- 300 • ARG3- 30 • ARG4- 120	
6	2 –(37500°) 3 – (207000°)	• ARG1- 30 • ARG2- 300 • ARG3- 30 • ARG4- 120	
7	(3600°)	• ARG1- 30 • ARG2- 300 • ARG3- 30 • ARG4- 120	New geometry is implemented by reducing the model size in order to reduce mesh elements and therefore processing time. Only two load steps are now considered, plunge and dwell.
8	(3600°)	• ARG1- 30 • ARG2- 300 • ARG3- 30 • ARG4- 120	
9	(3600°)	• ARG1- 30 • ARG2- 300 • ARG3- 30 • ARG4- 120	
10	(3600°)	• ARG1- 30 • ARG2- 300 • ARG3- 30 • ARG4- 120	Material properties changing with temperature are implemented for the two materials where before some only had one value considered at room temperature.
11	(3600°)	• ARG1- 30 • ARG2- 300 • ARG3- 30	

		• ARG4- 120	
12	(3600°)	• ARG1- 30 • ARG2- 300 • ARG3- 30 • ARG4- 120	
13	(3600°)	• ARG1- 30 • ARG2- 300 • ARG3- 30 • ARG4- 120	
14	(3600°)	• ARG1- 30 • ARG2- 150 • ARG3- 30 • ARG4- 120	
15	(3600°)	• ARG1- 30 • ARG2- 100 • ARG3- 30 • ARG4- 120	
16	(3600°)	• ARG1- 30 • ARG2- 200 • ARG3- 40 • ARG4- 120	
17	(3600°)	• ARG1- 30 • ARG2- 200 • ARG3- 40 • ARG4- 120	
18	(3600°)	• ARG1- 30 • ARG2- 300 • ARG3- 40 • ARG4- 120	
19	1250 (22500°)	• ARG1- 30 • ARG2- 300 • ARG3- 40 • ARG4- 120	
20	1250 (22500°)	• ARG1- 30 • ARG2- 300	

		• ARG3- 40 • ARG4- 120	
21	1250 (22500°)	• ARG1- 10 • ARG2- 300 • ARG3- 30 • ARG4- 120	

Based on the models, the following temperature results are represented in Figure 5.1. From time of 1 second, this is representative of the dwell time in the second time step. One can see that the temperature increases remarkably in a short space of time in the model.

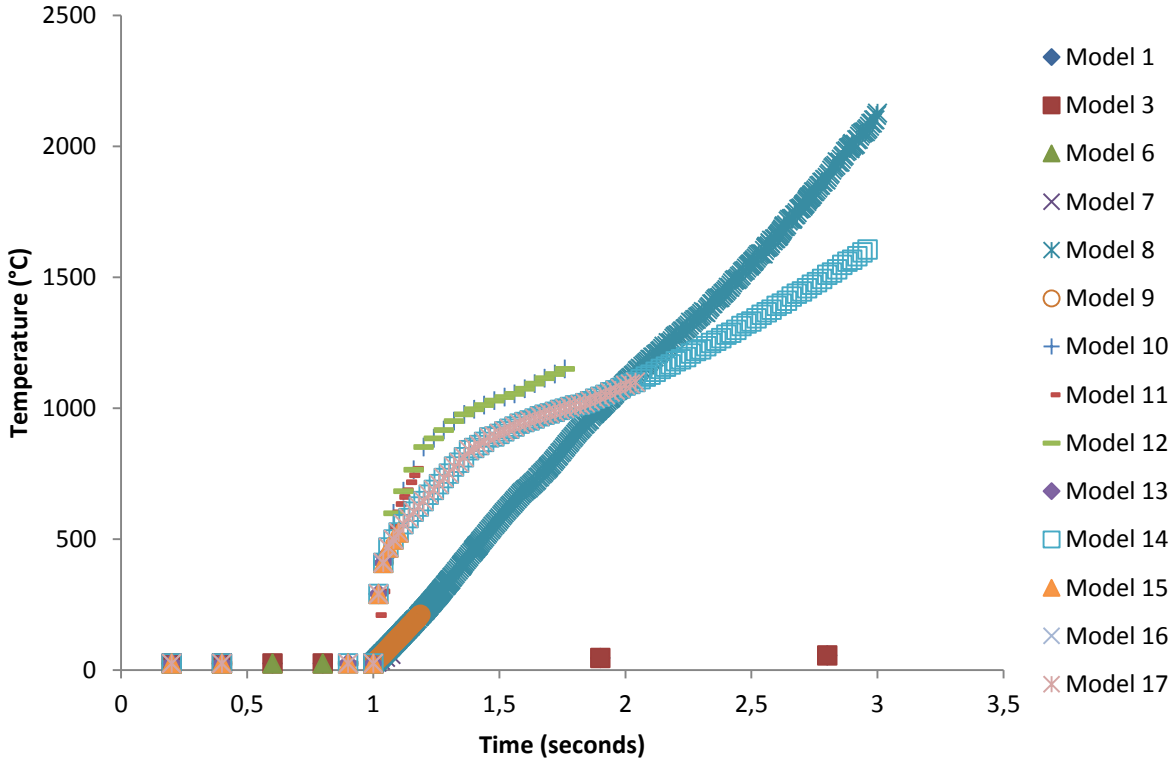


Figure 5.1: Temperature comparisons with various models

Calculating the heat flux transfer for each part in the model is related to the convection coefficient outlined in Table 5.1 and change in temperatures taken from the temperature results of the model. Total processed data can be found in Appendix 6: FEA model processed data.

5.2.1 Sample calculation for heat flux for FEA model

Heat flux is calculated as follows for the FEA model, since the convection coefficients and temperature values are known, one only requires the equation below [50] to calculate the heat transfer of each.

$$Q = h(\Delta T) \quad 5.1$$

For the heat transfer of the clamped tool of model 8 and average change in temperature taken as 853°C, where the convection coefficient is set to 120 W/m^{2}K

$$Q = 120(853)$$

$$Q = 102.4\ kW/m^2$$

5.2.2 Heat transfer values for FEA model

Table 5.2 displays the heat flux transfer. This is the average heat flux transfer calculated over the entire length of time for the dwell time.

Table 5.2: Heat flux transfer (kW/m^2) for various FEA models

Model Number	Heat flux transfer clamped tool	Heat flux transfer Shoulder of tool	Heat flux transfer from top plate	Heat flux transfer from bottom plate
8	102.4	25.6	60.95	256.09
10	109.03	27.26	42.21	272.58
12	109.03	27.26	42.21	272.58
14	127.19	31.80	59.11	158.99
17	100.08	25.01	45.29	166.79

Represented graphically in Figure 5.2, is to show the heat distribution of the heat generated from the tool to the work piece. Also shown between the surfaces is the frictional stress created between the tool and work piece surfaces. This frictional stress, gives some insight into the parts of the tool and work piece where there is higher frictional stress in areas as the tool rotates revealing that a higher temperature is expected at that point.

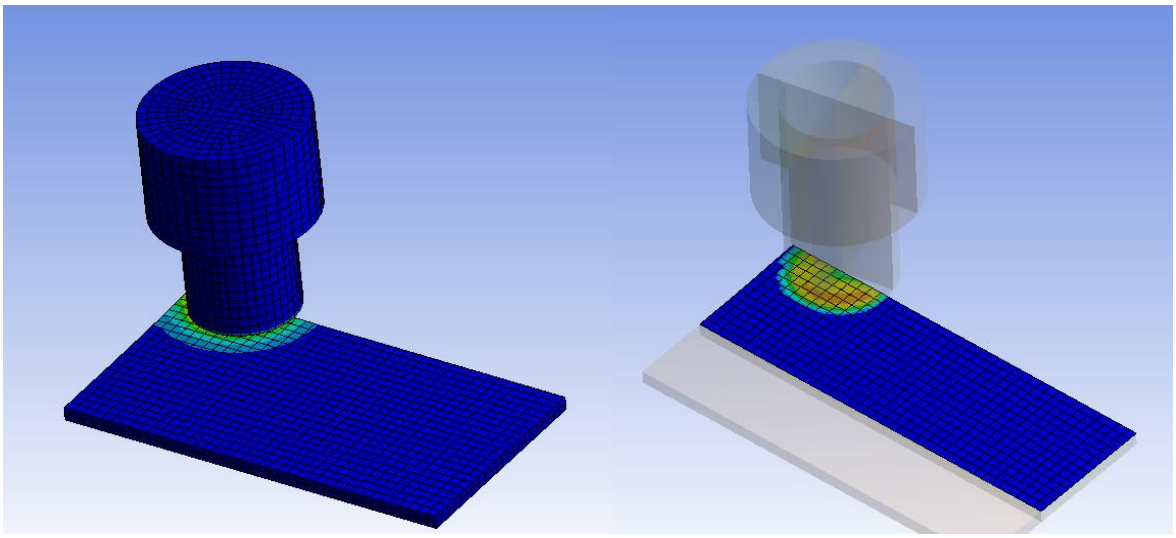


Figure 5.2: Heat distribution and frictional stress from tool to work piece

Figure 5.3, closely reveals the frictional stress between the surfaces and indicates where the frictional stress is higher as well as the direction of rotation is visible.

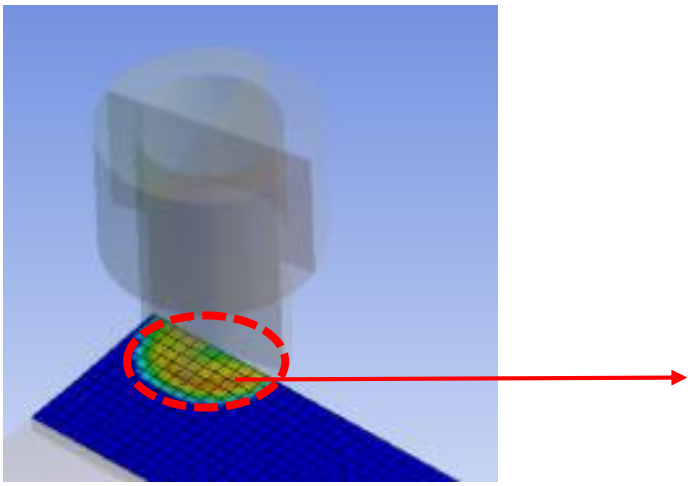
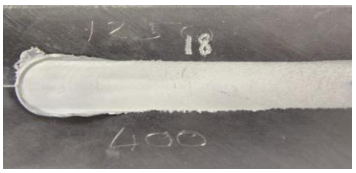
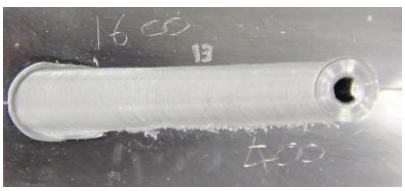


Figure 5.3: Frictional stress region between tool surface and work piece surface

5.3 Weld Trials

The following Table 5.3 represents the weld trials performed under various FSW process parameter conditions as indicated. The tool used is that as described in Figure 4.3 together with the aluminium alloy specified in Table 4:3.

Table 5.3: Weld trial parameters with images

Trial number	Rotation (rpm)	Feed rate (mm/min)	Images
1a	1250	400	
1b	1600	400	

1	1250	300	
2	1250	400	
3	1250	500	
4	1600	400	

Thermal imaging data

1. Spots were placed in areas of interest and temperatures were recorded along that point for the weld time. Average temperatures along the tool are also noted.
2. Based on these locations, temperatures at different times are considered for the dwell time and compared with temperatures of other weld trials.
3. A temperature increase rate is determined for each weld

4. Total heat transfer based on theory is calculated and is used to determine an approximate value for the convection coefficients to match this value. A contact variable is assumed to be sticking to calculate the aforementioned.
5. Further, these temperatures are determined along an approximate point of the weld line to compare with FEA.
6. The heat transfer can be used to compare with that of the FEA and conclusions may also be determined from the assumptions and approximations made.

5.3.1 Sample calculation for heat transfer values

Total heat transfer is calculated for the various conditions for the contact between the surface, namely, sticking, sliding or a combination of these two. The common parameters for describing the tool are outlined in Table 5.4;

Table 5.4: Tool parameters values

Symbol	Description	Value
R_s	Shoulder radius	12 mm
R_p	Pin radius	5 mm
R_c	Clamped tool radius	20 mm
H_p	Pin height	1.4 mm
ω	Rotation speed	130.9 rad/sec
A_S	Area of shoulder	113.1 mm^2
A_c	Area of clamped tool	314.16 mm^2
v	Velocity (ωr)	0.785 m/s (Shoulder speed)

Sticking condition, assumes the shear contact is equal to the yield stress of the material over the square root of three, therefore based on equation (2.17 the total heat generation is;

$$\tau_{contact} = \frac{\sigma_{ys}}{\sqrt{3}} = \frac{289MPa}{\sqrt{3}} = 166.85\ MPa$$

Therefore,

$$Q_{sticking,total} = \frac{2}{3}\frac{\sigma_{ys}}{\sqrt{3}}\pi\omega\left(\left(R_{shoulder}^3 - R_{probe}^3\right)(1-\tan\alpha) + R_{shoulder}^3 + 3R_{probe}^2 H_{probe}\right)$$

α= 0

So substituting the above parameters yields the result of;

$$Q_{sticking,total} = 11.08\ kW$$

For sliding conditions

$$\tau_{contact} = \mu P_{Contact}$$

$$P_{Contact} = \frac{F}{A_s}$$

The force is calculated using the CNC information given for the maximum power it has and for the maximum rotation it can produce. Based on Appendix 4: CNC information, the maximum power and maximum rotation it can produce is 2.2 kW and 2000 rpm respectively.

Assuming a linear relationship between these, and knowing the rotation of the test piece, an estimated power at which it is operating at for that particular rotation is therefore as follows;

$$\frac{Power}{Rotation} = \frac{P_{max}}{R_{max}} = \frac{P_1}{R_1}$$

$$\frac{2200}{2000} = \frac{P_1}{1250} \rightarrow P_1 = 1.375\ kW$$

$$\therefore F = \frac{P_1}{v} = \frac{1.375}{0.785} = 1.75\ kN$$

$$\therefore\ P_{Contact} = \frac{1.75 * 1000}{113.1 \div (1000 * 1000)} = 15.5\ MPa$$

The total heat transfer for pure sliding conditions is calculated using equation (2.18

$$Q_{sliding,total} = \frac{2}{3}\mu P_{contact}\pi\omega\left(\left(R_{shoulder}^3 - R_{probe}^3\right)(1 - \tan\alpha) + R_{shoulder}^3 + 3R_{probe}^2 H_{probe}\right)$$

$$Q_{sliding,total} = 411.2\ W$$

Then for a combination between sliding and sticking the heat transfer is between the values above;

$$Q_{sliding,total} < Q_{Combination,total} < Q_{sticking,total}$$

$$411.2\ W < Q_{Combination,total} < 11080\ W$$

The total heat flux is then calculated using equation 2.14;

$$q_{total} = \frac{3Q_{total}R_{shoulder}}{2\pi r_0}$$

Q_{total} is the total heat transfer for either sticking or sliding conditions

r_0 is the distance along the radius

$$q_{total,sticking} = \frac{3 \times 11080 \times 0.006}{2\pi \times 0.006} = 5291\ W/m^2$$

$$q_{total,sliding} = \frac{3 \times 411.2 \times 0.006}{2\pi \times 0.006} = 196.35\ W/m^2$$

Following relationships as described in section 2.3.5.1 Heat generation, the convection coefficients for the top surface of the work piece and bottom surface of the work piece are estimated. From equation 2.9,

$$q_2 = h_{q2}(T - T_0) + \varepsilon F \sigma_{SB}(T^4 - T_0^4)$$

$$q_2 = h_{q2}(T - (25 + 273.15)) + 0.11 \times 1 \times 5.67 \times 10^{-8}(T^4 - (273.15 + 25)^4)$$

$$Q_2 = h_{Q2}(T - 25)$$

For a temperature of 70.2°C= 343.35K

$$Q_2 = h_{Q2}(45.2)$$

$$q_2 = h_{q2}(45.2) + 37.4$$

The increase of heat content to the work piece described as Q is formulated as the additional heat flux

$$Q = h_Q(T - T_0)$$

$$Q = h_Q(45.2)$$

$$Q_1 = h_{Q2}(45.2) + h_{q2}(45.2) + 37.4 + h_Q(45.2)$$

The sum of convection coefficients

$$\frac{5291 - 37.4}{45.2} = h_{Q2} + h_{q2} + h_Q$$

$$116.23 = h_{Q2} + h_{q2} + h_Q$$

If we assume a percentage of each surface contributing to the heat transfer rate, estimation for the convection coefficients for each can be calculated. These percentage estimations are given in Table 5.5, where the convection coefficient value is also then calculated.

Table 5.5: Convection coefficients estimation for each contributing surface

	h_{q2} (W/m^{2}K)	h_{Q2} (W/m^{2}K)	h_Q (W/m^{2}K)
Percentage contribution	0.65	0.25	0.1
Value	75.5	29.05	11.62

Heat flux from tool shoulder equation 2.12 is as follows,

$$q_1 = \mu F \omega R 2\pi$$

$$q_1 = 0.4 \times 1750 \times 130.22 \times 0.006 \times 2\pi = 3455.75\ W/m^2$$

$$q_1 = q_1 A_S = 3455.75 \times 0.0001131 = 0.391\ W$$

If, $q_1 = h_{q1}(T - T_0)$, then

$$h_{q1} = \frac{q_1}{(T - T_0)} = \frac{3455.75}{45.2} = 76.45\ W/m^2K$$

This convection coefficient is only applicable for a temperature at 70.2°C.

This leads to the convection coefficient for the clamped tool to be calculated, using equation 2.6;

$$Q_3 = q_1 + Q_4$$

$$11080 = 0.391 + Q_4$$

$$Q_4 = 11080 - 0.391 = 11079.61\ W$$

$$h_{q1} = \frac{q_1}{A_C(T - T_0)} = \frac{11079.61}{0.000314 \times 45.2} = 35.27\ kW/m^2K$$

Average convection coefficients were calculated for the weld trails, based on the calculations above. The average convection coefficients are for the dwell period only. Table 5:8, represents the flux heat transfer for the different rotational speeds. It can be noted that for the same rotational speeds, the heat flux is the same as a result of the equation only have the tools parameters for influence and the contact stress which is influenced by the friction coefficient (which is assumed constant at a value of 0.4, for simplicity purposes for calculation) and force acting upon the work piece. If there are to be discrepancies for the values, this will surely come into effect with the force value, and should be determined experimentally as well.

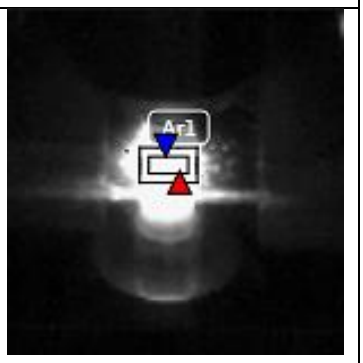
Though, for the purposes given a force value (dependant on the rotational speed) was determined and used in all calculations.

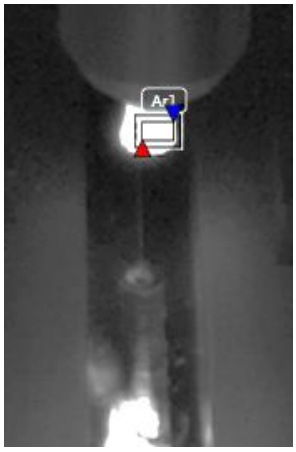
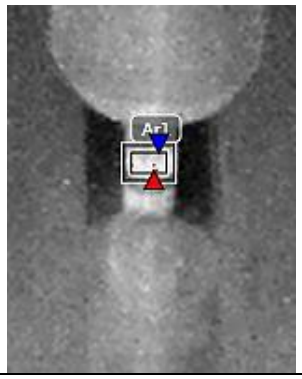
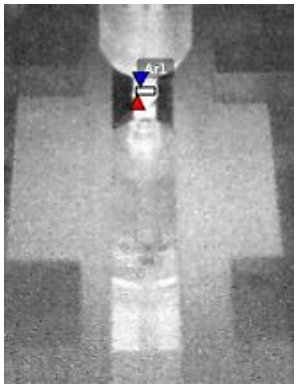
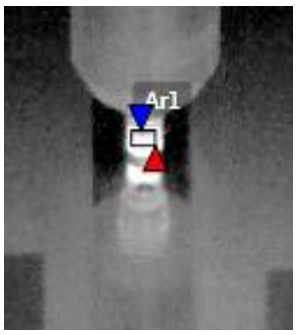
5.3.2 Convection coefficients and heat transfer values of weld trials

Based on the calculations above for the weld trials, the following data is represented for each model. Table 5.6 depicts the average convection coefficients found within the rectangular area shown in the images alongside for each trial number.

The square areas chosen where located between the tool and work piece areas. This is so that a uniform temperature comparison could be obtained instead of including areas of the work piece that are the retreating and advancing side of the tool.

Table 5.6: Average convection coefficients for the tool during dwell time

Trial number	h_{Q4} (kW/m^{2}K)	h_{q1} (W/m^{2}K)	Spot locations for average temperature on tool surface
1a	960.99	94.16	

1b	1399.22	107.13	 
3	1538.44	117.8	
4	2945.28	288.6	

The convection coefficients for each of the weld trials for the work piece surfaces is given below (Table 5.7), also to note the estimated contributions coming from each since the total heat transfer was calculated and each surface has a fraction of this.

Table 5.7: Average convection coefficients on work piece surfaces during the dwell period

Trial number	h_{q2} (W/m^2K)	h_{Q2} (W/m^2K)	h_Q (W/m^2K)
% Contribution of each	0.65	0.25	1
1a	14.85	5.7	2.28
1b	15.7	6.03	2.4
3	24	9.2	3.7
4	72.5	27.9	11.15

For sticking and sliding conditions, the following was obtained, where the sticking condition is largely affected by the rotation of the tool piece. These values of heat transfer for the various weld trials are shown below in Table 5.8.

Table 5.8: Heat transfer for sliding and sticking for dwell period

Trial number	Rotation (rpm)	Feed rate (mm/min)	Total Heat transfer (W) -Sliding	Total Heat transfer (W)-Sticking
1a	1250	400	196.35	5291.02
1b	1600	400	196.35	6772.51
1	1250	300	196.35	5291.02
2	1250	400	196.35	5291.02
3	1250	500	196.35	5291.02
4	1600	400	196.35	6772.51

Temperature results from the FLIR tools + software was obtained by placing points across the weld line. The results will be discussed in more detail in the discussion to follow, but other comments are made on the graphs to describe the different areas as well as certain discrepancies that appear which do affect the temperature output. This is to also to note the difference in temperatures from the advancing and retreating side and can be neatly shown in the graphs that follow. The locations for these spots for each weld trial are given in Table 5.9.

Table 5.9: Spot locations for temperature graphs

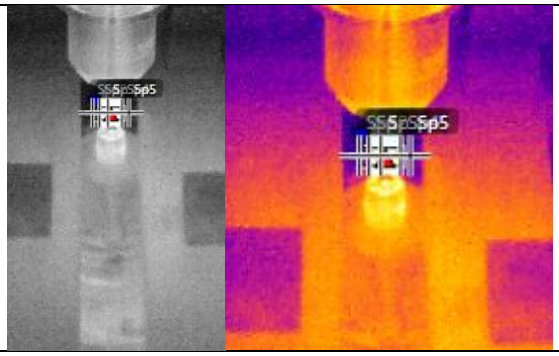
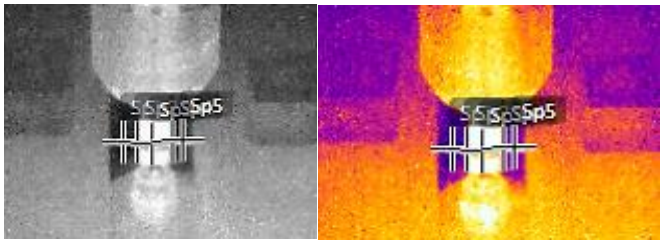
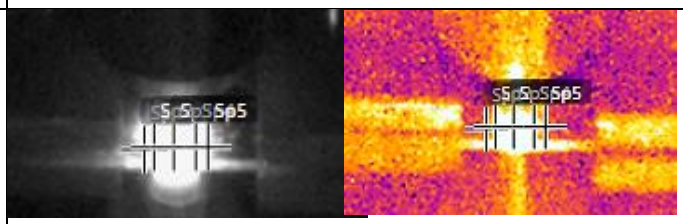
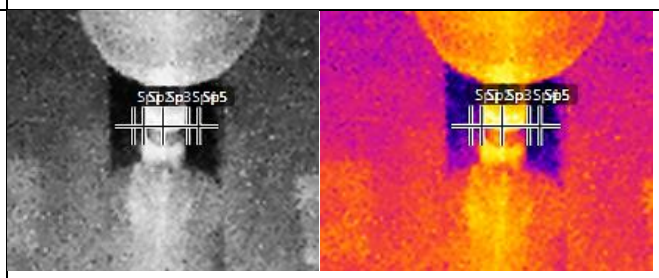
Weld trial number	Spot allocations for temperature data
3	
4	
1a	
1b	

Table 5.9 outlines the corresponding spot details which correlate with the specific graphs below. The temperature details were extrapolated from the FLIR tools + software which yielded the following graphs;

A few points to note are the following;

- Each part is shown which represents the dwell and feed rate phases
- The camera was set for values between 100°C and 650°C. This is for finer clarity of the image, since at higher temperatures, the resolution is not as clear. This is

also the reason as to why there are straight lines in the graphs for the maximum temperatures, since at these points, which may lie on the tool piece, are actually at a higher temperature than 650°C at the emissivity value set for the work piece.

- The emissivity value has an effect on the output temperature as discussed, and when performing the calculations for the tool piece surface, this value was changed in order to obtain a true temperature value for the tool. These graphs however, are set to the emissivity value calibrated for the work piece

This first Figure 5.4, clearly shows the behaviour of the temperature for the stages of the FSW process.

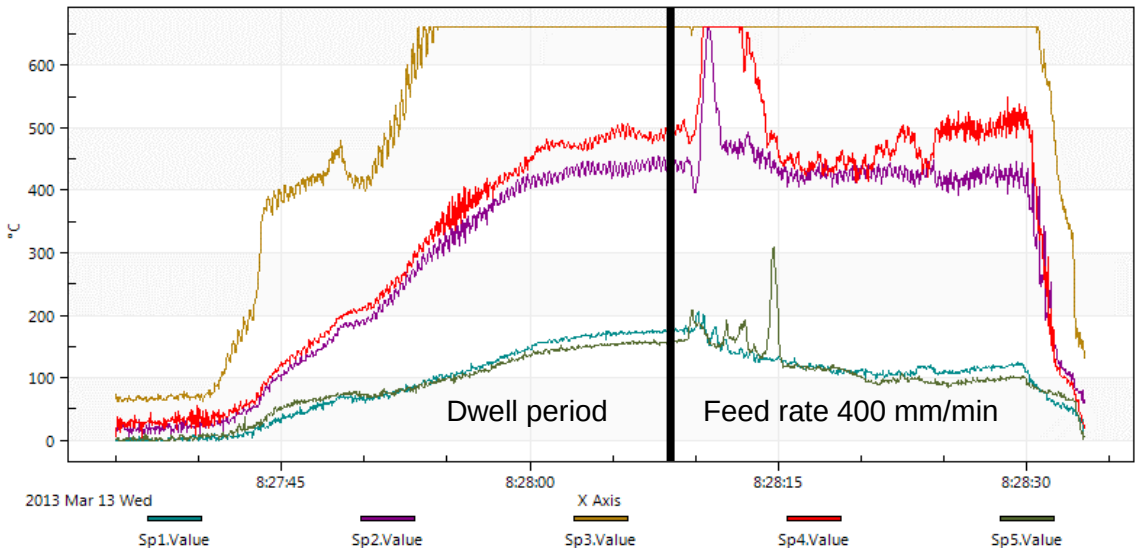


Figure 5.4: Temperature plot versus weld time for 1250 RPM and 500 mm/min feed rate weld trial

It can be noted that spot value 2 and spot value 1 are on the retreating side of the tool and spot value 4 and spot value 5 are on the advance side, since the temperature at point 1 and 2 are at lower temperatures than spot values 4 and 5. This is based, not only in literature where it was found that the advance side has a slightly higher temperature than the retreating side, but graphically it was noted which was the advance and retreating side of the tool.

In the next figure, Figure 5.5, with a higher rotation speed but slower federate, whereas before, the dwell time represents the temperature increasing over that period of time. Again as explained, the retreating and advancing side can be clearly depicted.

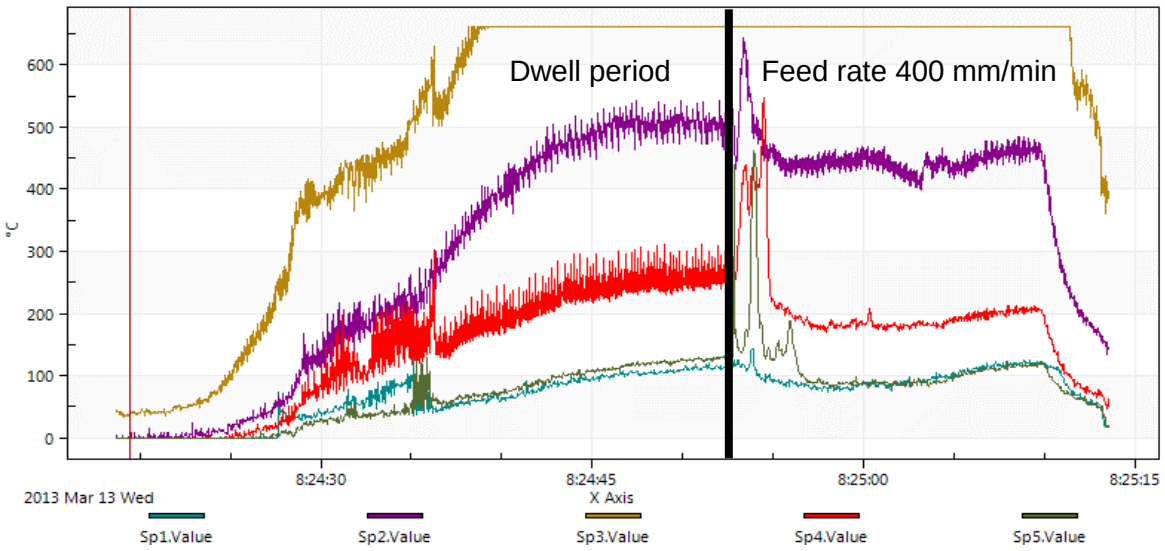


Figure 5.5: Temperature plot versus weld time for 1600 RPM and 400 mm/min feed rate weld trial 4

The next Figure 5.6, has the same parameters set for the rotation and feed rate as in Figure 5.4. The erratic behaviour of the lines represent the unsteady handling of the camera but it is still consistent with the temperature trend as seen in the previous figures.

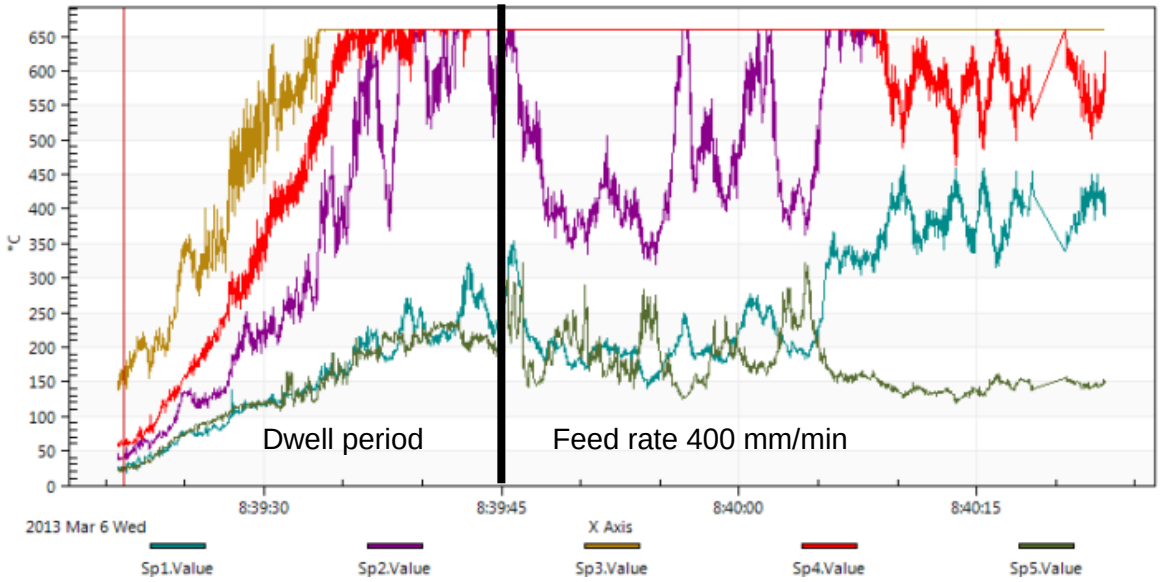


Figure 5.6: Temperature plot versus weld time for 1250 RPM and 400 mm/min feed rate weld 1a

The final figure, Figure 5.7, has the same parameters as that of Figure 6.5. Each phase of the FSW process is also represented and erratic behaviour for this set of results is the same as before where the camera handling was to blame but still follows the same trend for increasing temperature over a period of time for the dwell period.

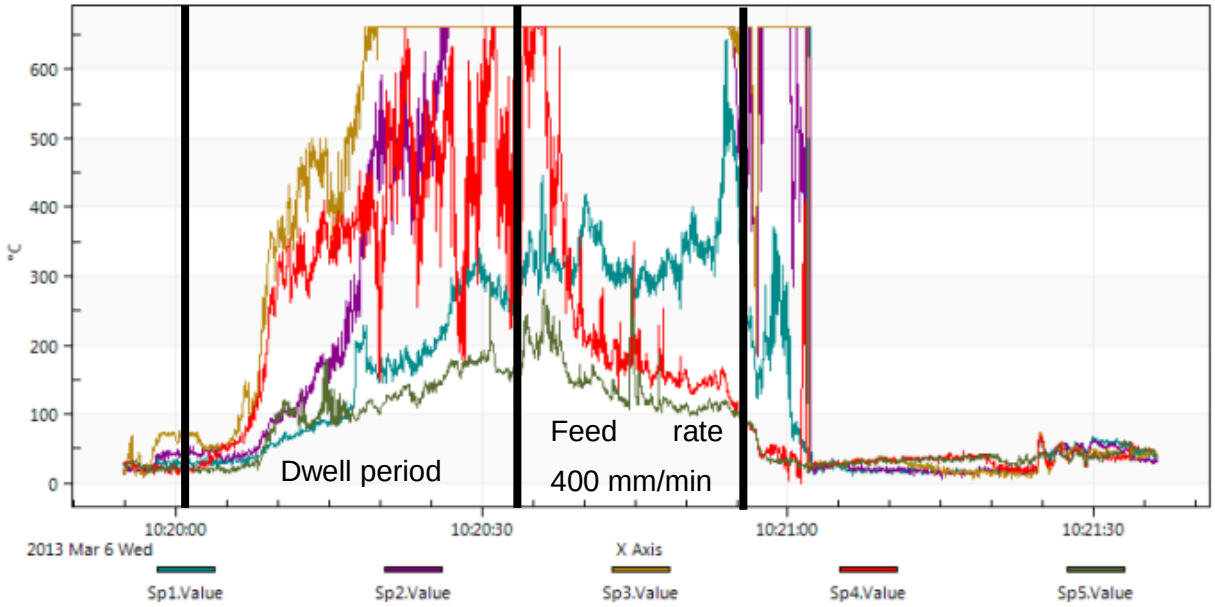


Figure 5.7: Temperature plot versus weld time for 1600 RPM and 400 mm/min feed rate weld 1b

The above graphs represent a similar trend for the various parameters set. The discrepancy of values (if required the same) and erratic behaviour of the lines could owe to the following;

- Unsteady camera and camera angle (As this camera angle influences the emissivity value)
- Other points already mentioned but summarised as follows;
    - Spot 1 and 2 are located on the retreating side of the tool and spots 4 and 5 on the advance side since these spots depict higher temperature values than spot 1 and 2.
    - Flat parts of the graph, represent the maximum limit of the range of temperature reached since the thermal imaging was recorded between 100°C and 650°C. This temperature range was chosen since we assume that the work piece material only reaches 80%-85% of its melting temperature which is only in the region of 450°C of the aluminium alloy

5.4 Summary

A temperature comparison was shown for the various FEA models run, whereby some correlation between some models existed. Heat flux transfer was calculated for the models that depicted strong correlation with each other. These values show a close relation for the heat flux of the tool, but the heat flux for the backing plate depicts a wide difference, which will need to be addressed.

Some images taken from the FEA for the frictional stress depicts an interesting phenomena which is already known, but clarified in the model. This is the direction in which the tool rotates and the effects of the advance and retreating side of the weld line. A higher frictional stress is thus experienced on the advance side of the weld and hence a higher temperature is expected in this region as well.

Weld trials were performed and images of these welds have been recorded. Since the convection of the work piece and tool are unknown, but the temperatures have been recorded, this data will be processed to estimate the convection coefficients for the relative surfaces and hence the heat flux can be calculated as well.

Temperatures across the weld are documented, whereby each begin and end phase has been shown. The temperatures in each phase also offer insight into the heat generation of the FSW process. It can be seen that during the weld, temperature increases gradually as the frictional contact between the two surfaces increases. During the feed rate, there is a slight drop in the temperature as the tool moves along the weld line. Although contributing factors could include the alignment of the thermal camera to the surface of the work piece.

Chapter 6

6. Results

6.1 Introduction

The results outlined are those taken from the processed data for comparison with the FEA model and weld trials. The following data will be compared and relationships will try be determined for further processing;

- Heat fluxes
- Temperatures
- Convection coefficients for surfaces
- Trend data for temperatures across the weld and for different parameters

6.2 Finite Element Modelling

The average heat flux for the tool and work piece are given in the table below after which the total heat flux transfer is given. The specified convection coefficients were used to calculate the following values (Table 6.1);

Table 6.1: Heat flux transfer values for certain FEA models specified

Model Number	q_1 heat flux transfer for tool kW/m^2	Q_4 heat flux transfer for the tool kW/m^2	q_2 heat flux transfer for the work piece kW/m^2	Q_2 heat flux transfer for the work piece kW/m^2
8	25.61	102.44	60.94	256.09
10	27.26	109.03	42.21	272.58
12	27.26	109.03	42.21	272.58
14	31.80	127.19	59.11	158.99
17	25.02	100.08	45.29	166.80

The total heat flux transfer were calculated using equations 2.5 and 2.6 and Table 6.2 displays the heat flux transfer for the values obtained in the FEA model. This is the average heat flux transfer calculated over the entire length of time for the dwell time. These calculated values are given in Table 6:2.

Table 6.2: Total heat flux transfer for FEA models

Model Number	Total heat flux transfer for tool kW/m^2	Total heat flux transfer for the work piece (Q_1-Q) kW/m^2
8	128	317.04
10	136.29	314.79
12	136.29	314.79
14	158.99	218.10
17	125.09	212.08

Average increase in temperature for the models was determined within the temperature result ranges obtained for the same period of time. The reason for this is that some models had more results for a longer process time where others did not, so a uniform comparison could be made by determining the average temperature increase (Table 6.3) within the same range.

Table 6.3: Average increase in temperature for FEA models

Model Number	Average increase in temperature (°C/s)
8	1048.05
10	1251.21
12	1251.21
14	779.38
17	949.65

6.3 Weld Trials

Results of the weld trials are represented below and were obtained using the same method as outlined in 5. Data Processing for sample calculation for the weld trials. Initially total heat flux was determined for the sliding and sticking conditions along the radius of the shoulder of the tool. It can be noted that in Table 6.4, the heat flux decreases outward and the reason for this is that the inner most part generates heat and this is generated outward.

Table 6.4: Total heat flux along radius for both contact conditions

Radius until shoulder radius (r_0)	Total heat flux (Sliding)- W/m^2	Total heat flux (Sticking)- W/m^2

0.001	1178.08	31746.14
0.0015	785.39	21164.09
0.002	589.04	15873.07
0.0025	471.23	12698.45
0.003	392.69	10582.05
0.0035	336.59	9070.32
0.004	294.52	7936.53
0.0045	261.80	7054.70
0.005	235.62	6349.23
0.0055	214.20	5772.02
0.006	196.35	5291.02

After determining the convection coefficients, these were used to determine the total heat flux and an average was taken over the dwell time period. This result is shown below in Table 6.5.

Table 6.5: Average for work piece of weld trials

Weld trial	Total heat flux transfer for the work piece (Q_1-Q) W/m^2
1a	4917.09
1b	6262.92
3	4897.98
4	6262.99

Based on the above, it can be seen for higher tool rotations, the heat flux is higher than for lower tool rotations, both which are also set at constant feed rate values.

Convection coefficients for the first two seconds were determined for the weld trials as this would give a uniform comparison with the FEA models time, for which it was analysed within. These average heat convection coefficients results for each weld trial are shown below in Table 6.6.

Table 6.6: Average heat convection coefficients before the first 2 seconds of the weld trial

Trial number	h_{q2} (W/m^{2}K)	h_{Q2} (W/m^{2}K)	h_Q (W/m^{2}K)

% Contribution of each	0.65	0.25	0.1
1a	88.22	33.93	13.57
1b	453.9	174.6	69.83
3	80.79	31.08	12.43
4	88.01	33.85	13.57

The same was done for the tools convection coefficients and to note the emissivity value for this data was changed to the emissivity value of the tool, since it is required to use the correct surface temperature for that particular surface. These results are recorded in Table 6.7.

Table 6.7: Convection coefficients for the tool for first 2 seconds of dwell time

Trial number	h_{q1} (W/m^2K)	h_{Q4} (MW/m^2K)
1a	522.08	5.32
1b	641.70	8.38
3	303.68	3.10
4	951.72	12.43

The change in temperature was also observed for future FEA comparison as the rate of temperature increase could help determine the heat generation rate that is inserted as a command in the FEA model. These changes in temperature are results obtained from the data obtained in the weld trials and are given in Table 6.8.

Table 6.8: Average change in temperature for the first 2 seconds of work piece and tool

Trial number	$T-T_O$ (Work piece)	$T^4-T_O^4$ (Work piece)	$T-T_O$ (Tool)
1a	38.79	5E09	7.36
1b	9.74	1.1E09	5.48
3	43.93	5.9E09	11.38
4	51.72	7.17E09	3.63

The above data reveals that average change in temperature has a higher increase in temperature rate for higher tool rotations. Although, trial 1b depicts change in temperature being lower for the higher tool rotation, these experiments also show erratic behaviour of points due to unsteady camera position and were initial tests performed as trials before trials 1-4 were achieved by including a procedure for the best possible recording of thermal data.

Below is the average increase in temperature rate, which one can again note the same trend as described in the change of temperature. Where, 1b shows a slower rate of increase which it should be higher due to the higher rotation of the tool causing a higher friction and hence heat generation increase between surfaces.

Table 6.9 depicts the increase in temperature over a 2 second dwell period for the work piece and tool for the weld trials performed.

Table 6.9: Average increase in temperature for work piece and tool for the entire dwell duration as well for the first 2 seconds of the dwell period are recorded.

Model number	Increase in temperature (Work piece) °C/s first 2 seconds and over dwell time		Increase in temperature (Tool) °C/s first 2 seconds and over dwell time	
1a	175.97	52.12	174.95	15.76
1b	174.92	28.63	1346.69	61.47
3	36.27	22.05	13.07	6.64
4	168.24	23.04	26.27	1.61

Heat flux (Table 6.10) for each is calculated as shown in the sample calculations in the data processing for the weld trials.

Table 6.10: Heat flux for work piece and tool during first 2 seconds of dwell time

Model number	q_2 (W/m^2)	Q_2 (W/m^2)	Q (W/m^2)	Q_1 (Total heat flux) (W/m^2)	q_1 (W/m^2)	Q_4 (MW/m^2)	Q_3 (MW/m^2)
1a	3.45E+03	1316.145	526.3803	5.29E+03	3842.51	39.155	39.159
1b	4.43E+03	1700.604	680.1442	6.81E+03	3516.52	45.922	45.926
3	3.59E+03	1365.344	546.0499	5.50E+03	3455.88	35.278	35.282
4	4.60E+03	1750.722	701.8404	7.05E+03	3454.74	45.121	45.124

Total heat flux for various surfaces depict higher values at higher rotation speeds. In comparison, between the different weld trials for the same parameters, similar values have been obtained, indicating some error but still fairly similar for the same rotation and feed rate values.

Error in calculated values based on differences between each are determined for each of the weld trials with the same parameters (Table 6.11).

Table 6.11: Error for total heat flux values on surfaces for weld trials of the same parameters

Trial comparison	Parameters	Error %
1a and 3	1250 RPM and 400mm/min	3.8 % difference
1b and 4	1600 RPM and 400mm/min	3.4 % difference

6.4 Comparison of FEA and weld trial results

A comparison of the heat flux and convection coefficients is represented below in Figure 6.1 for the FEA results and Weld trial results.

The following initial observations are made;

- The model heat flux values are far higher than the weld trial heat fluxes, this is due to the rotation values set for the model being a lot higher than the rotation values used in the weld trials.
- Heat flux Q_2 depicts a vast difference in a proportional relationship in comparison with FEA and weld trials. Q_2 depicts a higher value than that found in the weld trials. Based on this it is assumed that an initial assumption that this value contributes a higher percentage to the total heat flux is incorrect and has been corrected in the processed data based on result findings following this section.
- Heat flux q_1 and Q_4 depict a similar proportional relationship in comparison of FEA and weld trail results.
- q_2 requires more observation but it does reveal a similar proportional relationship depicted between the two comparisons.

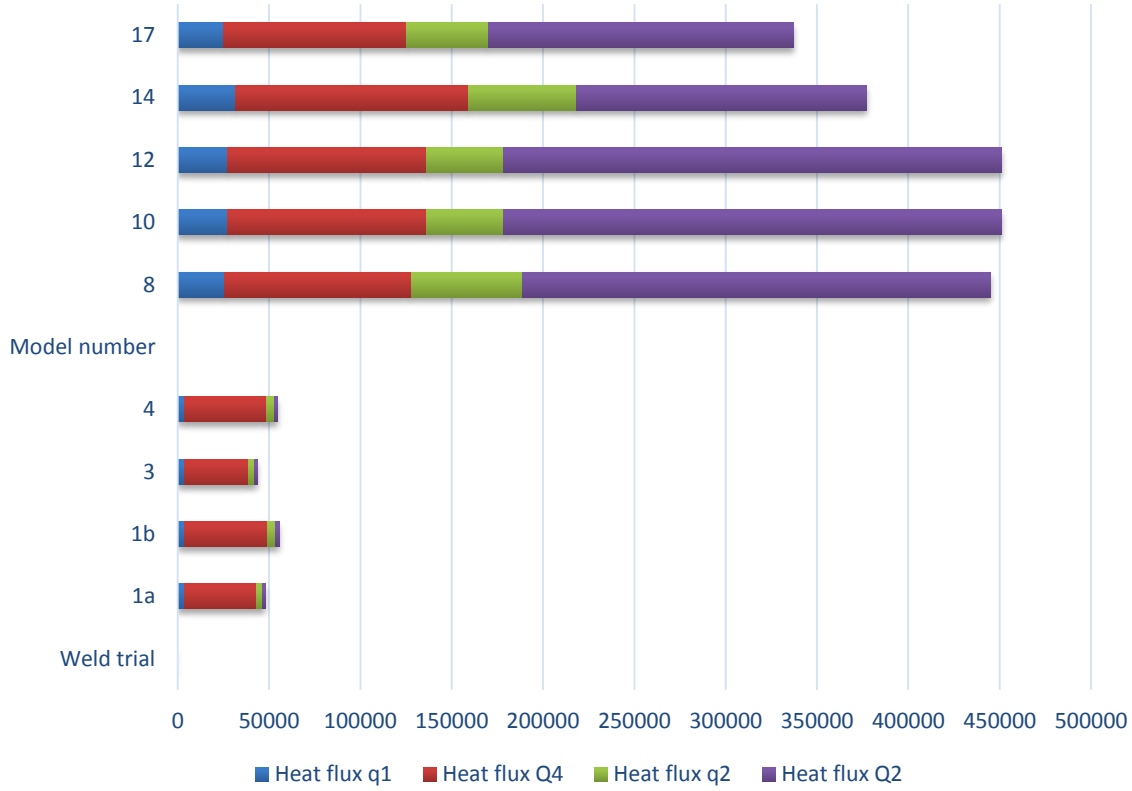


Figure 6.1: Heat flux comparison for each contributing surface for the FEA and weld trials

The following is observed for each of the convection coefficients for the weld trials and FEA model, these comparisons are represented graphically in Figure 6.2;

- Weld trials have a higher convection coefficient values than the FEA model initially used.
- Since the weld trials convection coefficients used a percentage value contributing to each and the values used in the FEA model were obtained from literature and manipulated when looking at various effects, the percentage contribution for the weld trials need to be adjusted accordingly.
- However, based on the higher values obtained for the convection coefficients for the weld trials, it can be assumed that the values used in the FEA are required to be of a higher value than initially assumed.
- H_{q1} and hQ_4 for the weld trials need to be changed for percentage contribution as this based on FEA models values, h_{Q4} requires a higher contribution and therefore value.

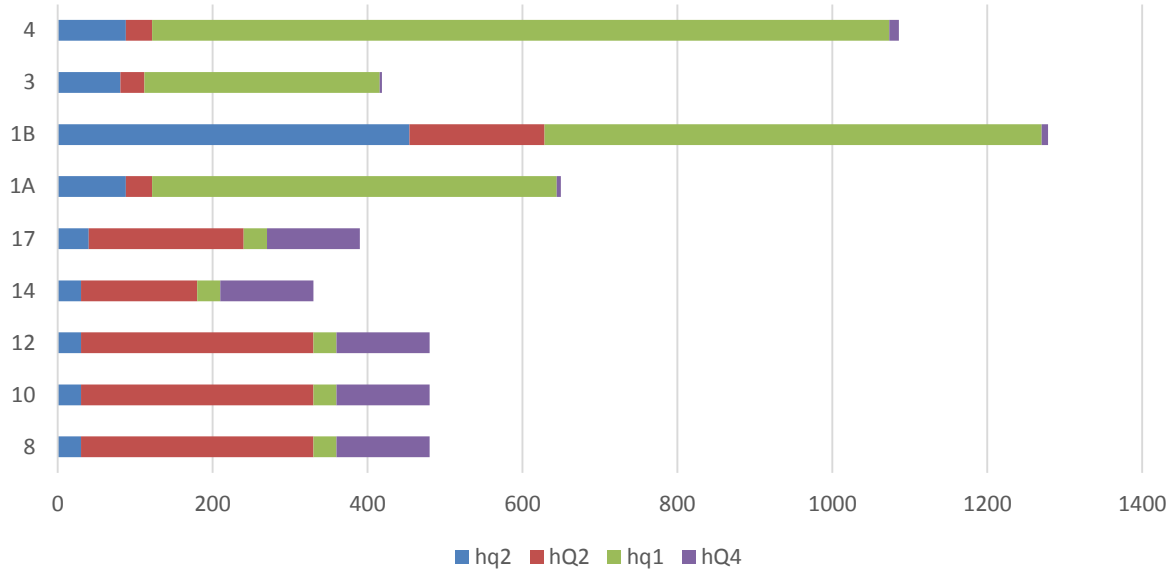


Figure 6.2: Convection contributions for each surface for the FEA and weld trials

The temperature results for each are compared and it can be seen that the temperature results obtained for the weld trials are far lower than those obtained for the FEA model. This is possibly due to the convection coefficients values being very different. This is represented in Figure 6.3, where the weld trial and FEA temperature results are represented on one graph to show the comparison.

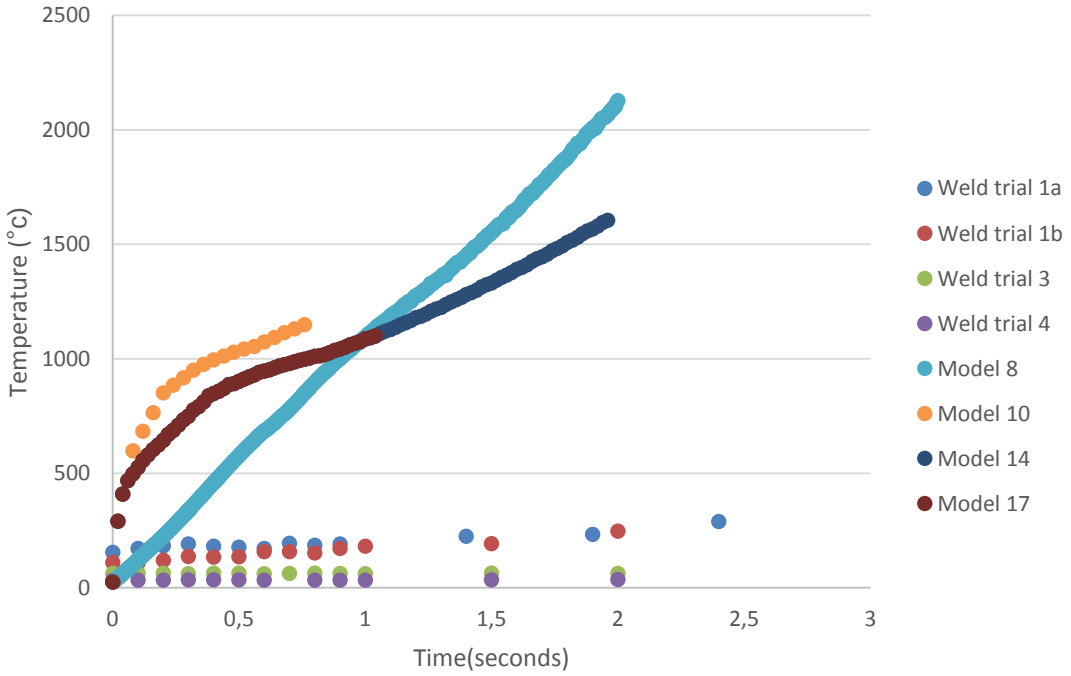


Figure 6.3: Temperature increase over time for the FEA and weld trials to compare

Based on the temperature graphs, each of the weld trial temperature results and model temperature results were observed separately to see if they followed the same trend. Also, for visual purposes, depicting each separately one is able to note that their trend similarities. Both temperature results were able to follow a polynomial trend to the power of 5.

Weld trial temperature results depict that at higher rotation speeds, higher temperatures are obtained which follows from previous results and processed data. The FEA model was analysed under a various rotation values and the models under comparison are those for which the rotation value is more than double that of the maximum rotation specified for the weld trials. This also adds to the fact as to why the temperatures are so high. These values are only being used, since the models which had the same rotation value set, did not have enough data results for a full comparison to be made.

Each of the temperature results for the weld trial and FEA model are represented separately for further information to be obtained. The first Figure 6.4, is that temperature result obtained for the weld trial.

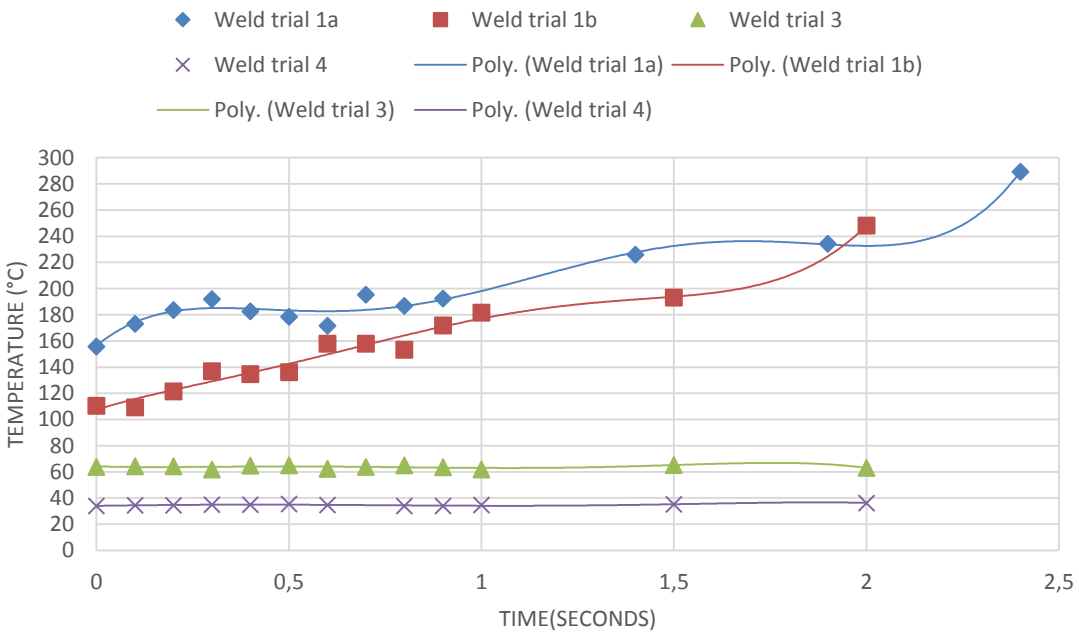


Figure 6.4: Weld trial temperature trend data

The second Figure 6.5, represents the temperature results obtained for the FEA model. Both graphs represent a similar trend in increase in temperature for that particular weld time. Although, the weld trials depict a slower rate of increase, it is then suggested that the convection coefficients initially assumed on the FEA model needs to be revised in order to decrease this temperature increase as it shows a rather rapid increase in temperature.

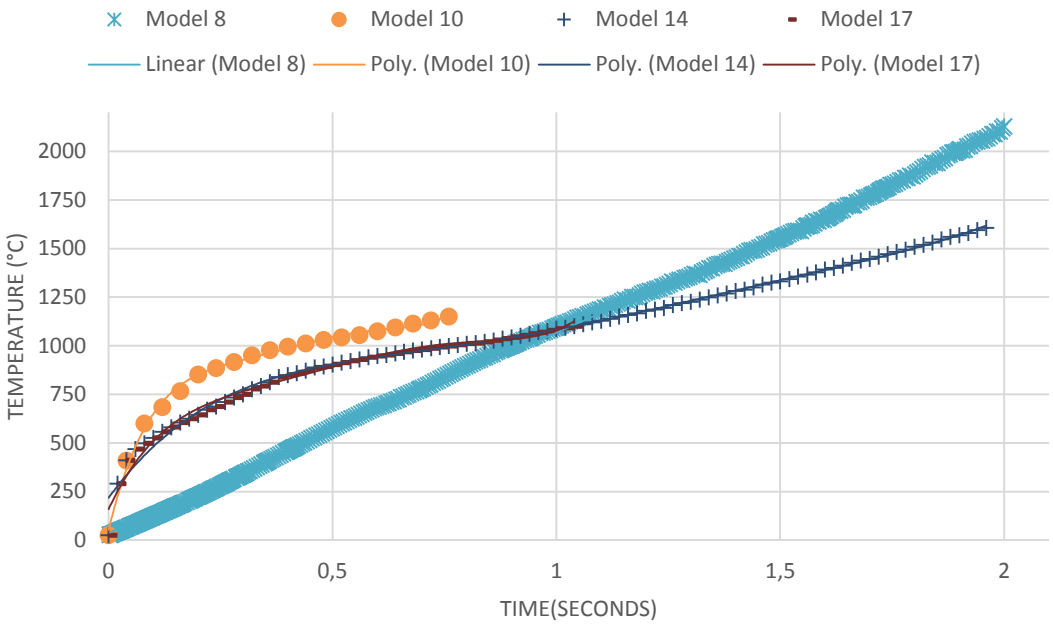


Figure 6.5: FEA temperature trend data

6.5 Processing data based on result findings

Since the model is based on literature attributes, especially for the convection coefficients and friction coefficients, the processed data shows that the dominant convection coefficient is that of the bottom surface of the work piece to the backing plate. Originally for the weld trial one assumed a low percentage contribution. This is now changed and the following results are shown, based on that the heat flux of bottom and top surface combined are 90% contributing to the total heat flux. This resulted in contributing factors for each surface being in an average of 10% and 80% respectively (Table 6.12).

Table 6.12: Revision of heat flux values for weld trials

Trial number	h_{q2} (W/m^{2}K)	h_{Q2} (W/m^{2}K)	h_Q (W/m^{2}K)
% Contribution of each	0.1	0.8	0.1
1a	12.43	99.44	12.43
1b	13.54	108.32	13.54
3	13.57	108.58	13.57
4	69.84	558.7	69.84

The above results are another assumption and this value for the backing plate would have errors since it is assumed as a convection coefficient which in fact it is conduction. However,

a similar trend can now be noted for the weld trials and FEA model convection values (Figure 6.6). Where the similarity is that the heat flux for Q_2 is far higher than that of q_2

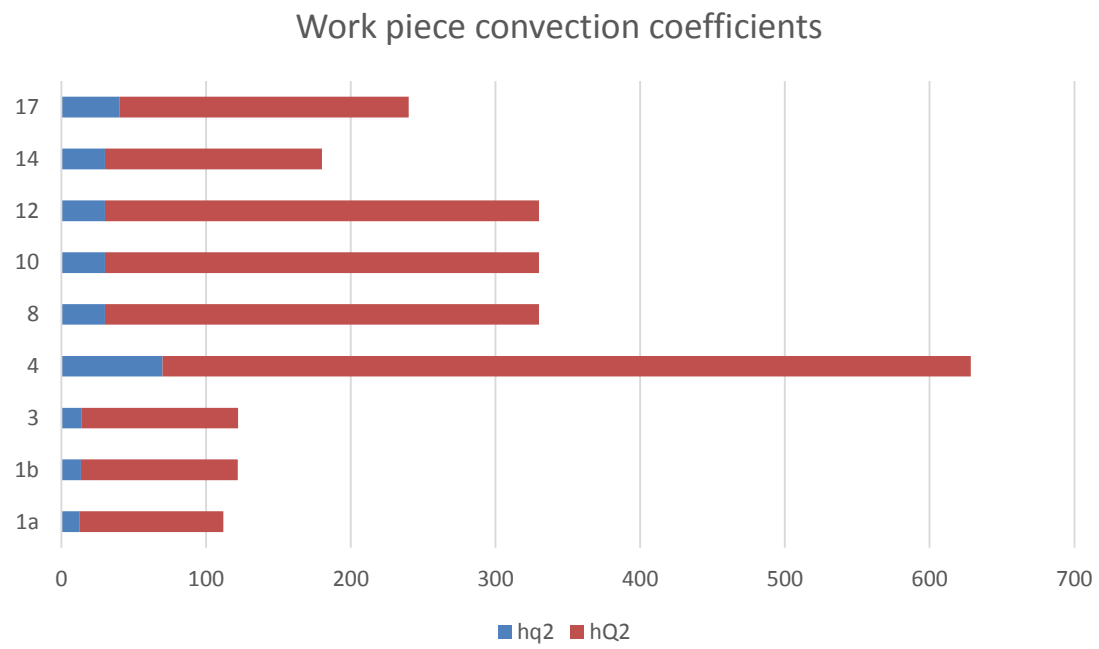


Figure 6.6: Work piece convection coefficients for FEA and weld trials after adjusted data contributions

6.6 Summary

Results based on the processed data is given, from which a comparison of the heat flux results for the FEA model and for the experimental weld trials can be compared. The temperature results of both are also be investigated.

The results of the temperature comparison prove to be challenging but a fair relationship can be determined in that the temperatures for each are increasing in a similar manner, which concludes that the model developed is a good representation of the FSW process in this regard.

The convection coefficients for the work piece surfaces need to be developed further in terms of those input into the model as models convection is a lot larger than that worked out for the weld trials, also their contributions of each surface convection coefficient do depict a similar relationship for each other.

Chapter 7

7. Discussion

7.1 Introduction

The order of discussion will first outline the model development and special mention to the whole process of the final model as it stands. The data for the FEA and for the weld trials obtained will be reviewed and any discrepancies discussed in more detail where applicable. After results for each will compared and future recommendations based on findings will also be briefly suggested. The optimisation of the parametric model will also be discussed further in terms of future development and what the current model contributes to enabling this.

7.2 Model development

The modelling of the FSW process was an on-going endeavour throughout the investigation. It was initially modelled using a basic guidance from the ANSYS APDL (ANSYS parametric design language) model of Zhu and Chao [20]. Certain parameters in the model were either clarified by literature or used or initial assumptions were made and later discussed and developed further where possible. An outlined version of the new model as that compared to the other models also developed in ANSYS as mentioned in 2.3.4 Current model features versus previous models developed, shows an advance in the FEA model developed not only in terms of user friendly interfaces (APDL versus the workbench) but also in terms of representation of the new command feature which together with the element SOLID 226 is able to represent the model in a more realistic manner by enabling the heat generated by friction to be simulated in the model.

Based on the heat generation ratios outlined in Scmhidt et al [34], the following heat contributions were determined and to justify the absence of the tool tip/probe in the model. The total heat generated was determined and using the ratios outlined in the equations [34] below;

$$f_{\text{shoulder}} = \frac{Q_1}{Q_{\text{total}}} = \frac{(R^3_{\text{shoulder}} - R^3_{\text{probe}})(1+\tan\alpha)}{(R^3_{\text{shoulder}} - R^3_{\text{probe}})(1+\tan\alpha) + R^3_{\text{probe}} + 3R^2_{\text{probe}}H_{\text{probe}}} \quad 7.1$$

$$f_{\text{probe side}} = \frac{Q_2}{Q_{\text{total}}} = \frac{3R^2_{\text{probe}}H_{\text{probe}}}{(R^3_{\text{shoulder}} - R^3_{\text{probe}})(1+\tan\alpha) + R^3_{\text{probe}} + 3R^2_{\text{probe}}H_{\text{probe}}} \quad 7.2$$

$$f_{\text{probe tip}} = \frac{Q_3}{Q_{\text{total}}} = \frac{R^3_{\text{probe}}}{(R^3_{\text{shoulder}} - R^3_{\text{probe}})(1+\tan\alpha) + R^3_{\text{probe}} + 3R^2_{\text{probe}}H_{\text{probe}}} \quad 7.3$$

The above equations resulted in the following percentage contribution, given in Table 7.1, for the proposed dimensions of the tool used.

Table 7.1: Percentage contributions for each part of the tool

Ratio	Percentage contribution (%)
$f_{probe\ side}$	10.8
$f_{probe\ tip}$	6.4

This amount conforms well to other literature, from which it states that 5% of heat generated due to friction (due to probe tip) flows into the tool and remaining amount of heat generated flows into the work piece [24].

This heat generation into the work piece is modelled as a command for the heat generated between the contact and target surface between the tool and work piece (Figure 7.1).

```
rmodif,CID,18,ARG2     !A real constant  FWGT, weight factor for
                       !the distribution of heat between the
                       !contact and target surfaces, 0.95
```

Figure 7.1: Extract from the contact command in FEA methodology

Changes in the model were made either to refine the model or to investigate the influences of particular parameters.

- Plunge depth changes in the model, initially to see the effects thereof since the deformation of the plates was shown as an issue, which it was then reduced. It was decided to use half the real plunge depth as in the experiment since this worked well with the model at the present time.
- Model size, this was reduced in order to reduce number of elements and hence processing time
- Material thermal properties. Initially, some thermal properties were set as commands in the workbench tree, since it was created in a structural transient analysis, but was later also seen as redundant since ANSYS has an Engineering Data block where this can all be inserted into. The thermal properties were added to the Engineering Data via a new component in the interface and not under the structural transient component as before. This then allows for the information to be read into the model.

- Rotation of the tool in the x co-ordinate was also changed. As outlined in the Methodology for the FEA modelling 2 methods were used for the calculation of this. Where one of the last models took the approach of both, by working out the degrees for a particular rotation and adjusting the time step accordingly.
- Convection coefficients were changed to see the effects on temperature, which one could then determine the rate of temperature increase in the model and compare to that of the rate of increase to the weld trials. These boundary conditions have a high uncertainty in the fact that little value is really known and it is suggested that more work is done in determining these values in order to obtain a better FEA model.

These changes contributed to the model analysis either in processing time, or to develop the model in a more realistic way in that all properties were accounted for correctly. The following results would not have been possible without these changes.

7.3 FEA model processed data

The heat flux transfer worked out for the FEA model was determined using the convection coefficients input and the temperature results obtained from the model. The results obtained for each of the sections;

- Clamped tool (ARG 4)
    - Shows little variation with change in value inserted
- Shoulder of the tool (ARG 3)
    - This value was kept similar for most of the models and very little variation exists in the results
- Top plate surface (ARG 1)
    - This value was kept the same throughout the models, and little variation exists between the models
- Bottom plate to backing plate (ARG2)
    - This is considered the most important value, as a definite difference in value exists for the variations inserted into the model for this convection coefficient. The model is proven to be according to literature in terms of that the heat flux is higher when the convection coefficients are higher, which the same result is obtained in the weld trials. It is immediately apparent when comparing these heat fluxes to the convection coefficients specified that in order for the heat to be transferred at a faster rate, the convection coefficients needs to be set to a higher value. When comparing it is seen that convection coefficients of 300 W/m^2K, the heat flux is over 250 kW/ m^2 and for convection coefficients between 150 W/m^2K and 200 W/m^2K, the heat flux ranges in the 159- 168 kW/

m^2. These heat flux transfers are also very high compared to the weld trials results. More reason as to why the convection coefficients need more attention.

The average increase in temperature for the FEA models correspond to the heat flux transfer obtained and hence the convection coefficient outlined for the bottom of the plate to the backing plate. It is clear that the heat transfer rate is higher at this higher convection coefficient than at a lower one.

7.4 Weld trial processed data

Results for the weld trials lead to interesting developments and outcomes. Although more than 4 weld trials were performed, it was decided to look at 4 in particular weld trials under similar conditions and steady state. Two of the weld trials for each are at 1200 and 1600 rpm respectively. Each set was performed at different times which also allowed one to see the conformity for the comparisons and how repeatable the procedure is. Although there are some discrepancies, results do show some similarity for valid conclusions to be drawn.

The initial results for the FLIR-temperature comparison for the same weld rotation for various weld trials compare fairly well, suggesting better results, whereas the last indicate a greater difference. Possible influences could be any of the following;

- Angle of camera changes further out on the weld line, therefore emissivity value might be different
- Reflective temperature has an influence on final temperature results as well
- There is also the possibility that the CNC machine has a discrepancy with input which results in the uncertainty that the rotation is set correctly, though this last may seem unlikely, it just ensures that these parameters need to be checked and ensured that they are correct.

Based on calculations performed to get the heat transfer coefficient with total heat transfer at particular temperatures, one is able to conclude whether sticking, sliding or a combination of each is occurring. Based on total heat flux transfer, one is able to conclude as to what condition the process is undergoing, it is assumed that based on the table for Total heat flux along radius for both contact conditions, values lie between the sticking and sliding condition. This conclusion is also comparable to literature and is outlined in [25]

Other notes on the temperature rate for FLIR;

- Heat flux transfer is higher at higher rotations than at lower rotations and this is due to the increase in friction generation rate between the two surfaces.

- For higher rotations, the rate of increase in the temperature is faster than those at lower rotations. This is a valid conclusion since higher rotations cause faster heat generation since friction coefficient increases at a faster rate. With this been said it can be concluded that the friction coefficient is some way influenced by the rotation parameter of the FSW process. It should be noted however, that for weld trials of 1a and 1b for the work piece, there is some discrepancy since the lower rotation exhibits a higher increase in temperature rate. Possible reasons for this could be due to the camera handling which would lead to, data points being inconsistent when processing the temperature results.

The total heat flux calculated for the tool using equation 10, clearly depicts the heat is mostly concentrated from the middle of the tool outwards and distributed along the weld line, where the temperature would be expected highest in the middle and gradually decrease from the weld line. This type of temperature measurement is difficult to measure experimentally and is where the FEA model would contribute to determining these temperatures. This would also lead to conclusions of the condition at the centre whether sticking is occurring at this point. Together with the aforementioned, correct parameters can then be selected to account for this and also would benefit the tool design.

The convection coefficients for the work piece were first based on an initial assumption that the heat from the top surface was the highest, this was to observe the effects thereof the varying surfaces and what type of convection coefficients one could expect. Average convection coefficients were determined for the dwell period and it can be noted that at higher rotations, the convection coefficients are higher, which relates to the rate at which the heat transfer is occurring. The tools convection coefficients, especially for the clamped part of the tool are very high. Though one can note that for the tools shoulder convection coefficients, they relate very similarly to the FEA convection coefficients used for the first few model runs, after which it was changed to a lower setting for observation purposes. It is however, concluded that for the tool shoulder convection coefficients, one could possibly use 100-300 W/m^2K when inserting this value into the FEA model.

Factors contributing to the convection coefficients of the clamped surface could be due to the force value worked out based on the operating conditions of the CNC machine. Since this force value was not measured, there is an uncertainty that it may not be correct. This value also affects that of the other values and could outline certain errors for the calculated heat transfer and hence the convection coefficients in the weld trial samples.

Temperature results obtained by placing spots across the weld line (Figures 5.4-5.7) , clearly indicate that a bell shape curve can be made for each of the data points set out in the figures for the temperature plots. The steadier the camera is set, the better the temperature results will be and can observed in the figures where there are erratic lines, although still depicting the correct trend, one will not be able to use those values as reliably as those results which show smoother increases in temperature.

The weld trial did however compare well to each other and although there are many precautions and consideration to take into account when setting up the experimental procedure for the thermal camera, it was noted that a percentage difference of less than 5% for the same parameters was obtained. This then proves to be a very good method in obtaining data since with the correct precautions and set up to consider, it makes the experimental procedure fairly repeatable and therefore a good comparison to be used with the FEA model temperature results.

7.5 Results comparison

Average increases in temperature indicate that the models temperatures are increasing at a higher rate than the actual weld trials. This is possibly due to the convection coefficients specified in the model as well the difference in rotation speeds specified in the model. The reason for the comparison of the different rotation speeds for the FEA with that to the weld trials is that the FEA model for those rotation speeds had more results to work with and compare then the previous models set out. One can notice though however, that the convection coefficient for the bottom of the work piece to the backing plate has an effect in the model. The higher this convection coefficient the faster the rate of temperature increase rate is. Also, therefore in the processing of the weld trials, the percentage of convection coefficients can be changed that h_{Q2} has a contributing factor than originally thought for the h_{q2} value. The convection coefficients for the clamped part of the tool and shoulder of the tool surface can be investigated further. After processing the results again to obtain better convection coefficients, one is able to make a better estimate of these values

Comparison of the heat flux transfer depicts higher values for the model than for the weld trials. It was mentioned that the convection coefficient for the bottom of the work piece should be changed and since the heat flux for the weld trials are much lower and hence their convection coefficients, it is suggested that a lower convection coefficient could be used for the bottom surface. Based on the bar graph for the coefficients, a relationship in terms of a percentage from view should be noted.

- For the models, it is noted that the heat flux for q_2 is much lower than that of Q_2 (which these relate to the top and bottom surface respectively). It can then be seen that for the weld trials this is in the reverse (but this is also the result of the percentage contributions chosen) Since in literature the bottom surface has a higher heat transfer rate and it is a result observed closely above, it can be suggested that for the weld trials, these values be altered and that the model does indeed depict the correct relationship between these two values.
- For the clamped and shoulder part of the tool, the models depict that indeed the clamped part of the tool has a higher value than that of the shoulder which can be seen more clearly in comparison for the heat transfers for these two values for the weld trials. Therefore, it can be concluded that the clamped tool part should indeed have a higher value than the shoulder, which also corresponds to the values obtained for the weld trials.
- However, as mentioned, the FEA model rotation value is at a higher degree and so although the values do not compare exact in number, in terms of correlation in percentage wise to each other it is comparable. It should also then be noted that for higher rotations speeds the convection coefficients and hence heat flux are much a higher and for a future recommendation a relationship of the rotational speed and convection coefficients can be further investigated.

Temperature comparisons for the weld trials and model show some varying degree between the values obtained. Although the model temperatures are far higher than the weld trial temperatures, they do follow the same trend of a curve and then increasing. The models do exhibit a higher increase in temperature, but this is due to the parameters inserted into the model. It is difficult to assume from these temperature values that the rotation inserted has a great affect (which under normal FSW circumstances should exhibit). The only conclusion that can be drawn as to why there may be the difference in the trends and that is again the convection coefficient specified for the bottom surface of the work piece, since a higher one was specified for model 10 and this is clearly shown a higher temperature increase and temperature result.

To see whether any relationship exists between the weld trials and temperatures, although the temperatures do not coincide, a polynomial line is fitted to each of the data points. Each of the lines were fitted with a polynomial line to the power of 5. This fitted very well for the trends with the weld trials having data points lying almost equally in and outside the line, indicating some error in the experimental results as is expected, but only slightly. Only one data trend does not consist with this polynomial fitting as this gave a linear trend of temperature

increasing for model 8. This could be an inaccurate result from the model, since the other trends follow quite well with one another and a possible reason could be the iterative workings for that particular model run. It is apparent however that for the weld trials temperatures obtained, higher rotations, results in higher temperature results.

After changing the convection coefficients percentage for the weld trials, one is able to depict a more comparable relationship between the bottom and top surface coefficients when compared between the experimental weld trials and model results. However, as noted in the Results section, this value for the backing plate is highly unstable since it has been assumed that it takes on a convection coefficient for modelling purposes when in fact it is conduction. So although, this comparison can be made, it is an assumption for both to compare.

In conclusion to the model developed, it is apparent that there are similarities between the model and weld trials in terms of the way the model behaves and one can conclude that the model does indeed depict the heat generation, but care and more extensive data is required for the model to operate within the correct conditions in order to achieve exact results.

7.6 Optimisation of parametric model

Based on the information obtained and alternate solutions that are required to be analysed for further research and findings, it is highly recommended that the optimisation of those thermal parameters needs to be done. Since this model is parametric, it has the potential to be used with modeFrontier which is an optimisation tool. One is able to use the experimental findings as objectives and since the model is parametric, these parameters can be optimised by reducing the minimum difference of the temperature field comparison of the experimental results and of the FEA model. This could optimise those parameter values i.e. convection coefficient, friction coefficient etc. as mentioned in section 3.3.5 Parametric model features.

Since the model has various parameters which are affected with one another, a response surface method (RSM) can be employed to optimise these values for the various parameters. A 3 dimensional response surface can be generated whereby the parameters at the minimum will be the optimal value. The RSM utilizes a Design of Experiment (DoE) approach.

Since the model is a parametric, one can appreciate that it can be implemented with this type of optimisation method relatively easily. However, the time to process these results can be extremely time consuming and is a fall back to the computational modelling aspect, but the information obtained from these models is far beyond that which can be seen experimentally. Thus, in determining a clear comparison with the experimental and FEA models, it is beneficial to use the FEA to obtain more results over a period of time. Based on the aforementioned with respect to processing time, this is the reason as to why this model has not been optimised

in this way. Since resources were limited and the time to process one solution within only the FEA model, the optimisation would have taken far longer to process since the surface of results for the FEA model alone for which it would require to input in modeFRONTIER, would be extensive in itself. Therefore, the processed results offer some insight as to what the parameter values might be, or at least the ranges in which they might be, for the convection coefficients, and a curve comparison for the temperatures of the FEA model and weld trials offer some revelation for an expected polynomial result that could be implemented to other criteria to determine temperatures for various rotations. Recommendations are set out for future work to be developed, not necessarily in the model itself, but more with respect to the computation time required to obtain other results and optimisation results.

7.7 Summary

Each of the sections above are discussed in detail and given support based on literature and results. The following summarises each of the sections outlined above;

- The development of the model went through various phases and resulted in depicting two phases of the FSW process
- The data processed for the FEA model and weld trials gave some valuable insight in terms of the convection coefficients that were used and calculated respectively
- A fair comparison can be made between the FEA model and the weld trials performed as temperature depicted a similar trend over time. This further supports the models reliability, although there is still room for improvement in the model
- Optimisation of the model is the next step in order to obtain values that have proven to have some uncertainty and due to the parametric behaviour of the model this is fairly reasonable to use with an optimisation tool such as modeFRONTIER

Chapter 8

8. Conclusions and recommendations

8.1 Introduction

The following conclusions and recommendations are listed below with reference to results found. During the course the study, the following workshops and conferences were attended by means of a selection process. The current work was presented at various stages of the study, where the following final conclusions have been expanded upon to those presented. The following events are listed in chronological order:

- HPC (High performance computing) - 2012
- IASSA 2012 (International Aerospace Symposium of South Africa) - 2012
- AeroMat (24th Advacnced Aerospace Materials and Processes) - 2013

The conclusions drawn are in adherence to the objectives outlined in the initial phase of the study and give a brief summary of those objectives achieved as well as important results obtained during the study that are applicable to each objective. The recommendations propose future work required and where attention is needed to further develop the study in order to achieve better results and more in depth knowledge of the FSW process.

8.2 Conclusions

- A thermo-mechanical model was developed using the new command features in ANSYS version 14.5, for the first two phases of the FSW process.
- Weld trials were performed for various rotational speeds and feed rates. The temperature during the process were recorded using the FLIR T640 thermal imaging camera. These experimental welds were processed using the FLIR tools + software in order to capture the temperatures at various points of the weld.
- Heat transfers and convection coefficients were calculated for the weld trials which was then used to compare with the FEA model. Due to the dissimilar inputs of the FEA model with that of the weld trials for comparison, the temperatures for the FEA model far exceed those of the weld trials which indicate that the rotation has a great effect on the temperature field. The convection coefficients input into the model need to be revised, but the temperature curves correlated to each other in comparison of trends,

which leads to the conclusion that the model does predict the correct heat generation in correspondence to the weld trials but more attention on the inputs of the model can be further developed and investigated should the time for processing be improved.

8.3 Recommendations

The following recommendations are for the FEA model as more processing time would allow for more results and a greater comparison with that of experimental findings. Although, the experimental procedure is also looked at for further development.

- Since the convection coefficients are highly influential on the output of temperature for the model, these values need to be checked and optimised in order to achieve a better result.
- The third step for the FSW process needs to be implemented so the feed rate can also be investigated as this will help in understanding the stresses incurred in the weld which can be compared to weld trials as well.
- The friction coefficient needs to be further investigated and a suggestion of a study to predict friction coefficients changing with temperature needs to be done as very little literature and findings are available on this subject. This value needs to be related to the FSW process parameters for the various phases of the weld. These results will be highly valuable when inserting inputs into a thermo mechanical modelling when predicting temperatures along the weld.
- Experimental procedure needs to be conducted more strictly, since the thermal imaging is extremely sensitive to environmental conditions. Although, these have been accounted for as much as possible, there is still minor discrepancies which could be why the results are not as consistent as if it were under perfect conditions. These perfect conditions for the setup include the exact angle the camera is set to the work piece and accounted for as the CNC table moves along the weld. Also, the camera needs to be kept as stable as possible and needs to be set so it is not affected by the vibrations of the CNC machine.
- A model with new parameter finding need to be run where the convection coefficient for the bottom of the work piece and backing plated needs to be made a lot higher than originally thought and other convection coefficients need to be adjusted as well.
- A relationship needs to be determined for the convection coefficients in order to manipulate the heat generation with what is happening realistically and this also corresponds to the material of the work piece and tool as well.
- Optimisation of parameters need to be investigated further, by creating a workflow for the parameters to modeFrontier which is an optimisation tool software. It’s

recommended that response surface method for optimisation be used since the temperature field is vast and an optimisation for all the values would require more than two variables.

Chapter 9

9. References

1) *Friction Stir Welding-Strong, Ductile and Environmentally Friendly.* Navy Metalworking Centre. Available: www.nmc.ctc.com. Accessed: July 2012.
2) Dr P. Colegrove, 2007. *Airbus evaluates Friction Stir Welding.* COMSOL News. A Technical Computing Magazine, Page 4-7.
3) Eclipse Aviation. 2012. Available: http://www.eclipse.aero/. Accessed: September 2012.
4) *Space Shuttle Technology Summary - Friction Stir Welding.* NASA Marshall Centre. Available: www.nasa.gov. Accessed: July 2012.
5) W.G. Babcock. 2003. *Friction Stir Welding Advances Joining Technology.* Ships- Navy Experts Explain the Newest Material & Structural Technologies. Volume 7, number 3. New York. AMPTIAC Quarterly.
6) J. De Backer and B. Verheyden, 2009. *Robotic Friction Stir Welding for Automotive and Aviation Applications*. University West, Master thesis, Mechanical Engineering.
7) *Joining-Friction Stir Welding.* The Aluminium Automotive Manual, 2002. Euoprean Aluminium Association. Available: auto@eaaa.be. Last accessed 31 January 2014
8) *Friction Stir Welding.* SAPA. SE-574 81 Sweden. Available: www.sapagroup.com. Last accessed 13 December 2013.
9) *Friction Stir Welding Technical Handbook.* ESAB, ISO 9001. Available: www.esab.com. Accessed: June 2012
10) R.S. Mishra and Z.Y. Ma. 2005. *Friction stir welding and processing.* Materials Science and Engineering R50 1-78. USA.
11) O. Masefield and P. Hartley, 2003. *ISTIR Friction Stir Welding Solutions.* MTS Systems Corporation, ISO 9001, USA.
12) G.J. Bendzsak, T.H North and C.B. Smith. *An Experimentally Validated 3D Model for Friction Stir Welding.* Department of Metallurgy and Material Science. University of Toronto, Canada and Tower Automotive Inc., Wisconsin, USA.
13) M. Song and R. Kovcevic. 2002. *Thermal modelling of friction stir welding in a moving coordinate system and its validation.* Research Centre for Advanced Manufacturing, Department of Mechanical Engineering. Southern Methodist University. USA.
14) E. Neumann 2004. Available: http://www.myphysicslab.com/numerical_vs_analytic.html. Accessed 5 January 2013.

15) B.Kural, M. Tabanoglu and H.T. Serindag. *Finite Element modelling of friction stir welding in aluminium alloys joint.* Mathematical and Computational applications Volume 18 pp122-131, 2013.

16) D. Stamenković, MSc (Eng), et al. *Finite Element Analysis of Residual Stress in Butt Welding Two Similar Plates*. Scientific Technical Review,Vol.LIX,No.1,2009. Serbia.

17) J. J. Muhsin, H. Moneer Tolephih and A. M. Muhammed, 2012. *Effect of friction stir welding parameters (rotation and transverse) speed on the transient temperature distribution in friction stir welding of AA 7020-T53*, ARPN Journal of Engineering and Applied Sciences, VOL. 7, NO. 4, APRIL 2012.

18) C.M. Chen, R. Kovacevic, 2003. *Finite Element modeling of friction stir welding-thermal and thermomechanical analysis*. International Journal of machine Tools and manufacture 43 (2003) 1319-1326. USA.

19) M. Malde, 2006. T*hermo mechanical modelling and optimization of friction stir welding*. December 2009 Master of Science in Industrial Engineering. B.E. Osmania University, Hyderabad, India, 2006.

20) X.K. Zhu and Y.J. Chao, 2001. *Effects of temperature-dependent material properties on welding simulation*. Computers and Structures 80 (2002) 967–976. Department of Mechanical Engineering, University of South Carolina, USA.

21) M Awang, V.H. Mucino, Z. Feng and S.A David, 2005. *Thermo-Mechanical Modeling of Friction Stir Spot welding process: Use of an explicit Adaptive Meshing scheme.* SAE International.

22) M. Grujicic, T. He, G. Arakere, H.V. Yalavarthy, C.F. Yen and B.A. Cheeseman, 2009. *Fully coupled thermo-mechanical finite element analysis of material evolution during friction-stir welding of AA5083*. Vol. 224 Part B: J. Engineering Manufacture JEMI 750.

23) Y. J. Chao, X. Qi and W. Tang, 2003. *Heat Transfer in Friction Stir Welding - Experimental and Numerical Studies.* Vol. 125, Journal of Manufacturing Science and Engineering FEBRUARY 2003 Transactions of the ASME.

24) M. Grujicic, G. Arakere, H.V. Yalavarthy, T. He, C.F. Yen, and B.A. Cheeseman, 2009. *Modeling of AA5083 Material-Microstructure Evolution during Butt Friction-Stir Welding*. ASM International, Journal of Materials Engineering and Performance, Volume 19(5) July 2010.

25) H. Li, D. Mackenzie and R. Hamilton. *Multi-Physics Simulation of Friction stir welding process.* Engineering computations journal. Research Article: EC-Apr-2009-0027.R1.

26) A. H. Kheireddine, A. A. Khalil, A.H. Ammouri, G.T. Kridli amd R.F. Hamade, 2013. *An Experimentally Validated Thermo-Mechanical Finite Element Model for Friction Stir Welding in Carbon Steels*. World Academy of Science, Engineering and Technology 76 2013, USA.

27) G.J. Bendzsak, T.H. North and C. B. Smith. *An Experimentally Validated 3D Model for Friction Stir Welding.* 52nd FSW Symposium. Univeristy of Ontario, Canada and Wisconsin USA.

28) P.A. Colegrove, H.R. Shercliff and R. Zettler. *A Model for Predicting the Heat Generation and Temperature in Friction Stir Welding from the Material Properties*. Science and Technology of Welding & Joining, Volume 12, Number 4, May 2007, pp. 284-297.

29) P.A. Colegrove. *Modelling of Friction Stir Welding*. A dissertation submitted to the University of Cambridge for the degree of Doctor of Philosophy, 2003.

30) P. Tasic, Dr I. Hajro and Dr D. Hodzic *Simplification possibilities for estimation of FSW process efficiency by* FEA. Journal of trends in Development of Machinery and Associated Technology Vol. 17 No.1 pp41-44, 2013.

31) R. Nandan, G.G. Roy, J. Lienert and T. DeBroy, 2006*. Numerical modelling of 3D plastic flow and heat transfer during friction stir welding of stainless steel*. Science and technology of welding and joining 2006. Vol. 11.

32) D. Sharma and Dr. R.K. Bhushan, 2013. *Thermomechanical Modeling of FSW: A Review*. International Journal of Emerging Technology and Advanced Engineering. Vol 3 Special Issue 2, January 2013. National conference on Machine Intelligence Research and Advancement, India.

33) P. Vilaca and L. Quintino, 2006. *Experimental and computational developments of FSW*. Welding equipment and Technology, 2006. ISSN 1221-4639. University of Lisbon, Portugal.

34) H. Schmidt, J. Hattel and J. Wert, 2004. *An analytical model for the heat generation in friction stir welding*. Modelling Simul. Mater. Sci. Eng. 12 143 Available: http://iopscience.iop.org/0965-0393/12/1/013 downloaded on 28/05/2010 at 23:17. Denmark. Accessed December 2013

35) R. Nandan, B. Prabu, A. De, and T. Debroy. *Improving Reliability of Heat Transfer and Materials Flow Calculations during Friction Stir Welding of Dissimilar Aluminium Alloys*. Welding Journal, October 2007, Vol. 86.

36) C. Hamilton, S. Dymek, and A. Sommers, 2010. *Characteristic Temperature Curves for Aluminium Alloys during Friction Stir Welding*. Welding journal, September 2010, VOL. 89.

37) S.A. Emam and A.E. Domiaty, 2009. *A Refined Energy-Based Model for Friction-Stir Welding*. World Academy of Science, Engineering and Technology 29 2009.

38) M.B. Đurđanović, M.M. Mijajlović, D.S. Milčić, D.S. Stamenković. *Heat Generation during Friction Stir Welding Process*. Tribology in industry, Vol. 31, No. 1&2, 2009.

39) A.K. Lakshminarayanan and V. Balasubramanian, 2007. *Process parameters optimization for friction stir welding of RDE-40 aluminium alloy using Taguchi technique*. Science Direct. Transactions of Nonferrous Metals Society of China.

40) J.T. Khairuddin, J. Abdullah, Z. Hussain and I.P. Almanar. *Principles and Thermo-Mechanical Model of Friction Stir Welding*. Chapter 9- Welding process, page 191-216.

41) S.A. Khodir. *Microstructure and Mechanical Properties of Friction Stir Welded Dissimilar Aluminum Joints of AA2024-T3 and AA7075-T6.* Materials Transactions, Vol. 48, No. 7 (2007) pp. 1928 to 1937 2007 The Japan Institute of Metals.

42) L. Cederqvist and A.P. Reynolds. *Factors Affecting the Properties of Friction Stir Welded Aluminum Lap Joints.*

43) A. K. Hussain and S.A. Quadri. *Evaluation of parameters of friction stir welding for aluminium AA6351 alloy*. International Journal of Engineering Science and Technology, Vol. 2(10), 2010, 5977-5984.

44) M.M. Mijajlovic, N.T. Pavlovic, S.V. Jovanovic, D.S. Jovanovic and M.D. Milicic. 2012. *Experimental studies of parameters affecting the heat generation in friction stir welding process.* Thermal Science, 2012, Volume 16. Pages S351-S362.

45) I. Martinez. *Thermal effects on materials*. 12 February 2013.

46) R.C. Rice, 2003. *Metallic materials properties development and standardization.* DOT/FAA/AR-MMPDS-01, Springfield Virginia.

47) *Alloy 2024 sheet and plate*. ALCOA mill products. Available: www.millproducts-alcoa.com.

48) Volume was prepared under ASM International Handbook Committee. *ASM Handbook Volume 1: Properties and selection: Irons steels and high performance alloys.*

49) Matweb:*Tool steel H13 Interlloy* Available: www.matweb.com, Accessed: 27 August 2012.

50) Matweb:*QR090 Supree Hot work Tool Steel*. Matweb Available: www.matweb.com, Accessed 15 August 2013.

51) Z. Na, 2012. *Finite element analysis of pressure on 2024 aluminium alloy created during restricting expansion-deformation heat-treatment*. Science Direct. Trans. Nonferrous Met. Soc. China 22(2012) 2226−2232.

52) Hyper Physics. Available: http://hyperphysics.phy-astr.gsu.edu/hbase/frict3.html Accessed: 19 December 2013.

53) 1963. *Friction and Wear at elevated temperatures.* Technical Documentary Report WADC-TR-59-603. Directorate of Materials and Processes.

54) F.M. Chester, 1994. *Effects of temperature on friction: Constitutive equations and experiments with quartz gouge.* Journal of Geophysical research, Vol 99. No. B4 pages 7247-7261.

55) Callster. *Chapter 17, Thermal properties, 12 February 2013*. Pages 713-729. Accessed: 15 October 2013.
56) J. Vlachopoulos and D. Strutt. *Basic heat transfer and some applications in polymer processing.* Vol 2, pages 21-33, SPE 2002.
57) *Infrared Energy, Emissivity, Reflection & Transmission*. Williamson Corporation, MA01742.
58) E. Fronapfel, 2006. *Emissivity Measurements of Common Construction.* InfraMation ITC 115 A 2006-05-22.
59) ANSYS HELP file, // Element Reference // I. Element Library // SOLID226. Accessed 20 January 2014.
60) D. Correia. *Research project* 2011.University of the Witwatersrand. 2012.
61) FLIR. *FLIR T640 camera*. Available: flir.com/aboutFLIR/. Accessed: 12 December 2013.
62) FLIR. *FLIR T640 camera*. FLIR-Tools-Manual. Accessed: 28 February 2013.
63) FLIR. *FLIR T640 camera* NET zero tools. Available: www.flir.com.
64) FLIR. *FLIR T640 camera* image specs. Available: www.flir.com.
65) FLIR. *FLIR T640 camera*. Available: www.flir.com. Accessed: October 2012.
66) FLIR. Available: http://www.flir.com/cs/emea/en/view/?id=41702 Accessed: 12 December 2013.
67) FLIR. *FLIR T640 camera*. Available: www.flir.com. Tech data-Camera Accessed: 27 Feb 2013.
68) MatWeb. Available: www.matweb.com, Accessed: 30 August 2012
69) MatWeb. Available: www.matweb.com, Accessed: 15 August 2012
70) MatWeb. Available: www.matweb.com, Accessed: 2 September 2012
71) J.G. Kaufman. *Properties of Aluminium Alloys: Tensile, Creep & Fatigue Data at High & Low*. Avaialble: http://books.google.co.za/books?id=3U_eQdnmzmwC&pg=PA1&lpg=PA1&dq=temperature+dependent+properties+of+aluminium&source=bl&ots=1h2Nal3MMb&sig=rr89HE6346k1iisfgJY4PsK7ofk&hl=en&sa=X&ei=ygMaUYH8BYSa1AXm5YCQDQ&ved=0CGMQ6AEwCTgK#v=onepage&q=temperature%20dependent%20properties%20of%20aluminium&f=false Accessed: October 2012.
72) G.S. Brady. *Materials Handbook.* Materials, their properties and uses. 15th Edition, McGraw Hill.
73) S. Babu, 1999. *Material and Surface Engineering for Precision Forging dies.* Precision forging consortium ohio aerospace institute and national cennter for manufacturing sciencecs. Ohio state University, USA.

74) *Table of Emissivity* Available: www.monarchinstrument.com. Obtained on: 20 Dec 2013.

Chapter 10

10. APPENDIX

10.1 Appendix 1: Further information on literature models

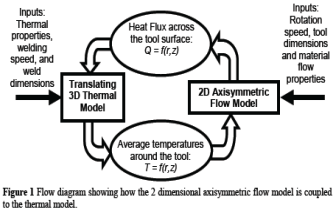
The tables are summarised version of the context found for each type of model in the literature survey.

Table 10.1: Numerical models investigated

Model ID	Model description	FSW process parameters and material properties	Parameters and assumptions
1 [15]	1. Only one plate is modelled due to symmetry. 2. SOLID70 is used which has 3D thermal conduction and can be used in steady state or transient thermal analysis. 3. Pin is incorporated in model. 4. Transient thermal analysis is used. 5. Moving heat source with heat distribution is used	Rotation- 800, 1000, 1200 rev/min Feed rates- 2.5 and 5 mm/s. 6061-T6 aluminium alloy plates, 3.1mm thick	5. Thermal conductivity and heat capacity are dependent on temperature. 6. Heat flux is applied to the interface of the tool shoulder, pin and work piece. 7. Convection coefficients- 30W/m^2 and 300W/m^2.
2 [30]	Tool serves as heat sink-Has constant ambient temperature on outside surface.	None given	Assumed: Maximum temperature does not exceed 500° C. Radiation is neglected. Material properties are temperature dependant.
3 [31]	Thermal conductivity, specific heat and yield strength depend on temperature and used in model.	304 Stainless steel	Assumptions- Heat is generated at constant rate for quasi-steady flow. Mass flow is non-Newtonian, incompressible, visco-plastic material. Partial sticking condition at surface of tool and work piece.
5 [21]	3D Dynamic fully coupled thermal-stress analysis. 2. C3D8RT Element is used which is an 8 node tri-linear displacement and temperature	Plunge rate- 2.668mm/sec (step1) Plunge rate-0.493mm/sec (Step2) Aluminium Alloy 6061-T6.1mm thick plate	Assumptions-Frictional contact is by Coulomb's frictional law and temperature dependent. Friction coefficient=0 at melting temperature of material
6 [22]	1. Fully coupled thermo mechanical model is created.	Fixed rotational speed range	Static and kinetic coefficients are set to a specific value. Arbitrary

	2. Nodal degrees of freedom include nodal velocities and nodal temperature. 3. Effect of local temperatures on for mechanical aspects are accounted for by temperature dependant material properties of the work piece.	• 200-400rev/min Aluminium alloy 5083-H321 thickness 3 mm	Langragian Eulerian formulation is used. Boundary conditions- Bottom of work piece is constrained, Tool rotation is maintained, fixed contact pressure applied over tool and work piece interface, work piece is still for first 2 seconds after which a constant material flow velocity is applied.
7 [23]	1. Study heat transfer of the work piece and tool. 2 DCAX4 element type used for the tool. 3. Heat source moves along work piece at same weld speed set for the tool. 4. Only half the work piece is modelled due to symmetry.	240 RPM and 2.36mm/sec weld speed. Aluminium alloy 2195 T8 8.1 mm thick	Used thermocouples in experiment to determine temperatures along weld. Temperature dependant material properties are used for the tool, thermal conductivity, specific heat and density. 30W/m^2°C is conductivity of top surface of work piece. Convection coefficient at bottom is dependent on temperature.
8 [16]	1. Thermal and mechanical welding simulation using a moving heat source and temperature dependent material properties. Used to predict residua stresses in butt welds. 2. SOLID70 element used for thermal analysis and SOLID45 used for structural analysis. 3. Change in thermal state causes change in mechanical state	Weld speed 5mm/sec ASTM 36 Steel plate (carbon steel), 3mm thick	Thermal stresses are results from the temperature distribution by thermal model from which mechanical analysis uses previous results to obtain displacements
9 [26]	3D thermo mechanical coupled model is developed. 2. Tetrahedral elements are used. 3. Backing plate and tool are for thermal analysis only.	(AISI 1045) Carbon steel, 3.2 mm thick	Constant mechanical properties defined in table those that are no present are dependent on temperature changes. Convective heat coefficient- 20 W/m^2 °C. Heat transfer between tool and work piece- 11kW/m^2 °C. Friction coefficient is dependent on temperature.
10 [20]	3D nonlinear thermal and thermo-mechanical analysis using FEA. 2. Investigate the effect of material properties which are temperature dependent on the transient temperature, residual stresses and distortion in welding process. 3. Thermal analysis performed which results are transferred to thermo-mechanical analysis	5025-H32 Aluminium alloy, 6.25mm thick	

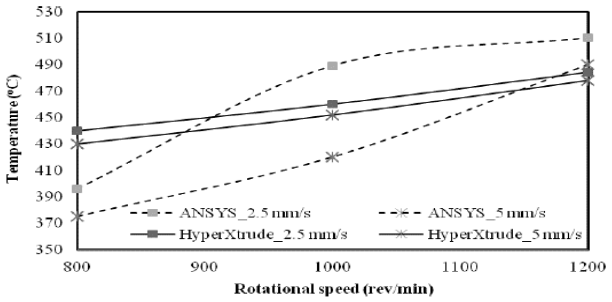
11 [13]	Moving co-ordinate is used to model the moving tool.	Aluminium Alloy 6061-T6.12.7mm thick plate Constant material properties	Yield stress strongly depends on temperature.
12 [27]	3D heat and material flow. 2. Analysis physical properties within the weld. 3. 3-D Navier stokes equations are used as well as non-linear dynamics. 4. Software offers temperature and heat generation field outputs as well as velocity profiles and pressure distributions.	Wed speed-20mm/sec. Tool rotation-1200rpm. Aluminium 6061-T6 7mm thick plate	1. Assumption that the material surrounding to tool is at eutectic temperature. 2. Constant temperature conditions are used.
13 [32]	Thermo-mechanical problem is modelled.		Thermo physical and thermo mechanical material properties are taken into account.
14 [17]	3D nonlinear thermal mechanical simulation. Arbitrary Langragian formulation is used. Predict numerical thermal distribution of aluminium alloy 7020-T53. SOLID70 is used for the thermal analysis. Heat loss is modelled by convection.	Welding speeds-40mm/min and 16mm/min. Rotation-900rpm and 1400 rpm. Aluminium alloy 7020-T53, 5 mm thick	K-Type thermocouples are used. Transient temperatures are recorded. Thermal analysis of FEA performed. Newton Raphson and non-linear equations are used in analysis.
15 [18]	Study thermal history and thermo mechanical process in butt welds. 2. Residual stress measured using X ray diffraction is used to validate model. Considering the mechanical effect of the tool, stresses in the weld can be determined by the impact of the thermal effect of the FSW.	Rotation-500rpm and welding speed is 140mm/min. Aluminium alloy 6061-T6, 6 mm thick	Temperature dependent properties are used up to a particular temperature (371Deg C) which after temperature dependent properties are extrapolated for the material. Constant friction coefficient is used. Langrangian FEM is used.
16 [33]	Computational modelling involves the following difficulties when developing this: Material deformation, heat generated due to sliding which depends on unknown		iSTIR is a thermal analytical model and is a 'reverse engineering approach'. Integra3D is code associated with the

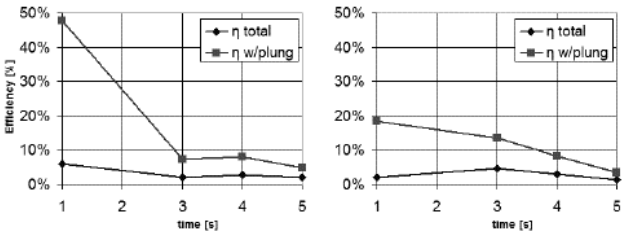
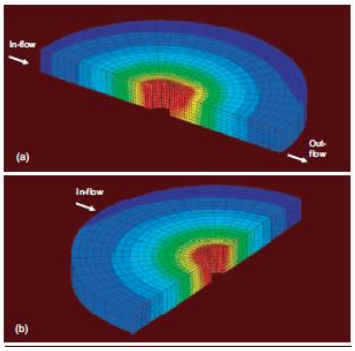
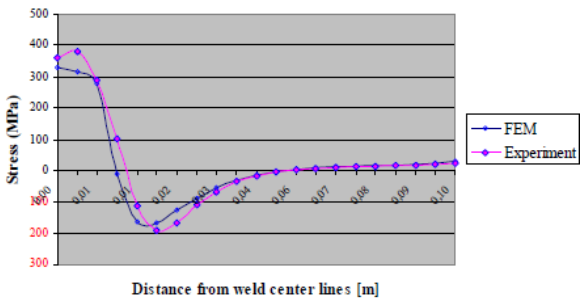
	friction coefficient, materials thermo-mechanical properties, thermal flow into the tool and work piece.		numerical modelling of FSW written in FORTRAN code.
17 [24]	Fully coupled thermo-mechanical FE model. Modelling of work piece material behaviour and interaction between plastic deformation and dynamic recrystallisation process.	Aluminium alloy 5083-H131	Heat generation equations are considered as well as heat and mass transfer equations are investigated using conservation equations of energy and momentum. Material flow of the work piece and temperature fields of the model are investigated. Process parameters and tool design are also considered.
18 [28]	Predicts heat generation from thermal properties, process parameters and physical attributes from the tool and work piece. Couples 3D thermal model which involves calculating the heat flow to a 2D axisymmetric flow model to calculate the heat generation.  **Figure 1** Flow diagram showing how the 2 dimensional axisymmetric flow model is coupled to the thermal model. Figure 10.1: Flow model depicting coupling for thermal model	Aluminium alloy 2024, 7449 and 6013 350rpm and 350mm/min	Thermal model is used to predict the temperature near the tool surface using the thermal properties associated with the process. The 2D axisymmetric model predicts the rotational flow around the tool. Thermal model involves four different pathways for the loss of heat which these are used as the convective heat transfer coefficient. This coefficient is temperature dependent but is difficult to determine since its sensitive to the material condition but since volume of material is small, assuming a room temperature value is a viable option.
19 [25]	Thermo mechanical coupled model is developed. C2D8RT elements are used which is an 8-node, 3D temperature displacement coupled element.	Aluminium 2024-T3, 3 mm thick	Convection coefficient of 1000W/m^{2}K is used for the bottom surface of the backing plate and the rest of the plate 10W/m^{2}K is used.
20 [19]	Studied model based optimisation approach to understand effect of input parameters. Using a developed model to study the temperature history of the weld as well as the residual stresses. SOLID70 is used. SOLID185 is used to model the plate and is switched from the SOLID 70 so it goes from thermal to structural.	304L stainless steel	Material properties used changing with temperature; Specific heat, thermal conductivity and density. Design of experiment technique is used to optimise the factors affecting the results of the process.
21 [29]	Main objective is to assist the design of tools by creating a numerical model. Visualises material flow for the FSW process.	Experimentally various process parameter were investigated on	Convection coefficient of 1000W/m^{2}K is used for the bottom surface of the backing plate and

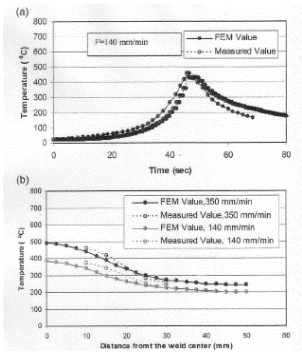
	Investigation into threaded and unthreaded tool profiles using 3D CFD model is also done but for purposes of the study undertaken only information regard temperature will be extracted for assumptions to be made for current model being developed. CFD modelling of flow around profiled FSW tooling is also investigated.	various thickness of plates. Aluminium alloy 7075	the rest of the plate 10W/m^{2}K is used.

Results for the numerical model are outlined and the software used for each is also stated.

Table 10.2: Results and issues discussed for numerical models

Model ID	Software used to develop model	Results and issues
1 [15]	ANSYS APDL and HyperXtrude	Differences are due to the different mathematical models used in the software. 2. Maximum temperatures obtained near the weld are higher than recrystallizing temperature of aluminium.  Figure 10.2: Rotational speed versus temperature result for numerical model 1
2 [30]	Not indicated	As weld time increases, efficiency ratio decreases. 2. Heat flux from friction is dependent on the dynamic friction coefficient and stresses. 3. Graph depicts efficiency decreasing with weld time taking into account plunge or without plunge. Issues

		• Calculating heat transfer efficiency has its complications and lacks accuracy.  Figure 10.3: Efficiency of weld over time for numerical model 2
3 [31]	Not indicated	Temperatures on advance side are higher than in retreating side due to higher local relative velocity.
5 [21]	ABAQUS/EXPLICIT	Higher maximum temperature was experienced at the tool/work piece and may be due to the approximated friction coefficients.
[22]	ABAQUS/EXPLICIT	Constant mechanical properties are used, not changing with temperature include- density and specific heat  Figure 10.4: Numerical model 6 modelling result
7 [23]	ABAQUS-Tool. WELDSIM-work piece	
8 [16]	ANSYS	Good comparison between experimental and FEM.  Figure 10.5: Stress along weld line result for numerical model 8

9 [26]	DEFORM 3D	A higher rotational speed in case 2 gave a peak temperature in the FEA model close to peak temperature found experimentally.
10 [20]	WELDSIM	Thermal conductivity, Yield stress and Young's modulus have certain effects on transient temperature, stress and distortion respectively. Average conductivity as well as using a constant conductivity at room temperature can be used to determine temperature. All thermal properties can be taken at room temperature. Yield stress has to be a function of temperature.
11 [23]	Not indicated	
12 [27]	STIR3D	Material flow results are given. Software models the flow structure and its irregularities consistently that is observed micro structurally.
13 [32]	Various models are discussed	
14 [17]	Experimental and ANSYS APDL	Results of both compare well, with a 2 % error. Axial load decreases with increase in rotational speed. Temperature on advance side is higher than retreating side. Temperature increases with rotation speed increasing. Issues • Friction is kept constant. Only thermal model is predicted.
15 [18]	ANSYS and X-ray diffraction used to measure the stresses in the weld.	Highest temperature is at centre of weld. Calculated values of temperature are higher than the measured temperatures but less after the maximum temperature. Higher welding speed produces lower temperatures in weld. Higher stress is produced by a higher weld speed.  Figure 10.6: Temperature results for numerical model 15

16 [33]	Discussion of computational and experimental FSW processes.	
17 [24]	ABAQUS/Explicit	Plastic strain results are discussed and material trajectories are concluded based on process parameters. Larger thermal gradients are observed in the front of the tool. Higher rotational speed results in higher temperatures.
18 [28]	Steady state thermal model is created in FLUENT.	Appears as if the boundary condition at the shoulder is a slip condition, but using a smaller contact radius, a stick condition (simpler model) can be used to predict heat generation.
19 [25]	ABAQUS/Explicit	Temperature dependent properties, young's modulus, friction coefficient and shear stress can result in better temperature predictions.
20 [19]	ANSYS with parametric studies	Peak temperature increases with weld speed. Work piece temperature decreases with increase of weld speed. Issues • Two stages are carried out, from transient thermal analysis to a non-linear structural analysis. Process variables are limited and future work is suggested to perform optimisation on a process model which includes more input variables and output responses.
21 [29]	FLUENT	Slip model indicates that different tool designs affect condition whether sticking or slip is occurring or both.

Table 10.3: Analytical models investigated

Model ID	**Model description**	**FSW process parameters and material properties**	**Parameters and assumptions**
3 [34]	Estimate heat generation based on different contact conditions	Rotation speed-400rpm, welding speed-120mm/min, plunge depth 0.2mm. Aluminium Alloy 2024-T3	Yield stress is dependent on temperature.

4 [35]	Heat, momentum and solute transport model with a fixed grid finite difference method is used.	Aluminium alloy 1200 and aluminium alloy 6061	Friction coefficient, sticking condition, heat transfer coefficient at bottom surface and extent of viscous dissipation are important parameters considered that affect output results.
5 [36]	Predict maximum temperature using characteristic curves to determine temperatures for Sc-modified and Al-Zn-Mg-Cu alloy. Uses Mikron M7815 thermal imaging camera to obtain temperature profile.	225,250,300 & 400 rev/min Sc-modified and Al-Zn-Mg-Cu alloy	Friction coefficient is dependent on temperature. Calculations changed friction coefficient depending in energy levels value and was adjusted accordingly.
6 [37]	Investigates the heat generated due to plastic deformation within work piece and the friction between the surfaces using an energy based model.	Aluminium alloy 6000 and 7000 series.	Average value of friction coefficient for sticky condition is 0.5 and 0.25 for sliding condition and is dependent on the energy value.
7 [13]	Moving co-ordinate is used to model the moving tool.	Aluminium Alloy 6061-T6.12.7mm thick plate	Yield stress strongly depends on temperature.
8 [38]	Mathematical model shows the geometrical conditions for heat generation		Two basic tribological processes are involved- Pure sliding associated with adhesion and pure sticking associated with the deformation part of the process. Constant pressure and friction coefficient is assumed.

9 [39]	Investigate optimised properties to improve tensile strength of the joint. Uses Taguchi parametric design approach.	RDE-40 aluminium alloy, 6 mm thick	Taguchi method determines most influential parameters which are independent of variation in environmental conditions. Uses an orthogonal array.
10 [40]	Predicts the transient temperature profile and stresses developed as well as the 3D force components. Various cases are considered for the model. Case 1 and 2 assume sliding condition, case 3 assumes sticking condition, case 4 is experiment plunge force and first three cases are theoretical plunge force.	Aluminium alloy 6061-T6, 7 mm thick	It describes the friction coefficient being constant during the static phase and temperature dependant when kinetic friction is taken into account as a result of the condition being sliding or non-sticking. Plastic dissipation heat generation occurs at higher temperatures due to the frictional heat and is said to only be significant during the dwell phase and welding of the process. Constant friction coefficient but for sliding condition, is dependent on temperature. After sliding, sticking condition is assumed.

Table 10.4: Results for analytical models

Model ID	**Results and issues observed**
3 [34]	Close to sticking condition is concluded.
4 [35]	Parameters mentioned important affect the temperature fields: Friction coefficient Slip condition

5 [36]	As welding energy increases, discrepancies with relation to experimental data and predicted temperature data exists. Issues • Formula used to calculate weld energy per unit length does not take into account heat generation due to plastic deformation.
6 [37]	Heat due to plastic deformation has a significant effect on the temperature results.
8 [38]	Combination of sliding and sticking condition exists. Issues • Uncertainties in values for combination of sliding and sticking exist with mathematical model.
9 [39]	(% contribution)Rotational speed (41%0, traverse speed (33%) and axial force (21%) affect tensile strength significantly.
10 [40]	Experimental depicts a profile that is similar to case 4 for the plunge force but similar to case 3 for the tool torque. Issues • Assumes either slip or sticking condition between rotating tool and work piece. This is not always the case.

The following table summarise the parameters and material properties that was used as well as any other valid assumptions made for each.

Table 10.5: Experimental studies investigated

Model ID	**Model description**	**FSW process parameters and material properties**	**Parameters and assumptions**
1 [41]	Investigates effect of rotational speed for joining dissimilar materials.	Aluminium Alloy 2024-T3 and Aluminium Alloy 7075 T6 3mm thick Constant weld speed-100 mm/min. Rotation speeds-400,800,1600, 2000 /min	Peak temperature and deformation rates influence the microstructure and grain size during the FSW process.

2 [43]	Investigating lap joints of aluminium alloys	Aluminium 2024-T3 and Aluminium 7075-T6, 2.29mm thick Table 1 — Welding Parameter and Overlap Shear Test Data Weld No. / Tool No. / WS (mm/s) / RS (rpm) / SP/DP / SE (mm) / F Load (kN) R (R1) Loaded / F Locations R (R1) Loaded / F Load (kN) A (R2) Loaded 1 1 2.3 495 SP — 7.0 A,B 14.0 2 2 2.3 495 SP — n/a n/a 8.3 3 3 2.3 495 SP — 8.0 t.o. 9.4 4 4 2.3 495 SP — n/a n/a 5.6 5 5 2.3 495 SP — 8.5 A, B 12.2 6 6 2.3 495 SP — 10.9 A, B 14.0 7 9 2.3 300 SP — 21.4 A, B 15.6 8 1 2.3 495 DP 3.8 14.4 R1, T 15.1 9 6 2.3 495 DP 3.8 17.8 R1, T 17.7 10 6 2.3 495 DP 6.4 18.3 R1, T 19.6 11 6 3.3 495 DP 3.8 16.7 R1, T 18.6 12 6 3.3 638 DP 3.8 17.7 R1, T 14.9 13 6 3.3 638 DP 6.4 16.7 R1, T 17.1 14 6 3.3 638 DP 8.9 18.0 R1,T 20.3 15 6 4.2 983 DP 5.1 16.1 R1, T 16.7 16 6 4.2 833 DP 5.1 15.6 R1, T 17.0 17 5 3.3 495 DP 5.8 15.7 R1, T 18.1 18 5 5.6 495 DP 5.8 17.7 R1, T 17.9 19 7 2.3 300 DP 8.9 19.6 R1, T 21.4 20 7 2.3 495 DP 8.9 16.4 R1, T 16.6 21 8 2.3 300 DP 8.9 20.0 R1, T 23.0 22 8 3.3 495 DP 8.9 20.9 R1, T 23.8 23 9 2.3 300 DP 8.9 22.8 R1, T 22.6 24 9 3.3 495 DP 8.9 23.2 R1, T HAZ 23.3 25 9 4.2 833 DP 8.9 20.9 R1, T 22.4 Figure 10.7: Table of welding parameters for experimental work	Table 2 — Tool Dimensions Tool No. / Pin Length (mm) / Pin Diameter (mm) / Shoulder Diameter (mm) 1 4.0 5.1 12.7 2 4.0 4.4 12.7 3 3.0 5.1 12.7 4 3.0 4.4 12.7 5 4.0 5.9 12.7 6 3.0 4.8 15.7 7 3.6 9.7 25.4 8 3.3 9.7 25.4 9 3.0 9.7 25.4 Figure 10.8: Tool dimensions for experimental
4 [43]	Tensile strength and hardness for the FSW process is evaluated under various process parameters.	770rpm and 75mm/min. 130rpm and 900 rpm with same weld speed. 90mm/min and 900rpm. Aluminium alloy 6351, 6 mm thick	Uses Vickers hardness and radiography to measure outputs welds with various parameters. Important process parameters- Feed rate, depth of penetration and spindle speed (rotation). Ratio of tool speed to weld speed is 4:3
5 [44]	Analytical model to estimate heat generation and the parameters that affect this are investigated.	Aluminium alloy 2024-T351, 6mm thick. Table 1. Proposed technological parameters for welding of Al 2024 T351 [4] Recommended diapason/value / Optimal values Tool rotation speed: n = 750-1180 rpm / n = 910 rpm Plunging speed: v_z – no recommended value / v_z – not determined Travel speed: v_x = 46-150 mm/min. = 0.77-2.5 mm/s / v_x = 0.062 mm/rev. = 0.9403 mm/s Tilt angle: ≤5° / 1°-2° Welding length: l = 50 mm / l = 100 mm Figure 10.9: Table of tool parameters for experimental	Dominant influencing parameters are, tool geometry, technological parameters, delivered loads, tribological parameters (Friction coefficient, contact and shear stresses), temperature of the work piece and mechanism of heat generation. Friction coefficient is taken as a constant.

10.2 Appendix 2: Material properties

The material properties come from the references in Matweb [68-70]

Table 10.6: Aluminium alloy 2024 properties changing with temperature

Temperature (°C)	Thermal conductivity (W/mK)	Specific Heat (J/kgK)	Elastic modulus (MPa)	Yield strength (MPa)	Density (kg/m^3)	Thermal expansion coefficient (/10^-6)
20	164	881	72.4	473	2780	14
100	182	927	66.5	416.5	2780	23.018
200	194	1047	63.5	293.5	2780	24.509
300	202	1130	60.4	239.8	2780	25.119
400	210	1210	56.1	150	2780	25.594
500	220	1300	50	100	2780	26.637

Table 10.7: Aluminium Alloy 2024 T3

Physical Properties	Metric	Comments
Density	2.78 g/cc	AA; Typical
Mechanical Properties	**Metric**	**Comments**
Hardness, Brinell	120	AA; Typical; 500 g load; 10 mm ball
Hardness, Knoop	150	Converted from Brinell Hardness Value
Hardness, Rockwell A	46.8	Converted from Brinell Hardness Value
Hardness, Rockwell B	75	Converted from Brinell Hardness Value
Hardness, Vickers	137	Converted from Brinell Hardness Value
Tensile Strength, Ultimate	>= 440 MPa	Drawn tube
	>= 475 MPa	Wire, rod, and bar (rolled or cold finished); T36
	483 MPa	AA; Typical
	34.0 MPa @Temperature 371 °C	
	52.0 MPa @Temperature 316 °C	
	76.0 MPa @Temperature 260 °C	

	186 MPa @Temperature 204 °C	
	379 MPa @Temperature 149 °C	
	455 MPa @Temperature 100 °C	
	483 MPa @Temperature 24.0 °C	
	496 MPa @Temperature -28.0 °C	
	503 MPa @Temperature -80.0 °C	
	586 MPa @Temperature -196 °C	
	>= 435 MPa @Thickness 0.203 - 3.25 mm	Flat sheet
	>= 440 MPa @Thickness 3.28 - 6.32 mm	Flat sheet
	>= 395 MPa @Diameter <=6.32 mm	Wire, rod, bar and shapes (extruded)
	>= 395 MPa @Diameter <=6.32 mm	Extruded tube
	>= 415 MPa @Diameter 6.35 - 19.0 mm	Wire, rod, bar and shapes (extruded)
	>= 415 MPa @Diameter 6.35 - 19.0 mm	Extruded tube
	>= 450 MPa @Diameter 19.0 - 38.07 mm	Wire, rod, bar and shapes (extruded)
	>= 450 MPa @Diameter 19.0 - 38.07 mm	Extruded tube
	>= 470 MPa @Diameter >=38.1 mm	Wire, rod, bar and shapes (extruded); Area 25-32 in^2
	>= 470 MPa @Diameter >=38.1 mm	Extruded tube; Area 25-32 in^2
	>= 485 MPa @Diameter >=38.1 mm	Wire, rod, bar and shapes (extruded); Area <25 in^2
	>= 485 MPa @Diameter >=38.1 mm	Extruded tube; Area <25 in^2
Tensile Strength, Yield	>= 290 MPa	Drawn tube
	345 MPa	AA; Typical

	>= 360 MPa	Wire, rod, and bar (rolled or cold finished); T36
	>= 290 MPa @Thickness 0.203 - 3.25 mm	Flat sheet
	>= 290 MPa @Thickness 3.28 - 6.32 mm	Flat sheet
	>= 290 MPa @Diameter <=6.32 mm	Wire, rod, bar and shapes (extruded)
	>= 290 MPa @Diameter <=6.32 mm	Extruded tube
	>= 305 MPa @Diameter 6.35 - 19.0 mm	Wire, rod, bar and shapes (extruded)
	>= 305 MPa @Diameter 6.35 - 19.0 mm	Extruded tube
	>= 315 MPa @Diameter 19.0 - 38.07 mm	Wire, rod, bar and shapes (extruded)
	>= 315 MPa @Diameter 19.0 - 38.07 mm	Extruded tube
	>= 315 MPa @Diameter >=38.1 mm	Extruded tube; Area 25-32 in^2
	>= 330 MPa @Diameter >=38.1 mm	Wire, rod, bar and shapes (extruded); Area 25-32 in^2
	>= 330 MPa @Diameter >=38.1 mm	Extruded tube; Area <25 in^2
	>= 360 MPa @Diameter >=38.1 mm	Wire, rod, bar and shapes (extruded); Area <25 in^2
	28.0 MPa @Strain 0.200 %, Temperature 371 °C	
	41.0 MPa @Strain 0.200 %, Temperature 316 °C	
	62.0 MPa @Strain 0.200 %, Temperature 260 °C	
	138 MPa @Strain 0.200 %, Temperature 204 °C	
	310 MPa @Strain 0.200 %, Temperature 149 °C	
	331 MPa @Strain 0.200 %, Temperature 100 °C	

	345 MPa @Strain 0.200 %, Temperature 24.0 °C	
	352 MPa @Strain 0.200 %, Temperature -28.0 °C	
	359 MPa @Strain 0.200 %, Temperature -80.0 °C	
	427 MPa @Strain 0.200 %, Temperature -196 °C	
Elongation at Break   	>= 10.0 %	Wire, rod, and bar (rolled or cold finished); T36
	10.0 - 16.0 %	Drawn tube
	11.0 % @Temperature 149 °C	
	16.0 % @Temperature 100 °C	
	17.0 % @Temperature -80.0 °C	
	17.0 % @Temperature -28.0 °C	
	17.0 % @Temperature 24.0 °C	
	18.0 % @Temperature -196 °C	
	23.0 % @Temperature 204 °C	
	55.0 % @Temperature 260 °C	
	75.0 % @Temperature 316 °C	
	100 % @Temperature 371 °C	
	10.0 - 15.0 % @Thickness 0.203 - 3.25 mm	Flat sheet
	>= 15.0 % @Thickness 3.28 - 6.32 mm	Flat sheet
	18.0 % @Thickness 1.59 mm	AA; Typical
	>= 8.00 % @Diameter >=38.1 mm	Extruded tube; Area 25-32 in^2

	>= 8.00 % @Diameter >=38.1 mm	Wire, rod, bar and shapes (extruded); Area 25-32 in^2
	>= 10.0 % @Diameter 19.0 - 38.07 mm	Wire, rod, bar and shapes (extruded)
	>= 10.0 % @Diameter >=38.1 mm	Wire, rod, bar and shapes (extruded); Area <25 in^2
	>= 10.0 % @Diameter <=6.32 mm	Extruded tube
	>= 10.0 % @Diameter 6.35 - 19.0 mm	Extruded tube
	>= 10.0 % @Diameter 19.0 - 38.07 mm	Extruded tube
	>= 10.0 % @Diameter >=38.1 mm	Extruded tube; Area <25 in^2
	>= 12.0 % @Diameter <=6.32 mm	Wire, rod, bar and shapes (extruded)
	>= 12.0 % @Diameter 6.35 - 19.0 mm	Wire, rod, bar and shapes (extruded)
Modulus of Elasticity	73.1 GPa	AA; Typical; Average of tension and compression. Compression modulus is about 2% greater than tensile modulus.
Notched Tensile Strength	379 MPa	2.5 cm width x 0.16 cm thick side-notched specimen, K_t = 17.
Ultimate Bearing Strength	855 MPa	Edge distance/pin diameter = 2.0
Bearing Yield Strength	524 MPa	Edge distance/pin diameter = 2.0
Poisson's Ratio	0.330	
Fatigue Strength	138 MPa @# of Cycles 5.00e+8	completely reversed stress; RR Moore machine/specimen
Machinability	70 %	0-100 Scale of Aluminium Alloys
Shear Modulus	28.0 GPa	
Shear Strength	283 MPa	AA; Typical
Electrical Properties	**Metric**	**Comments**
Electrical Resistivity	0.00000582 ohm-cm @Temperature 20.0 °C	AA; Typical
Thermal Properties	**Metric**	**Comments**
CTE, linear	21.1 µm/m-°C @Temperature -50.0 - 20.0 °C	

	22.9 µm/m-°C @Temperature 20.0 - 100 °C	
	23.2 µm/m-°C @Temperature 20.0 - 100 °C	AA; Typical; average over range
	23.8 µm/m-°C @Temperature 20.0 - 200 °C	
	24.7 µm/m-°C @Temperature 20.0 - 300 °C	
	24.7 µm/m-°C @Temperature 20.0 - 300 °C	average
Specific Heat Capacity	0.875 J/g-°C	
Thermal Conductivity	121 W/m-K	AA; Typical at 77°F
Melting Point	502 - 638 °C	AA; Typical range based on typical composition for wrought products 1/4 inch thickness or greater. Eutectic melting is not eliminated by homogenization.
Solidus	502 °C	AA; Typical
Liquidus	638 °C	AA; Typical
Processing Properties	Metric	Comments
Annealing Temperature	413 °C	
Solution Temperature	493 °C	
Component Elements Properties	Metric	Comments
Aluminium, Al	90.7 - 94.7 %	As remainder
Chromium, Cr	<= 0.10 %	
Copper, Cu	3.80 - 4.90 %	
Iron, Fe	<= 0.50 %	
Magnesium, Mg	1.20 - 1.80 %	
Manganese, Mn	0.30 - 0.90 %	
Other, each	<= 0.050 %	
Other, total	<= 0.15 %	
Silicon, Si	<= 0.50 %	
Titanium, Ti	<= 0.15 %	

Zinc, Zn	<= 0.25 %	

Table 10.8: Aluminium Alloy 2024 T6

Physical Properties	Metric	Comments
Density	2.78 g/cc	AA; Typical
Mechanical Properties	**Metric**	**Comments**
Hardness, Brinell	125	500 kg load/10 mm ball
Hardness, Knoop	157	Estimated from Brinell
Hardness, Rockwell A	48	Estimated from Brinell
Hardness, Rockwell B	78	Estimated from Brinell
Hardness, Vickers	142	Estimated from Brinell
Tensile Strength, Ultimate	>= 415 MPa	Wire, rod, and bar (rolled or cold finished); T62
	>= 425 MPa	Wire, rod, and bar (rolled or cold finished)
	>= 427 MPa	
	34.0 MPa @Temperature 371 °C	
	52.0 MPa @Temperature 316 °C	
	76.0 MPa @Temperature 260 °C	
	179 MPa @Temperature 204 °C	
	310 MPa @Temperature 149 °C	
	448 MPa @Temperature 100 °C	
	476 MPa @Temperature 24.0 °C	
	483 MPa @Temperature -28.0 °C	
	496 MPa @Temperature -80.0 °C	
	579 MPa @Temperature -196 °C	

	>= 435 MPa @Thickness 12.7 - 76.2 mm	Sheet and plate; T62
	>= 440 MPa @Thickness 0.254 - 12.7 mm	Sheet and plate; T62
Tensile Strength, Yield  	>= 315 MPa	Wire, rod, and bar (rolled or cold finished); T62
	>= 345 MPa	
	>= 345 MPa	Wire, rod, and bar (rolled or cold finished)
	>= 345 MPa @Thickness 0.254 - 12.7 mm	Sheet and plate; T62
	>= 345 MPa @Thickness 12.7 - 76.2 mm	Sheet and plate; T62
	28.0 MPa @Strain 0.200 %, Temperature 371 °C	
	41.0 MPa @Strain 0.200 %, Temperature 316 °C	
	62.0 MPa @Strain 0.200 %, Temperature 260 °C	
	131 MPa @Strain 0.200 %, Temperature 204 °C	
	248 MPa @Strain 0.200 %, Temperature 149 °C	
	372 MPa @Strain 0.200 %, Temperature 100 °C	
	393 MPa @Strain 0.200 %, Temperature 24.0 °C	
	400 MPa @Strain 0.200 %, Temperature -28.0 °C	
	407 MPa @Strain 0.200 %, Temperature -80.0 °C	
	469 MPa @Strain 0.200 %, Temperature -196 °C	
Elongation at Break	5.00 %	

 	>= 5.00 %	Wire, rod, and bar (rolled or cold finished)
	>= 5.00 %	Wire, rod, and bar (rolled or cold finished); T62
	10.0 % @Temperature -80.0 °C	
	10.0 % @Temperature -28.0 °C	
	10.0 % @Temperature 24.0 °C	
	10.0 % @Temperature 100 °C	
	11.0 % @Temperature -196 °C	
	17.0 % @Temperature 149 °C	
	27.0 % @Temperature 204 °C	
	55.0 % @Temperature 260 °C	
	75.0 % @Temperature 316 °C	
	100 % @Temperature 371 °C	
	>= 5.00 % @Thickness 0.254 - 12.7 mm	Sheet and plate; T62
	>= 5.00 % @Thickness 12.7 - 76.2 mm	Sheet and plate; T62
Modulus of Elasticity	72.4 GPa	Estimated from other heat treatments.
poison's Ratio	0.330	Estimated from other heat treatments.
Fatigue Strength	124 MPa @# of Cycles 5.00e+8	Completely reversed; R. R. Moore Machine and specimen.
Machinability	70 %	0-100 Scale (A=90; B=70; C=50; D=30; E=10)
Shear Modulus	27.0 GPa	Estimated from similar Al alloys.
Shear Strength	283 MPa	
Electrical Properties	**Metric**	**Comments**
Electrical Resistivity	0.00000449 ohm-cm @Temperature 20.0 °C	AA; Typical

Thermal Properties	Metric	Comments
CTE, linear	21.1 µm/m-°C @Temperature -50.0 - 20.0 °C	
	22.9 µm/m-°C @Temperature 20.0 - 100 °C	
	23.2 µm/m-°C @Temperature 20.0 - 100 °C	AA; Typical; average over range
	23.8 µm/m-°C @Temperature 20.0 - 200 °C	
	24.7 µm/m-°C @Temperature 20.0 - 300 °C	
	24.7 µm/m-°C @Temperature 20.0 - 300 °C	average
Specific Heat Capacity	0.875 J/g-°C	
Thermal Conductivity	151 W/m-K	AA; Typical at 77°F
Melting Point	502 - 638 °C	AA; Typical range based on typical composition for wrought products 1/4 inch thickness or greater. Eutectic melting is not eliminated by homogenization.
Solidus	502 °C	AA; Typical
Liquidus	638 °C	AA; Typical
Processing Properties	**Metric**	**Comments**
Annealing Temperature	413 °C	
Solution Temperature	493 °C	
Aging Temperature	191 °C	8 to 16 hr at temperature
Component Elements Properties	**Metric**	**Comments**
Aluminium, Al	90.7 - 94.7 %	As remainder
Chromium, Cr	<= 0.10 %	
Copper, Cu	3.80 - 4.90 %	
Iron, Fe	<= 0.50 %	
Magnesium, Mg	1.20 - 1.80 %	
Manganese, Mn	0.30 - 0.90 %	
Other, each	<= 0.050 %	

Other, total	<= 0.15 %	
Silicon, Si	<= 0.50 %	
Titanium, Ti	<= 0.15 %	
Zinc, Zn	<= 0.25 %	

Table 10.9: Overview of hot-work tool steel

Physical Properties	Metric	Comments
Density	6.45 - 8.19 g/cc	Average value: 7.76 g/cc Grade Count:55
Particle Size	6.70 - 12.0 µm	Average value: 9.27 µm Grade Count:4
Chemical Properties	**Metric**	**Comments**
Critical Temperature	732 - 924 °C	Average value: 817 °C Grade Count:9
Mechanical Properties	**Metric**	**Comments**
Hardness, Brinell	160 - 594	Average value: 294 Grade Count:16
Hardness, Knoop	431 - 660	Average value: 575 Grade Count:5
Hardness, Rockwell C	26.0 - 66.0	Average value: 49.7 Grade Count:52
Hardness, Vickers	325 - 632	Average value: 500 Grade Count:7
Tensile Strength, Ultimate	1010 - 2310 MPa	Average value: 1650 MPa Grade Count:34
Tensile Strength, Yield	800 - 1900 MPa	Average value: 1400 MPa Grade Count:31
Elongation at Break	8.00 - 15.5 %	Average value: 11.2 % Grade Count:15
Elongation at Yield	12.0 - 16.0 %	Average value: 13.3 % Grade Count:4
Reduction of Area	15.0 - 55.0 %	Average value: 41.3 % Grade Count:20
Modulus of Elasticity	203 - 228 GPa	Average value: 210 GPa Grade Count:36
Bulk Modulus	140 GPa	Average value: 140 GPa Grade Count:4
Charpy Impact	2.71 - 55.0 J	Average value: 24.1 J Grade Count:14

Machinability	45.0 - 95.0 %	Average value: 69.9 % Grade Count:18
Shear Modulus	80.0 - 81.0 GPa	Average value: 80.5 GPa Grade Count:4
Abrasion	3.76 - 186	Average value: 88.6 Grade Count:3
Electrical Properties	**Metric**	**Comments**
Electrical Resistivity	0.0000500 - 0.0000590 ohm-cm	Average value: 0.0000524 ohm-cm Grade Count:7
Thermal Properties	**Metric**	**Comments**
CTE, linear	7.00 - 14.3 µm/m-°C	Average value: 12.3 µm/m-°C Grade Count:27
Specific Heat Capacity	0.418 - 0.461 J/g-°C	Average value: 0.457 J/g-°C Grade Count:13
Thermal Conductivity	3.60 - 42.0 W/m-K	Average value: 27.7 W/m-K Grade Count:29
Transformation Temperature	785 - 913 °C	Average value: 850 °C Grade Count:7
Processing Properties	**Metric**	**Comments**
Processing Temperature	540 - 1220 °C	Average value: 918 °C Grade Count:9
Annealing Temperature	399 - 900 °C	Average value: 774 °C Grade Count:12
Component Elements Properties	**Metric**	**Comments**
Carbon, C	0.300 - 2.10 %	Average value: 0.459 % Grade Count:64
Chromium, Cr	1.10 - 6.80 %	Average value: 4.49 % Grade Count:64
Iron, Fe	82.3 - 96.0 %	Average value: 90.7 % Grade Count:50
Manganese, Mn	0.250 - 1.50 %	Average value: 0.476 % Grade Count:50
Molybdenum, Mo	0.200 - 5.00 %	Average value: 1.76 % Grade Count:61
Nickel, Ni	1.00 - 1.70 %	Average value: 1.53 % Grade Count:6
Silicon, Si	0.200 - 1.50 %	Average value: 0.785 % Grade Count:58

Sulphur, S	0.00100 - 0.0100 %	Average value: 0.00373 % Grade Count:15
Tungsten, W	1.00 - 9.15 %	Average value: 5.37 % Grade Count:7
Vanadium, V	0.100 - 5.40 %	Average value: 0.919 % Grade Count:62

Table 10.10: H13 Hot work tool steel

Physical Properties	Metric	Comments
Density	7.75 g/cc	
Chemical properties	**Metric**	**Comments**
Critical temperature	732-924 °C	Average value 817°C
Mechanical Properties	**Metric**	**Comments**
Hardness, Rockwell C	46	70°F; sample was oil quenched from 1875°F (1024°C) and double tempered at 1100°F (593°C)
	29.0 @Temperature 538 °C	
	37.5 @Temperature 427 °C	
	39.5 @Temperature 316 °C	
	40 @Temperature 260 °C	
	41 @Temperature 204 °C	
	42.5 @Temperature 149 °C	
	43 @Temperature 93.3 °C	
Modulus of Elasticity	207 GPa	
	159 GPa @Temperature 538 °C	
	186 GPa @Temperature 204 °C	
	190 GPa @Temperature 427 °C	
	197 GPa @Temperature 316 °C	

	200 GPa @Temperature 93.3 °C	
Charpy Impact	20.3 J	V-Notch; sample was oil quenched from 1875°F (1024°C) and double tempered at 1100°F (593°C)
Machinability	65.0 - 70.0 %	of a 1% carbon steel
Thermal Properties	**Metric**	**Comments**
CTE, linear	10.4 µm/m-°C @Temperature 26.7 - 93.3 °C	at 47 to 48 HRC
	11.3 µm/m-°C @Temperature 26.7 - 204 °C	at 47 to 48 HRC
	12.4 µm/m-°C @Temperature 26.7 - 427 °C	
	13.1 µm/m-°C @Temperature 26.7 - 649 °C	at 47 to 48 HRC
	13.5 µm/m-°C @Temperature 26.7 - 816 °C	at 47 to 48 HRC
Thermal Conductivity	17.6 W/m-K @Temperature 27.0 °C	
	23.4 W/m-K @Temperature 204 °C	
	26.8 W/m-K @Temperature 649 °C	
Component Elements Properties	**Metric**	**Comments**
Carbon, C	0.40 %	
Chromium, Cr	5.25 %	
Iron, Fe	90.6 %	As Balance
Manganese, Mn	0.40 %	
Molybdenum, Mo	1.35 %	
Silicon, Si	1.0 %	
Sulphur, S	0.0010 %	
Vanadium, V	1.0 %	

Reference 47 and 53

Table 10.11: Conversion of U.S units to standard Unit's

A.4 Conversion of U.S. Units of Measure Used in MMPDS to SI Units

Quantity or Property	To Convert From U. S. Unit	Multiply by[a]	SI Unit[b]
Area	$in.^2$	645.16[c]	Millimeter^2 (mm^2)
Force	lb	4.4482	Newton (N)
Length	in.	25.4[c]	Millimeter (mm)
Stress	ksi	6.895	Megapascal (MPa)[d]
Stress intensity factor	ksi $\sqrt{in.}$	1.0989	Megapascal $\sqrt{meter}$ ($MPa \cdot m^{1/2}$)[d]
Modulus	10^3 ksi	6.895	Gigapascal (GPa)[d]
Temperature	°F	$\frac{F + 459.67}{1.8}$	Kelvin (K)
Density (ω)	$lb/in.^3$	27.680	Megagram/meter^3 (Mg/m^3)
Specific heat (C)	Btu/lb·F (or $Btu \cdot lb^{-1} \cdot F^{-1}$)	4.1868[c]	Joule/(gram·Kelvin) ($J/g \cdot K$) or ($J \cdot g^{-1} \cdot K^{-1}$)
Thermal conductivity (K)	$Btu/[(hr)(ft^2)(F)/ft]$ (or $Btu \cdot hr^{-1} \cdot ft^{-2} \cdot F^{-1} \cdot ft$)	1.7307	Watt/(meter·Kelvin) $W/(m \cdot K)$ or ($W \cdot m^{-1} \cdot K^{-1}$)
Thermal expansion (α)	in./in./F (or $in. \cdot in.^{-1} \cdot F^{-1}$)	1.8	Meter/meter/Kelvin $m/(m \cdot K)$ or ($m \cdot m^{-1} \cdot K^{-1}$)

a Conversion factors to give significant figures are as specified in ASTM E 380, NASA SP-7012, second revision. NBS Special Publication 330, and *Metals Engineering Quarterly*. Note: Multiple conversions between U.S. and SI units should be avoided because significant round-off errors may result.

b

Prefix	Multiple	Prefix	Multiple
giga (G)	10^9	milli (m)	10^{-3}
mega (M)	10^6	micro (μ)	10^{-6}
kilo (k)	10^3		

c Conversion factor is exact.

d One Pascal (Pa) = one Newton/meter^2.

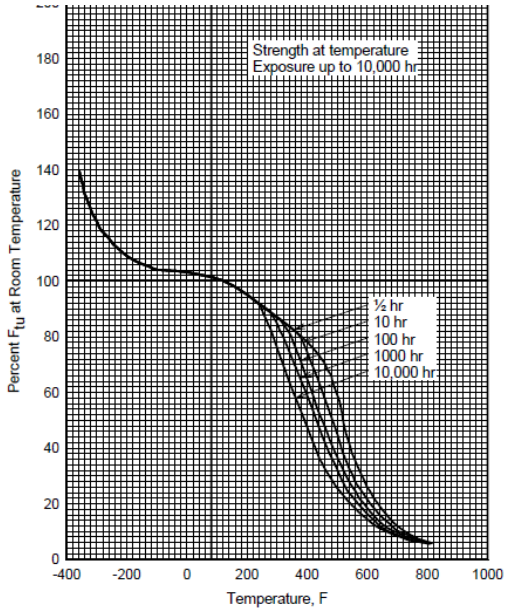


Figure 10.10: Ultimate tensile strength of AL2024 changing with

Reference 47 and 72

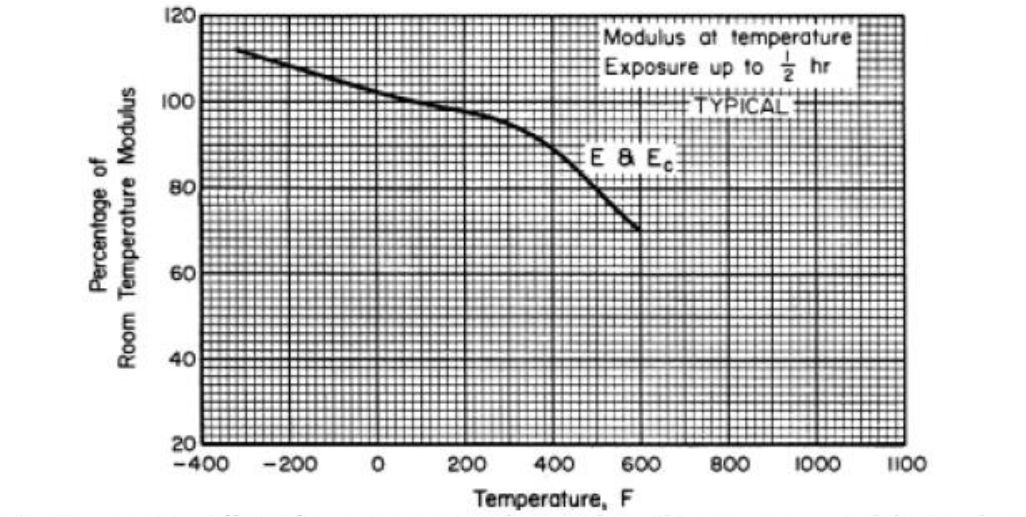


Figure 10.11: Young's modulus of Al2024 changing with temperature

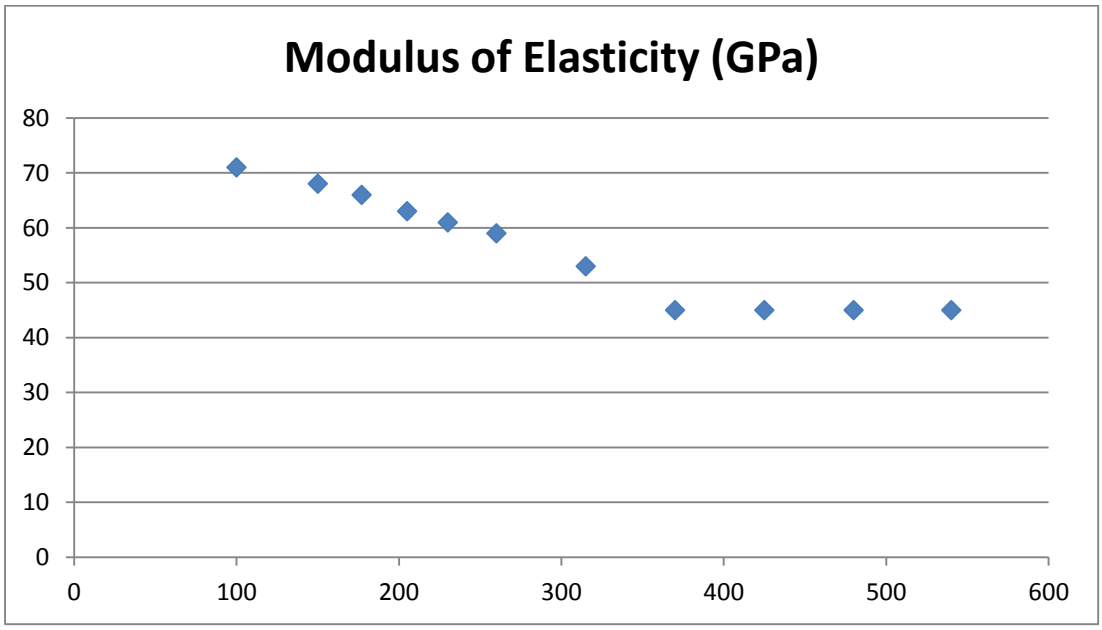


Figure 10.12: Modulus of Elasticity changing with temperature for Aluminium 2024

Reference73

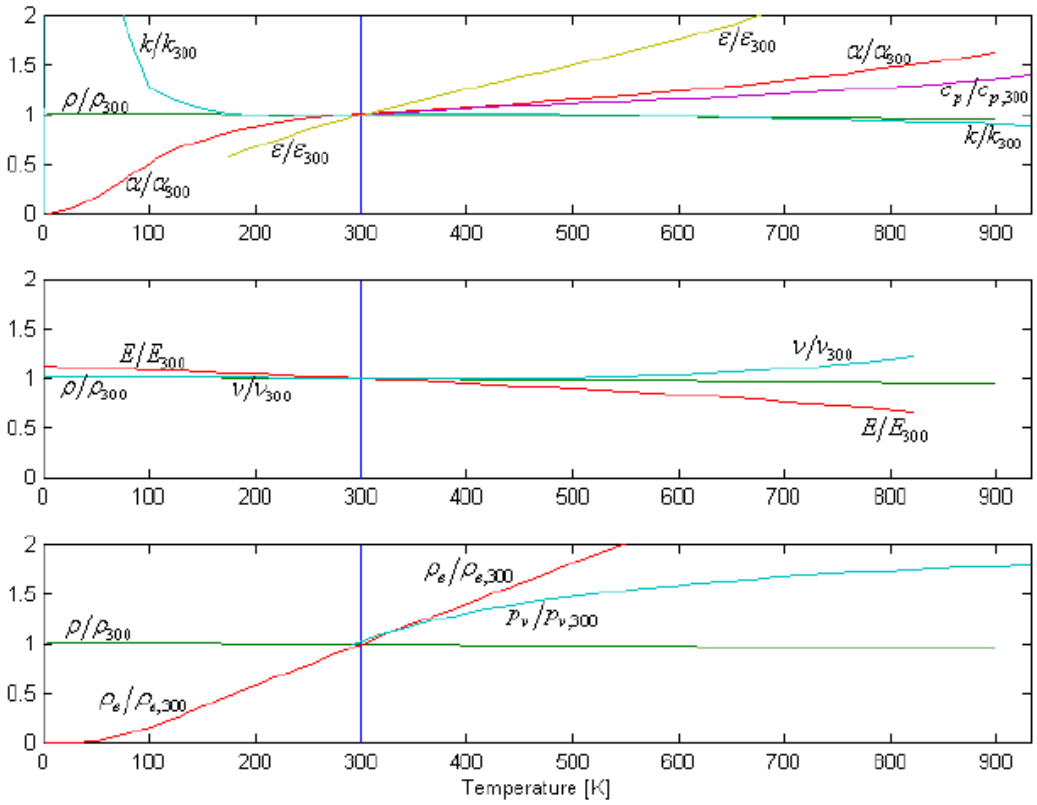


Figure 10.13: Variation with temperature for aluminium material properties relative to their value of 300K

	E [GPa]	ν	$\sigma_{fluency=0,2\%}$ [MPa]	$\varepsilon_{fluency=0,2\%}$ [%]	σ_{break} [MPa]	ε_{break} [%]	$\alpha \cdot 10^6$ [1/K]	ρ [kg/m^3]
Metals								
Aluminium	74	0.33	40	0,35	200..500	50	24	2710
Alu. alloys	69..72	0.33	300		90..500	5..40	23..25	2720
Alu. alloy 2024-T4 (Al, 4.5%Cu, 1.5%Mg)	73	0.32	330		470		23	2770
Brass	92	0.33	100..300		300..500		18..20	8780
Bronze	100	0.31	150..500		350..500		17..19	8800
Copper	120	0.34	70		400..500		17	8910
Iron (Cast iron)	70..140	0.36	200..600		100..800	2..20	9..12	7300
Steels								
Carbon steel	207	0.30	200..1000	0,30	400..1500	20	12	7900
Carbon steel AISI 1018 (0.18%C, 0.8%Mn)	198	0.30	390		500	27	12	7800
Carbon steel EN-335 (0.24%C, 1.7%Mn)	199	0.32	335	0,10	490..630	20	12	7860
Invar steel (36%Ni)	140	0.30					1.7	8000
Stainless steel	193..204	0.30	200..1500		400..1400	20	10..17	7900
Platinum	150	0.38			240		9	21470
Titanium	110	0.32	700		800..900		9	4530

Figure 10.14: Table representation of typical values for material properties

Reference 75

Table 10.13: Thermal expansion coefficient increasing with temperature for H13 tool steel

Type	Density		µm/m K from 20 °C to				
	g/cm^3	lb/in.^{3}	100 °C	200 °C	425 °C	540 °C	650 °C
W1	7.84	0.282	10.4	11.0	13.1	13.8(a)	14.2(b)
W2	7.85	0.283	...	...	14.4	14.8	14.9
S1	7.88	0.255	12.4	12.6	13.5	13.9	14.2
S2	7.79	0.281	10.9	11.9	13.5	14.0	14.2
S5	7.76	0.280	...	...	12.6	13.3	13.7
S6	7.75	0.279	...	...	12.6	13.3	...
S7	7.76	0.280	...	12.6	13.3	13.7(a)	13.3
O1	7.85	0.283	...	10.6(c)	12.8	14.0(d)	14.4(d)
O2	7.66	0.277	11.2	12.6	13.9	14.6	15.1
O6	7.70	0.277	...	11.2	12.6	12.9	13.7
O7	7.8	0.282	...	...	...	...	...
A2	7.86	0.284	10.7	10.6(c)	12.9	14.0	14.2
A6	7.84	0.283	11.5	12.4	13.5	13.9	14.2
A7	7.66	0.277	...	...	12.4.	12.9	13.5
A8	7.87	0.284	...	...	12.0	12.4	12.6
A9	7.78	0.281	...	...	12.0	12.4	12.6
A10	7.68	0.278	12.8	13.3	...	...	...
D2	7.70	0.278	10.4	10.3	11.9	12.2	12.2
D3	7.70	0.278	12.0	11.7	12.9	13.1	13.5
D4	7.70	0.278	...	...	12.4	...	...
D5	...	...	...	...	...	12.0	...
H10	7.81	0.281	...	...	12.2	13.3	13.7
H11	7.75	0.280	11.9	12.4	12.8	12.9	13.3
H13	7.76	0.280	10.4	11.5	12.2	12.4	13.1
H14	7.89	0.285	11.0	...	...	...	...

Reference 74

Table 10.14: Emissivity for Aluminium alloy of various surface specifications

Aluminum	as received, plate	100	T	0.09
Aluminum	as received, sheet	100	T	0.09
Aluminum	cast, blast cleaned	70	SW	0.47
Aluminum	cast, blast cleaned	70	LW	0.46
Aluminum	dipped in HNO_3, plate	100	T	0.05
Aluminum	foil	27	10 µm	0.04
Aluminum	foil	27	3 µm	0.09
Aluminum	oxidized, strongly	50–500	T	0.2–0.3
Aluminum	polished	50–100	T	0.04–0.06
Aluminum	polished plate	100	T	0.05
Aluminum	polished, sheet	100	T	0.05
Aluminum	rough surface	20–50	T	0.06–0.07
Aluminum	roughened	27	10 µm	0.18
Aluminum	roughened	27	3 µm	0.28
Aluminum	sheet, 4 samples differently scratched	70	SW	0.05–0.08
Aluminum	sheet, 4 samples differently scratched	70	LW	0.03–0.06
Aluminum	vacuum deposited	20	T	0.04

Reference 73, 74 and 55

Table 10.15: Theoretical emissivity values for various materials

Material	Temp °F (°C)	ε Emissivity
Alloys		
20-Ni, 24-CR, 55-FE, Oxid.	392 (200)	.90
20-Ni, 24-CR, 55-FE, Oxid.	932 (500)	.97
60-Ni , 12-CR, 28-FE, Oxid.	518 (270)	.89
60-Ni , 12-CR, 28-FE, Oxid.	1040 (560)	.82
80-Ni, 20-CR, Oxidized	212 (100)	.87
80-Ni, 20-CR, Oxidized	1112 (600)	.87
80-Ni, 20-CR, Oxidized	2372 (1300)	.89
Aluminum		
Unoxidized	77 (25)	.02
Unoxidized	212 (100)	.03
Unoxidized	932 (500)	.06
Oxidized	390 (199)	.11
Oxidized	1110 (599)	.19
Oxidized at 599°C (1110°F)	390 (199)	.11
Oxidized at 599°C (1110°F)	1110 (599)	.19
Heavily Oxidized	200 (93)	.20
Heavily Oxidized	940 (504)	.31
Highly Polished	212 (100)	.09
Roughly Polished	212 (100)	.18
Commercial Sheet	212 (100)	.09
Highly Polished Plate	440 (227)	.04
Highly Polished Plate	1070 (577)	.06
Bright Rolled Plate	338 (170)	.04
Bright Rolled Plate	932 (500)	.05
Alloy A3003, Oxidized	600 (316)	.40
Alloy A3003, Oxidized	900 (482)	.40
Alloy 1100-0	200-800 (93-427)	.05
Alloy 24ST	75 (24)	.09
Alloy 24ST, Polished	75 (24)	.09
Alloy 75ST	75 (24)	.11
Alloy 75ST, Polished	75 (24)	.08
Bismuth, Bright	176 (80)	.34
Bismuth, Unoxidized	77 (25)	.05
Bismuth, Unoxidized	212 (100)	.06

Table 10.16: Values of thermal properties of some materials

Material	c_p *(J/kg-K)*[a]	α_l $[(°C)^{-1} \times 10^{-6}]$[b]	k *(W/m-K)*[c]	L $[\Omega\text{-}W/(K)^2 \times 10^{-8}]$
		Metals		
Aluminum	900	23.6	247	2.20
Copper	386	17.0	398	2.25
Gold	128	14.2	315	2.50
Iron	448	11.8	80	2.71
Nickel	443	13.3	90	2.08
Silver	235	19.7	428	2.13
Tungsten	138	4.5	178	3.20
1025 Steel	486	12.0	51.9	—
316 Stainless steel	502	16.0	15.9	—
Brass (70Cu-30Zn)	375	20.0	120	—
Kovar (54Fe-29Ni-17Co)	460	5.1	17	2.80
Invar (64Fe-36Ni)	500	1.6	10	2.75
Super Invar (63Fe-32Ni-5Co)	500	0.72	10	2.68

Table 10.17: Yield stress at various conditions

Temper	Thickness in. (mm)	Tensile Strength ksi (MPa)	Yield Strength ksi (MPa)	Elongation %
0-Sheet & plate	0.010-0.499 (0.25-12.44)	32.0 (max) (220)	14.0 (max) (96)	12
T3-Flat Sheet	0.008-0.249 (0.203-6.32)	63-64 (434-441)	42 (289)	10-15
T351-Plate*	0.250-4.000 (6.35-101.60)	64-57 (441-393)	42-41 (289-282)	12-4
T4-Coiled Sheet	0.010-0.125 (0.254-3.16)	62 (427)	40 (276)	12-15
T81-Flat Sheet	0.010-0.249 (0.254-6.32)	67 (462)	58 (400)	5
T851-Plate	0.250-1.499 (6.35-38.07)	67-66 (462-455)	58-57 (400-393)	5
*Strength Decreases as thickness increases				

10.3 Appendix 3: ANSYS APDL commands

The following commands are outlined in more detail and are laid out in reference to the ANSYS help file [54].

ET

ET, *ITYPE*, *Ename*, *KOP1*, *KOP2*, *KOP3*, *KOP4*, *KOP5*, *KOP6*, *INOPR*
Defines a local element type from the element library.

ITYPE
Arbitrary local element type number. Defaults to 1 + current maximum.

Ename
Element name (or number) as given in the element library in Chapter 4 of the *Element Reference*. The name consists of a category prefix and a unique number, such as PIPE288. The category prefix of the name (PIPE for the example) may be omitted but is displayed upon output for clarity. If *Ename* = 0, the element is defined as a null element.

KOP1, KOP2, KOP3, . . . , KOP6
KEYOPT values (1 through 6) for this element, as described in the *Element Reference*.

INOPR
If 1, suppress all element solution printout for this element type.

Notes

The **ET** command selects an element type from the element library and establishes it as a local element type for the current model. Information derived from the element type is used for subsequent commands, so the **ET** command(s) should be issued early. (The *Element Reference* describes the available elements.)

A special option, *Ename* = 0, permits the specified element type to be ignored during solution without actually removing the element from the model. *Ename* may be set to zero only after the element type has been previously defined with a nonzero *Ename*. The preferred method of ignoring elements is to use the select commands (such as **ESEL**).

KOPn are element option keys. These keys (referred to as KEYOPT(*n*)) are used to turn on certain element options for this element. These options are listed under "KEYOPT" in the input table for each element type in the *Element Reference*. KEYOPT values include stiffness formulation options, printout controls, and various other element options. If KEYOPT(7) or greater is needed, input their values with the **KEYOPT** command.

The **ET** command only defines an element type local to your model (from the types in the element library). The **TYPE** or similar [**KATT**, **LATT**, **AATT**, or **VATT**] command must be used to point to the desired local element type before meshing.

To activate the ANSYS program's LS-DYNA explicit dynamic analysis capability, use the **ET** command or its GUI equivalent to choose an element that works only with LS-DYNA (such as SHELL163). Choosing LS-DYNA in the Preferences dialog box does *not* activate LS-DYNA; it simply makes items and options related to LS-DYNA accessible in the GUI.

ESEL

ESEL, *Type*, *Item*, *Comp*, *VMIN*, *VMAX*, *VINC*, *KABS*

Selects a subset of elements.

Type

Label identifying the type of select:

- **S** — Select a new set (default).
- **R** — Reselect a set from the current set.
- **A** — Additionally select a set and extend the current set.
- **U** — Unselect a set from the current set.
- **ALL** — Restore the full set.
- **NONE** — Unselect the full set.
- **INVE** — Invert the current set (selected becomes unselected and vice versa).
- **STAT** — Display the current select status.

The following fields are used only with *Type* = S, R, A, or U:

Item

Label identifying data, see *Table 143: ESEL - Valid Item and Component Labels*. Some items also require a component label. If *Item* = PICK (or simply "P"), graphical picking is enabled and all remaining command fields are ignored (valid only in the GUI). Defaults to ELEM. If *Item* = STRA (straightened), elements are selected whose midside nodes do not conform to the curved line or non-flat area on which they should lie. (Such elements are sometimes formed during volume meshing [**VMESH**] in an attempt to avoid excessive element distortion.) You should graphically examine any such elements to evaluate their possible effect on solution accuracy.

Comp

Component of the item (if required). Valid component labels are shown in *Table 143: ESEL - Valid Item and Component Labels* below.

VMIN

Minimum value of item range. Ranges are element numbers, attribute numbers, load values, or result values as appropriate for the item. A component name (as specified on the **CM** command) may also be substituted for *VMIN* (*VMAX* and *VINC* are ignored).

VMAX

Maximum value of item range. *VMAX* defaults to *VMIN* for input values.
For result values, *VMAX* defaults to infinity if *VMIN* is positive, or to zero if *VMIN* is negative.

VINC

Value increment within range. Used only with integer ranges (such as for element and attribute numbers). Defaults to 1. *VINC* cannot be negative.

KABS

Absolute value key:

- **0** — Check sign of value during selection.
- **1** — Use absolute value during selection (sign ignored).

Command Default

All elements are selected.

Notes

Selects elements based on values of a labeled item and component. For example, to select a new set of elements based on element numbers 1 through 7, use **ESEL**,S,ELEM,,1,7. The subset is used when the ALL label is entered (or implied) on other commands, such as **ELIST**,ALL. Only data identified by element number are selected. Selected data are internally flagged; no actual removal of data from the database occurs. Different element subsets cannot be used for different load steps [**SOLVE**] in a **/SOLU** sequence. The subset used in the first load step will be used for all subsequent load steps regardless of subsequent **ESEL** specifications.

This command is valid in any processor.

Elements crossing the named path (see **PATH** command) will be selected. This option is only available in PREP7 and POST1. If no geometry data has been mapped to the path (i.e., via **PMAP** and **PDEF** commands), the path will assume the default mapping option (**PMAP**,UNIFORM) to map the geometry prior to selecting the elements. If an invalid path name is given, the **ESEL** command is ignored (status of selected elements is unchanged). If there are no elements crossing the path, the **ESEL** command will return zero elements selected.

For selections based on non-integer numbers (coordinates, results, etc.), items that are within the range *VMIN* - *Toler* and *VMAX* + *Toler* are selected. The default tolerance *Toler* is based on the relative values of *VMIN* and *VMAX* as follows:

- If *VMIN* = *VMAX*, *Toler* = 0.005 x *VMIN*.
- If *VMIN* = *VMAX* = 0.0, *Toler* = 1.0E-6.
- If *VMAX* ≠ *VMIN*, *Toler* = 1.0E-8 x (*VMAX* - *VMIN*).

Use the **SELTOL** command to override this default and specify *Toler* explicitly.

Item	Comp	Description
ELEM		Element number.
ADJ		Elements adjacent to element *VMIN* (*VMAX* and *VINC* fields are ignored). Only elements (of the same dimensionality) adjacent to lateral faces are considered. Progression continues until edge of model or until more than two elements are adjacent at a face.
CENT	X, Y, Z	X, Y, or Z location in the active coordinate system.
TYPE		Element type number.
ENAME		Element name (or identifying number).

EMODIF

EMODIF, *IEL*, *STLOC*, *I1*, *I2*, *I3*, *I4*, *I5*, *I6*, *I7*, *I8*
Modifies a previously defined element.

IEL
Modify nodes and/or attributes for element number *IEL*. If ALL, modify all selected elements [ESEL]. If *IEL* = P, graphical picking is enabled and all remaining command fields are ignored (valid only in the GUI). A component name may also be substituted for *IEL*.

STLOC
Starting location (*n*) of first node to be modified or the attribute label. If *n*, modify element node positions *n*, *n*+1, etc. (*n* = 1 to 20). For example, if *STLOC* = 1, *I1* refers to the first node, *I2*, the second, etc. If *STLOC* = 9, *I1* refers to the ninth node, *I2*, the tenth, etc. Attributes are also modified to the currently specified values (use -*n* to modify only nodes and not attributes). If zero, modify only the attributes to the currently specified values. If MAT, TYPE, REAL, ESYS, or SECNUM, modify only that attribute to the *I1* value.

I1, I2, I3, . . . , I8
Replace the previous node numbers assigned to this element with these corresponding values. A (blank) retains the previous value (except in the *I1* field, which resets the *STLOC* node number to zero). For attributes, replace the existing value with the *I1* value (or the default if *I1* is zero or blank).

Notes

The nodes and/or attributes (MAT, TYPE, REAL, ESYS, and SECNUM values) of an existing element may be changed with this command.

Thermal boundary condition commands set for the convection coefficients taken from the ANSYS help file [54]

CMSEL

CMSEL, *Type*, *Name*, *Entity*

Selects a subset of components and assemblies.

Type

Label identifying the type of select:

S — Select a new set (default).

R — Reselect a set from the current set.

A — Additionally select a set and extend the current set.

U — Unselect a set from the current set.

ALL — Also select all components.

NONE — Unselect all components.

Name

Name of component or assembly whose items are to be selected (valid only if *Type* = S, R, A, or U).

Graphical picking is enabled if *Type* is blank and *Name* = PICK (or simply "P").

Entity

If *Name* is blank, then the following entity types can be specified:

VOLU — Select the volume components only.

AREA — Select the area components only.

LINE — Select the line components only.

KP — Select the keypoint components only.

ELEM — Select the element components only.

NODE — Select the node components only.

Notes

Selecting by component is a convenient adjunct to individual item selection (e.g., **VSEL**, **ESEL**, etc.). **CMSEL**, ALL allows you to select components **in addition** to other items you have already selected.

If *Type* = R for an assembly selection [**CMSEL**,R,<*assembly-name*>], the reselect operation is performed on each component in the assembly in the order in which the components make up the assembly. Thus, if one reselect operation results in an empty set, subsequent operations will also result in empty sets. For example, if the first reselect operation tries to reselect node 1 from the selected set of nodes 3, 4, and 5, the operation results in an empty set (that is, no nodes are selected). Since the current set is now an empty set, if the second reselect operation tries to reselect any nodes, the second operation also results in an empty set, and so on. This is equivalent to repeating the command **CMSEL**,R,<*component-name*> once for each component making up the assembly.

This command is valid in any processor.

SF

SF, *Nlist*, *Lab*, *VALUE*, *VALUE2*
Specifies surface loads on nodes.

Nlist

Nodes defining the surface upon which the load is to be applied. Use the label ALL or P, or a component name. If ALL, all selected nodes [NSEL] are used (default). If P, graphical picking is enabled and all remaining command fields are ignored (valid only in the GUI).

Lab

Valid surface load label. Load labels are listed under "Surface Loads" in the input table for each element type in the *Element Reference*.

Discipline	Surface Load Label	Label Description
Structural	PRES	pressure
	FREQ	frequency (harmonic analyses only)
Thermal	CONV[*1*]	convection
	HFLUX[*1*]	heat flux
	RAD	radiation
	RDSF	surface-to-surface radiation

1. Thermal labels CONV and HFLUX are mutually exclusive.
2. For an acoustic analysis, apply the fluid-structure interaction flag (Label = FSI) to only the FLUID29, FLUID30, FLUID220, and FLUID221 elements.
3. For a fluid-solid interaction analysis, apply the field-surface interface flag (Label = FSIN) twice: once for the fluid side (FLUID141 or FLUID142 elements) and once for the solid side.

VALUE

Surface load value or table name reference for specifying tabular boundary conditions.
If *Lab* = PRES, *VALUE* is the real component of the pressure.
If *Lab* = CONV, *VALUE* is typically the film coefficient and *VALUE2* (below) is typically the bulk temperature. If *VALUE* = -*N*, the film coefficient may be a function of temperature and is determined from the HF property table for material *N* [MP]. The temperature used to evaluate the film coefficient is usually the average between the bulk and wall temperatures, but may be user-defined for some elements. For acoustic harmonic and transient analyses, *VALUE* is the attenuation coefficient of the surface.
If *Lab* = MCI, *VALUE* indicates current direction (-1; current flow into the element face (IN), +1; current flow out of the element face (OUT). If *Lab* = RAD, *VALUE* is surface emissivity.
If *Lab* = PORT, *VALUE* is a port number representing a waveguide exterior port. The port number must be an integer between 1 and 50.
If *Lab* = SHLD, *VALUE* is surface conductivity for high-frequency electromagnetics. For acoustics, *VALUE* is the surface normal velocity in harmonic analysis and the surface normal acceleration in transient analysis.
If *Lab* = IMPD, *VALUE* is resistance in ohms/square for high-frequency electromagnetics. For acoustic harmonic response analyses, *VALUE* is resistance in (N)(s)/m^3 if *VALUE* > 0 and is conductance in mho if *VALUE* < 0. In acoustic transient analyses, VALUE2 is not used.
If *Lab* = RDSF, *VALUE* is the emissivity value; the following conditions apply: If *VALUE* is between 0 and 1, apply a single value to the surface. If *VALUE*= -*N*, the emissivity may be a function of the temperature, and is determined from the EMISS property table for material *N* (MP). The material *N* does not need to correlate with the underlying solid thermal elements.
If *Lab* = FSIN in a Multi-field solver (single or multiple code coupling) analysis, *VALUE* is the surface interface number.
If *Lab* = FSIN in a unidirectional ANSYS to CFX analysis, *VALUE* is not used unless the ANSYS analysis is performed using the Multi-field solver.

VALUE2

Second surface load value (if any).
If *Lab* = PRES, *VALUE2* is the imaginary component of the pressure. Imaginary pressures can only be used by SURF153, SURF154 and SURF159, and can only be used for a full harmonic analysis (**HROPT**,FULL), or by a mode superposition harmonic analysis (**HROPT**,MSUP) if the mode extraction method is Block Lanczos (**MODOPT**,LANB), PCG Lanczos (**MODOPT**,LANPCG), or Supernode (**MODOPT**,SNODE).
If *Lab* = CONV, *VALUE2* is the bulk temperature for thermal analyses. For acoustic analyses, VALUE2 is not used.
If *Lab* = RAD, *VALUE2* is the ambient temperature.
If *Lab* = SHLD, *VALUE2* is relative permeability (defaults to 1.0) for high-frequency electromagnetics. For acoustic analyses, VALUE2 is the phase angle of the normal surface velocity (defaults to zero) for harmonic response analyses while VALUE2 is not used for transient analyses.
If *Lab* = IMPD, *VALUE2* is reactance in ohms/square for high-frequency electromagnetics. For acoustics, *VALUE2* is reactance in (N)(s)/m^3 if *VALUE* > 0 and is the product of susceptance and angular frequency if *VALUE* < 0.
If *Lab* = RDSF, *VALUE2* is the enclosure number. Radiation will occur between surfaces flagged with the same enclosure numbers. If the enclosure is open, radiation will also occur to ambient. If *VALUE2* is negative radiation direction is reversed and will occur inside the element for the flagged radiation surfaces. Negative value of enclosure number is applicable for FLUID141 and FLUID142 elements, to model radiation occurring between surfaces inside the fluid domain.
If *Lab* = FSIN in a unidirectional ANSYS to CFX analysis, *VALUE2* is the surface interface number (not available from within the GUI).
If *Lab* = PORT, *VALUE2* is not used.

Notes

Individual nodes may not be entered for this command. The node list is to identify a surface and the *NList* field must contain a sufficient number of nodes to define an element surface. The loads are internally stored on element faces defined by the specified nodes. All nodes on an element face (including midside nodes, if any) must be specified for the face to be used, and the element must be selected.

If all nodes defining a face are shared by an adjacent face of another selected element, the face is not free and will not have a load applied. If more than one element can share the same nodes (for example, a surface element attached to a solid element), select the desired element type before issuing the **SF** command. The **SF** command applies only to area and volume elements.

For shell elements, if the specified nodes include face one (which is usually the bottom face) along with other faces (such as edges), only face one is used. Where faces cannot be uniquely determined from the nodes, or where the face does not fully describe the load application, use the **SFE** command. A load key of 1 (which is typically the first loading condition on the first face) is used if the face determination is not unique. A uniform load value is applied over the element face.

See the **SFBEAM** command for applying surface loads to beam elements. See the **SFGRAD** command for an alternate tapered load capability. See the **SFFUN** command for applying loads from a node vs. value function. Also see the **SFE** command for applying tapered loads on individual element faces. Use the **SFDELE** command to delete loads applied with this command. Use the **SFCUM** command to accumulate (add) surface loads applied with **SF**.

Tabular boundary conditions (*VALUE* = %*tabname*% and/or *VALUE2* = %*tabname*%) are available for the following surface load labels (*Lab*) only: PRES (real and/or imaginary components), CONV (film coefficient and/or bulk temperature) or HFLUX, DFLUX (diffusion flux), and RAD (surface emissivity and ambient temperature). Use the ***DIM** command to define a table.

This command is also valid in PREP7.

TB

TB, *Lab*, *MAT*, *NTEMP*, *NPTS*, *TBOPT*, *EOSOPT*, *FuncName*

Activates a data table for material properties or special element input.

For a list of *elements* and the material models they support (*Lab* value), see *Element Support for Material Models* in the *Element Reference*.

For a list of *material models* and the elements that support them, see *Material Model Element Support* in the *Material Reference*.

Lab

Material model data table type:

AHYPER — Anisotropic hyperelasticity.

ANEL — Anisotropic elasticity.

ANISO — Anisotropic plasticity.

BB — Bergstrom-Boyce.

BH — Magnetic field data.

BISO — Bilinear isotropic hardening using von Mises or Hill plasticity.

BKIN — Bilinear kinematic hardening using von Mises or Hill plasticity.

CAST — Cast iron.

CDM — Mullins effect (for isotropic hyperelasticity models).

CGCR — Fracture criterion for crack growth simulation (**CGROW**).

CHABOCHE — Chaboche nonlinear kinematic hardening using von Mises or Hill plasticity.

CNDE — Anisotropic electric current conductivity.

CNDM — Anisotropic magnetic current conductivity.

COMP — Composite damage (explicit dynamic analysis).

CONCR — Concrete element data.

CREEP — Creep. Pure creep, creep with isotropic hardening plasticity, or creep with kinematic hardening plasticity using both von Mises or Hill potentials.

CTE — Instantaneous coefficient of thermal expansion.

CZM — Cohesive zone.

DISCRETE — Explicit spring-damper (discrete).

DMGE — Damage evolution law.

DMGI — Damage initiation criteria.

DP — Classic Drucker-Prager plasticity.

DPER — Anisotropic electric permittivity.

EDP — Extended Drucker-Prager (for granular materials such as rock, concrete, soil, ceramics and other pressure-dependent materials).

ELASTIC — Elasticity. For full harmonic analyses, properties can be defined as frequency- or temperature-dependent (**TBFIELD**).

EOS — Equation of state (explicit dynamic analysis).

EVISC — Viscoelastic element data (explicit dynamic analysis).

EXPE — Experimental data.

FCON — Fluid conductance data (explicit dynamic analysis).

FCLI — Material strength limits for calculating failure criteria.

FLUID — Fluid.

FOAM — Foam (explicit dynamic analysis).

FRIC — Coefficient of friction based on Coulomb's Law or user-defined friction.

GASKET — Gasket.

GCAP — Geological cap (explicit dynamic analysis).

GURSON — Gurson pressure-dependent plasticity for porous metals.

HFFDLD — Frequency-dependent lossy dielectric.

HFLM — Film coefficient data.

HILL — Hill anisotropy. When combined with other material options, simulates plasticity, viscoplasticity, and creep -- all with the Hill potential.

HONEY — Honeycomb (explicit dynamic analysis).

HYPER — Hyperelasticity material models (Arruda-Boyce, Blatz-Ko, Extended Tube, Gent, Mooney-Rivlin [default], Neo-Hookean, Ogden, Ogden Foam, Polynomial Form, Response Function, Yeoh, and user-defined).

INTER — User-defined contact interaction.

JOIN — Joint (linear and nonlinear elastic stiffness, linear and nonlinear damping, and frictional behavior).

KINH — Multilinear kinematic hardening using von Mises or Hill plasticity.

LSEM — Anisotropic electric and magnetic loss tangents.

MELAS — Multilinear elasticity.

MISO — Multilinear isotropic hardening using von Mises or Hill plasticity.

MKIN — Multilinear kinematic hardening using von Mises or Hill plasticity.

MOONEY — Mooney-Rivlin hyperelasticity (explicit dynamic analysis).

MPLANE — Microplane.

MUR — Anisotropic relative permeability.

NLISO — Voce isotropic hardening law (or power law) for modeling nonlinear isotropic hardening using von Mises or Hill plasticity.

PERF — Porous Media. Johnson-Champoux-Allard equivalent fluid model of porous media.

PIEZ — Piezoelectric matrix.

PLASTIC — Nonlinear plasticity with stress-vs.-plastic strain data.

PLAW — Plasticity laws (explicit dynamic analysis).

PM — Porous Media. Coupled pore-fluid diffusion and structural model of porous media.

PRONY — Prony series constants for viscoelastic materials.

PZRS — Piezoresistivity.

RATE — Rate-dependent plasticity (viscoplasticity) when combined with the BISO, MISO, NLISO or PLASTIC material options, or rate-dependent anisotropic plasticity (anisotropic viscoplasticity) when combined with the HILL and BISO, MISO, NLISO or PLASTIC material options.
The exponential visco-hardening option includes an explicit function for directly defining static yield stresses of materials.
The Anand unified plasticity option requires no combination with other material models.

SDAMP — Material structural damping coefficient. For full harmonic analyses, damping coefficients can be defined as frequency- or temperature-dependent properties (**TBFIELD**). SDAMP specifies damping in terms of the loss factor, which is equal to 2x the damping ratio.
For the relationship between SDAMP,**DMPRAT** and **MP**,BETD, see *"Notes"*.
When specifying frequency-dependent damping, specify the material property via **TB**,ELAS.

SHIFT — Shift function for viscoelastic materials.

SMA — Shape memory alloy for simulating hysteresis superelastic behavior with no performance degradation. Plane stress is not supported.

STATE — User-defined state variables. Valid with **TB**,USER and used with the UserMat subroutine. Also valid with **TB**,CREEP (when *TBOPT* = 100) and used with the UserCreep subroutine.

SWELL — Swelling strain function.

UNIAXIAL — Uniaxial stress-strain relation associated with the Cast iron material model.

USER — User-defined material model (general-purpose except for incompressible material models).

MAT

Material reference number. The default value is 1.

NTEMP

The number of temperatures for which data will be provided (if applicable). Specify temperatures via the **TBTEMP** command.

NPTS

For most labels where *NPTS* is defined, the number of data points to be specified for a given temperature. Define data points via the **TBDATA** or **TBPT** commands.

EOSOPT

Indicates which equation of state model will be used. Used only for explicit dynamics, and only when *Lab* = EOS.

1 — Linear polynomial equation of state

2 — Gruneisen equation of state

3 — Tabulated equation of state

FuncName

The name of the function to be used (entered as %*tabname*%, where *tabname* is the name of the table created by the Function Tool). Valid only when *Lab* = JOIN (joint element material) and nonlinear stiffness or damping are specified on the *TBOPT* field (see *Joint Element Specifications (JOINT)*). The function must be previously defined using the Function Tool. To learn more about how to create a function, see *Using the Function Tool* in the *Basic Analysis Guide*.

TBDATA

TBDATA, *STLOC*, *C1*, *C2*, *C3*, *C4*, *C5*, *C6*
Defines data for the material data table.

STLOC

Starting location in table for entering data. For example, if *STLOC* = 1, data input in the *C1* field applies to the first table constant, *C2* applies to the second table constant, etc. If *STLOC*=5, data input in the *C1* field applies to the fifth table constant, etc. Defaults to the last location filled + 1. The last location is reset to 1 with each TB or TBTEMP command.

C1, C2, C3, . . . , C6

Data values assigned to six locations starting with *STLOC*. If a value is already in this location, it is redefined. A blank value leaves the existing value unchanged.

Notes

Defines data for the table specified on the last TB command at the temperature specified on the last TBTEMP command (if applicable). The type of data table specified in the last TB command determines the number of data values needed in **TBDATA**. Data values are linearly interpolated for temperatures that fall between user defined TBTEMP values. See *Material Models* in the *Material Reference* for the number of data values required for different material behavior options.

This command is also valid in SOLUTION.

TBTEMP

TBTEMP, *TEMP*, *KMOD*
Defines a temperature for a material data table.

PREP7: Data Tables
MP ME ST PR PRN <> <> <> EM <> DY PP EME MFS

TEMP
Temperature value (defaults to 0.0 if *KMOD* is blank).
KMOD
If blank, *TEMP* defines a new temperature. If an integer, 1 to NTEMP (from the **TB** command), modify that previously defined temperature to the *TEMP* value, unless *TEMP* is blank, then that previously defined temperature is reactivated. Use **TBLIST** to list temperatures and data. The next **TBDATA** or **TBPT** commands also add or change the data at this temperature. If *KMOD* = CRIT (and *TEMP* is blank), the next **TBDATA** values are failure-criteria keys. If *KMOD* = STRAIN (and *TEMP* is blank), the next **TBDATA** values are strains as described for the MKIN property option. (See *Material Models* in the *Material Reference*.)

Notes

The **TBTEMP** command defines a temperature to be associated with the data on subsequent **TBPT** or **TBDATA** commands.

The defined temperature remains active until the next **TBTEMP** command is issued.

Data values must be defined with the temperatures in ascending order. Temperatures previously associated with a data table may also be modified.

This command is also valid in SOLUTION.

RMODIF

RMODIF, *NSET*, *STLOC*, *V1*, *V2*, *V3*, *V4*, *V5*, *V6*
Modifies real constant sets.

NSET
Existing set to be modified.
STLOC
Starting location in table for modifying data. For example, if *STLOC* = 1, data input in the *V1* field is the first constant in the set. If *STLOC* = 7, data input in the *V1* field is the seventh constant in the set, etc. Must be greater than zero.
V1
New value assigned to constant in location *STLOC*. If zero (or blank), a zero value will be assigned.
V2, V3, V4, . . . , V6
New values assigned to constants in the next five locations. If blank, the value remains unchanged.

Notes

Allows modifying (or adding) real constants to an existing set [R] at any location.

This command is also valid in SOLUTION.

KEYOPT

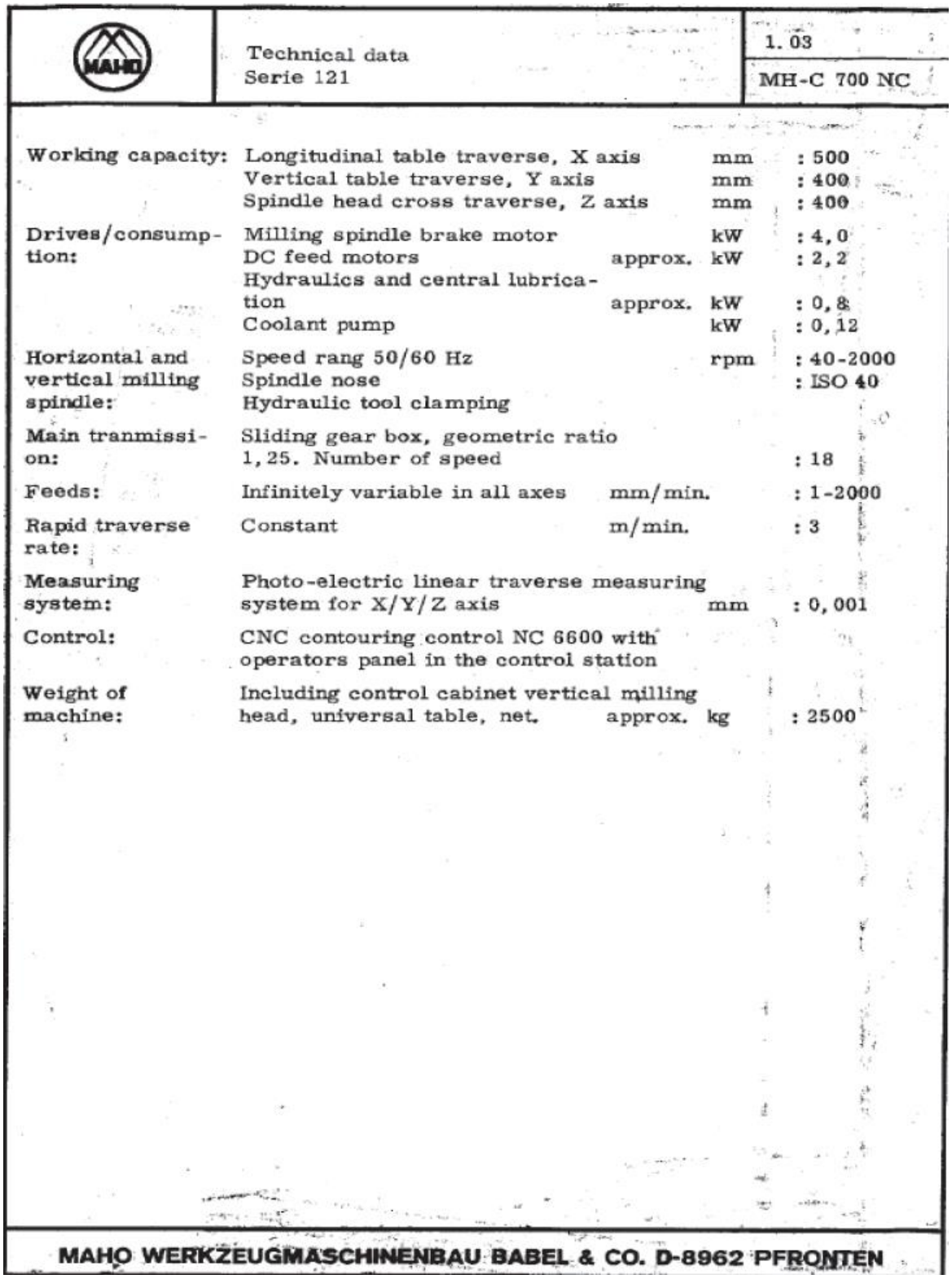
KEYOPT, *ITYPE*, *KNUM*, *VALUE*
Sets element key options.

ITYPE
Element type number as defined on the ET command.
KNUM
Number of the KEYOPT to be defined (KEYOPT(*KNUM*)).
VALUE
Value of this KEYOPT.

Notes

Alternative to inputting KEYOPT values on ET command. Must be used if KEYOPT(7) or greater values are to be input. *ITYPE* must first be defined with the ET command.

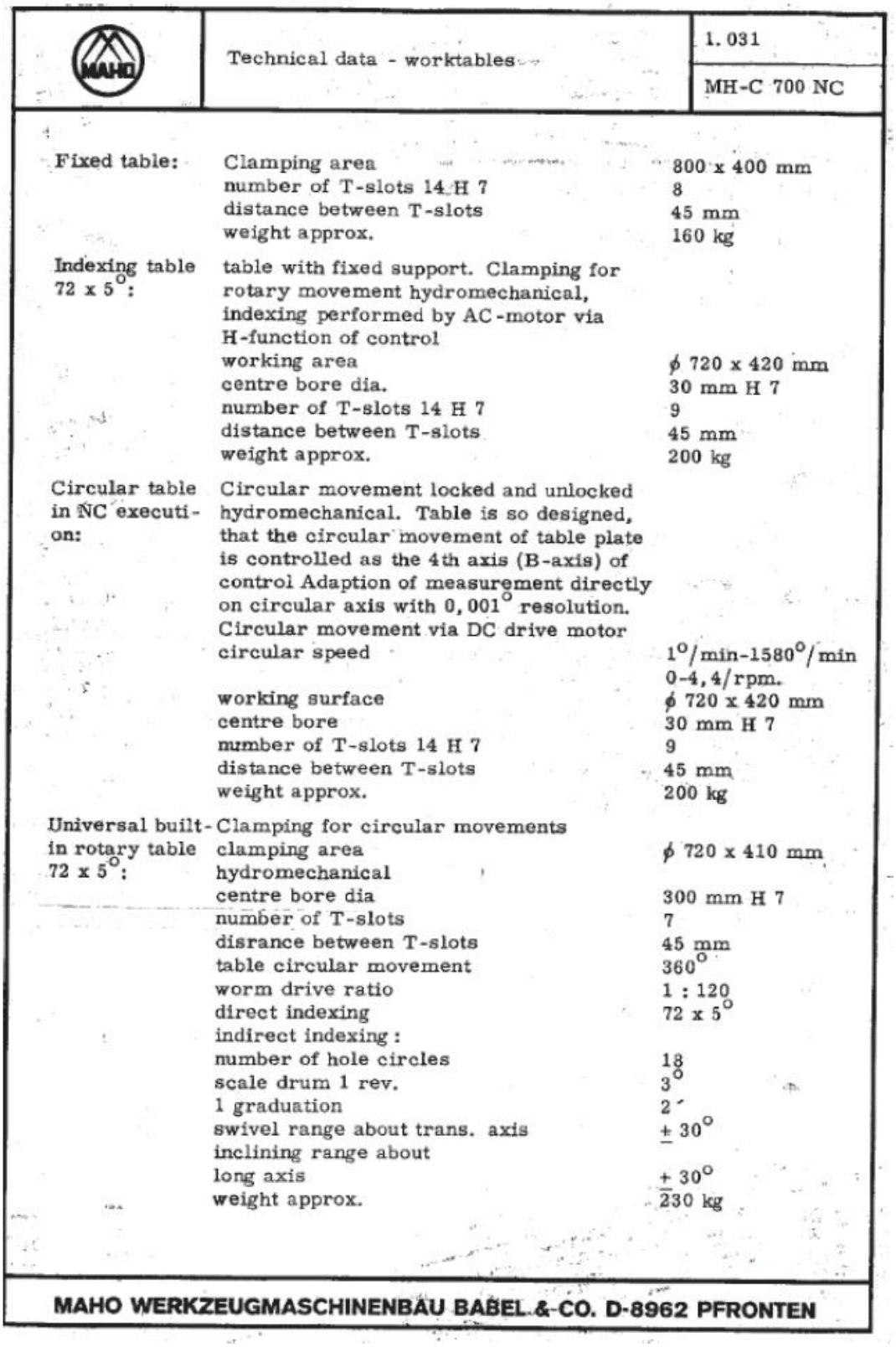
10.4 Appendix 4: CNC information



	Technical data Serie 121			1. 03 MH-C 700 NC
Working capacity:	Longitudinal table traverse, X axis		mm	: 500
	Vertical table traverse, Y axis		mm	: 400
	Spindle head cross traverse, Z axis		mm	: 400
Drives/consumption:	Milling spindle brake motor		kW	: 4,0
	DC feed motors	approx.	kW	: 2,2
	Hydraulics and central lubrication	approx.	kW	: 0,8
	Coolant pump		kW	: 0,12
Horizontal and vertical milling spindle:	Speed rang 50/60 Hz		rpm	: 40-2000
	Spindle nose			: ISO 40
	Hydraulic tool clamping			
Main tranmission:	Sliding gear box, geometric ratio 1,25. Number of speed			: 18
Feeds:	Infinitely variable in all axes	mm/min.		: 1-2000
Rapid traverse rate:	Constant	m/min.		: 3
Measuring system:	Photo-electric linear traverse measuring system for X/Y/Z axis		mm	: 0,001
Control:	CNC contouring control NC 6600 with operators panel in the control station			
Weight of machine:	Including control cabinet vertical milling head, universal table, net.	approx.	kg	: 2500

MAHO WERKZEUGMASCHINENBAU BABEL & CO. D-8962 PFRONTEN

Figure 10.15: CNC specification



	Technical data - worktables	1.031
		MH-C 700 NC
Fixed table:	Clamping area	800 x 400 mm
	number of T-slots 14 H 7	8
	distance between T-slots	45 mm
	weight approx.	160 kg
Indexing table 72 x 5°:	table with fixed support. Clamping for rotary movement hydromechanical, indexing performed by AC-motor via H-function of control	
	working area	ϕ 720 x 420 mm
	centre bore dia.	30 mm H 7
	number of T-slots 14 H 7	9
	distance between T-slots	45 mm
	weight approx.	200 kg
Circular table in NC execution:	Circular movement locked and unlocked hydromechanical. Table is so designed, that the circular movement of table plate is controlled as the 4th axis (B-axis) of control Adaption of measurement directly on circular axis with 0,001° resolution. Circular movement via DC drive motor	
	circular speed	1°/min-1580°/min 0-4,4/rpm.
	working surface	ϕ 720 x 420 mm
	centre bore	30 mm H 7
	number of T-slots 14 H 7	9
	distance between T-slots	45 mm
	weight approx.	200 kg
Universal built-in rotary table 72 x 5°:	Clamping for circular movements	
	clamping area	ϕ 720 x 410 mm
	hydromechanical	
	centre bore dia	300 mm H 7
	number of T-slots	7
	disrance between T-slots	45 mm
	table circular movement	360°
	worm drive ratio	1 : 120
	direct indexing	72 x 5°
	indirect indexing :	
	number of hole circles	18
	scale drum 1 rev.	3°
	1 graduation	2´
	swivel range about trans. axis	± 30°
	inclining range about long axis	± 30°
	weight approx.	230 kg

MAHO WERKZEUGMASCHINENBAU BABEL & CO. D-8962 PFRONTEN

Figure 10.16: CNC technical data specification

10.5 Appendix 5: Tool and Pin Geometry

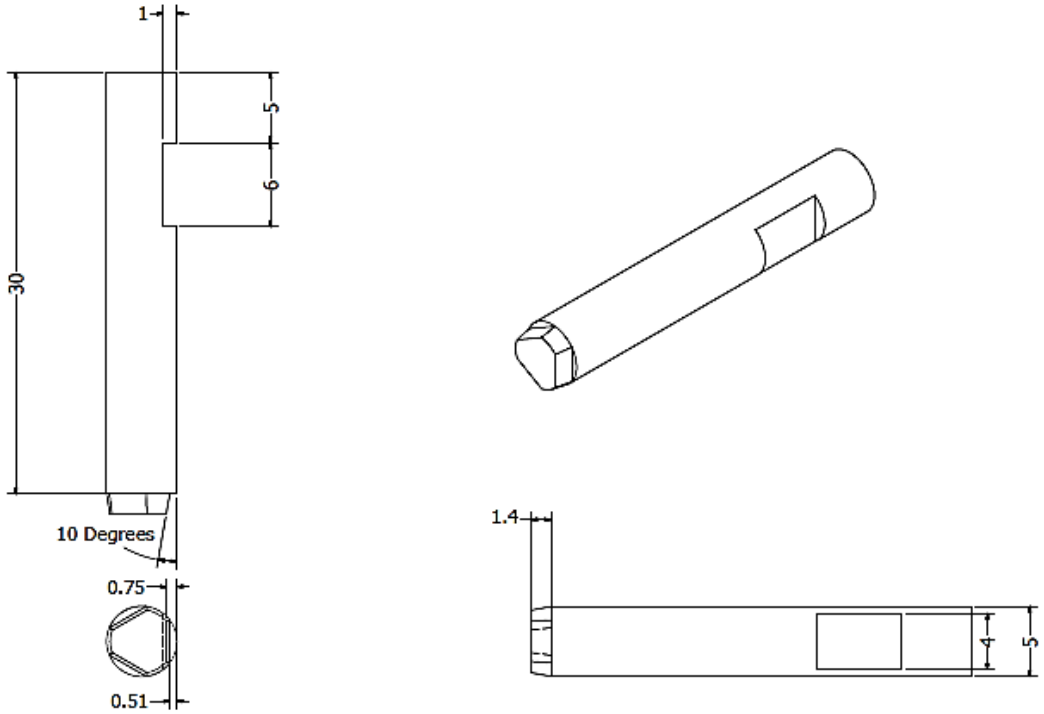


Figure 10.17: Pin geometry

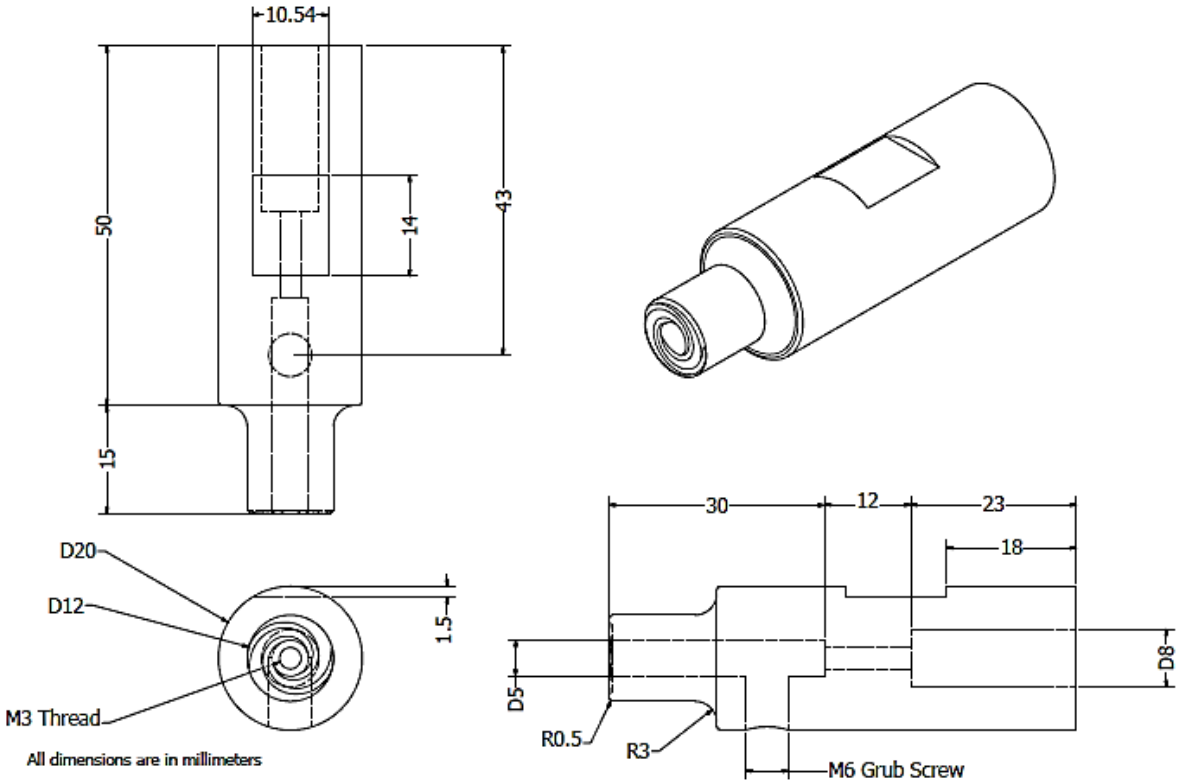


Figure 10.18: Tool geometry

10.6 Appendix 6: FEA model processed data

Table 10.18: Average heat flux for FEA models

		Average heat flux	13505.61	54022.46	22466.54	135056.1
Model			q1	Q4	q2	Q2
8	Ambient	25	hq1	hQ4	hq2	hQ2
Time	Temperature	Delta T	30	120	30	300
1.0028	26.833	1.833	54.99	219.96	56.213223	549.9
1.025	48.24	23.24	697.2	2788.8	714.4584	6972
1.04	62.91	37.91	1137.3	4549.2	1167.5655	11373
1.0501	72.472	47.472	1424.16	5696.64	1463.8732	14241.6
1.0606	82.546	57.546	1726.38	6905.52	1776.932	17263.8
1.0706	92.565	67.565	2026.95	8107.8	2089.2348	20269.5
1.0802	102.77	77.77	2333.1	9332.4	2408.3689	23331
1.0902	112.64	87.64	2629.2	10516.8	2718.0741	26292
1.1012	123.92	98.92	2967.6	11870.4	3073.3551	29676
1.1202	142.9	117.9	3537	14148	3674.5928	35370
1.1225	145.28	120.28	3608.4	14433.6	3750.3058	36084
1.1307	153.63	128.63	3858.9	15435.6	4016.53	38589
1.1408	164.04	139.04	4171.2	16684.8	4349.769	41712
1.1501	173.28	148.28	4448.4	17793.6	4646.851	44484
1.1603	184.01	159.01	4770.3	19081.2	4993.441	47703
1.1691	193.28	168.28	5048.4	20193.6	5294.3186	50484
1.1811	205.48	180.48	5414.4	21657.6	5692.4371	54144
1.1908	215.34	190.34	5710.2	22840.8	6016.054	57102
1.2011	226.64	201.64	6049.2	24196.8	6389.073	60492
1.211	236.53	211.53	6345.9	25383.6	6717.5026	63459
1.2208	246.67	221.67	6650.1	26600.4	7056.2094	66501
1.2302	258.19	233.19	6995.7	27982.8	7443.5402	69957
1.2415	271.25	246.25	7387.5	29550	7886.048	73875
1.2502	280.46	255.46	7663.8	30655.2	8200.3717	76638
1.2524	282.96	257.96	7738.8	30955.2	8286.0261	77388
1.3014	340.41	315.41	9462.3	37849.2	10296.917	94623
1.4007	460.71	435.71	13071.3	52285.2	14830.974	130713
1.4034	464.11	439.11	13173.3	52693.2	14966.731	131733
1.4048	464.73	439.73	13191.9	52767.6	14991.537	131919
1.4062	467.01	442.01	13260.3	53041.2	15082.896	132603
1.4083	469.3	444.3	13329	53316	15174.869	133290
1.4104	472.32	447.32	13419.6	53678.4	15296.493	134196
1.4114	473.66	448.66	13459.8	53839.2	15350.58	134598
1.4125	474.79	449.79	13493.7	53974.8	15396.249	134937

1.4132	475.47	450.47	13514.1	54056.4	15423.756	135141
1.414	475.25	450.25	13507.5	54030	15414.855	135075
1.4148	477.23	452.23	13566.9	54267.6	15495.043	135669
1.4164	477.71	452.71	13581.3	54325.2	15514.508	135813
1.4195	481.29	456.29	13688.7	54754.8	15659.988	136887
1.4226	486.64	461.64	13849.2	55396.8	15878.415	138492
1.4273	492.14	467.14	14014.2	56056.8	16104.255	140142
1.432	497.91	472.91	14187.3	56749.2	16342.608	141873
1.4367	503.58	478.58	14357.4	57429.6	16578.273	143574
1.4422	510.24	485.24	14557.2	58228.8	16856.941	145572
1.4478	516.86	491.86	14755.8	59023.2	17135.955	147558
1.4533	523.5	498.5	14955	59820	17417.867	149550
1.4589	529.85	504.85	15145.5	60582	17689.426	151455
1.4645	536.7	511.7	15351	61404	17984.551	153510
1.47	543.14	518.14	15544.2	62176.8	18264.111	155442
1.4756	549.7	524.7	15741	62964	18551.007	157410
1.4811	556.29	531.29	15938.7	63754.8	18841.41	159387
1.4867	562.34	537.34	16120.2	64480.8	19109.985	161202
1.4922	568.89	543.89	16316.7	65266.8	19402.914	163167
1.4978	575.27	550.27	16508.1	66032.4	19690.428	165081
1.5033	582.14	557.14	16714.2	66856.8	20002.477	167142
1.6033	687.93	662.93	19887.9	79551.6	25159.868	198879
1.702	783.32	758.32	22749.6	90998.4	30470.018	227496
1.802	900.51	875.51	26265.3	105061.2	38050.38	262653
1.9009	1003.8	978.8	29364	117456	45898.029	293640
2.0016	1096.8	1071.8	32154	128616	54072.922	321540
2.253	1317.7	1292.7	38781	155124	78679.497	387810
2.5002	1551.9	1526.9	45807	183228	114952.73	458070
2.7511	1828.2	1803.2	54096	216384	175656.72	540960
3	2127.8	2102.8	63084	252336	270291.24	630840

Table 10.19: Average heat flux for FEA models

		Average heat flux	27257.98	109031.9	42207.2	272579.8
Model			q1	Q4	q2	Q2
10	Ambient	25	hq1	hQ4	hq2	hQ2
Time	Temperature	Delta T	30	120	30	300
0.2	25	0	0	0	0	0
0.4	25	0	0	0	0	0
0.9	25	0	0	0	0	0
1	25	0	0	0	0	0

1.04	409.14	384.14	11524.2	46096.8	12826.53	115242
1.08	599.29	574.29	17228.7	68914.8	20792.83	172287
1.12	683.76	658.76	19762.8	79051.2	24943.01	197628
1.16	765.64	740.64	22219.2	88876.8	29432.43	222192
1.2001	851.6	826.6	24798	99192	34730.31	247980
1.24	885.48	860.48	25814.4	103257.6	37004.82	258144
1.28	917.05	892.05	26761.5	107046	39227.93	267615
1.32	951.01	926.01	27780.3	111121.2	41737.48	277803
1.3601	976.38	951.38	28541.4	114165.6	43696.28	285414
1.4	995.84	970.84	29125.2	116500.8	45249.58	291252
1.44	1012	987	29610	118440	46574.11	296100
1.48	1029.2	1004.2	30126	120504	48019.37	301260
1.5201	1043	1018	30540	122160	49206.04	305400
1.5601	1055.2	1030.2	30906	123624	50275.67	309060
1.6001	1074.8	1049.8	31494	125976	52035.4	314940
1.6401	1093.8	1068.8	32064	128256	53791.12	320640
1.68	1114.3	1089.3	32679	130716	55742.12	326790
1.72	1130.8	1105.8	33174	132696	57356.33	331740
1.76	1150.1	1125.1	33753	135012	59295.5	337530
		Average heat flux	27257.98	109031.9	42207.2	272579.8
Model			q1	Q4	q2	Q2
12	Ambient	25	hq1	hQ4	hq2	hQ2
Time	Temperature	Delta T	30	120	30	300
0.2	25	0	0	0	0	0
0.4	25	0	0	0	0	0
0.9	25	0	0	0	0	0
1	25	0	0	0	0	0
1.04	409.14	384.14	11524.2	46096.8	12826.53	115242
1.08	599.29	574.29	17228.7	68914.8	20792.83	172287
1.12	683.76	658.76	19762.8	79051.2	24943.01	197628
1.16	765.64	740.64	22219.2	88876.8	29432.43	222192
1.2001	851.6	826.6	24798	99192	34730.31	247980
1.24	885.48	860.48	25814.4	103257.6	37004.82	258144
1.28	917.05	892.05	26761.5	107046	39227.93	267615
1.32	951.01	926.01	27780.3	111121.2	41737.48	277803
1.3601	976.38	951.38	28541.4	114165.6	43696.28	285414
1.4	995.84	970.84	29125.2	116500.8	45249.58	291252
1.44	1012	987	29610	118440	46574.11	296100
1.48	1029.2	1004.2	30126	120504	48019.37	301260
1.5201	1043	1018	30540	122160	49206.04	305400
1.5601	1055.2	1030.2	30906	123624	50275.67	309060
1.6001	1074.8	1049.8	31494	125976	52035.4	314940

1.6401	1093.8	1068.8	32064	128256	53791.12	320640
1.68	1114.3	1089.3	32679	130716	55742.12	326790
1.72	1130.8	1105.8	33174	132696	57356.33	331740
1.76	1150.1	1125.1	33753	135012	59295.5	337530

Table 10.20: Heat flux transfer for FEA model

		Average heat flux	32710.43	130841.7	62222.88	163552.2
Model			q1	Q4	q2	Q2
14	Ambient	25	hq1	hQ4	hq2	hQ2
Time	Temperature	Delta T	30	120	30	150
0.2	25	0	0	0	0	0
0.4	25	0	0	0	0	0
0.9	25	0	0	0	0	0
1	25	0	0	0	0	0
1.1	525.54	500.54	15016.2	60064.8	17504.9	75081
1.12	557.04	532.04	15961.2	63844.8	18874.6	79806
1.14	581.08	556.08	16682.4	66729.6	19954.16	83412
1.18	624.31	599.31	17979.3	71917.2	21976.11	89896.5
1.22	670.29	645.29	19358.7	77434.8	24250.62	96793.5
1.26	710.02	685.02	20550.6	82202.4	26328.92	102753
1.28	733.79	708.79	21263.7	85054.8	27626.36	106318.5
1.3	749.98	724.98	21749.4	86997.6	28534.49	108747
1.32	777.07	752.07	22562.1	90248.4	30100.28	112810.5
1.36	812.88	787.88	23636.4	94545.6	32263.58	118182
1.38	839.31	814.31	24429.3	97717.2	33932.43	122146.5
1.4	848.52	823.52	24705.6	98822.4	34529.02	123528
1.42	858.98	833.98	25019.4	100077.6	35216.27	125097
1.44	871.73	846.73	25401.9	101607.6	36068.19	127009.5
1.46	888.37	863.37	25901.1	103604.4	37204.08	129505.5
1.48	892.71	867.71	26031.3	104125.2	37504.9	130156.5
1.52	912.43	887.43	26622.9	106491.6	38896.13	133114.5
1.54	921.81	896.81	26904.3	107617.2	39572.15	134521.5
1.56	929.81	904.81	27144.3	108577.2	40156.14	135721.5
1.6	946.87	921.87	27656.1	110624.4	41424.76	138280.5
1.66	969	944	28320	113280	43118.85	141600
1.68	975.07	950.07	28502.1	114008.4	43593.32	142510.5
1.7	980.71	955.71	28671.3	114685.2	44038.02	143356.5
1.74	993.64	968.64	29059.2	116236.8	45071.72	145296
1.76	998.2	973.2	29196	116784	45441.04	145980
1.8	1010.8	985.8	29574	118296	46474.66	147870

1.82	1013.4	988.4	29652	118608	46690.37	148260
1.9	1043.8	1018.8	30564	122256	49275.58	152820
1.92	1051.1	1026.1	30783	123132	49914.03	153915
1.94	1061.2	1036.2	31086	124344	50808.91	155430
1.96	1068.3	1043.3	31299	125196	51446.1	156495
1.98	1075.8	1050.8	31524	126096	52126.57	157620
2	1087.3	1062.3	31869	127476	53184.87	159345
2.04	1100	1075	32250	129000	54374.9	161250
2.1	1128.5	1103.5	33105	132420	57128.93	165525
2.14	1150	1125	33750	135000	59285.3	168750
2.22	1186.4	1161.4	34842	139368	63096.97	174210
2.26	1209	1184	35520	142080	65569.18	177600
2.34	1249.3	1224.3	36729	146916	70187.67	183645
2.38	1268	1243	37290	149160	72425.54	186450
2.4	1281.6	1256.6	37698	150792	74092.04	188490
2.42	1288.8	1263.8	37914	151656	74987.82	189570
2.44	1299.5	1274.5	38235	152940	76336.55	191175
2.46	1314	1289	38670	154680	78198.15	193350
2.5	1331.7	1306.7	39201	156804	80524.38	196005
2.54	1356.7	1331.7	39951	159804	83913.23	199755
2.58	1376.9	1351.9	40557	162228	86742	202785
2.62	1399.6	1374.6	41238	164952	90020.2	206190
2.64	1411.3	1386.3	41589	166356	91751.8	207945
2.66	1426.7	1401.7	42051	168204	94075.38	210255
2.68	1438	1413	42390	169560	95812.92	211950
2.72	1457.9	1432.9	42987	171948	98941.09	214935
2.76	1482.1	1457.1	43713	174852	102865.1	218565
2.8	1509.3	1484.3	44529	178116	107436.9	222645
2.82	1518.4	1493.4	44802	179208	109005.4	224010
2.84	1530.9	1505.9	45177	180708	111192.5	225885
2.86	1547.3	1522.3	45669	182676	114119.7	228345
2.8801	1559.8	1534.8	46044	184176	116395.6	230220
2.9	1567.8	1542.8	46284	185136	117872.8	231420
2.92	1580.1	1555.1	46653	186612	120175.6	233265
2.94	1595.1	1570.1	47103	188412	123036.6	235515
2.9601	1606	1581	47430	189720	125152.4	237150

Table 10.21: Heat flux transfer for FEA model

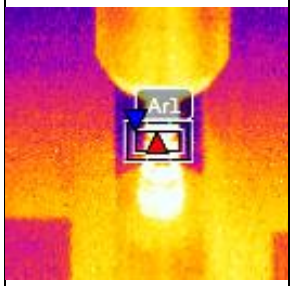
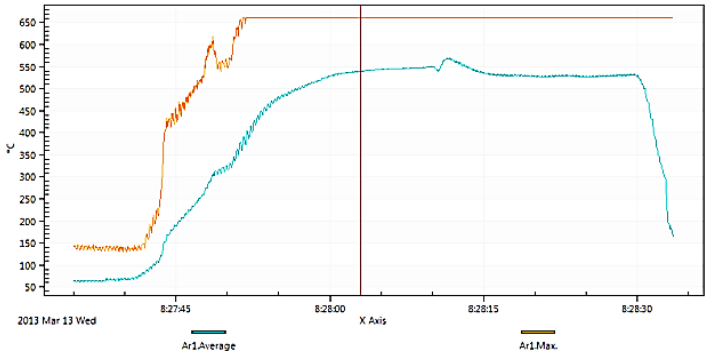
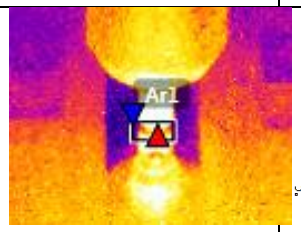
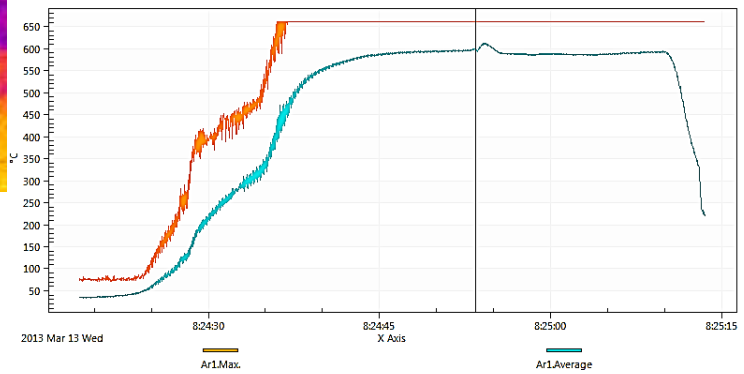
		Average heat flux	25018.96	100075.9	45287.41	166793.1
Model			q1	Q4	q2	Q2

17	Ambient	25	hq1	hQ4	hq2	hQ2
Time	Temperature	Delta T	30	120	40	200
0.2	25	0	0	0	0	0
0.4	25	0	0	0	0	0
0.9	25	0	0	0	0	0
1	25	0	0	0	0	0
1.02	290.79	265.79	7973.7	31894.8	11213.14	53158
1.0401	410.33	385.33	11559.9	46239.6	16724.98	77066
1.0601	468.46	443.46	13303.8	53215.2	19575.71	88692
1.0801	498.64	473.64	14209.2	56836.8	21109.27	94728
1.1001	525.64	500.64	15019.2	60076.8	22515.57	100128
1.12	557.05	532.05	15961.5	63846	24195.54	106410
1.1401	581.15	556.15	16684.5	66738	25518.85	111230
1.16	604.74	579.74	17392.2	69568.8	26844.87	115948
1.18	624.33	599.33	17979.9	71919.6	27970.37	119866
1.2001	645.33	620.33	18609.9	74439.6	29202.6	124066
1.2201	670.43	645.43	19362.9	77451.6	30712.05	129086
1.24	688.08	663.08	19892.4	79569.6	31798.49	132616
1.26	710.13	685.13	20553.9	82215.6	33186.13	137026
1.28	734.01	709.01	21270.3	85081.2	34728.67	141802
1.3	750.24	725.24	21757.2	87028.8	35801.64	145048
1.32	777.26	752.26	22567.8	90271.2	37634.08	150452
1.3401	792.42	767.42	23022.6	92090.4	38688.4	153484
1.3601	813.29	788.29	23648.7	94594.8	40171.89	157658
1.3801	839.56	814.56	24436.8	97747.2	42094.12	162912
1.4	848.72	823.72	24711.6	98846.4	42779.26	164744
1.42	859.27	834.27	25028.1	100112.4	43578.17	166854
1.44	871.98	846.98	25409.4	101637.6	44554.86	169396
1.4601	888.75	863.75	25912.5	103650	45867.84	172750
1.4801	892.98	867.98	26039.4	104157.6	46203.48	173596
1.5	902.87	877.87	26336.1	105344.4	46995.35	175574
1.52	912.64	887.64	26629.2	106516.8	47787.56	177528
1.54	922.01	897.01	26910.3	107641.2	48556.76	179402
1.5601	929.93	904.93	27147.9	108591.6	49214.25	180986
1.5801	941.61	916.61	27498.3	109993.2	50196.3	183322
1.6	947.01	922.01	27660.3	110641.2	50655.41	184402
1.6201	953.09	928.09	27842.7	111370.8	51176.22	185618
1.6401	960.94	935.94	28078.2	112312.8	51854.8	187188
1.66	969.19	944.19	28325.7	113302.8	52575.54	188838
1.68	975.23	950.23	28506.9	114027.6	53108.18	190046
1.7001	980.84	955.84	28675.2	114700.8	53606.72	191168
1.72	987	962	28860	115440	54158.4	192400

1.74	993.8	968.8	29064	116256	54772.63	193760
1.76	998.33	973.33	29199.9	116799.6	55184.9	194666
1.7801	1004.5	979.5	29385	117540	55750.42	195900
1.8	1011	986	29580	118320	56351.22	197200
1.82	1013.6	988.6	29658	118632	56593	197720
1.8401	1020.3	995.3	29859	119436	57219.9	199060
1.8601	1027.6	1002.6	30078	120312	57909.35	200520
1.88	1037.2	1012.2	30366	121464	58826.31	202440
1.9001	1044.1	1019.1	30573	122292	59492.68	203820
1.9201	1051.5	1026.5	30795	123180	60214.21	205300
1.94	1061.5	1036.5	31095	124380	61200.69	207300
1.96	1068.8	1043.8	31314	125256	61929.23	208760
1.98	1076.2	1051.2	31536	126144	62675.08	210240
2	1087.7	1062.7	31881	127524	63849.01	212540
2.0201	1093.2	1068.2	32046	128184	64416.92	213640
2.04	1100.5	1075.5	32265	129060	65177.21	215100
3	1109.4	1084.4	32532	130128	66114.34	216880

10.7 Appendix 7: Average temperature plots

Table 10.22: Temperature plots for average temperatures on work piece

Weld trial number	Average point locator	Temperature plot
3		
4		

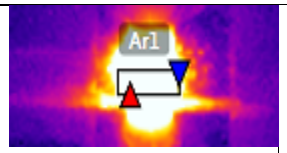
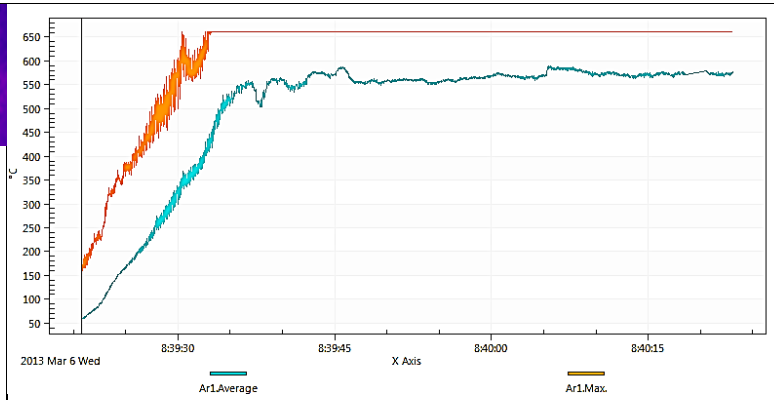
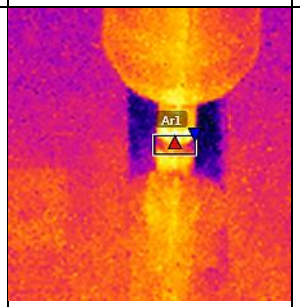
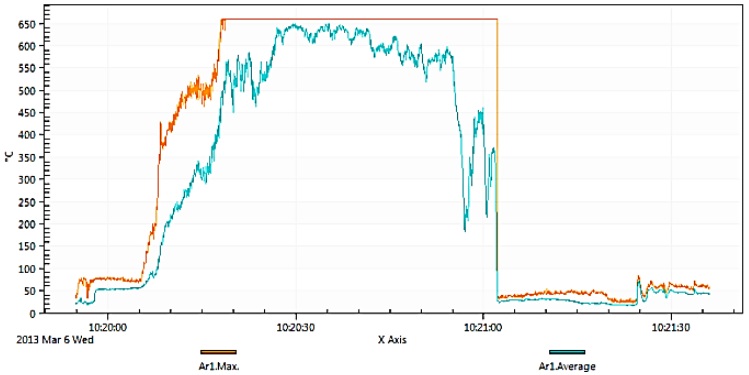
1a		
1b		

Table 10.23: Calculated values used for processed data

	$Q_{sticking}$	$Q_{sliding}$
Heat transfer (W)	11080	411.23
Total heat flux (W/m^2)	5291.02	196.35
Area shoulder	0.000113097	

F (radiation view factor)	1	
Emissivity	0.11	
Stefan Boltzman	5.67E-08	W/m^2K

Table 10.24: 1250 RPM and 500mm/min processes data

				Average convection coefficients	24.008	9.234	3.694
Atmospheric temperature	25				Contributions		
	Average temperature				0.65	0.25	0.1
Relative time	Delta T	$T^4-T_0^4$	q_2 radiation	Sum of convections	h_{q2}	h_{Q2}	h_Q
0	38.77	4.98E+09	31.08	135.68	88.19	33.92	13.57
0.1	39.42	5.08E+09	31.70	133.43	86.73	33.36	13.34
0.2	39.39	5.08E+09	31.68	133.51	86.78	33.38	13.35
0.3	36.86	4.69E+09	29.27	142.76	92.79	35.69	14.28
0.4	39.76	5.14E+09	32.03	132.28	85.98	33.07	13.23
0.5	40.12	5.19E+09	32.38	131.08	85.20	32.77	13.11
0.6	37.33	4.76E+09	29.72	140.94	91.61	35.24	14.09
0.7	38.74	4.98E+09	31.05	135.79	88.26	33.95	13.58
0.8	40.01	5.17E+09	32.28	131.43	85.43	32.86	13.14
0.9	38.64	4.96E+09	30.96	136.11	88.47	34.03	13.61
1	36.94	4.71E+09	29.35	142.43	92.58	35.61	14.24
1.5	40.30	5.22E+09	32.55	130.49	84.82	32.62	13.05
2	38.00	4.87E+09	30.35	138.42	89.98	34.61	13.84
2.5	40.00	5.17E+09	32.26	131.47	85.45	32.87	13.15

3	39.15	5.04E+09	31.45	134.35	87.33	33.59	13.43
3.5	41.54	5.41E+09	33.76	126.55	82.26	31.64	12.66
4	42.70	5.60E+09	34.90	123.09	80.01	30.77	12.31
4.5	41.04	5.33E+09	33.27	128.10	83.27	32.03	12.81
5	45.18	5.99E+09	37.37	116.28	75.59	29.07	11.63
5.5	42.10	5.50E+09	34.30	124.88	81.17	31.22	12.49
6	46.57	6.22E+09	38.78	112.79	73.32	28.20	11.28
6.5	50.34	6.85E+09	42.71	104.25	67.76	26.06	10.43
7	58.61	8.30E+09	51.76	89.39	58.10	22.35	8.94
7.5	71.38	1.07E+10	67.01	73.19	47.57	18.30	7.32
8	74.69	1.14E+10	71.23	69.89	45.43	17.47	6.99
8.5	95.23	1.60E+10	100.08	54.51	35.43	13.63	5.45
9	129.85	2.57E+10	160.01	39.51	25.68	9.88	3.95
9.5	153.91	3.39E+10	211.19	33.00	21.45	8.25	3.30
10	163.67	3.76E+10	234.43	30.89	20.08	7.72	3.09
11	191.33	4.95E+10	308.75	26.04	16.93	6.51	2.60
12	216.92	6.25E+10	389.68	22.60	14.69	5.65	2.26
13	249.68	8.22E+10	512.49	19.14	12.44	4.78	1.91
14	283.75	1.07E+11	665.81	16.30	10.60	4.08	1.63
15	298.91	1.19E+11	743.33	15.21	9.89	3.80	1.52
16	338.15	1.56E+11	973.15	12.77	8.30	3.19	1.28
17	377.49	2.00E+11	1250.40	10.70	6.96	2.68	1.07
18	415.13	2.51E+11	1565.13	8.98	5.83	2.24	0.90
19	440.38	2.90E+11	1806.12	7.91	5.14	1.98	0.79
20	456.68	3.17E+11	1975.43	7.26	4.72	1.82	0.73
25	503.15	4.04E+11	2521.99	5.50	3.58	1.38	0.55
30	517.85	4.35E+11	2715.97	4.97	3.23	1.24	0.50
34	522.45	4.46E+11	2778.88	4.81	3.13	1.20	0.48
34.8	524.82	4.51E+11	2811.74	4.72	3.07	1.18	0.47

Table 10.25: 1600 RPM and 400mm/min processes data

			25				72.50	27.886	11.154
			Average temperature						
Relative time	Ar1.Max.	Ar1.Average	Delta T	$T^4-T_0^4$	q_2 radiation	Sum of convections	h_{q2}	h_{Q2}	h_Q
0	72.4	34.1	9.1	1.01E+09	6.3	745.3	484.4	186.3	74.5
0.1	74.5	34.4	9.4	1.04E+09	6.5	723.2	470.1	180.8	72.3
0.2	73.1	34.5	9.5	1.06E+09	6.6	712.4	463.0	178.1	71.2
0.3	74.9	34.9	9.9	1.10E+09	6.9	685.7	445.7	171.4	68.6
0.4	75.9	34.9	9.9	1.10E+09	6.9	682.3	443.5	170.6	68.2
0.5	76.6	35.4	10.4	1.16E+09	7.3	648.8	421.7	162.2	64.9
0.6	75.9	34.7	9.7	1.08E+09	6.7	699.8	454.9	175.0	70.0
0.8	75.5	34.0	9.0	1.00E+09	6.3	748.5	486.5	187.1	74.8
0.9	76.6	33.9	8.9	9.84E+08	6.1	762.0	495.3	190.5	76.2
1	74.2	34.6	9.6	1.07E+09	6.6	706.2	459.0	176.6	70.6
1.5	74.9	35.2	10.2	1.13E+09	7.1	665.5	432.6	166.4	66.6
2	79.9	36.3	11.3	1.26E+09	7.9	600.5	390.3	150.1	60.0
2.5	74.9	35.9	10.9	1.22E+09	7.6	623.0	404.9	155.7	62.3
3	79.9	37.5	12.5	1.41E+09	8.8	539.8	350.9	135.0	54.0
3.5	75.2	39.2	14.2	1.61E+09	10.0	477.7	310.5	119.4	47.8
4	74.5	38.7	13.7	1.55E+09	9.7	494.0	321.1	123.5	49.4
4.5	78.3	42.3	17.3	2.00E+09	12.5	390.2	253.7	97.6	39.0
5	81.3	44.6	19.6	2.29E+09	14.3	344.4	223.9	86.1	34.4
5.5	83.2	47.2	22.2	2.63E+09	16.4	304.0	197.6	76.0	30.4
6	106.5	55.7	30.7	3.79E+09	23.6	220.0	143.0	55.0	22.0
6.5	125.4	60.8	35.8	4.54E+09	28.3	188.3	122.4	47.1	18.8
7	138.3	71.7	46.7	6.24E+09	38.9	144.3	93.8	36.1	14.4
7.5	182.2	87.3	62.3	8.97E+09	56.0	107.8	70.1	27.0	10.8

8	163.2	84.8	59.8	8.51E+09	53.1	112.4	73.0	28.1	11.2
8.5	225.5	108.3	83.3	1.33E+10	82.7	80.3	52.2	20.1	8.0
9	235.9	117.5	92.5	1.54E+10	96.0	72.2	46.9	18.0	7.2
9.5	275.0	129.2	104.2	1.83E+10	114.2	63.9	41.5	16.0	6.4
10	367.0	171.2	146.2	3.11E+10	193.8	45.0	29.3	11.3	4.5
11	398.8	212.4	187.4	4.77E+10	297.4	34.6	22.5	8.6	3.5
12	406.9	244.5	219.5	6.39E+10	398.5	29.0	18.9	7.3	2.9
13	440.9	257.9	232.9	7.16E+10	446.6	27.2	17.7	6.8	2.7
14	465.2	280.2	255.2	8.58E+10	535.3	24.4	15.9	6.1	2.4
15	456.7	302.2	277.2	1.02E+11	633.9	22.1	14.4	5.5	2.2
16	498.6	337.8	312.8	1.31E+11	819.8	19.0	12.4	4.8	1.9
17	627.9	401.3	376.3	1.99E+11	1241.5	14.7	9.6	3.7	1.5
18	660.6	457.2	432.2	2.77E+11	1725.7	11.7	7.6	2.9	1.2
19	660.6	489.7	464.7	3.31E+11	2062.8	10.1	6.6	2.5	1.0
20	660.6	528.6	503.6	4.05E+11	2527.7	8.4	5.5	2.1	0.8
24	660.6	577.8	552.8	5.16E+11	3220.5	6.4	4.2	1.6	0.6
25	660.6	584.7	559.7	5.34E+11	3328.1	6.2	4.0	1.5	0.6
30	660.6	593.8	568.8	5.57E+11	3474.1	5.8	3.8	1.4	0.6
34.7	660.64	597.38	572.38	5.66E+11	3532.65	5.66	3.68	1.42	0.57

Table 10.26: 1250 RPM and 400mm/min processes data

	234	234	25				14.85176	5.712214	2.284886
			Average temperature						
Relative time	Ar1.Max.	Ar1.Average	Delta T	$T^4-T_0^4$	q_2 radiation	Sum of convections	h_{q2}	h_{Q2}	h_Q
0.0	58.8	155.7	33.8	4.24E+09	26.5	155.7	101.2	38.9	15.56587
0.1	60.5	173.1	35.5	4.49E+09	28.0	148.3	96.4	37.1	14.82744

0.2	62.7	183.7	37.7	4.82E+09	30.0	139.7	90.8	34.9	13.96863
0.3	63.5	192.0	38.5	4.94E+09	30.8	136.8	88.9	34.2	13.67588
0.4	64.2	182.8	39.2	5.05E+09	31.5	134.1	87.1	33.5	13.40708
0.5	63.9	178.6	38.9	5.01E+09	31.2	135.1	87.8	33.8	13.50982
0.6	67.0	171.8	42.0	5.48E+09	34.2	125.3	81.4	31.3	12.5254
0.7	69.0	195.3	44.0	5.80E+09	36.2	119.5	77.7	29.9	11.94916
0.8	70.0	186.8	45.0	5.97E+09	37.2	116.6	75.8	29.2	11.6636
0.9	72.3	192.4	47.3	6.33E+09	39.5	111.1	72.2	27.8	11.11328
1.4	80.4	226.1	55.4	7.71E+09	48.1	94.7	61.6	23.7	9.471914
1.9	94.9	234.3	69.9	1.05E+10	65.2	74.7	48.6	18.7	7.473036
2.4	111.9	289.4	86.9	1.41E+10	87.8	59.9	38.9	15.0	5.987887
2.9	132.6	332.7	107.6	1.92E+10	119.7	48.1	31.2	12.0	4.807262
3.4	148.0	350.5	123.0	2.35E+10	146.8	41.8	27.2	10.5	4.183919
3.9	159.7	358.5	134.7	2.72E+10	169.6	38.0	24.7	9.5	3.802808
4.4	171.1	371.5	146.1	3.10E+10	193.5	34.9	22.7	8.7	3.490124
4.9	186.5	403.6	161.5	3.67E+10	229.1	31.3	20.4	7.8	3.134742
5.4	196.7	413.1	171.7	4.08E+10	254.6	29.3	19.1	7.3	2.933912
5.9	208.3	417.3	183.3	4.58E+10	285.8	27.3	17.7	6.8	2.730709
6.4	231.9	464.0	206.9	5.72E+10	356.6	23.8	15.5	6.0	2.384735
6.9	234.6	431.3	209.6	5.86E+10	365.3	23.5	15.3	5.9	2.349881
7.4	262.9	501.2	237.9	7.47E+10	465.9	20.3	13.2	5.1	2.02785
7.9	284.5	520.1	259.5	8.88E+10	554.0	18.3	11.9	4.6	1.825296
8.4	274.2	476.4	249.2	8.19E+10	510.5	19.2	12.5	4.8	1.918325
8.9	328.0	601.1	303.0	1.23E+11	765.2	14.9	9.7	3.7	1.493728
9.4	325.9	585.3	300.9	1.21E+11	754.1	15.1	9.8	3.8	1.507653
9.9	347.4	594.3	322.4	1.40E+11	875.4	13.7	8.9	3.4	1.369772
10.9	358.0	565.0	333.0	1.51E+11	940.5	13.1	8.5	3.3	1.306438
11.9	400.8	604.4	375.8	1.98E+11	1237.2	10.8	7.0	2.7	1.078819
12.9	486.6	660.6	461.6	3.25E+11	2029.3	7.1	4.6	1.8	0.706532

13.9	529.5	660.6	504.5	4.07E+11	2539.4	5.5	3.5	1.4	0.545424
14.9	542.4	660.6	517.4	4.35E+11	2710.3	5.0	3.2	1.2	0.498751
15.9	547.7	660.6	522.7	4.46E+11	2782.5	4.8	3.1	1.2	0.479909
16.9	509.8	660.6	484.8	3.68E+11	2294.8	6.2	4.0	1.5	0.618004
17.9	555.4	660.6	530.4	4.63E+11	2889.4	4.5	2.9	1.1	0.452839
18.9	563.5	660.6	538.5	4.82E+11	3007.2	4.2	2.8	1.1	0.424069
19.9	548.8	660.6	523.8	4.49E+11	2797.3	4.8	3.1	1.2	0.476094
23.9	573.4	660.6	548.4	5.06E+11	3154.5	3.9	2.5	1.0	0.389572
24.9	583.3	660.6	558.3	5.30E+11	3306.3	3.6	2.3	0.9	0.355508

Table 10.27: 1600 RPM and 400mm/min processes data

			25				15.69965	6.038328	2.415331
			Average temperature						
Relative time	Ar1.Max.	Ar1.Average	Delta T	$T^4-T_0^4$	q_2 radiation	Sum of convections	h_{q2}	h_{Q2}	h_Q
11	110.4757	65.1139	40.1139	5.19E+09	32.3729	168.025	109.2162	42.00625	16.8025
11.1	109.3475	62.84063	37.84063	4.84E+09	30.19984	178.1765	115.8147	44.54411	17.81765
11.2	121.4244	65.53498	40.53498	5.26E+09	32.78026	166.2695	108.0752	41.56737	16.62695
11.3	136.8601	71.40181	46.40181	6.19E+09	38.61598	145.1214	94.3289	36.28034	14.51214
11.4	134.8627	69.55487	44.55487	5.89E+09	36.74634	151.1791	98.26639	37.79477	15.11791
11.5	136.1131	71.41502	46.41502	6.19E+09	38.62947	145.0798	94.30186	36.26994	14.50798
11.6	158.0221	74.97602	49.97602	6.79E+09	42.3205	134.6684	87.53444	33.66709	13.46684
11.7	158.0221	77.26545	52.26545	7.18E+09	44.75413	128.7228	83.66983	32.1807	12.87228
11.8	153.4224	78.38091	53.38091	7.37E+09	45.95726	126.0105	81.9068	31.50261	12.60105
11.9	172.0042	84.56928	59.56928	8.47E+09	52.84305	112.8042	73.32275	28.20106	11.28042
12	181.7805	91.61823	66.61823	9.8E+09	61.13396	100.7438	65.48349	25.18596	10.07438
12.5	193.2529	82.66311	57.66311	8.13E+09	50.68356	116.5706	75.77092	29.14266	11.65706

13	248.257	102.0649	77.06492	1.19E+10	74.33708	86.91598	56.49539	21.729	8.691598
13.5	373.5997	130.3175	105.3175	1.86E+10	115.9911	63.2043	41.08279	15.80107	6.32043
14	366.5801	169.878	144.878	3.06E+10	190.9856	45.42803	29.52822	11.35701	4.542803
14.5	394.7305	199.7999	174.7999	4.21E+10	262.7736	37.24108	24.2067	9.310271	3.724108
15	411.1035	205.715	180.715	4.47E+10	278.6805	35.93409	23.35716	8.983521	3.593409
15.5	417.8037	216.5644	191.5644	4.96E+10	309.4279	33.73844	21.92998	8.43461	3.373844
16	434.9037	239.6404	214.6404	6.12E+10	381.9711	29.77324	19.3526	7.443309	2.977324
16.5	452.7363	233.7993	208.7993	5.81E+10	362.6548	30.69865	19.95412	7.674662	3.069865
17	498.0389	253.6553	228.6553	6.91E+10	431.0855	27.73355	18.02681	6.933388	2.773355
17.5	475.335	264.7754	239.7754	7.58E+10	472.9475	26.27276	17.0773	6.568191	2.627276
18	506.0691	278.4906	253.4906	8.47E+10	528.2796	24.63299	16.01144	6.158247	2.463299
18.5	484.9437	280.1079	255.1079	8.58E+10	535.0829	24.45015	15.8926	6.112537	2.445015
19	507.6013	322.594	297.594	1.18E+11	736.3386	20.28324	13.18411	5.07081	2.028324
19.5	488.1126	318.9557	293.9557	1.15E+11	717.3221	20.59898	13.38934	5.149745	2.059898
20	510.4512	306.6121	281.6121	1.05E+11	655.3677	21.72187	14.11922	5.430468	2.172187
21	512.0737	327.9176	302.9176	1.23E+11	764.7984	19.83283	12.89134	4.958207	1.983283
22	525.992	371.1584	346.1584	1.64E+11	1025.573	16.60204	10.79133	4.150511	1.660204
23	619.9727	449.1229	424.1229	2.64E+11	1648.103	12.08236	7.853536	3.020591	1.208236
24	660.6422	553.4455	528.4455	4.59E+11	2862.423	7.399224	4.809496	1.849806	0.739922
25	660.6422	501.1757	476.1757	3.52E+11	2192.894	9.617492	6.25137	2.404373	0.961749
30	660.6422	522.4693	497.4693	3.93E+11	2449.892	8.689214	5.647989	2.172304	0.868921
35	660.6422	646.3103	621.3103	7.07E+11	4408.382	3.805068	2.473294	0.951267	0.380507
36	660.6422	640.8669	615.8669	6.9E+11	4303.755	4.008585	2.605581	1.002146	0.400859
37	660.6422	630.4821	605.4821	6.59E+11	4109.269	4.398545	2.859054	1.099636	0.439855
37.6	660.6422	625.5092	600.5092	6.44E+11	4018.48	4.586158	2.981003	1.146539	0.458616

10.8 Appendix 8: Conferences and workshops

During the course of my two year Masters the following workshops and conferences were attended by means of a selection process whereby I was chosen to present the current work and explore different avenues of resources available. The following events are listed in chronological order;

- HPC (High performance computing)
    - This was a 6 day course to advance ones knowledge in high performance computing. It involved a greater understanding of the actual language in which programs are written in and manipulating these and integrating certain commands in order to increase the process time of the program.
    - It expanded and broadened one's mind with the interactions of other students across South Africa. Although the course involved in depth knowledge of programming, it was useful to gain an understanding of a particular avenue in increasing process time should one have the time to rewrite the codes in which the programme used was written by software developers.
- IASSA 2012 (International Aerospace Symposium of South Africa)
    - C.C. Topper, C. Polese, F. Pietra, *Optimisation of the Thermal Model for the Friction Stir Welding Process*, IASSA 2012 International Aerospace Symposium of South Africa, 17-18 September, Centurion, South Africa, 2012. Candice C. Topper: 3rd Best Student Presentation Prize. ISBN-978-0-620-54586-0.
    - This conference involved American delegates from the US army who attended and partook in the conference discussing Aeronautical related topics and issues.
    - There were many interesting subjects discussed in the aeronautical field as well as an interaction of local companies where present as well. This created an environment where one could interact and find out what is happening in the South African industry.

- My presented work won a third prize award amongst all the delegates that presented throughout the two days. This is featured in the AeSSA newsletter of October 2012 and can be seen in Appendix 8: Conferences and workshops.

- AeroMat (24th Advacnced Aerospace Materials and Processes)
  - C.C. Topper, C. Polese, F. Pietra, Multi-Objective Optimisation of Thermo-Mechanical Modelling of Friction Stir Welding. Aeromat 2013 Conference and Exposition, April 2-5, 2013, Bellevue, Washington, USA.
  - This conference was held internationally in the area of Seattle, Washington, USA. It involved many candidates and companies from America as well as other international countries. Included with this opportunity was the travel grant granted by the University in order to assist with travel costs involved in attending the conference in the USA.
  - Being chosen to present amongst other individuals from international countries, one was able to show what the University of the Witwatersrand had to offer on an international scale and that we have a lot of potential to expand to a higher calibre of internationally recognised degree and University.
  - Conversing with various academics including those from I-STIR, which is a company that produces the machines to perform FSW and members from TWI (The Welding Institute), who were the first to develop the FSW process, it was an opportunity to expand one's knowledge of the subject and to develop a greater understanding of the possibilities for the FSW process.

The abstracts submitted and letters of acceptance can be found in Appendix 6 for more information.

AeSSA Best Student Presentations at IASSA 2012:

1st: Andrew Wood - *Wind Tunnel Testing of a Semi-Span Wing with Oscillating Gurney Tabs to Induce Vortex Wake Instability* (Wits)

2nd: Ridhwaan Suliman - *A Partitioned Finite Volume-Finite Element Fluid Structure Interaction Scheme with Applications to Flutter Analysis* (Tuks)

3rd: Candice Topper - *Optimisation of Finite Element Thermal Model for the Friction Stir Welding Process* (Wits)



Student Prize Giving at the Awards Dinner, from left Karen van Breukelen, Rob Jonkers, Candice Topper

Figure 10.19: Extract for prize winners from AeSSA newsletter of October 2012

below in more detail with reference to abstract and references letters submitted together with acceptance letters and emails and any other output from thereof.

Workshop HPC

Letter of application with acceptance email

2012 HPC School
Application Form

Applicant Details:

Surname: Topper

First name(s): Candice Catherine

ID Number *8802030024088*
Or Passport Number

Country of Citizenship. South African

Residential Address
286 Birchin Road
Mondeor

Gender: Female

Ethnicity: White

Degree Registered for in 2012: MSc Engineering

University: Witwatersrand

Department: School of Aeronautical, Mechanical and Industrial Engineering

Email Address: cands.kat@gmail.com

Cell Phone Number: *072 688 1474*

Other Telephone Number:

Figure 10.20: Application to attend HPC workshop, part 1

Academic Record

Letter of Recommendation Attached:	***YES*** *(delete whichever is inapplicable)*
Academic Transcript Attached:	***YES*** *(delete whichever is inapplicable)*

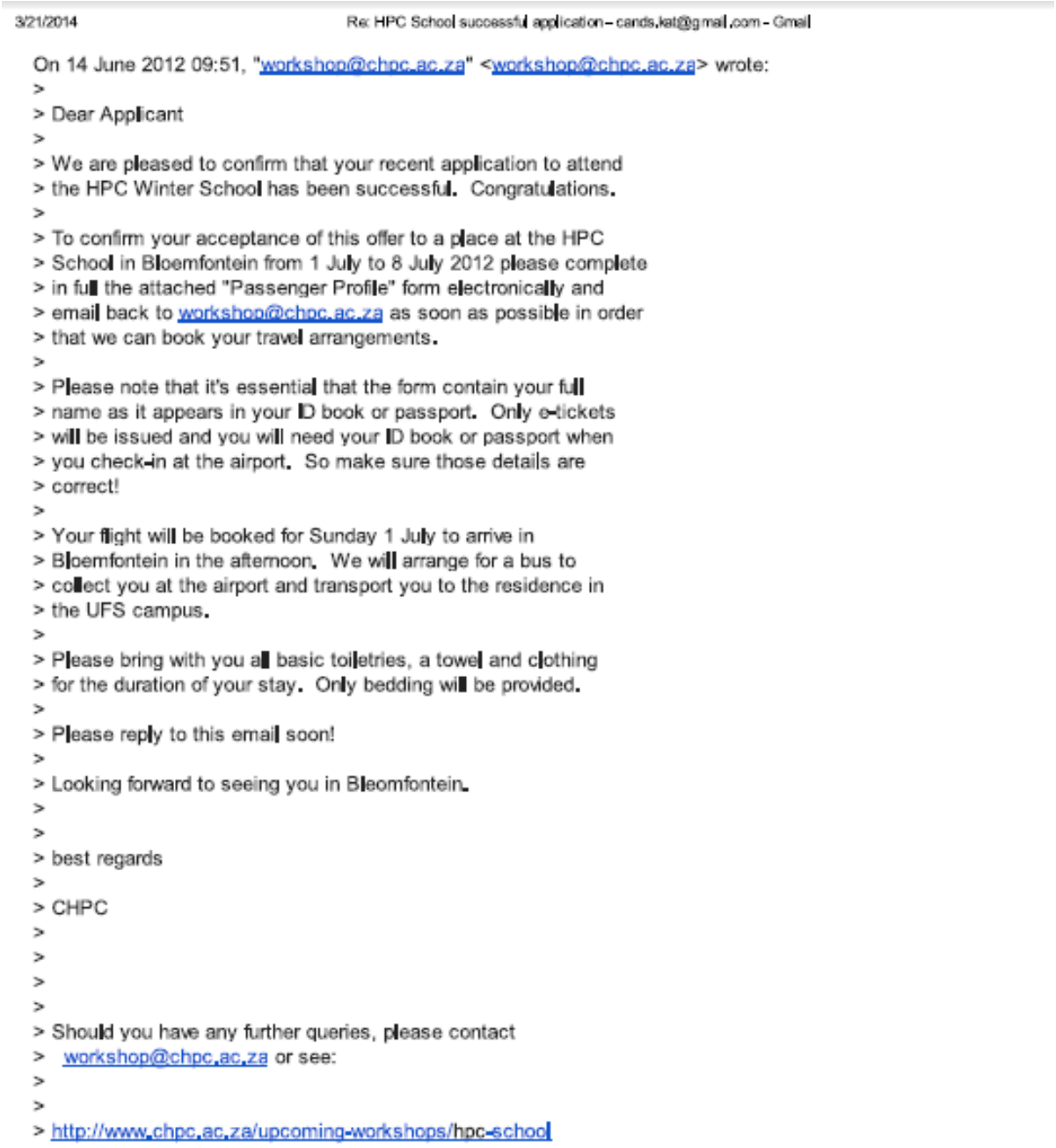
Motivation

Explain why you should be considered as one of the participants in the 2012 HPC School? (Not more than 100 words)	Based on my current knowledge of programming and being a graduate engineer, one is always looking to further their skills and this particular area is of great importance for future use. Always wanting to dissect and find a more feasible, simple solution, enhancing my own program skills would be of great benefit in applying it to my current studies and future career.
Briefly describe your programming skills and experience, including mention of programming languages and projects completed. (Not more than 100 words)	Programming skills include basic knowledge of Matlab and C++. In second year (2009) completed projects for both the languages and obtained an A for the Matlab project and a C for the C++ project. Both languages were taught in a period of approximately 4 months combined, which gave a suitable amount of time to grasp basic concepts of the two different languages. Throughout the undergraduate degree, Matlab proved to be a useful tool when doing calculations. Other programming skills include currently, learning ANSYS parametric design language (APDL) which is applicable to my postgraduate degree.

Research Plan

Are you currently registered for a postgraduate degree‡ in 2012? OR Do you intend to continue with a postgraduate degree in 2013?	**Currently enrolled in a postgraduate degree in 2012** (delete whichever is inapplicable)
Postgraduate Degree (eg MscEngng) current or future:	MSc Eng
Subject:	Research in Friction Stir Welding
Department:	School of Aeronautical, Mechanical and Industrial Engineering
University:	Witwatersrand
Name of (current or potential) Supervisor:	Professor C Polese
Contact detail for **supervisor**: Email	claudia.polese@wits.ac.za
Contact detail for **supervisor**: Telephone	
Research Topic: (Not more than 100 words)	Research is being done on Friction Stir Welding of Aluminium plates. As a start ANSYS is being used to simulate the effects of the process onto the material. Knowing how the material is deforming and stresses incurred by this friction process one is then able to design for a better tool which incurs the least amount of damage to the material and hence a more productive way of joining materials together. A program is being used first to try simulate as closely possible to reality of the process as doing actual tests can become expensive.

Figure 10.21: Application to attend HPC workshop, part 2



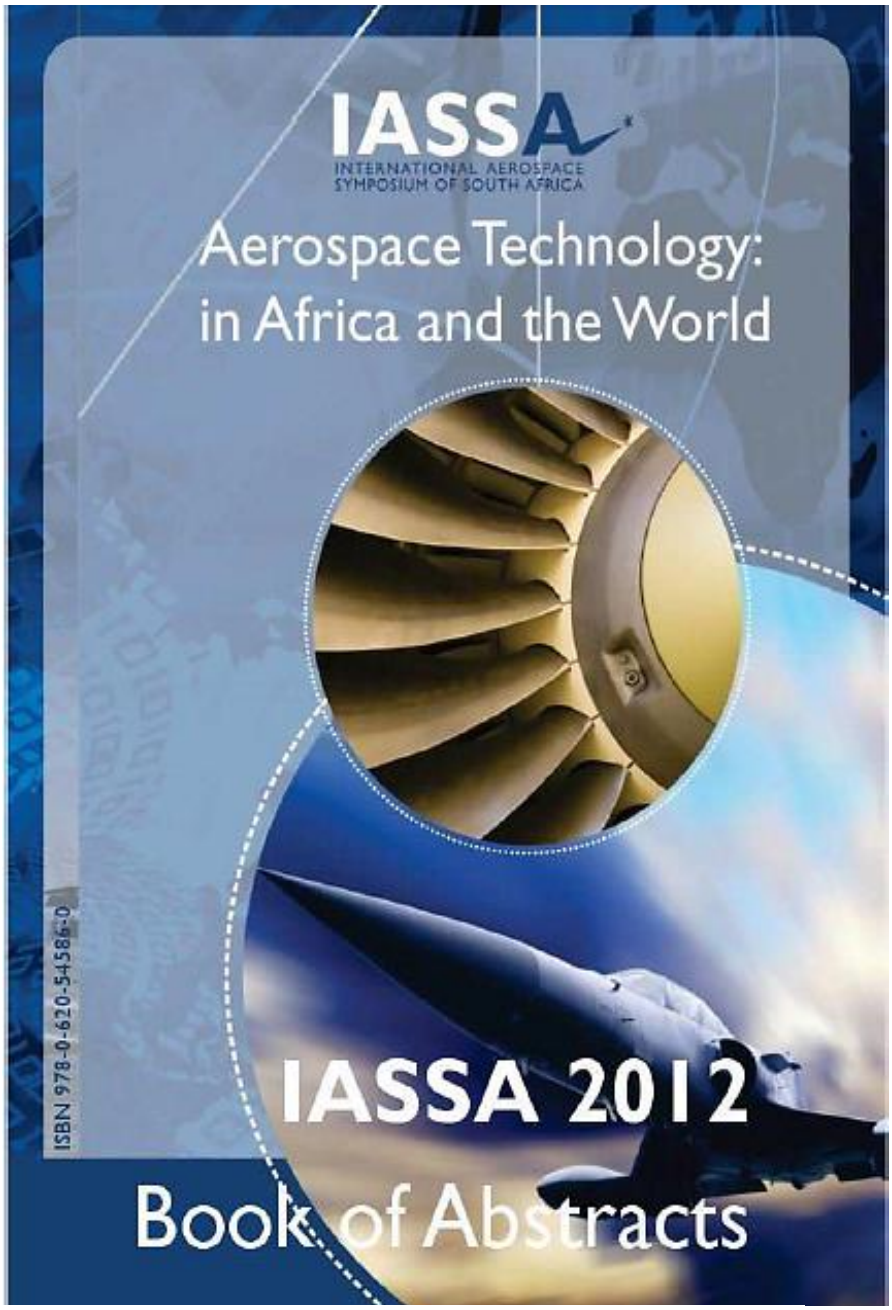
3/21/2014 Re: HPC School successful application – cands.kat@gmail.com - Gmail

On 14 June 2012 09:51, "workshop@chpc.ac.za" <workshop@chpc.ac.za> wrote:
>
> Dear Applicant
>
> We are pleased to confirm that your recent application to attend
> the HPC Winter School has been successful. Congratulations.
>
> To confirm your acceptance of this offer to a place at the HPC
> School in Bloemfontein from 1 July to 8 July 2012 please complete
> in full the attached "Passenger Profile" form electronically and
> email back to workshop@chpc.ac.za as soon as possible in order
> that we can book your travel arrangements.
>
> Please note that it's essential that the form contain your full
> name as it appears in your ID book or passport. Only e-tickets
> will be issued and you will need your ID book or passport when
> you check-in at the airport. So make sure those details are
> correct!
>
> Your flight will be booked for Sunday 1 July to arrive in
> Bloemfontein in the afternoon. We will arrange for a bus to
> collect you at the airport and transport you to the residence in
> the UFS campus.
>
> Please bring with you all basic toiletries, a towel and clothing
> for the duration of your stay. Only bedding will be provided.
>
> Please reply to this email soon!
>
> Looking forward to seeing you in Bloemfontein.
>
>
> best regards
>
> CHPC
>
>
>
>
> Should you have any further queries, please contact
> workshop@chpc.ac.za or see:
>
>
> http://www.chpc.ac.za/upcoming-workshops/hpc-school

Figure 10.22: Acceptance letter from HPC

Conference IASSA

The following extracts are taken from the IASSA 2012 book of abstracts.



IASSA 2012 Book of Abstracts
© The Aeronautical Society of South Africa 2012

Edited by:
Karen van Breukelen

Published by:
The Aeronautical Society of South Africa, (Association incorporated under section 21)
Registration number 2000/026325/08, P.O. Box 11928 Die Hoewes 0163
September 2012

ISBN-978-0-620-54586-0

IASSA 2012 is proudly convened by the Aeronautical Society of South Africa (AeSSA) and the Flight Test Society of South Africa (FTSSA) and incorporates the Technical Aerospace and Unmanned Systems Conference (TAUSC).

IASSA 2012 Organising Committee
Karen van Breukelen, AeSSA
Rob Jonkers, AeSSA
Derick Matthee, FTSSA
Thomas Jones, TAUSC

IASSA 2012 Conference Administration
Esther Torlage

IASSA 2012 Technical Review Committee
Japie van Wyk
Barbara Barbieri
Des Barker
Japie Engelbrecht
Danie Hattingh
Jim Huston
Thomas Jones
Deon Labuschagne
Anton Maneschijn
Jimoh Pedro
Chris Redelinghuys
Robert Reid
Glen Snedden

Acknowledgements
The IASSA 2012 Organising Committee would like to thank the following institutions (in alphabetical order) for their support:
Aerospace Industry Support Initiative
Aerosud
CSIR
Denel Dynamics
Denel Aerostructures
Department of Science & Technology
Marenco Engineering Technologies Africa
National Aerospace Centre
South African National Space Agency (SANSA)
Technology Innovation Agency (TIA)

Contents

Control and Automation 7

Flight Control System for an Autonomous Parafoil 7
Autonomous Landing of a Helicopter on a Moving Deck through Monocular Vision 7
Robust Flight Control of a UAV with Asymmetric Damage to its Primary Lifting Surface 8
Extending the Flight Envelope Evaluation of a Quad Rotor Aircraft 9
Autonomous Return to Base of the SLADe II Quad-rotor Vehicle 9
A Generic Local Planning Method for a Fixed-Wing UAV in Cluttered, Dynamic Environments 10
A Multi-Mode Upset Recovery Flight Control System for Large Transport Aircraft 11
Motion Planning Algorithms for Autonomous Navigation for a Rotary Wing UAV 12
Optimal Active Fault Detection for Open Loop Stable Linear Systems 13
Autonomous Take-off and Landing of the SLADe II Quad-rotor Vehicle 13

Aerodynamics and Simulation 14

A Partitioned Finite Volume-Finite Element Fluid-Structure Interaction Scheme with Applications to Flutter Analysis 14
AHRLAC Aerodynamic Control Surface Design 15
Multi-disciplinary Optimization and Rapid Configuration Studies in Preliminary UAV Design 16
Aerodynamics of Combined Trailing-Edge Modifications 17
Automated Analysis of Aircraft Configurations for Safe Separation Enabled by Quantitative Grading of Results 18
Inferring the Optimum Glide Slope and Trim Setting of a Parafoil from Flight Tests and Design of Experiments 19
An Interactive Boundary Layer Modelling Methodology for Aerodynamic Flows 20
Wind Tunnel Testing of a Semi-Span Wing with Oscillating Gurney Tabs to Induce Vortex Wake Instability 21
The Use of Simulators in the Design of Marenco Swisshelicopter SKYe SH09 23
Some Experiences of the Cape Rocket Society 23
Wing Trailing Vortex Paths in Formation Flight 24

Manufacturing, Materials and Structures 24

Investigation of Post-Machining Residual Stress, of a Grade 5 Titanium Alloy, for Minimum Quantity Lubrication and Flood Cooling Regimes 24
Optimisation of Friction Stir Welding Tools and Process Parameters 25
Optimisation of Finite Element Thermal Model for the Friction Stir Welding Process 26
Characterisation of Friction Stir Welded (FSW) AA5083-H111 27
Water Confinement Influences on the Laser Shock Peening Process 28
Optimisation of the Micro Cutter Path Strategies in the Machining of Ti-6Al-4V 29

Aircraft Subsystems 30

Condensation Heat Transfer in Aerospace 30
Design, Manufacture and Optimization of a Single Stage Axial Flow Turbine Section of a Turbojet Engine 31
Performance Modelling of a Radial Compressor for a Micro Turbojet Application 32
Nanotubes as Heat Transfer Medium in High Performance Aerospace Heat Exchangers 33

Figure 10.24: Featured title in IASSA book of abstracts

Optimisation of Finite Element Thermal Model for the Friction Stir Welding Process

CC Topper[1]*, C Polese[1] and F Pietra[2]

1 University of the Witwatersrand and 2 University of Pretoria (cands.kat@gmail.com)

The following research is primarily focused on the simulation of the thermal effects on the Friction Stir Welding (FSW) process on aluminium alloys for aerospace applications. The main objective is to be able to realistically characterise the thermal input of a FSW process by means of an accurate parametric Finite Element thermal model, verified using thermal imaging camera data as benchmark.

FSW is a solid state joining process. A rotating tool is plunged into the join line between two clamped plates. The heat transfer input mechanism in the FSW process is due to the frictional contact between the tool and the work-piece plates. Since the FSW process occurs at solid state, no melting occurs and hence the yield strength of the material is temperature dependent.

Obtaining accurate measurements of temperature for the FSW process has proven to be challenging. Preliminary experimental observations in obtaining temperature variations in the material was performed using thermocouples but issues arose, one being the inability to obtain a complete thermal representation of the tool and the work-piece as thermocouples were placed along the FS weld only as control points. Research is to be undertaken using a thermal imaging camera. The type of camera to be used has a sensitivity that is able to detect temperature differences as small as 0.04℃. This experimental approach can give direct information of the temperature at all points of the work-piece, obtaining a complete external thermal assessment of the process. This is also beneficial in obtaining images of the temperature distribution in the tool itself also if it is rotating and partly submerged into the work-piece.

Since the temperature field directly affects the final residual stress distribution in the joint, an accurate thermal model of the FSW process is required to assimilate the numerical simulation with the process that actually occurs in reality. The new release of the FE software ANSYS Release 14 is being used. This novel version is capable of modelling the specific features required to assimilate the FSW process by using the ANSYS Parametric Design Language (APDL). The APDL language has new specific features designed for frictional heat generation, plastic heat generation and temperature controlled bonding contacts. The formulation of the model is based upon the thermal-mechanical model specifically developed by Zhu and Chao [*1*]. ANSYS APDL language is parametric by nature so it is well suited to be efficiently implemented into a multi-objective optimization platform, such as the modeFRONTIER software, in order to further improve the FSW simulation.

The quantitative experimental data obtained from the thermal imaging camera can be used to match and verify the numerical results of the FSW FE model. An accurate FSW thermal model will help to achieve a deeper understanding of the different phases of the process and an enhanced control of the key parameters of this technology, significantly reducing the required testing phase.

Reference:

[1] Technology Demonstration Guide, ANSYS Inc. release 14.0

Figure 10.25: Abstract as found in IASSA book of Abstracts

AERONAUTICAL SOCIETY OF SOUTH AFRICA

(Association incorporated under section 21)
Registration number 2000/026325/08
P.O. Box 11928 Die Hoewes 0163
Tel / Fax: (012) 662 5113
Email: admin@aessa.org.za
Web: www.aessa.org.za

A DIVISION OF THE ROYAL AERONAUTICAL SOCIETY

18-Sept-2012

Dear Candice Topper

Congratulations on your award as presented to you on behalf of IASSA 2012.
The value of the award is R 2000-00. In order to make the required payment, please provide your bank details to the Society Administration Officer as detailed below so that we can make an Internet based payment.

All the best and enjoy your award.

Rob Jonkers
AeSSA President

Karen van Breukelen
IASSA Organiser

Prof. Japie Van Wyk
IASSA Technical Committee Chair

*Please send your banking details to:
AeSSA Admin Officer Contact details
Esther Torlage
Email: e.torlage@aerosud.co.za
Tel: 012 662 5113
Fax: 012 662 5198

DIRECTORS:
RP JONKERS, GH JANSEN VAN RENSBURG, PROF JP MEYER, PROF AJ VAN WYK, DR RS HURLIN, G CORDERLEY, KP KING, DR C LAW, R POWRIE, JS MONK, CT BUTLER, PROF A BASSON, MAJ GEN W THACKWRAY, CAPT S POPRAWA, MS K VAN BREUKELEN, G SNEDDEN, PROF L DALA, B GERRYTS, D LOOTS

Figure 10.26: Prize awarded for presentation at IASSA 2012

Conference AeroMat

Abstract submitted to the AeroMat committee and as seen on the website once it was accepted.



30/01/2013 24th Advanced Aerospace Materials and Processes (AeroMat) Conference and Exposition: Multi-Objective Optimization of Thermo-Mechanical Modellin...

AeroMat CONFERENCE AND EXPOSITION

Industry Partner: ATI

April 2-5, 2013 • Bellevue, Washington USA • Meydenbauer Center

Start | At-A-Glance | Browse by Day | Author Index

Multi-Objective Optimization of Thermo-Mechanical Modelling of Friction Stir Welding

Wednesday, April 3, 2013: 9:30 AM
403 (Meydenbauer Center)

***Ms. Candice C. Topper** , University of the Witwatersrand, Johannesburg, South Africa*
Prof. Claudia Polese , University of the Witwatersrand, Johannesburg, South Africa
Mr. Francesco Pietra , University of Pretoria, Pretoria, South Africa

The following research is primarily focused on the development of a reliable thermo-mechanical model of the Friction Stir Welding (FSW) for aerospace applications.

The main objective is to realistically simulate the FSW process characteristics using a synergic approach of advanced Finite Element (FE) modelling together with high-resolution thermal imaging.

Since FSW occurs at a solid state, the heat input mechanism, based on a complex frictional contact between the rotating tool and the workpiece, is strongly affected by several temperature-dependent material properties.

The new release of ANsys 14 FE software has innovative Parametric Design Language (APDL) command features specifically designed for frictional heat generation, plastic heat generation and temperature controlled bonding contacts, perfectly suited for a FSW process simulation that can efficiently be implemented into a multi-objective optimization platform, i.e. modeFRONTIER.

Experimentally, thermocouples are insufficient in obtaining complete thermal representations of the tool and workpiece as they can be used only as control points along the weld. Instead a high-resolution, high-sensitivity infrared (IR) camera and an IR real-time digital storage and analysis software can provide precise temperature information at all visible points, obtaining a complete external thermal assessment of the process.

Applying a Taguchi Design of Experiments method, FSW trials were performed on a standard aluminium alloy for airframe structures, using a Triflat design tool, and modifying the primary parameters for heat generation within the operating window. Welds were thermally monitored using a FLIR T640 IR camera to create a significant database to be used to optimize the developed ANsys/modeFRONTIER FSW parametric model.

An accurate FSW thermo-mechanical simulation will help to achieve a deeper understanding of the different phases of the FSW process and an enhanced control of the key parameters of this technology, substantially reducing the testing phase required to frame a robust sweet-spot.

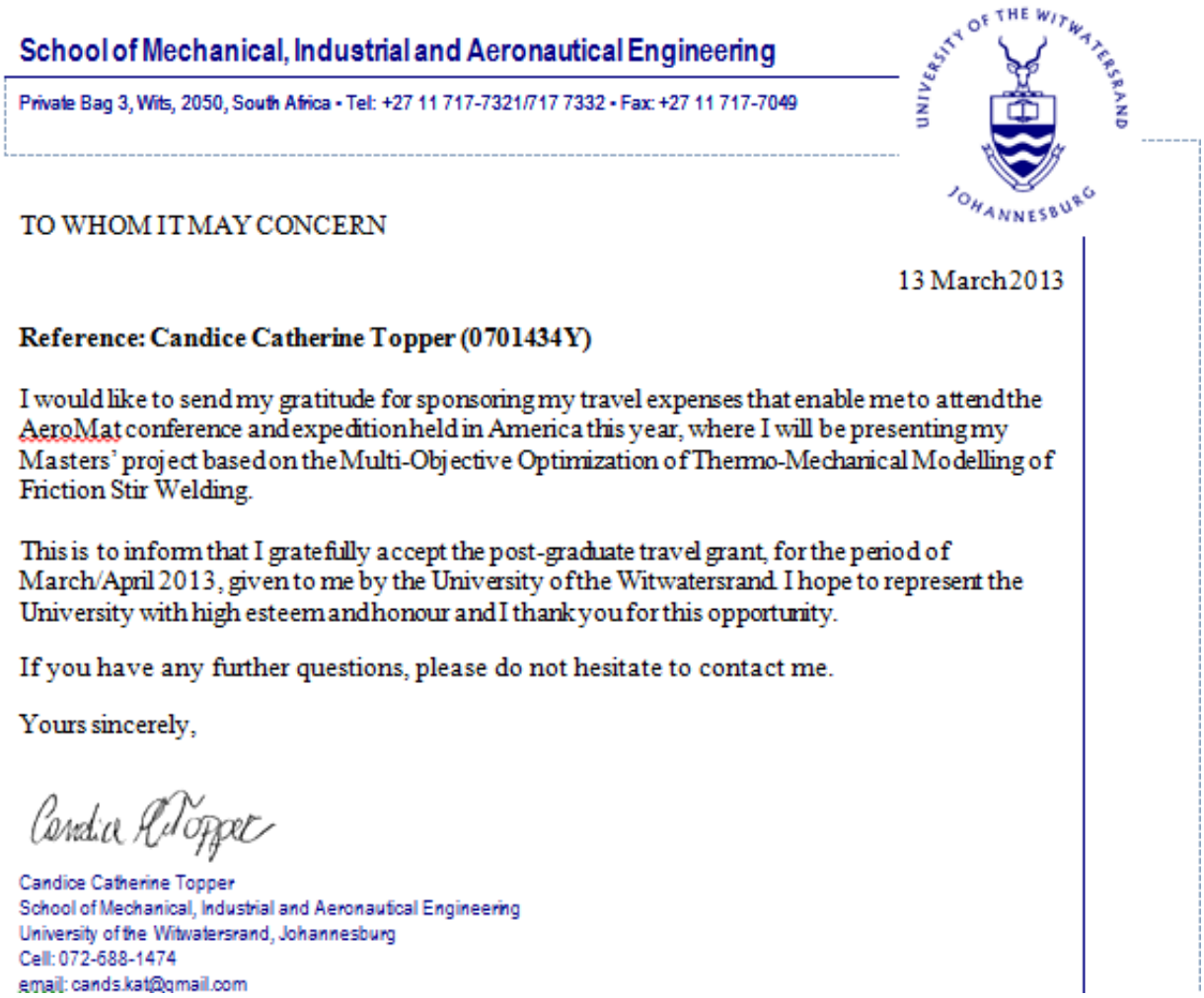
See more of: Welding & Joining - III
See more of: Welding & Joining

Figure 10.27: Extract of Abstract submitted from AeroMat website

Letter of acceptance to attend the conference in the USA, together with the travel grant that was given to assist with costs

25-Mar-13	000009	Refund - Stipends ALL	TRAVEL GRANT	9,000.00

Figure 10.28: Travel grant in Student account



School of Mechanical, Industrial and Aeronautical Engineering

Private Bag 3, Wits, 2050, South Africa • Tel: +27 11 717-7321/717 7332 • Fax: +27 11 717-7049

TO WHOM IT MAY CONCERN

13 March 2013

Reference: Candice Catherine Topper (0701434Y)

I would like to send my gratitude for sponsoring my travel expenses that enable me to attend the AeroMat conference and expedition held in America this year, where I will be presenting my Masters' project based on the Multi-Objective Optimization of Thermo-Mechanical Modelling of Friction Stir Welding.

This is to inform that I gratefully accept the post-graduate travel grant, for the period of March/April 2013, given to me by the University of the Witwatersrand. I hope to represent the University with high esteem and honour and I thank you for this opportunity.

If you have any further questions, please do not hesitate to contact me.

Yours sincerely,

Candice Catherine Topper
School of Mechanical, Industrial and Aeronautical Engineering
University of the Witwatersrand, Johannesburg
Cell: 072-688-1474
email: cands.kat@gmail.com

Figure 10.29: Acceptance letter for travel grant

Claudia Polese

From: Candice Topper <cands.kat@gmail.com>
Sent: Tuesday, January 15, 2013 10:39 AM
To: Claudia Polese
Subject: Fwd: AeroMat 2013 Acceptance Letter and Program Details

---------- Forwarded message ----------
From: <jaime.creighton@gmail.com>
Date: Mon, Jan 14, 2013 at 7:04 PM
Subject: AeroMat 2013 Acceptance Letter and Program Details
To: candice.topper@students.wits.ac.za

Dear Candice C. Topper:

On behalf of the AeroMat 2013 Organizing Committee, I would like to personally congratulate you on the acceptance of your abstract entitled, "Multi-Objective Optimization of Thermo-Mechanical Modelling of Friction Stir Welding" (ID# 34174). The knowledge and expertise of participants like you make it possible to consistently deliver the quality conference our attendees have come to expect.

This letter has been sent to you because your name was submitted as the presenting author. If you are not the presenting author, please notify Jaime Creighton at jaime.creighton@asminternational.org as soon as possible. If you submitted more than one abstract, you will receive a separate notification for each abstract.

AeroMat 2013 will be held April 2-4, 2013 at the Meydenbauer Center in Bellevue, Washington.

If you encounter any reason to cancel your presentation, it is extremely important that you notify Jaime Creighton immediately, so that we can adjust the program accordingly and seek a replacement. Also, if there is any change to the presenting author between now and the conference, please contact Jaime Creighton with the new presenting author information as soon as possible. If you have any questions, please contact Jaime Creighton directly at (440) 338-5151 ext. 5581, or by e-mail at jaime.creighton@asminternational.org.

IMPORTANT NOTICE FOR INTERNTATIONAL PRESENTERS:
Travel to the United States
Meeting attendees from countries that require a visa to enter the United States are reminded that the process of obtaining a visa may take several months. You are strongly encouraged to plan ahead and begin the application process early. Visa applications should be submitted for processing as early as possible and absolutely no later than 90 days prior to travel. Plan today. If you require a Visa Letter or have any questions, please contact Jaime Creighton directly at jaime.creighton@asminternational.org.

VISA WAIVER PROGRAM UPDATE – MUST READ
Eligible citizens or nationals traveling under the Visa Waiver Program are REQUIRED to register for ESTA (Electronic System for Travel Authorization), which was launched by the U.S. Department of Homeland Security in August 2008. It is a fully automated, electronic system for screening at any time prior to travel. A visa waiver will not be permitted unless you are registered for ESTA. More information can be obtained by going to http://www.cbp.gov/xp/cgov/travel/id_visa/esta/

PRESENTATION DETAILS*
Paper Title: Multi-Objective Optimization of Thermo-Mechanical Modelling of Friction Stir Welding (ID #34174)
Session Title: Welding & Joining - III
Date: Wednesday, April 3, 2013
Session Start Time: 8:30 AM
Your Presentation Time: 10:30 AM
Location: 403, Meydenbauer Center
*Changes to the schedule may occur between now and the conference. If your assigned time or room changes, you will be notified.

You will have 30 minutes for your presentation, which includes 5 minutes to answer questions from the audience. Meeting rooms are equipped with a computer (with CD-ROM and USB capability), podium microphone, laser pointer, a projection screen and data projector.

For electronic presentations, we recommend that you maintain 0.75" (19mm) margins on each slide and use a minimum 24-point font. Black or dark text on a white or light background is also recommended for best visual clarity.

NOTE: AeroMat does not produce a proceedings, which means you do not have to submit a manuscript or a PowerPoint Presentation for publication. Please bring your PowerPoint presentation with you to the conference to upload prior to your presentation.

ABSTRACT CHANGES (DUE NO LATER THAN February 8, 2013):
Technical abstracts will available online before the conference, on the mobile app, and will be printed in the final program. If you have not yet submitted your abstract, or need to revise it, please email your revised version to Jaime Creighton@asminternational.org. Note: The abstract must be 300 words or less. (No figures, tables or graphs).

SPEAKER BIOGRAPHY (DUE NO LATER THAN March 15, 2013):
If you have not already submitted your speaker biography online, please submit a 25-word description of your professional background no later than March 15, 2013 - please email Jaime Creighton with your bio at jaime.creighton@asminternational.org. This information will be used by your Session Chair to introduce you at the conference.

CONFERENCE REGISTRATION:
Speakers are required to pay a reduced registration fee (participant registration) and are expected to be registered for the conference by March 4, 2013. Registration details will be available online at by January 18, 2013.
http://www.asminternational.org/content/Events/aeromat/registration.jsp

HOUSING RESERVATIONS:
The headquarters hotel for AeroMat 2013 is the Hyatt Regency Bellevue. You may make your reservation online at http://www.asminternational.org/content/Events/aeromat/travel.jsp. The conference rate of $184.00/night (plus taxes) is only available until March 11, 2013 and is subject to availability. It is advised that you secure your hotel room for AeroMat 2013 on or before March 11, 2013.

DAY OF PRESENTATION:
All presenting authors are asked to meet in the meeting room of your presentation 30 minutes prior to the start of your session. This will allow all speakers the opportunity to meet their session chair and go over any final conference details and audio visual concerns. Your attendance is VERY IMPORTANT.

MOBILE APP:
This year, AeroMat will feature a Mobile App during the conference. The app will provide key information regarding the technical program, exposition and social events. More information will be provided closer to the conference on how to download the app and stay connected.

Once again, on behalf of the entire AeroMat 2013 Organizing Committee, thank you for your support of this important conference series. Please spread the word about your involvement within your organization and to your colleagues! We look forward to seeing you in Bellevue.

Please direct all requests and any questions to Jaime Creighton, Event Planner at ASM International at (440) 338-5151 ext. 5581, or by e-mail at jaime.creighton@asminternational.org.

Regards,
ASM International®

Dr. James D. Cotton
AeroMat 2013 Chairman

Figure 10.30: Acceptance letter to attend AeroMat conference

Post-GraduateTravel Grant: Final Report

Conference:	**AeroMat 2013 Conference & Exposition**
	Oral Presentation: Multi-Objective Optimisation of Thermo-Mechanical Modelling of Friction Stir Welding
Candidate:	**Candice C Topper (0701434Y)**
Supervisor:	**Claudia Polese**
Date:	**20/05/2013**

AeroMat Conference

The following project was presented at the AeroMat conference held in Seattle, WA, USA. Organised by the ASM international and in partner with ATI and various sponsors such as Boeing, the conference is involved in presenting new innovative technologies relating to aeronautical materials.

ASM is an engineering and scientific society and are involved in everything relating to materials. Members are able to share their ideas through conferences such as the AeroMat Conference and Expositions which is targeted at aerospace materials. ASM is partnered with many organisations, from academic Universities and government to Industries, not only within their country but international ones as well. They also belong to societies as well as they are members to of American Society of Association Executives (ASAE) and Council of Engineering and Scientific Society Executives (CESSE) to name a few. Their industry partner ATI (Allegheny Technologies Incorporated) is part of the development and manufacturing of the advanced aerospace materials and also the technically complex cast and forged components being used today.

With over ten various topics discussed at the conference, the Welding & Joining session was the particular area of validity for the presented project on FSW. Also part of the Welding & Joining session include Linear Friction Welding, Laser Welding and Electron Beam Welding, all of which were presented on what is currently developing in each topic either in industry or research being conducted in Universities.

Other members included in this particular session were TWI (The Welding Institute) which are the developers of the FSW process. Other big companies include Boeing, who are undertaking research in FSW and I-STIR technology, who manufacture the machines to perform the welds. Universities that were involved, include; University of Washington, USA, Witwatersrand University, SA, University of Manitoba, Canada.

Sessions of conference

The session of the conference that this presentation was part of, involved the Welding and Joining sessions, where the project was presented in Welding and Joining III. This particular topic was divided into three sessions and the various projects and innovations spoken about are listed below;

Welding and Joining I

- Recent Developments in Friction Stir Welding
- Characterisation of Friction Stir Welding in Aluminium Alloy 7055 using Microhardness and Differential Scanning
- Charpy Impact Testing of Friction Stir Welded Titanium
- Comparison of Friction Stir Welded and Stationary Shoulder Friction Stir Welded Dissimiliar AA2024/AA7050 Butt Joints with Comparable Energy

Welding and Joining II

- Wide-Gap Braze Repair of Single Crystal Aerospace Superalloys
- Electron Beam Probing to Assure Process and Product
- Effect of Welding Parameters on Residual Stress Distribution in A6056-T4 Friction Stir Welds
    - This was presented by the University of the Witwatersrand

Welding and Joining III

- New Development in Aluminium Welding Wire-Alloy 4943
- Linear Friction Welding for Low Cost Manufacturing
- Multi-Objective Optimisation of Thermo-Mechanical Modelling of Friction Stir Welding
- Investigation of Vapour Plume and Molten Pool in Pulsed and Continuous Keyhole Welding Based on Three-Dimensional Dynamic Model.
    - This presentation was very interesting and the person presenting (W. Tan, Y Shin, Purdue University, W. Lafayette, IN) displayed remarkable intellect in presenting project on its difficult technicality.

Based on the above presentation presented under this particular topic, shows an advanced progression of the work and the league at which this project was presented.

Content of presented work

The following research is primarily focused on the development of a reliable thermo-mechanical model of the Friction Stir Welding (FSW) for aerospace applications.

The main objective is to realistically simulate the FSW process characteristics using a synergic approach of advanced Finite Element (FE) modelling together with high-resolution thermal imaging. Since FSW occurs at a solid state, the heat input mechanism, based on a complex frictional contact between the rotating tool and the workpiece, is strongly affected by several temperature-dependent material properties. The new release of ANsys 14 FE software has innovative Parametric Design Language (APDL) command features specifically designed for frictional heat generation, plastic heat generation and temperature controlled bonding contacts, perfectly suited for a FSW process simulation that can efficiently be implemented into a multi-objective optimization platform, i.e. modeFRONTIER.

Experimentally, thermocouples are insufficient in obtaining complete thermal representations of the tool and workpiece as they can be used only as control points along the weld. Instead a high-resolution, high-sensitivity infrared (IR) camera and an IR real-time digital storage and analysis software can provide precise temperature information at all visible points, obtaining a complete external thermal assessment of the process.

Applying a Taguchi Design of Experiments method, FSW trials were performed on a standard aluminium alloy for airframe structures, using a Triflat design tool, and modifying the primary parameters for heat generation within the operating window. Welds were thermally monitored using a FLIR T640 IR camera to create a significant database to be used to optimize the developed ANsys/modeFRONTIER FSW parametric model.

An accurate FSW thermo-mechanical simulation will help to achieve a deeper understanding of the different phases of the FSW process and an enhanced control of the key parameters of this technology, substantially reducing the testing phase required to frame a robust sweet-spot.

A brief schematic of the content of the presentation is shown below, describing the certain topics discussed on the Masters project.

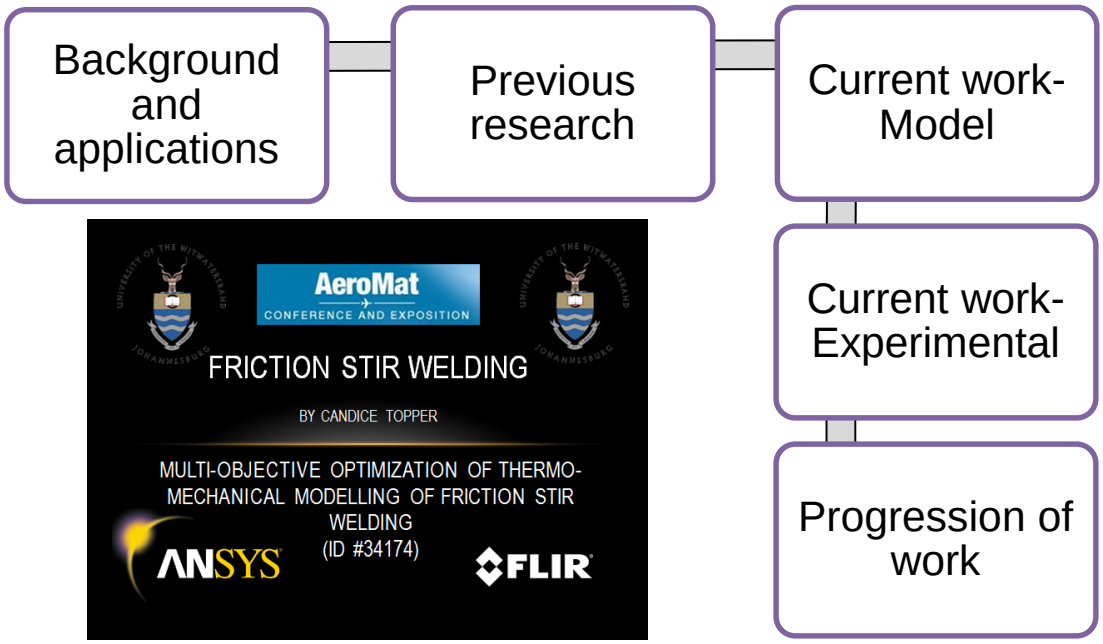


Figure 10.31: Overview of presentation

The project presented covered the details of FSW and its advantages associated with it. Previous work was discussed on other models already developed based on the FSW process. Various results from other models were discussed more thoroughly as to how it applies to the current model being developed and what precautions and considerations need to be made. The developing model was discussed in detail which moved onto the experimental testing being undertaken adjacent to it. After which it was summarised as to what has been achieved so far and where the project stands to what is still required.

The presented work was appreciated by those who attended the session and displayed the high standard that it was being presented at alongside other professionals and academics.

Remarks

The presentation went well, and there were questions asked that showed interest in the idea of what was being presented. Approached by a few attendees and academics from the conference in order to discuss the project further, displayed a valuable networking opportunity that allows one to be able to expand ones project with many others having attempted or completed similar outcomes to ones' project and enhancing the calibre and expertise of the project itself.

Outcomes

- For Welding and Joining III, the presentations were very interesting and displayed a great amount of advanced technology and innovation. To be presenting alongside such high esteemed academics and professionals was a wonderful opportunity not only to advocate the University but for ones' own self confidence.
- Presentation of project was a success, where a few contacts were made and are being followed up so one is able to enhance the knowledge in the particular field of interest.
- Presenting at an international conference exposed the University outside of the bounds of the country and enables others to see the high standard and excellence we are capable of competing with.
- Approached by an individual to speak about my model is to be followed up as they have done similar research but it will be investigated as to what they were considering important and which is applicable to the current project being undertaken.
- During the exhibition intervals, made contact with an individual who works for the I-STIR technologies company. He had a lot of interesting remarks on the process and the samples on display were interesting to look at, considering their machines are capable of friction stir welding approximately 30mm of aluminium alloy.
- Also approached by one of the TWI members who also presented, and offered to help if I had any questions and to get in contact with one of the sources I have started researching when beginning my project.
- Conversing with academics from other Universities was interesting to hear what they have been working on in the field of aeronautical materials and what other processes and manufacturing techniques are available.
- The overall experience was an opportunity not to be missed. It expanded ones' own mind in terms of conversing with other engineers in fields and who are expertise in those particular areas of topics, not only in the field which I presented in but in other topics that were interesting as well.